



MAX-PLANCK-GESELLSCHAFT

**Role of Histone Modifications in the Recruitment of  
Remodeling Complex RSC and Lysine Deacetylase Hst2 to Chromatin**

Dissertation

to the Faculty of Chemistry and Chemical Biology  
at the Technical University of Dortmund

in fulfilment of the requirements for the degree of  
**Doctorate of Natural Sciences (Ph.D.)**

prepared at the  
Max Planck Institute of Molecular Physiology, Dortmund

By

Neha Jain

Parts of this thesis has been published in:

Jain, N\*, Tamborrini D\*, Evans B, Chaudhary S, Wilkins J.B & Neumann, H. Interaction of RSC chromatin remodelling complex with nucleosomes is modulated by H3 K14 acetylation and H2B SUMOylation *in vivo*. *iScience* (2020) (\*equal contribution).

Parts of this thesis is currently under review:

Jain, N., Janning, P. & Neumann, H. 14-3-3 protein Bmh1 triggers short-range compaction of mitotic chromosomes by recruiting sirtuin deacetylase Hst2. *Journal of Biological Chemistry* (2020).

The figures used in this thesis are adapted and/or extended from the original publications.

Contributions:

All experiments in this thesis were performed and analyzed by Neha Jain, with the exception of the data shown in Figure, 12-13, 22-24 and 26 which were produced by Dr. Bryan J. Wilkins; all MS analysis in this thesis were performed by Petra Janning and HRMS facility at Max Planck Institute, Dortmund.

1<sup>st</sup> Referee: Prof. Dr. Stefan Raunser

Director Structural Biochemistry

Max-Planck-Institute of Molecular Physiology, Dortmund.

2<sup>nd</sup> Referee: Prof. Dr. Daniel Summerer

Chair for Chemical Biology of Nucleic Acids

Faculty of Chemistry and Chemical Biology,

TU Dortmund University, Dortmund.

Date of submission: 26.06.2020

Dedicated to my late grandmother and mother

“Be the change you want to see in this world” - Mahatma Gandhi

## Formal declaration

The work described in this dissertation was carried out between February 2017 and August 2020 under the supervision of Prof. Dr. Stefan Raunser in the laboratory of Prof. Dr. Heinz Neumann at the Max-Planck-Institute of Molecular Physiology, Dortmund.

I hereby declare that I carried out the work independently and did not use any aid, other than the ones mentioned.

## Eidesstattliche Erklärung

Die vorliegende Arbeit wurde in der Zeit von February 2017 bis August 2020 am Max-Planck-Institut für Molekulare Physiologie in Dortmund unter der Anleitung von Prof. Dr. Stefan Raunser in dem Labor von Prof. Dr. Heinz Neumann durchgeführt.

Hiermit erkläre ich, dass ich die vorliegende Arbeit selbstständig und nur mit den angegebenen Hilfsmitteln angefertigt habe.

## Table of Contents

<b>ABSTRACT .....</b>	<b>1</b>
<b>ZUSAMMENFASSUNG .....</b>	<b>3</b>
<b>INTRODUCTION .....</b>	<b>5</b>
1.1 CHROMATIN ARCHITECTURE AND FUNCTION .....	5
1.1.1 DNA as the storehouse of genetic information .....	5
1.1.2 Histones and Nucleosomes .....	7
1.1.3 Post Translational Modifications on Histones .....	10
1.2 READERS, WRITERS AND ERASERS OF HISTONE PTMS.....	13
1.2.1 ATP dependent Chromatin Remodelers .....	13
1.2.2 Roles of RSC Complex in chromatin dynamics .....	14
1.2.3 Structural insights into the function of RSC Complex.....	15
1.2.4 What regulates the RSC Complex? .....	17
1.3 CHROMOSOME CONDENSATION.....	19
1.3.1 Higher-Order organization of Mitotic Chromosomes by Condensins .....	19
1.3.2 Nucleosome-Nucleosome interactions in Chromosome Compaction.....	21
1.3.3 Other factors regulating Chromosome Condensation .....	24
1.4 GENETIC CODE EXPANSION AS A TOOLKIT FOR PROBING PROTEIN INTERACTIONS AND FUNCTIONS .....	24
1.4.1 Principles of Genetic Code Expansion .....	25
1.4.2 Usage of Genetic Code Expansion for the incorporation of light inducible Crosslinkers into Proteins .....	28
1.4.3 Applications of the Genetic Code Expansion system for the study of PTMs .....	32
<b>2 MATERIALS AND METHODS .....</b>	<b>35</b>
2.1 MATERIALS AND APPLIANCES .....	35
2.1.1 Equipments, Consumable Supplies and Chemicals .....	35
2.1.2 Buffers and Solutions.....	38
2.1.3 Kits.....	41
2.1.4 Peptides.....	41
2.1.5 Softwares .....	42
2.1.6 Strains .....	42
2.1.7 Plasmids.....	42
2.1.8 Primers.....	42
2.2 METHODS.....	42

2.2.1 DNA Methods .....	42
2.2.2 Protein Methods.....	47
2.2.3 Yeast Methods and Crosslinking.....	56
<b>3 RESULTS.....</b>	<b>66</b>
3.1 IDENTIFICATION OF CHROMATIN INTERACTION TOPOLOGY WITH GENETICALLY ENCODED UV-CROSSLINKER .....	66
3.2 INVESTIGATION OF PROTEINS ASSOCIATING WITH HISTONES AT SINGLE AMINO ACID RESOLUTION.....	72
3.2.1 Analysis of Histone H2B T51 pBPA and crosslink products.....	72
3.2.2 Analysis of Histone H3 T80 pBPA and crosslink products .....	77
3.2.3 Immunoprecipitation of Histones and crosslinks at diverse sites.....	81
3.3 INVESTIGATION OF RSC-NUCLEOSOME INTERACTION IN VIVO USING GCE .....	83
3.3.1 Footprint of Sth1, catalytic subunit of RSC Complex onto Nucleosome.....	84
3.3.2 Binding of the H3 tail by Sth1 depends on H3 K14 Acetylation.....	88
3.3.3 RSC preferentially interacts with SUMOylated H2B In Vivo.....	91
3.3.4 RSC recognizes previously SUMOylated Nucleosomes in vivo.....	93
3.3.5 Induction of GAL1 gene as a readout of RSC interaction with SUMOylated Nucleosomes .....	95
3.3.6 Modulation of Sth1-Nucleosome interactions during the Cell Cycle.....	97
3.3 INVESTIGATION OF H3S10 PHOSPHORYLATION MEDIATED RECRUITMENT OF DEACETYLASE HST2.....	99
3.3.1 Recruitment of Deacetylase Hst2 To H3S10ph in Mitosis.....	99
3.3.2 Identification of Hst2 interaction partners and PTMs using Proteomics.....	101
3.3.3 Candidate proteins as missing Link in Chromosome Condensation Cascade .....	105
3.3.4 Effect Of Bmh1/2 knockouts on H4K16ac Levels.....	106
3.3.5 Characterization of interaction between Hst2 and Bmh1 in vivo.....	109
3.3.6 Interaction between Wildtype Hst2 and Bmh1 .....	112
3.3.7 Purification of Genetically Encoded Phosphorylated Hst2 .....	114
3.3.8 Characterization of interaction between phosphorylated Hst2 and Bmh1 in vitro .....	116
3.3.9 Effect of individual phosphosite mutants on H4K16ac levels using CRISPR/Cas9 Genome Editing .....	118
3.3.10 Investigating potential Kinases of Hst2.....	120
<b>DISCUSSION .....</b>	<b>122</b>
4.1 IN VIVO CROSSLINKING OF HISTONES IN <i>S. CEREVISIAE</i> .....	122
4.2 INSIGHTS INTO RSC COMPLEX INTERACTION WITH NUCLEOSOME IN VIVO .....	126

<i>4.3 IDENTIFICATION OF 14-3-3 PROTEIN BMH1 IN TRIGGERING SHORT RANGE CHROMOSOME CONDENSATION</i>	132
<b>SUPPLEMENTARY INFORMATION</b>	<b>138</b>
<i>SUPPLEMENTARY TABLES</i>	138
<i>SUPPLEMENTARY FIGURES</i>	144
<b>REFERENCES</b>	<b>154</b>
<b>ACKNOWLEDGEMENTS</b>	<b>170</b>

## List of Figures

Figure 1: Schematic illustration of packaging of DNA into higher-order structures in a cell.....	6
Figure 2 : Structure of Nucleosome.....	9
Figure 3 : Schematic illustration of Post translational modifications on Histones. ....	12
Figure 4 : RSC–nucleosome complex structure. ....	17
Figure 5 : Complementary pathways of chromosome condensation in eukaryotic cells. ....	23
Figure 6 : Tools for the success of Genetic Code Expansion. ....	27
Figure 7 : Genetically encoded crosslinker amino acids for in vivo crosslinking. ....	30
Figure 8 : Reaction mechanism of in vivo photo-induced crosslinking by pBPA.....	31
Figure 9 : Genetic encoding of phosphoserine into proteins.....	32
Figure 10 : Chromatin Crosslinking pipeline with encoded UV-Crosslinker, pBPA.....	66
Figure 11 : Comparative growth of Wildtype and Histone mutants.....	69
Figure 12 : in vivo crosslink pattern across Histone H2A and H2B.....	70
Figure 13 : in vivo crosslink pattern across Histone H3 and H4.....	71
Figure 14 : Immunoprecipitation of H2B T51pBPA crosslink products for MS analysis. ....	74
Figure 15 : MS analysis of H2B T51pBPA crosslink products. ....	75
Figure 16 : MS analysis of H2B T51pBPA crosslink products. ....	76
Figure 17 : Immunoprecipitation of H3 T80 pBPA crosslink products for MS analysis. ....	77
Figure 18 : MS analysis of H2B T80pBPA crosslink products. ....	79
Figure 19 : MS analysis of H2B T80pBPA crosslink products. ....	80
Figure 20 : Immunoprecipitation of diverse histones and crosslink products for MS analysis. ....	82
Figure 21: Molecular weight shift approach. ....	83
Figure 22 : Identification of Sth1-histone H2A crosslink products. ....	84
Figure 23 : Identification of Sth1-histone H2B crosslink products.....	85
Figure 24 : Identification of Sth1-histone H3 crosslink products.....	86
Figure 25 : Mapping the interaction surface of Sth1 on the nucleosome in vivo.....	87
Figure 26 : Crosslinking of the H3 tail to Sth1 is regulated by H3 K14ac. ....	90

Figure 27 : RSC preferentially interacts with SUMOylated H2B in vivo.....	92
Figure 28 : RSC recognizes previously SUMOylated nucleosomes. ....	94
Figure 29 : Effect of SUMOylation on GAL1 mRNA levels. ....	96
Figure 30 : Effect of the cell cycle stage on Histone-Sth1 crosslink efficiency.....	98
Figure 31 : Hst2 shows no interaction with H3S10D peptide in vitro.....	100
Figure 32 : Identification of Hst2 interaction partners and PTMs by MS analysis. ....	103
Figure 33 : Interaction of Hst2 with Mcm2 and Cdc28.....	104
Figure 34 : 14-3-3 proteins as candidates for recruiting Hst2 to H3S10ph.....	106
Figure 35 : Hst2 and Bmh1 knockout have same effect on H4K16ac.....	108
Figure 36 : Hst2 and Bmh1 interact in vivo.....	110
Figure 37 : Bmh1 interacts with Hst2 in vivo at endogenous levels only in G2/M. ....	111
Figure 38 : Wildtype Hst2 shows no interaction with Bmh1/2. ....	113
Figure 39 : Purification of singly phosphorylated Hst2 by GCE. ....	115
Figure 40 : Phosphorylation of Hst2 enhances catalytic activity and mediates interaction with Bmh1 in vitro. ....	117
Figure 41 : Genome Editing of Hst2.....	119
Figure 42 : AuroraB delta45/InBox Incenp and Ipl-1/Sli15 phosphorylate Hst2 in vitro. ....	121
Figure 43 : Modulation of RSC complex by histones and their PTMs. ....	130
Figure 44 : Model for histone tails mediated chromatin compaction. ....	134

## List of Tables

<i>Table 1 : Overview of instruments used in this study.</i>	35
<i>Table 2 : Overview of Laboratory supplies used in this study.</i>	36
<i>Table 3 : Overview of chemicals/reagents used in this study.</i>	37
<i>Table 4 : Overview of commonly used buffers and solutions.</i>	38
<i>Table 5 : Overview of media used in this study.</i>	39
<i>Table 6 : Overview of antibiotics used in growth media and agar plates.</i>	40
<i>Table 7 : Overview of enzymes used.</i>	40
<i>Table 8 : Overview of standard markers used.</i>	40
<i>Table 9 : Overview of antibodies used.</i>	41
<i>Table 10 : Overview of antibody conjugated beads used.</i>	41
<i>Table 11 : Overview of kits used.</i>	41
<i>Table 12 : Overview of peptides used for ITC.</i>	41
<i>Table 13 : Overview of softwares used.</i>	42
<i>Table 14 : Composition of Polyacrylamide Gels for SDS-PAGE.</i>	48
<i>Table 15 : Overview of E.coli strains used during this study.</i>	138
<i>Table 16 : Overview of yeast strains used during this study.</i>	138
<i>Table 17 : Overview of plasmids used in this study.</i>	139
<i>Table 18 : Overview of primers used in this study.</i>	141

## List Of Acronyms

aaRS : aminoacyl tRNA synthetase

ADP : adenosine di-phosphate

AID : auxin induced degron

AMP-PNP : adenylyl-imidodiphosphate

APEX : ascorbate peroxidase

ATP : adenosine triphosphate

BD : bromodomain

BioID : proximity-dependent biotin identification

BLI : biolayer interferometry

BSA : Bovine serum albumin

cDNA : complementary DNA

ChIP : Chromatin Immunoprecipitation

CPC : Chromosomal passenger complex

CRISPR : clustered regularly interspaced short palindromic repeats

CTD : C-terminal-domain

ddH<sub>2</sub>O : double-distilled water

DNA : deoxyribonucleic acid

dNTP : deoxynucleoside triphosphate

DSB : double-strand break

dsDNA : double-stranded DNA

DTT : dithiothreitol

E.coli : Escherichia coli

ECL : enhanced chemiluminescence

EDTA : ethylenediaminetetraacetic acid

EM : Electron Microscopy

ESI : Electrospray Ionization

FACS : fluorescence activated cell sorting

FDR : False discovery rate

FLuc : firefly luciferase

FRET : Förster/fluorescence resonance energy transfer

GCE : genetic code expansion

GFP : green fluorescent protein

gRNA : guide ribonucleic acid

HDACs : histone deacetylases

His : histidine

HPLC : High Performance Liquid Chromatography

HRP : horseradish peroxidase

iBAQ : intensity Based Absolute Quantification

IP : Immunoprecipitation

ITC : isothermal calorimetry

kan : kanamycin

KDAC : lysine deacetylases

LB : lysogeny broth

LEU : leucine

LFQ : Label-free quantification

M barkeri : Methanosarcina barkeri

M mazei : Methanosarcina mazei

M. jannaschii : Methanocaldococcus jannaschii

MOPS : 3-(N-Morpholino)propanesulfonic acid

mRNA : messenger RNA

MS : mass spectrometry

MWCO : molecular weight cut off

NAD : nicotinamide adenine dinucleotide

NES : nuclear export sequence

NTD : N-terminal domain

OD600 : optical density at 600 nm wavelength

ORF : open reading frame

PAGE : polyacrylamide gel electrophoresis

pAzF : 4-Azido-L-phenylalanine

pBPA : p-benzoyl-L-phenylalanine

PCR : Polymerase Chain Reaction

PEG : polyethylene glycol

pH : pleckstrin homology

PMSF : phenylmethanesulfonyl fluoride

PTMs : posttranslational modifications

PVDF : polyvinylidene difluoride

qPCR : quantitative Polymerase Chain Reaction

RF : release factor

rpm : revolutions per minute

RT : room temperature

*S. cerevisiae* : *Saccharomyces cerevisiae*

SDS : sodium dodecyl sulfate

SEC : size exclusion chromatography

SHL : superhelical location

SILAC : stable isotope labeling by amino acids in cell culture

SnAC : Snf2 ATP-coupling

*S. pombe* : *Schizosaccharomyces pombe*

ssDNA : single-stranded DNA

SUMO : Small Ubiquitin-like Modifier

TAD : Topologically Associated Domain

UV : ultraviolet

WT : wildtype



## ABSTRACT

How DNA, an extremely enormous blueprint of life is stored within miniscule cells has always remained enigmatic. A cell has not just to condense DNA to meet space limitations but also concurrently permit access to its information. Therefore, it has evolved highly malleable factors so as to fulfill these needs for dynamic changes of chromatin. Such factors include chromatin remodeling enzymes that use ATP hydrolysis to edit DNA-histone contacts and diverse proteins which modify histones to either alter the stability and DNA binding properties of the histones or signal the recruitment of further factors. Conceivably, the most dramatic alteration in the structure of chromatin is the formation of iconic X-shaped chromosomes which are maximally condensed in mitosis, just afore a parent cell is prepared to separate its genetic information into two daughter cells.

A key question is how these factors locate their target sites on chromatin and achieve their biological functions in complex physiological setting. A prominent hurdle in the investigation of modifications and interactions of chromatin in cellular context is their low affinity and high spatio-temporal nature. To overcome these limitations, my PhD project aimed at leveraging recent advances in genetically encoded unnatural amino acid mutagenesis. Notably, photoactivatable chemical crosslinker amino acid pBPA was efficiently introduced into cellular histones and subsequently photocrosslinking allowed ensnaring histone interaction partners. This was combined with quantitative proteomics approach to characterize the direct interactors for few histone sites. One of my research objectives was focused on the chromatin remodeller RSC complex, which is the only essential remodeler in yeast and is implicated in many DNA-related processes such as transcription, replication and DNA repair. Genetic code expansion helped reveal the interaction of the RSC ATPase subunit Sth1 to depend on H3 K14 acetylation by Gcn5. In contrast to popular belief, this modification was shown not to

recruit RSC to chromatin but mediate its interaction with neighboring nucleosomes. A preference of RSC for H2B SUMOylated nucleosomes was detected *in vivo*. Furthermore, RSC was shown not to be ejected from chromatin in mitosis, but its mode of nucleosome binding differed between interphase and mitosis. Collectively, *in vivo* studies used here showed that RSC recruitment to specific chromatin targets encompasses multiple histone modifications most probably in conjuncture with other components such as histone variants and transcription factors too. Last part of my thesis was dedicated to investigating the molecular mechanism behind the histone modification H3 S10 phosphorylation mediated chromosome compaction in mitosis. In budding yeast, mitotic chromosome compaction is licensed by the kinetochores where recruitment of Aurora Kinase B initiates a cascade of events commencing with phosphorylation of H3 S10, which eventually signals the recruitment of lysine deacetylase Hst2 and leads to the unmasking of H4 K16. The exposed H4 tails interact with the acidic patch of neighboring nucleosomes to drive short-range compaction of chromatin. Here, I demonstrated that the interaction of Hst2 with H3 S10ph is mediated by the 14-3-3 protein Bmh1. This phosphorylated Hst2-Bmh1 interaction is cell cycle dependent, reaching its maximum in M phase. I could recapitulate the binding event *in vitro* by purifying genetically encoded phosphorylated Hst2. Furthermore, I also showed that phosphorylation at C-terminal residues of Hst2 stimulates its deacetylase activity releasing a previously identified autoinhibition of the enzyme. Hence, the data presented here revealed Bmh1 as a key player in the mechanism of licensing of chromosome compaction in mitosis.

## ZUSAMMENFASSUNG

Wie DNA, der extrem große Bauplan des Lebens, in winzigen Zellen gespeichert wird ist immer noch ein ungelöstes Rätsel. Während eine Zelle ihre DNA kondensieren muss da ihr nur beschränkt Platz zur Verfügung steht, muss sie gleichzeitig auch Zugriff die Informationen ermöglichen. Daher hat es anpassungsfähige Faktoren entwickelt, um dieser Anforderungen an einer dynamischen Änderung des Chromatins zu ermöglichen. Diese Faktoren umfassen Chromatin-Remodelling-Enzyme, die mittels ATP-Hydrolyse DNA-Histon-Kontakte zu modulieren, oder verschiedene Proteine die Histone modifizieren, um deren Stabilität und DNA-Bindungseigenschaften zu verändern oder die Rekrutierung weiterer Faktoren zu signalisieren. Die vielleicht dramatischste Veränderung in der Struktur des Chromatins ist die Bildung von ikonischen X-förmigen Chromosomen, welche während der Mitose vollständig kondensiert werden. Dies erlaubt den Elternzelle ihre genetische Information in zwei Tochterzellen aufzuteilen.

Eine Schlüsselfrage ist, wie diese Faktoren ihr Ziel auf Chromatin finden und ihre biologischen Funktionen in diesem komplexen physiologischen Umfeld ausüben. Eine große Hürde für das Verständnis der Wechselwirkungen von Modifikationen und Chromatin im zellulären Kontext ist die geringe Affinität und hohe räumlich-zeitliche Natur dieser. Um diese Einschränkungen zu überwinden nutzte in meiner Promotion die jüngsten Fortschritte in der Codierung von unnatürlicher Aminosäure. Insbesondere wurde die photoaktivierbare, chemische reaktiven, pBPA wurde effizient in zelluläre Histone eingeführt, mit welchem Histon-Interaktionspartner kovalent gebunden werden konnten. Dieser ansatz wurde mit quantitativer Massenspektrometrie kombiniert um die direkten Integratoren für einige Histon positionen zu identifizieren. Eines meiner Ziele war der Chromatin-Remodeller-RSC-Komplex (Remodels the Structure of Chromatin), welcher ein wesentliche Remodeler in Hefen ist und an vielen Prozessen wie Transkription, Replikation und DNA-Reparatur beteiligt ist. Durch in-vivo-

Photovernetzung konnte ich neue Einblicke in die Wechselwirkung des RSC-Komplexes mit dem Nukleosom in seiner physiologischen Umgebung gewinnen. Diese zeigte das H3-K14-Acetylierung durch Gcn5 notwendig ist für die Interaktion der RSC ATPase-Untereinheit Sth1 mit Nukleosomen. Hierbei wird der RSC Komplex nicht zu Nukleosomen rekrutiert welche die Modifikation tragen, sondern deren Nachbar Nukleosomen. Zudem wurde *in vivo* eine Präferenz von RSC für H2B-SUMOylierte Nukleosomen beobachtet. Darüber hinaus wurde gezeigt, dass RSC während der Mitose nicht aus dem Chromatin entfernt wird, sondern dass sich die Nukleosomenbindung zwischen Interphase und Mitose unterscheidet. Zusammengefasst zeigen meine *In-vivo*-Studien, dass die RSC-Rekrutierung für bestimmte Chromatin-Ziele abhängig von mehreren Histonmodifikationen ist, welche höchstwahrscheinlich in Kombination mit anderen Komponenten wie Histonvarianten und Transkriptionsfaktoren auftreten. Der letzte Teil meiner Arbeit untersuchte den molekularen Mechanismus hinter der durch die Histonmodifikation H3 S10-Phosphorylierung verursachten Chromosomenverdichtung während der Mitose. In Hefe wird die mitotische Chromosomenverdichtung von Kinetochoren lizenziert. Die Rekrutierung von Aurora Kinase B löst eine Kaskade von Ereignissen aus beginnend mit Phosphorylierung von H3 S10, was die Rekrutierung der Lysin-deacetylase Hst2 und die Entfernung von H4 K16ac signalisiert. Die nicht modifizierten H4-Arme interagieren mit der sauren Bindetasche auf dem benachbarten Nukleosomen, um die kurzreichweitige Verdichtung von Chromatin voranzutreiben. Hier haben wir gezeigt, dass die Interaktion von phosphorylierten Hst2 mit H3 S10ph durch das 14-3-3-Protein Bmh1 vermittelt wird. Die Hst2-Bmh1-Interaktion ist zellzyklusabhängig und erreicht in der M-Phase ihr Maximum. Wir haben genetisch phosphoryliertes Hst2 gereinigt und gezeigt, dass die Phosphorylierung an C-terminalen Resten von Hst2 dessen Deacetylaseaktivität stimuliert. Daher identifizierten die hier präsentierten Daten Bmh1 als einen Schlüsselakteur im Mechanismus der Lizenzierung der Chromosomenverdichtung während der Mitose.

# INTRODUCTION

## 1.1 CHROMATIN ARCHITECTURE AND FUNCTION

### 1.1.1 DNA AS THE STOREHOUSE OF GENETIC INFORMATION

Deoxyribonucleic acid, or DNA, is a molecule that functions as the universal carrier of genetic instructions. Its inheritance and alterations through years of evolution have led to the plethora of lifeforms on earth today. Its discovery dates back to 1869, when Friedrich Miescher fortuitously discovered what he called "nuclein" in the nuclei of human white blood cells, which we now call as deoxyribonucleic acid (DNA)<sup>1</sup>. This landmark discovery unlocked doors to understanding of possibly the most complicated and vital biomolecule.

Experiments carried out by Oswald T. Avery and colleagues in 1944 recognized DNA as the carrier of genetic information<sup>2</sup>. Later, works of James Watson and Francis Crick on pre-existing X-ray crystallography data from Rosalind Franklin molded the basis of structure of DNA<sup>3</sup>.

Essentially, DNA is a polynucleotide composed of multiple monomers called nucleotides. Each nucleotide contains a phosphate group, a sugar called deoxyribose, and one of the four nitrogen-containing nucleobases, namely, cytosine (C), guanine (G), adenine (A), or thymine (T). The phosphate group and deoxyribose form the backbone of the DNA molecule, in which they are covalently linked through 3', 5' - phosphodiester bonds. Usually, a single string of such polynucleotides is called a single-stranded DNA (ssDNA) and two of them coalesce to shape the DNA double helix.

The human genome consists of approximately  $3.2 \times 10^9$  nucleotides distributed over 46 different chromosomes. While on one hand, each base pair is on an average 0.34 nm long, if the entire DNA were to be stretched from end to end it would be 2

m in length. On the other hand, the average eukaryotic cell size is only about 2-10  $\mu\text{m}$  in diameter. Despite of this space constraint, an extremely long DNA molecule is somehow encased in numerous hierarchical layers to be able to fit inside a miniscule cell (Figure 1).

Two conflicting themes arise in this mode of chromatin organization. Even though proper packaging of DNA within cells is essential, such dense packaging can constrain the accessibility of the underlying DNA. To meet this need, chromatin has evolved exceedingly malleable elements which have the capability to manoeuvre the underlying genetic information.

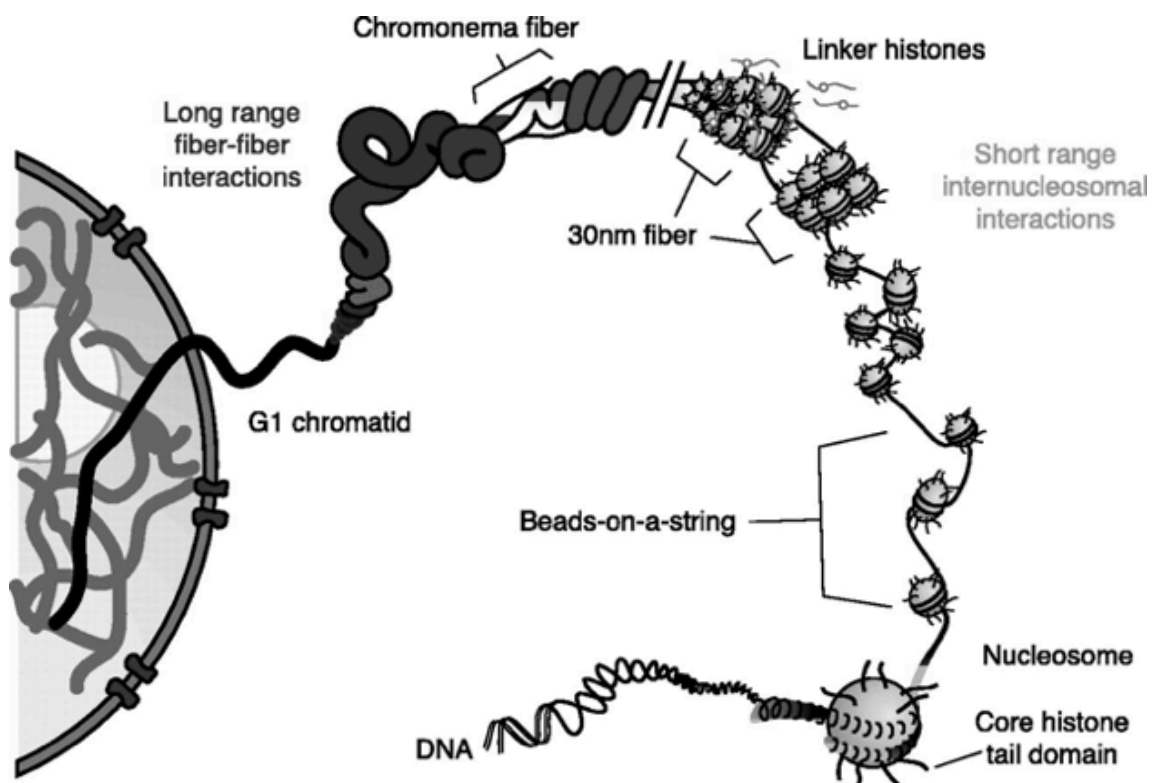


Figure 1: Schematic illustration of packaging of DNA into higher-order structures in a cell.

(From Horn and Peterson, 2002<sup>4</sup>).

## 1.1.2 HISTONES AND NUCLEOSOMES

In eukaryotes, fundamental level of compaction of DNA commences by packaging of 147 base pairs of DNA double helix 1.67 times around the so called histone proteins in a structure called nucleosome<sup>5,6</sup>(Figure 2A,B). 10 base pairs contribute to one superhelical turn of DNA such that each nucleosome is created of 15 such turns. These DNA locations are termed as superhelical locations (SHL) such that SHL0 or nucleosomal dyad is at the centre of the nucleosome and moving on either side one superhelical turn would bring to the similar location on the symmetrical halves of the nucleosome.

Each nucleosome is composed of an 'octamer' of two copies each of highly conserved histones H2A, H2B, H3 and H4. Histones were discovered by Albrecht Kossel in 1884, they are small proteins (~100-140 amino acids) and are significantly basic in nature at physiological pH of 7-8. Owing to their enormous proportion of positively charged lysine and arginine residues, they are able to counteract the negative charge of DNA<sup>6,7</sup>.

Structurally, all histones share a 'histone fold' formed of three alpha helices linked by two loop domains<sup>8</sup>(Figure 2). It is this helical arrangement which permits for interaction between H2A/H2B and H3/H4 histone dimers, precisely in a head-tail fashion, also called the 'handshake motif'. Surplus interactions encompass the four-helix bundle interactions which hitch the rest of the histone heterodimers collectively<sup>9,8</sup>(Figure 2D).

Other than the structured histone fold domains, the rest of the histone protein comprises of unstructured N-terminal (H2A, H2B, H3 and H4) and C-terminal (H2B) tails (Figure 2C). Contrary to original beliefs that DNA completely wraps histones, significant portion of histones protrude outside of the confined nucleosome core in the form

of these flexible tails and are largely more accessible, e.g. to proteases like trypsin, than the histone fold domains<sup>10</sup> and to numerous other regulatory classes of enzymes.

In *S. cerevisiae*, two copies each of the core histone genes exist<sup>11</sup>. Although the genes encoding the major histones are essential for viability, deletion strains with either one gene set are still feasible<sup>12</sup>. Expression of the histone genes is associated to cell cycle, following DNA replication in S phase of the cell cycle<sup>13</sup>, histones are placed on both branches of the replication fork. These genes share broad sequence similarities and are expressed throughout the S phase of the cell cycle. For each type of histone except H4, another class of histones called histone variants have arisen. These variants include H2A.X, H2A.Z, Macro-H2A, H2A.B, H3.3, and also the linker histones H1. These have specific expression, localization and species-distribution patterns and often confer distinctive structural and functional features. For example, H2A.Z has an extended acidic patch, which can modify action of interacting proteins such as that of ATP-dependent chromatin remodelers<sup>14,15</sup>. Crosstalk between variants and post translational modifications further magnifies the control of histones over chromatin landscape. Such as, a recent report of acetylation of H2A.Z histones to regulate RNA transcription in African trypanosomes<sup>16</sup>. The positioning of the linker histone on the nucleosome has been known to effect the packaging of chromatin<sup>17</sup>.

The regional incorporation of an extensive assortment of posttranslational histone marks and histone variants renders every nucleosome exclusive and provides them the potential to control key processes. Considering their critical functions, mutation(s) or the deregulation of histones or their variants have been shown to drive tumor initiations and developments in a multitude of cancers<sup>18,19</sup>.

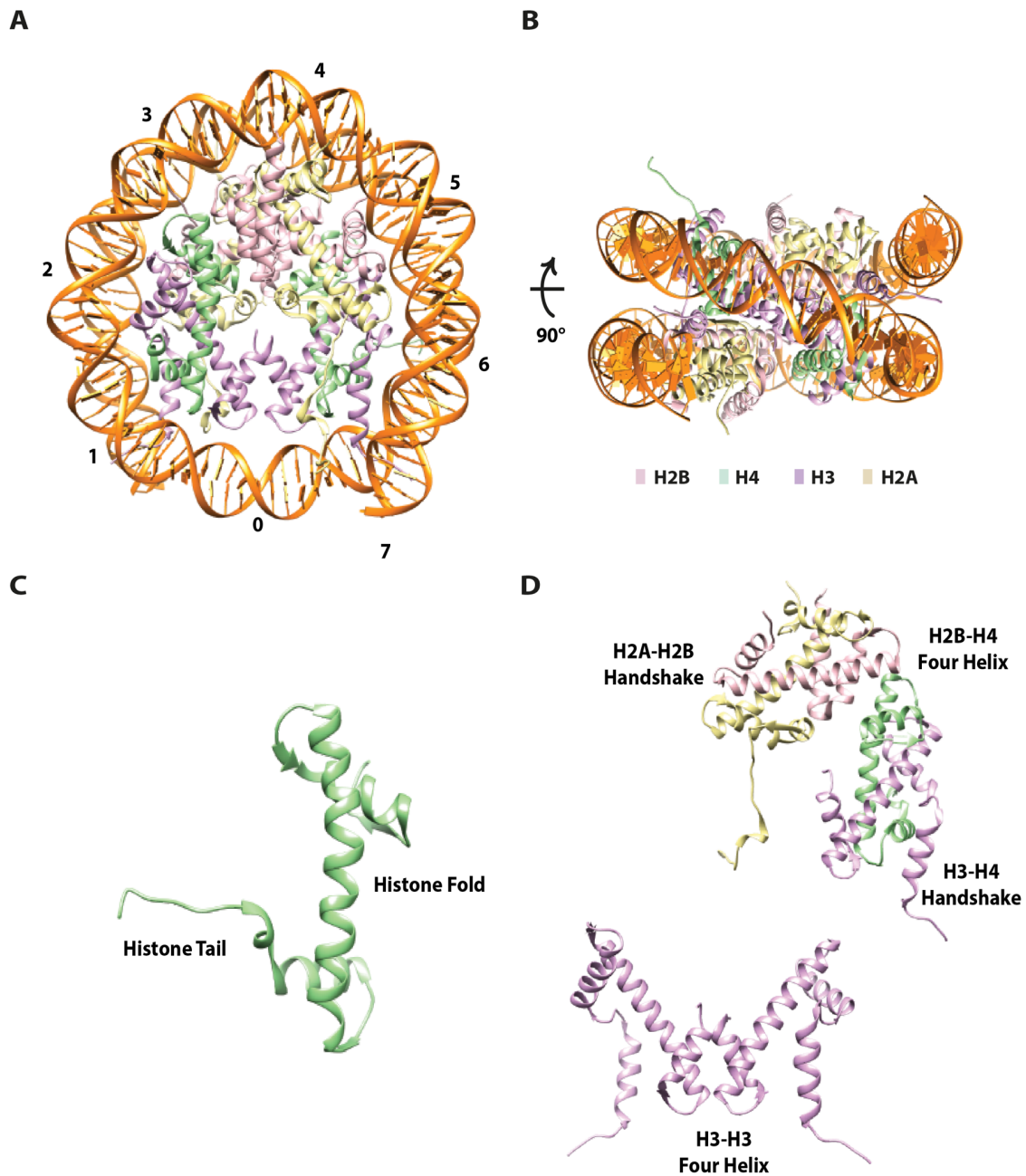


**Figure 2 : Structure of Nucleosome.**

(A), (B) Crystal structure of the nucleosome at 3.1 Å resolution (pdb 11D3). Numbers indicate SHL positions. (C) Common structural features of histones include core fold domains and unstructured tail domains. (D) Handshake interactions hold histones together, and four-helix bundle interactions hold histone heterodimers together. (Figure prepared using pdb file 11D3 in Chimera software).

### 1.1.3 POST TRANSLATIONAL MODIFICATIONS ON HISTONES

Histones harbor additional chemical groups called posttranslational modifications (PTMs) which greatly augment their regulatory potential. These PTMs are primarily enhanced at the protruding N or C terminal tails but can also occur on the solvent-exposed parts of their nucleosome core regions<sup>20,21</sup>(Figure 3). Addition of these groups can have a myriad of effects on the nucleosomes : amending the net charge of histones, modifying inter-nucleosomal interactions, acting as 'flagposts' facilitating the recruitment and or interaction of exclusive proteins or enzymes, aiding in DNA unwrapping and rewrapping in a procedure called 'DNA breathing'<sup>22,23,22</sup>.

PTMs are highly varied in nature. They can be small, neutral functional groups such as methyl-, acetyl- or charged moieties like phosphate, ADP-ribose. They can also be small proteins such as Ubiquitin or SUMO (Small Ubiquitin-like Modifier). Most of these modifications are amino acid in particular. Acetylation and Ubiquitination mainly occur at lysine, methylation at arginine and lysine, phosphorylation is of serine and threonine, ADP-ribosylation of glutamate and SUMOylation of lysine. Conventionally, PTMs have been identified by Edman degradation, amino acid analysis, isotopic labeling and identified and quantified by western blots and Chromatin immunoprecipitation. More recently, many histone PTMs have been determined by the advancement of mass spectrometric techniques. The presence of covalent modifications in proteins alters the molecular weight, and this mass increment or deficit can be detected by MS <sup>16,25</sup>. With the discovery of acyl chains, such as propionylation and butyrylation<sup>26</sup>, crotonylation<sup>27</sup>, succinylation<sup>20</sup>, malonylation<sup>29</sup>, 2-hydroxyisobutyrylation<sup>30</sup>, and glutarylation<sup>31</sup>, the landscape of lysine modifications has significantly extended.

PTMs are introduced in a very synchronized fashion in response to external or internal cues by particular writer proteins and are read by specific enzymes<sup>32</sup> with their specific

domains such as bromo-domains for the recognition of acetylated<sup>33</sup> or chromo-domains for methylated lysine<sup>34</sup>. Most of the PTMs are small excluding addition of ubiquitin and SUMO which outcome in large covalent changes. Both these modifications are deposited by a dedicated set of enzymes: E1-activating, E2-conjugating and E3-ligating enzymes<sup>35</sup>. Many PTMs can be erased and are therefore revocable such as acetylation which is consigned by the activity of HATs (histone acetyl transferases)<sup>36</sup> and can be erased by HDACs (histone deacetylases)<sup>37,38</sup>.

Most of the PTMs act individually or in combination accumulating at defined regions of the genome, forming active or repressed states. For example, H3K4Me3, H3K9Ac and general H4Ac are associated with active states<sup>39</sup> whereas H3K9Me3 and H3K27Me3 with repressed states<sup>40</sup>. Addition of acetylation of lysine residues generally masks the positive charge, this reduction in charge results in weakening of histone-DNA interaction and consequently leads to more open accessible chromatin. Moreover, additional negative charges such as phosphorylation of serine can destabilize histone-DNA interactions. Most of the histone PTMs show extensive cross talk<sup>41</sup>. For example, a signaling cascade that initiates by phosphorylation of H3 T3 by Haspin Kinase leads to recruitment of CPC, and phosphorylation of S10 by Aurora B. This signal is then translated in recruiting a Sirtuin, Hst2 which detaches acetyl group from K16 on H4 tails. This unmasking of positive charge leads to interaction of H4 tail with neighboring H2A-H2B acidic patch and plays a central role in the development of higher-order chromatin structures in mitosis.

The extent of PTM varies strongly depending upon, for example, the kind of modification, the sequence and structure of the protein and the physiological state of the cell<sup>42</sup>. Mostly, only a small fraction of the target protein is modified<sup>43</sup>. PTMs are also transient in nature, with turnover rates varying depending on the kind of modification: days for lysine methylation and minutes for lysine acetylation. The use of activated

precursor molecules such as ATP, acetyl-CoA and NAD<sup>+</sup> as co-substrates also couples numerous modification reactions to metabolism.

Patterns of PTMs are frequently named 'Histone code' or epigenetic signature<sup>44</sup>. Most of the PTMs are also extremely conserved. Dysregulation of histone PTMs can lead to dramatic changes in chromosomal processes. It can shift gene expression that are frequently observed in human cancers<sup>45,46</sup> and mutations have also been associated with neurological, developmental and autoimmune disorders.

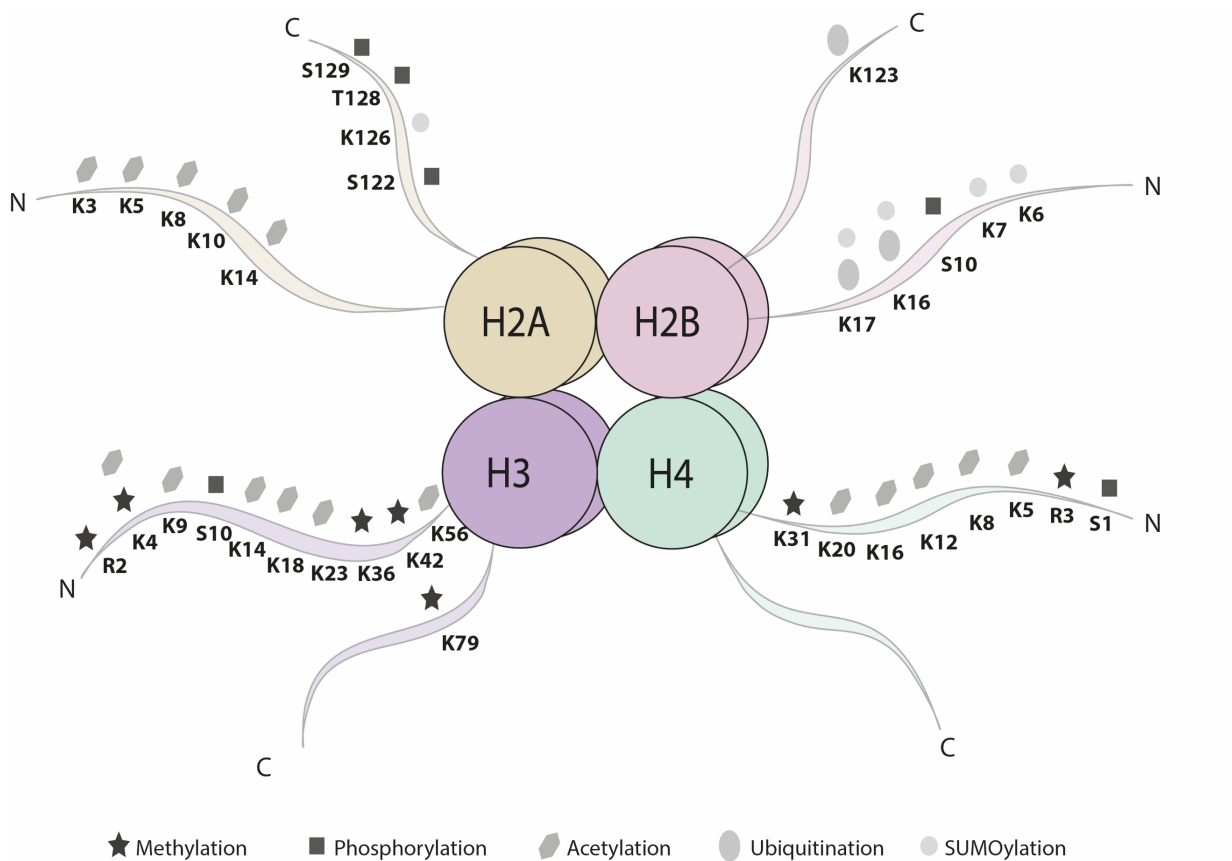


**Figure 3 : Schematic illustration of Post translational modifications on Histones.**

Schematic representation of the histone octamer core with protruding N-terminal tails and C-terminal parts. For H2A, other than K8 acetylation rest all the modifications are on histone variant, H2A.Z.(Figure prepared from Rando and Winston, 2012<sup>47</sup>).

## 1.2 READERS, WRITERS AND ERASERS OF HISTONE PTMS

Many proteins involved in PTM decoding are modularly organized, including combinations of Writer, Reader and Eraser domains. These help chromatin to meet with challenges of accessibility in addition to storage. Some modifying enzymes and proteins identifying histone modifications occur in multi-subunit protein complexes, linked to chromatin remodeling.

### 1.2.1 ATP DEPENDENT CHROMATIN REMODELERS

One of the chief classes of epigenetic readers are ATP-dependent chromatin remodelers. They utilize energy derived from ATP hydrolysis to stimulate DNA deformation which can propagate throughout the nucleosome by sliding, ejecting, relocating or replacing nucleosomes<sup>48</sup>. They distinguish PTMs on histones via specialized domains such as bromodomain, chromodomain and ultimately regulate the fate of those nucleosomes. Eukaryotes have four different families of chromatin remodeling complexes: switch/sucrose non-fermentable (SWI/SNF), imitation switch (ISWI), Inositol 80 (INO80) and chromodomain helicase DNA-binding (CHD)<sup>49,50</sup>. Although they share a similar ATPase domain and unifyingly bind the nucleosome two turns away from the dyad, they vary in their mechanism of action probably due to differences in their subunit compositions and targeting mechanisms to the nucleosomes. It is intriguing how cells have evolved these diverse remodelers to carry out complex chromosomal processes with their unique among overlapping functions. For example, ISWI and CHD subfamily of remodelers reign deposition of histones, the maturation of nucleosomes and their regular spacing, SWI/SNF subfamily remodelers primarily modify chromatin by repositioning nucleosomes, ejecting octamers or evicting histone dimers. Remodelers of the INO80 subfamily alter nucleosome composition by substituting canonical with variant histones. Deletion of most of the subunits lead to varieties of cellular defects primarily involving rupture of chromatin processes such as transcription, replication and repair. It is no surprise that defects in several remodeler subunits show utmost

appearance in diseases like cancers and developmental disorders. Therefore, a great amount of effort is required to understand these complexes and their mechanisms. Recently, a surge of high-resolution structural studies on several remodelling complexes have only commenced to shed light on their interaction with nucleosomes and hint towards their mechanism of action<sup>51</sup>.

### 1.2.2 ROLES OF RSC COMPLEX IN CHROMATIN DYNAMICS

The RSC (Remodels the Structure of Chromatin) complex is comprised of 15 subunits including the ATP-dependent catalytic subunit, Sth1, and was first identified based on the homology of Sth1 to Swi2/Snf2<sup>52</sup>. RSC is imperative for yeast survival and is 10 times more abundant than SWI/SNF<sup>1,53</sup>. Loss of function mutants in the core components of the RSC complex cause cell cycle arrest in G2/M<sup>52</sup>. RSC exists as two distinct isoforms that share core subunits including the ATPase subunit Nps1/Sth1 but contain either Rsc1 or Rsc2.

Nucleosomes mostly impede access to DNA. Global mapping of nucleosome positioning have revealed insights into promoter architecture, such that a so called '+1 nucleosome' is positioned at a relatively fixed distance from the transcription start site (TSS) and the positioning of the pre-initiation complex<sup>54,55</sup>. Immediately upstream of the +1 nucleosome is a Nucleosome Depleted/Free Region (NDR/NFR) and it is followed by an array of constant-spaced nucleosomes throughout the gene body. RSC complex plays pivotal roles in governing nucleosome positioning and in turn DNA template related processes such as transcription and replication. For instance, RSC counteracts encroachment from flanking nucleosomes and facilitates the binding of Gal4 to the *UASg* regulating GAL1 transcription levels<sup>56</sup>. It is required globally for RNA polymerase II transcription specifically during acute stress<sup>57,58,59</sup>. It retains transcription start site choice and transcription initiation<sup>60</sup>. RSC is enriched at the promoters of genes encoding histones, RNA polymerase III, small nucleolar RNAs, and mitochondrial proteins, apart from genes whose products are involved in nonfermentable carbon

metabolism, the nitrogen discrimination pathway and two major classes of stress response genes, TOR-regulated genes and cell wall integrity genes<sup>61</sup>. Recruitment of RSC to particular promoters can lead to either repression or activation of transcription by creating NFR. RSC enhances Cohesin loading onto DNA, thus being part of another important process of chromatin architecture<sup>62</sup>. *In vitro*, RSC is directly and specifically essential, and in few cases even sufficient, to set up nucleosome positioning<sup>63</sup>.

Additional roles of RSC include double-strand break (DSB) repair, specifically by homologous recombination (HR)<sup>64</sup>, preventing segregation defects<sup>65</sup>, maintaining ploidy by promoting spindle pole body insertion<sup>66</sup>.

### 1.2.3 STRUCTURAL INSIGHTS INTO THE FUNCTION OF RSC COMPLEX

Recently, single particle Cryo-EM studies have revealed high resolution structural information of RSC complex in association with nucleosome (Figure 4)<sup>67,68,69</sup>. It is partitioned into five protein modules: The core body module which operates as a scaffold for the rest of the flexible modules designated as: DNA-interacting, ATPase, arm and actin-related protein (ARP) modules. The DNA-interacting module binds extra-nucleosomal DNA and is involved in the detection of promoter DNA elements that impact RSC functionality<sup>70</sup>. The ATPase and arm modules sandwich the nucleosome disc with the Snf2 ATP-coupling (SnAC) domain and the finger helix, respectively and aid in nucleosome selection. For example, Sth1 interacts with the N-terminal H4 tail which is heavily acetylated. One of the lobes of the ATPase module engages with the edge of the nucleosome at SHL+2 and the other around SHL -6, towards which the N-terminal tail of histone H3 protrudes. Based on the directionality of translocation<sup>71</sup> it has been recommended that the ATPase domain passages DNA in small step size, one bp at a time into the direction of dyad across the entire nucleosome<sup>72,73</sup>. This expedites access to promoter DNA. Sfh1 subunit of the arm module with its very conserved four arginine residues in the finger helix (R397, R400, R401 and R404) interacts with the acidic patch of which three residues are identified to be frequently mutated

in cancers. The arm module of Sfh1 could mediate interaction with H2A.Z nucleosomes which have a more prominent acidic patch and consequently might explain their penchant for H2A.Z containing nucleosomes<sup>15</sup>. The arm–octamer interaction may also elucidate why ubiquitination of histone H2B counteracts RSC function<sup>74</sup>. The ubiquitin moiety is linked to H2B residue K123 and, while flexible, can assume a position that sterically interferes with the arm–octamer interaction. The ARP module couples RSC ATPase activity to DNA translocation and controls the remodeling activity. Fluctuations in mobility of ARP modules are probably transmitted through the hinge which is between the HSA and lobe1 region of the ATPase domain and thereby impacts its translocation ability which also sheds light on how regulation of remodeling mechanism is a key feature of ARPs<sup>75</sup>.

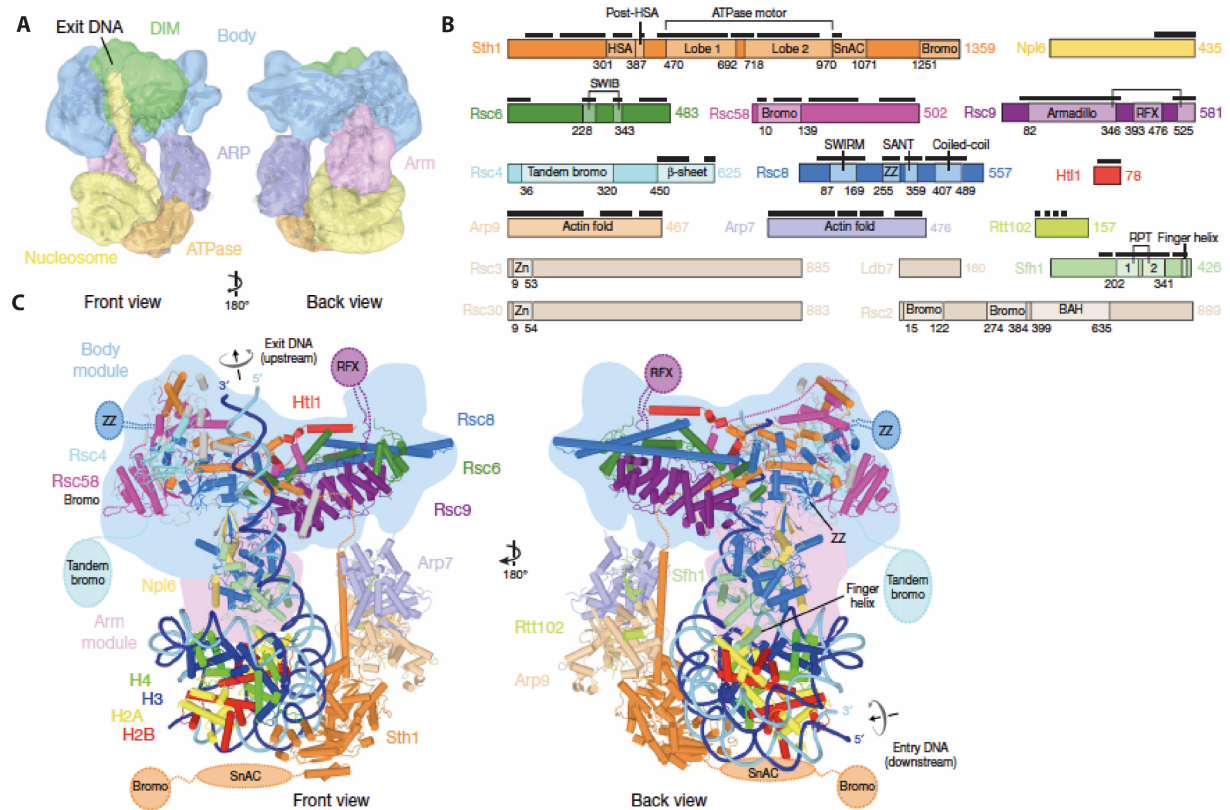


**Figure 4 : RSC–nucleosome complex structure.**

(A) Low pass filter maps showing two views of RSC-nucleosome structure with the overall cryo-EM architecture. (B) Domain architecture of various RSC subunits. (C) Cartoon representation of two views of the RSC nucleosome structure. (Figure from Wagner et.al, 2020<sup>69</sup>)

### 1.2.4 WHAT REGULATES THE RSC COMPLEX?

As described in the previous section, the structure of RSC complex has established a charter for improved understanding of this complex as well its human homologs, BAF/PBAF complexes which are most commonly dysregulated in cancers<sup>76–78</sup>. Nonetheless, because of the flexible tethering of its distinctive domains, their structure, substrate inclination, and interaction with the nucleosome remains essentially undetermined. , the regional assimilation of an extensive assortment of posttranslational histone marks and histone variants renders each nucleosome unique, in this case how does RSC unambiguously distinguish its unique substrate in the face of all other nucleosomes? What are its target sites on genomic loci? What is its particular binding mechanism to its substrate and how is it regulated in terms of changes to cell cycle,

or environmental stimuli such as stress? Further studies are necessary to evaluate these mechanisms.

Lately solved structure of nucleosome-bound human BAF complex disclosed similar nucleosome-binding mode as nucleosome-bound RSC in addition to considerable differences<sup>79</sup>. The fact that BAF complexes are extremely critical in human health, additionally reinforces the case that the RSC complex, the only essential remodeler in yeast, is a strong model system to study the mechanisms through which the activities of remodeler-nucleosome substrate are modulated. A major portion of my thesis is devoted to address some of the questions poised above.

## 1.3 CHROMOSOME CONDENSATION

Perhaps the most dramatic transition in architecture of chromatin is its condensation into chromosomes. This averts the formation of entanglements of chromosome arms throughout the separation of sister chromatids which safeguards faithful segregation of genome from one generation to the next. Instead, chromosome condensation of arms transforms them into compact rigid rod like structures which have extremely low likelihood of getting stuck at the spindle midzone during anaphase. Errors in condensation can cause entanglements which can shape bridges or lead to breakage in chromosomes and ultimately damage to portions of the genome for one of the two daughter cells often labelled as aneuploidy. This condition over consecutive rounds of cell divisions can give rise to cancers. The manner of condensation is vastly conserved among metazoans but the underlying molecular mechanisms that orchestrate this event remain elusive.

### 1.3.1 HIGHER-ORDER ORGANIZATION OF MITOTIC CHROMOSOMES BY CONDENSINS

Chromatin organization varies dramatically throughout cell cycle<sup>1</sup>. Whilst in interphase chromatin is structured into compartments and Topologically Associated Domains (TADs), that are assumed to relate to DNA loops<sup>81,82,83,84</sup>, in Metaphase this spatial organization is entirely vanished, creating loss of boundaries, obstruction of transcription and large-scale compaction which is attained through assembling of chromatin into an array of compressed chromatin loops. These dissimilar degrees of chromatin organization are attributed largely to the Structural Maintenance of Chromosomes or SMC Complexes. Actually, evidences had emerged as early as in late 70s and 80s where electron-microscopic images of histone depleted chromosomes revealed extended DNA "halos" connected to a central, linear protein core that still resembled a native mitotic chromosome. Topoisomerase II<sup>85,86</sup> and condensin<sup>87,88</sup> were identified as the key constituents of this scaffold fraction leading to the hypothesis that

condensation of chromosomes in mitosis is propelled by action of these proteins. Condensins were first shown to be necessary for chromosome condensation *in vitro* in *Xenopus* egg extracts<sup>89</sup>. From a structural point of view, eukaryotic condensin is a pentameric protein complex, fairly resembling a semi-closed ring in electron microscopy images. Indeed, the two coiled-coil SMC (Structure of Mitotic Chromatin; Smc2 and Smc4) subunits of condensin turn back onto themselves to interact with other so-called non-kleisin subunits (Brn1, Ycg1 and Ycs4) to close the ring. Recently, structural studies have delineated how condensins use ATP hydrolysis to extrude loops of DNA<sup>90,91,92,93</sup>. This has been further reinforced by real time visualizations of ATP dependent loop extrusions and compaction by yeast in addition to human condensins<sup>94,95</sup>. How loop extrusion enterprises compaction remains largely unidentified. Condensins achieve chromosomal compaction using a mixture of looping structures<sup>96</sup>. Recently, Golfier and colleagues have expanded on the use *Xenopus* egg extracts to reconstruct and image loop extrusion of single DNA molecules during the cell cycle. Their results show that condensin extrudes asymmetric loops in metaphase, whereas cohesin extrudes symmetric loops in interphase<sup>97</sup>. Valuable cell biological information emanated from considering the localization of condensins during the cell cycle, as in budding yeast, condensins localize exclusively to the nucleus. Conversely, condensation does not take place until a very definite time in mitosis, thus what factors synchronize the action of condensins on DNA? Crosstalk from PTMs on condensins or its interactions with certain mitotic factors could synchronize this. Moreover, activity of Aurora B kinase might be important. In budding yeast Aurora B (Ipl1) activity directly regulates H3 S10 phosphorylation. Cells depleted of Ipl1 show defective compaction in rDNA locus<sup>98,99</sup>.

### 1.3.2 NUCLEOSOME-NUCLEOSOME INTERACTIONS IN CHROMOSOME COMPACT- TION

Although condensins are critical for upholding the architecture of chromosomes, their depletion has no dramatic effect on global chromatin compaction<sup>100,101</sup>. This indicates roles of additional factors in compaction. Indeed, is the nature of chromatin itself capable of driving compaction? Nucleosomes are the obvious distinctive feature of chromatin as compared to a naked piece of DNA. They predominantly prevent transcription but also contribute to compaction in certain ways. Presence of linker histones have shown to modulate chromatin structure by increasing linker length *in vivo* and stabilizing 30nm fibers *in vitro*<sup>102</sup>. Histone PTMs are known to affect chromatin structure either by altering the physico-chemical properties of the nucleosome or by aiding as attachment sites for regulatory proteins<sup>103</sup>.

Histone methylation has been shown to form repressive domains which likely influence chromatin structure and form heterochromatin regions. These in turn recruit heterochromatin and Polycomb group proteins which are lately thought to contribute to liquid–liquid phase separation<sup>104,105</sup>, although it is not known whether this directly encompasses modulating intranucleosomal interactions.

*In vitro*, acetylation inhibits the folding of the nucleosome array<sup>106</sup>, in fact acetylation at H4 K16 alone is adequate to do so<sup>107</sup>. Many solved crystal structures, involving that of a tetranucleosome array, underline the significance of interactions between the positively charged H4 tail of one nucleosome, and the negatively charged H2A acidic patch of another nucleosome<sup>9,108</sup>. *In vivo*, elevated histone acetylation levels mark open chromatin in interphase, increasing accessibility and reducing nucleosome clustering<sup>109,110</sup>. Most histone PTMs fluctuate precisely with cell cycle<sup>111</sup>. H4 K16 acetylation mark peaks during S phase and is completely reduced during G2/M phase of mitosis<sup>112</sup>. The modifications that surge throughout mitosis are particularly histone

phosphorylation's, including H3 T3 and H3 S10. These modifications are deposited by mitotic specific kinases such as the Haspin kinase for T3 and the Aurora Kinase B as part of the Chromosomal Passenger Complex (CPC)<sup>113,114</sup>. Intricate feedback mechanisms between these kinases confirm each other's presence, especially at mitotic centromeres<sup>115</sup>. Commencing at kinetochores, Aurora B mediated H3 S10 phosphorylation has been shown to impose compaction via two pathways : one comprising shugoshin and the other lysine deacetylase Hst2<sup>116,117</sup>. While shugoshin perhaps controls compaction by regulating condensin<sup>118,119</sup>. The role of Hst2 is to remove acetyl groups from H4 K16 which exposes the positive charge on lysine and thus facilitate interaction of the H4 tail with the acidic patch of neighboring nucleosomes<sup>117</sup>. This short range compaction propelled by histone phosphorylation and is a condensin independent process (Figure 5)<sup>120,121</sup>. Part of my thesis involved dissecting the molecular mechanisms by which Hst2 is recruited to the H3 S10 phosphorylation in mitosis to induce internucleosomal compaction and thereby regulate chromatin landscape.

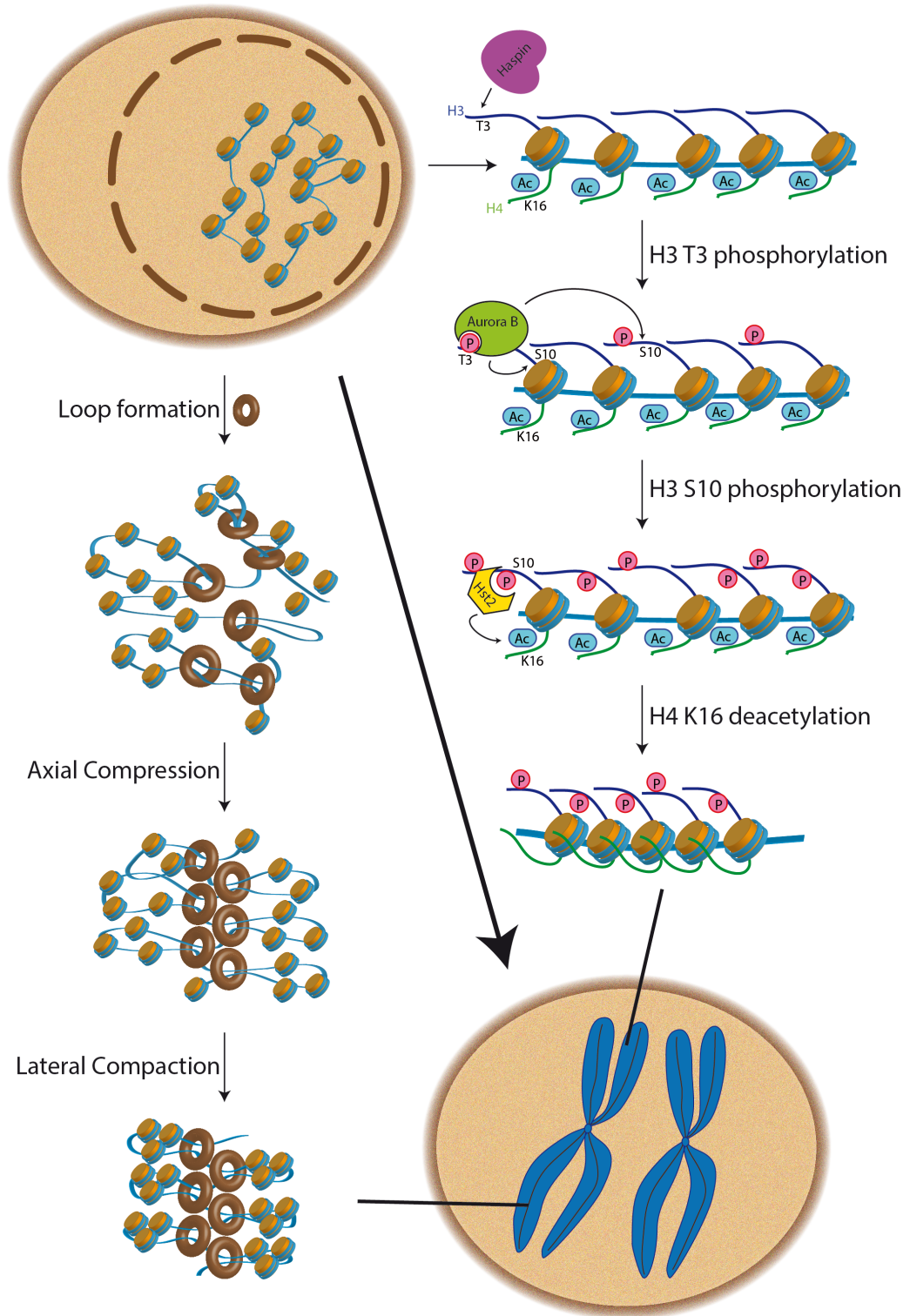


**Figure 5 : Complementary pathways of chromosome condensation in eukaryotic cells.**

Condensin-driven condensation (left) leads to loop formation, which are subsequently compacted in axial and lateral direction. Histone tails driven internucleosomal interactions lead to local chromatin compaction in Mitosis (right) (Figure from Antonin and Neumann<sup>121</sup>).

### 1.3.3 OTHER FACTORS REGULATING CHROMOSOME CONDENSATION

Chromosomes can still condense in circumstances where H3 S10ph is abolished or condensin activity is prohibited. This has fueled investigations of additional factors which regulate chromosome condensation. For example, the chromokinesin KIF4, which when codepleted with condensins causes loss of chromosome morphology<sup>101</sup>. Condensins demand other factors like Repo-Man–PP1 in the regulation of chromosome architecture during mitosis in addition to cooperation with factors such as Ki-67, a protein localizing to and establishing the periphery of mitotic chromosomes, averting clumping of individual chromosomes in the center of the metaphase plate<sup>122,123</sup>. Proteomic analysis have disclosed novel promising candidates of condensation<sup>124</sup>. A microscopy-based screen in fission yeast *S. pombe* led to the identification of probable factors involved in the condensation process<sup>125</sup>.

The sections above emphasize the giant steps that were employed to understand the process of condensation. Nonetheless, the accurate molecular mechanisms that orchestrate this cardinal process remain still unresolved.

### 1.4 GENETIC CODE EXPANSION AS A TOOLKIT FOR PROBING PROTEIN INTERACTIONS AND FUNCTIONS

Genetic information stored within DNA is transcribed into RNA which is ultimately translated in the form of 20 canonical amino acids into proteins. This passage of information is denoted to as the central dogma of molecular biology. Associations between proteins both in time and space shape each and every process that proceeds within a cell. Therefore, it is crucial to recognize them in their native context. Normally the 20 canonical amino acids determine the structural and functional fate of every protein. However, Genetic code expansion (GCE) allows the incorporation of unnatural amino acids into a protein of interest and permits repurposing of biological systems already found in nature. This equips proteins with multifarious structural and functional

properties and paves way for new means to address biological questions<sup>126,127</sup>. In my PhD, I want to leverage some of the tools of GCE to mechanistic and molecular details of processes pertaining to chromatin. My aims are to genetically encode and incorporate unnatural crosslinker amino acid 4-Benzoyl-L-phenylalanine (pBPA) into histone proteins in an effective manner to site-specifically investigate protein-protein interactions within the chromatin landscape of living yeast. With a combination of *in vivo* crosslinking, immunoprecipitation and mass spectrometry-based approach, I want to further quantitatively establish the local composition of trapped interactors to chromatin. Using the same approach, I want to dissect the mechanism of interaction between the chromatin remodeler RSC and the nucleosome. This will accelerate characterization of previously unknown modes of regulation of chromatin reader proteins. Lastly, I aim to employ the potential of GCE to mimic PTMs on a particular eraser protein called Hst2 to aid in discerning its mechanisms of action on chromatin compaction. In the following section, I discuss some of the necessities, usage and potentials of GCE.

### 1.4.1 PRINCIPLES OF GENETIC CODE EXPANSION

A cell employs only 61 of its possible 64 codons to direct the synthesis of 20 canonical amino acids into all proteins. The remaining three codons amber (UAG), Opal (UGA) and ochre (UAA) are used for termination of translation, and hence also known as 'stop' codons. GCE is founded on the idea of utilizing this degeneracy of the genetic code to unleash the full power of amino acid diversities. With the exception for amino acids such as selenocysteine and pyrrolysine the code is recited by an evolutionarily conserved protein biosynthesis machinery<sup>128</sup>. This system comprises of an aminoacyl-tRNA synthetase (aaRS), which aminoacylates its cognate tRNA with a particular amino acid. The aminoacylated tRNA is decoded on the ribosome in retort to a cognate codon in the mRNA during translational elongation, controlling to the addition of an amino acid into the protein polymer.

So as to achieve site-specific incorporation of an unnatural amino acid, an orthogonal aaRS/tRNA pair is indispensable (Figure 6), which must decode a codon that does not relate to any canonical amino acid. Since stop codons are unassigned, they are repurposed for unnatural amino acid incorporation by 'suppression'. The amber stop codon (UAG) is most recurrently used for this purpose due to its slightest usage and rare occurrence in most essential genes<sup>129,130</sup>.

One of the key aspects for the successful application of GCE is the orthogonality of the evolved aaRS/tRNA pair with respect to the host. For example, a *M.janaschii* - derived TyrRS-tRNA<sub>CUA</sub> pair is usually employed in bacteria<sup>131</sup>; *E. coli* derived TyrRS-tRNA<sub>CUA</sub> and LeuRS-tRNA<sub>CUA</sub> are used in eukaryotic cells; and PylRS-tRNA<sub>CUA</sub> pairs from some methanogens such as *M.barkeri* and *M.mazei* are orthogonal in both bacteria and eukaryotic cells formulating that there is no cross-reactivity<sup>132,133</sup>.

The pair is arranged by selection through directed evolution whereby by means of error prone PCR or degenerate primers, the mixture of active site mutants of synthetase is cloned into a plasmid such that it is able to charge the tRNA with a novel amino acid. This comprises a two-step process, where the plasmids are transported into cells expressing an essential gene bearing amber codon in the company of non-natural or natural amino acid and a second where plasmids are introduced into cells with amber codon in a toxic gene, however without non-natural amino acid such that only those survive which unambiguously distinguish the non-natural amino acid<sup>132</sup>.

Another impediment that can bother efficiency of GCE is the competition with release factors (RF1 in *E.coli* and eRF1 in eukaryotes) which terminate protein synthesis in retort to amber codons. To address this issue, an orthogonal ribosome was evolved which was no longer compatible with RF1 as well as RF1 was temporarily or constitutively deleted from several *E.coli* strains<sup>134,135</sup>. Other than RF1, optimization of



## 1.4.2 USAGE OF GENETIC CODE EXPANSION FOR THE INCORPORATION OF LIGHT INDUCIBLE CROSSLINKERS INTO PROTEINS

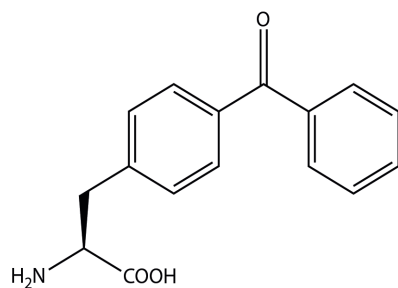
One of the classes of crosslinkers that have been used to reveal interactions *in vivo* are UV inducible in nature<sup>127</sup>. They vary in their functional moieties such as aryl azide, aryl diazirine, benzophenone and trifluoromethylphenyl (Figure 7) and accordingly in properties such as activation wavelength, crosslinking efficiency, linker lengths, hydrophobicity and charge. Each of these crosslinker has their exclusive aids and caveats which need be taken into contemplation while experimental designs to guarantee optimal crosslinking while diminishing the metabolic cargo of cells. In my thesis, I have used the benzophenone pBPA for all *in-vivo* crosslinking studies.

Benzophenones have several advantages over other UV crosslinkers<sup>141</sup>. Firstly, they are more stable than others. Secondly, they can be easily activated at nondamaging wavelength of 350-365 nm of light. Thirdly, after activation they can preferentially interact with unreactive C-H bonds, even in the presence of solvent and bulk nucleophiles, forming covalent crosslink adducts by hydrogen abstraction (Figure 8). The excited state persists only for 80-120 ms followed by return to the ground state as well as capacity of re-excitement<sup>142</sup>. On the contrary, the photoactivation of ABK, pAzF and DiZPK is irreversible. Also, the applicability of pAzF in living cells can potentially be diminished by reduction of the azide to an amine in cellular environment<sup>143</sup>. Other advantages of pBPA include high crosslinking yield, commercial availability and ease of handling. Few disadvantages of pBPA are hydrophobicity and therefore bulkiness which can affect incorporation efficiency at different sites. Moreover, pBPA has a certain penchant for crosslinking with methionine also called "methionine magnet", which can shift crosslinking contacts in company of methionines<sup>144</sup>. Infrequently, benzophenones can react in dark which can add to irregular crosslinking patterns<sup>145</sup>. Photocrosslinking with pBPA was primarily employed in *E. coli* where Chin and colleagues evolved the archeal *M. jannaschii* TyrRS/tRNACUA pair to successfully introduce pBPA

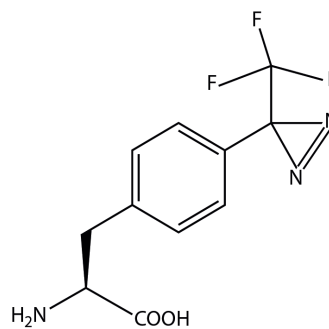
into myoglobin and GST protein<sup>146</sup>. Since then it has been incorporated with high translational efficiency and fidelity in multiple interaction contexts in *E.coli*, including studies mapping the interaction surface between SecY and SecA the two components involved in protein translocation across the plasma membrane<sup>147, 148</sup> or insights into substrate binding by bacterial chaperone ClpB<sup>149</sup>.

Usage of pBPA has proven to be extremely fruitful in Eukaryotes, especially in yeast. Several studies have employed pBPA mediated GCE in *S. cerevisiae* for elucidating site-specific interactions as well as mapping the interaction landscape of whole protein surfaces. Chin and coworkers evolved bacterial TyrRS/tRNATyrCUA pair orthogonal to yeast by mutagenesis of the implicated five amino acids of the AARS and their subsequent selection in yeast based on auxotrophy and antibiotic resistance<sup>150</sup>. pBPA mediated crosslinking has been specially used in cases where other conventional approaches have proven unsuccessful, where the interactions need to be studied in native contexts as well as cases where the structural and subsequently mechanistic information of processes has been scarce. For example, in the analysis of membrane transport processes such as ERAD (ER-associated protein degradation) pathway, where pBPA mediated crosslinking identified role of Der1 in movement of misfolded proteins through the endoplasmic reticulum membrane<sup>151,152,153</sup> and mitochondrial import machinery where several groups have employed comprehensive BPA-crosslinking study to elucidate the network between the outer- and inner membrane complexes<sup>154</sup> and on the architecture of the outer membrane translocator complex (the TOM complex) for the translocation of substrate proteins<sup>155</sup>. In a study scanning 61 different surface-exposed positions of the TATA-binding protein (TBP) by site-specific incorporation of pBpa led to the identification and mapping of several interaction partners, including the Spt-Ada-Gcn5 acetyltransferase (SAGA) complex<sup>156</sup>.

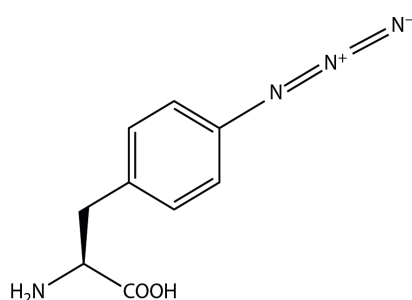
**A**



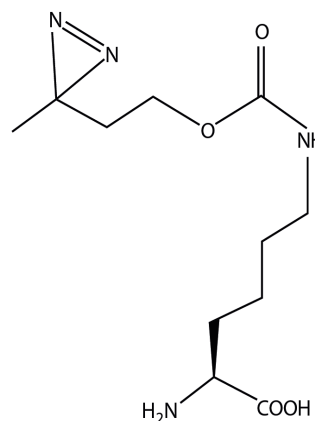
**B**



**C**



**D**



**E**

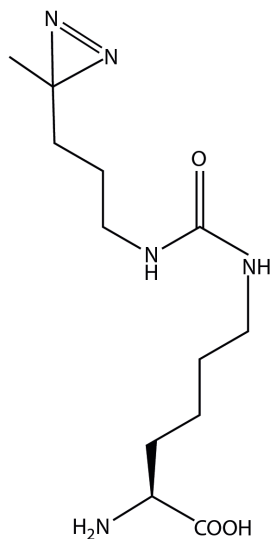


**Figure 7 : Genetically encoded crosslinker amino acids for *in vivo* crosslinking.**

Chemical structures of genetically encoded crosslinker amino acids. A) p-benzoyl-L-phenylalanine (pBPA) B) p-azido-L-phenylalanine (pAzF) C) p-trifluoromethyl-diaziriny-L-phenylalanine (tmdF) D) 3'-azibutyl-N-carbamoyl-lysine (ABK) E) 3-(3-methyl-3H-diazirine-3-yl)-propaminocarbonyl-N $\epsilon$ -L-lysine (DiZPK).

Amber suppression technology has been favorably utilized in Epigenetics<sup>157</sup>. Substituting N-terminal domain of histone H2A with pBPA exposed the downstream events of H3 S10 phosphorylation driving chromatin condensation<sup>117</sup>. Novel role of Pob3 subunit in FACT binding to H2A–H2B was recognized in a screen of the interaction interface of the histone chaperone complex FACT (facilitates chromatin transcription) with the nucleosome<sup>158</sup>. Using BPA inclusion in both the H3 K9me3 reading chromodomain and the dimerization negotiating HP1 chromoshadow domain, it was disclosed that heterochromatin protein 1 (HP1) bridges fibres in condensed chromatin, thus stabilizing the compacted state<sup>159</sup>. Another formidable use of pBPA crosslinking was to establish how the Paf1 complex regulates H2B ubiquitination levels in budding yeast<sup>160</sup>. In addition to use of pBPA in yeast, it has been extensively employed in mammalian cells for pathways such as EGFR signaling and the analysis of GPCRs (G-protein-coupled receptors)<sup>161,162</sup>.

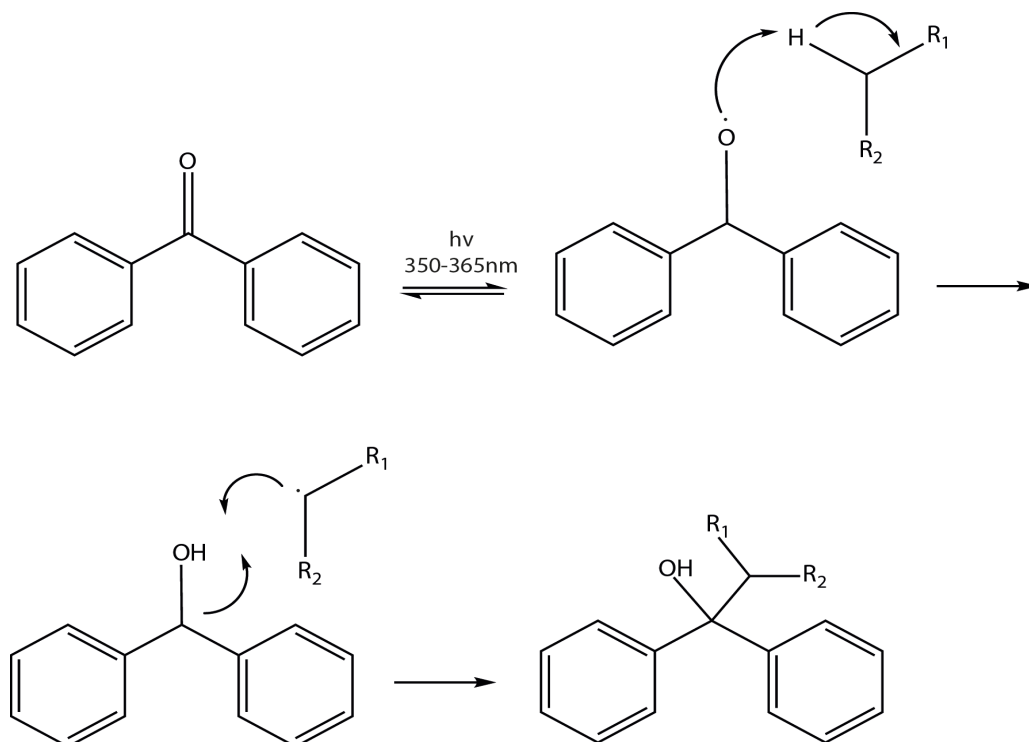


**Figure 8 : Reaction mechanism of *in vivo* photo-induced crosslinking by pBPA.**

Mechanism of reversible radical formation by pBPA upon activation by light

### 1.4.3 APPLICATIONS OF THE GENETIC CODE EXPANSION SYSTEM FOR THE STUDY OF PTMS

The past decade has witnessed the swift growth in miscellany and possibility for therapeutic purposes of GCE, aiding a plethora of applications, involving protein imaging, engineering, mechanistic and structural investigations, and functional regulation. Unnatural amino acids containing spectroscopic probes, post-translational modifications, metal chelators, photo affinity labels, and other chemical moieties have been selectively incorporated into proteins. This has paved way for latest means to regulate and apprehend biological functions and postulate new approaches for biomedical research. Examining the roles of PTMs has been impeded by a limited synthetic access to proteins with outlined PTM patterns. While recombinant proteins with specific modifications have been created by chemical ligation, is restricted only to N- or C-terminal modification of a narrow range of proteins that lack cysteine residues and tolerate chemical treatment. Developing the genetic code has shown promising results in the study of PTM, like serine, threonine and tyrosine phosphorylation (Figure 9) and lysine acetylation, crotonylation and hydroxyisobutyrylation .

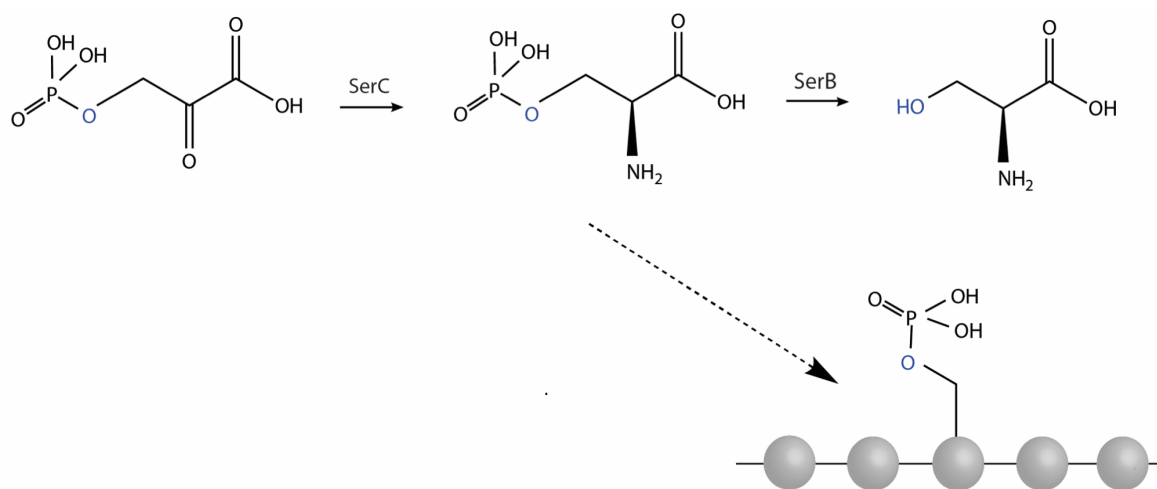


**Figure 9 : Genetic encoding of phosphoserine into proteins.**

serC deletion and overexpression of serB enables the site-specific incorporation of phosphoserines into proteins.

Intriguingly, phosphoserine is the most copious phosphoamino acid in eukaryotes which is not encoded by the genetic code, instead synthesized post translationally as an intermediate in a two-step pathway for synthesis of cysteine into proteins in certain methanogenic Archaeal bacteria. An aminoacyl-tRNA synthetase (SepRS) aminoacylates phosphoserine to tRNA<sup>Cys</sup><sub>GCA</sub> creating pSer-tRNA<sup>Cys</sup><sub>GCA</sub> in the first step, which is then converted to Cys-tRNA<sup>Cys</sup><sub>GCA</sub> by Sep tRNA:Cys tRNA synthase. Finally, elongation factor EF1 $\alpha$ , homolog of EF-Tu, takes it to ribosomes. By evolving these enzymes into SepRS9/tRNA<sup>Sep</sup> and EF-Sep21, Lee and colleagues demonstrated that H3S10 phosphorylation directly stimulates H3 acetylation by SAGA in the context of nucleosomal arrays<sup>163</sup>. Additional group synthesized the activated form of human mitogen-activated ERK activating kinase 1 (MEK1) with either one or two Sep residues cotranslationally inserted in their canonical positions (Sep218, Sep222)<sup>139</sup>. Recently, Rogerson and colleagues have established that alteration of EF-Tu is needless for the incorporation of phosphoserine. They also went a step ahead to show the feasibility of incorporating non-hydrolysable analog of phosphoserine, 2-amino-4-phosphonobutyric acid into proteins by overexpression of serB and deletion of serC phosphatase. This can help mimic constitutively active kinases and provide insights into complexes formed between phosphatase and their substrates<sup>164</sup>. Genetic encoding of phosphoserine bearing ubiquitin dimers linked via different lysines provided insights into substrate selectivity of E3 ligase and other deubiquitinases<sup>165</sup>. Evolved RS/trna pair with a EF-1 $\alpha$ -Sep, that enhances phosphoserine incorporation, and a mutant of eRF1, Beránek and colleagues were able to demonstrate synthetic activation of MEK1 kinase also in mammalian cells<sup>166</sup>. Other than phosphoserine, both phosphothreonine and phosphotyrosine with its non-hydrolyzable analog have been successfully encoded in E.coli<sup>167,168</sup>.

PTMs such as acetylation have been studied using GCE. For instance, a 7-fold upsurge in DNA breathing using single-molecule FRET experiments was perceived upon

reconstitution of nucleosomal arrays carrying genetically encoded acetyl-lysine<sup>169</sup>. In an alternative study genetically encoded acetylation at H3K56 and H3K14 in nucleosomes promoted different gap-filling pathways by inhibiting DNA polymerase  $\beta$  activity<sup>170</sup>.

GCE have also revealed in what way different PTMs crosstalk with each other. Example, genomic stability maintenance was studied by highlighting the acetylation-phosphorylation cascade in the detecting and fixing of chromosome attachment errors during mitosis<sup>171</sup>. Fluorescence levels on acetyl lysine containing GFP was used to ascertain deacetylation activity of sirtuins such a CobB, SIRT1 and SIRT2<sup>172</sup>. Genetic encoding of Ne -propionyllysine (PrK), Ne -butyryllysine (BuK) and Ne -crotonyllysine (CrK) and Ne -formyllysine are amongst the other few PTMs to be assimilated into histones<sup>173,174, 163,101</sup>.

## 2 MATERIALS AND METHODS

### 2.1 MATERIALS AND APPLIANCES

#### 2.1.1 EQUIPMENTS, CONSUMABLE SUPPLIES AND CHEMICALS

##### 2.1.1.1 LABORATORY DEVICES AND INSTRUMENTS

Table 1 : Overview of instruments used in this study.

Application	Instrument	Company
Agarose gel. electrophoresis	Agarose gel electrophoresis system	Carl Roth GmbH
Cell Lysis	Ultra Centrifugal Mill ZM 200	Retsch
	Sonifier 250	Branson
	Microfluidizer	Hyland Scientific
	Dounce tissue grinder set (#D9063)	Sigma
Centrifuges	Avanti-J20 XPI centrifuge JLA 8.1000 and JA-25.50 Tirotor	Beckman Coulter
	Allegra X-22 R	Beckman Coulter
	Centrifuge 5810 R	Eppendorf
	Centrifuge 542-4	Eppendorf
Chemiluminescence	Biostep-Celvin S	Biostep
Chromatography	ÄKTApurifier 10 (#28-4062-64)	GE Healthcare
	ÄKTAprime/plus (#11-0013-13)	Amersham
Columns	HiLoad™ 26/60 Superdex™ 75	GE Healthcare
	HiLoad™ 26/60 Superdex™ 200	GE Healthcare
	HiTrap SP Sepharose FF	GE Healthcare
Crosslinking apparatus	UV-lamp, VL-208.BL, 365nm tubes, 2x8W	Vilber Luomat
DNA	Trans illuminator	Thermo Fisher scientific
Documentation	Thermo printer UP-D895	Sony
	Perfection V850 Pro	Epson
Electrophoresis Chamber	Criterion™ Blotter with plate electrodes	Bio-Rad
	Mini Trans-Blot R Electrophoretic Transfer Cell	Bio-Rad
	Trans-Blot Turbo	Bio-Rad
	XCell SureLock R Mini-Cell and XCell IITM Blot Module	Life Technologies
Gel Doc™ XR	Gel documentation system	Bio-Rad
Glass beads	Glass beads	Carl Roth GmbH
Flow Cytometry	BD Accuri C6 Plus flow cytometer 660517	BD Biosciences
Incubator/Shaker	New Brunswick™ Innova® E42/42R	Eppendorf I
	New Brunswick™ Excella® E24/E24R	Eppendorf
	Incubation Shaker Multitron	INFORS HT
	Rotamax 120 Shaker	Heidolph
ITC	ITC200 micro calorimeter	GE Healthcare

Luciferase	FluoStar Omega Microplate Reader	BMG Labtech
Microscope	LSM 900	Zeiss
PCR & qPCR	Labcyler Basic (011-103), Thermoblock 48 (012-102), Thermoblock 96 (012-103)	SensoQuest GmbH
	CFX96 Touch Real-Time PCR Detection System	Bio-Rad
pH-meter	pH-meter	Mettler Toledo
Polr Supply Unit	Power Supply 300V	VWR International
	Power Supply MP-250V	Major Science
	Power Pac	Bio-Rad
Spectrophotometer	BioPhotometer	Eppendorf
	NanoDrop ND-1000	Thermo Scientific
Thermomixer	Eppendorf R-Thermomixer comfort™	Eppendorf

### 2.1.1.2 CONSUMABLE SUPPLIES

**Table 2 : Overview of Laboratory supplies used in this study.**

Application	Supplies/Equipments	Company
Concentrators	Amicon Ultra-15 Centrifugal Filter Units with different MWCOs	Millipore
Glasswares	Erlenmeyer flask (100 mL, 300 mL, 1000 mL, 2000 mL) Borosilicate flasks (100 mL, 250 mL, 500 mL, 1000 mL), pipettes (20 mL, 10 mL, 5 mL)	Schott
Blotting membrane	Immobilon R-P PVDF Membrane (#IPVH00010)	Millipore
Cuvette	Cuvettes (#67.742)	SARSTEDT
Dialysis	Dialysis Membrane MWCO 12.4 kDa	Sigma
	Spectra/Por R Dialysis Membrane MWCO 6-8.000	Spectrum Laboratories Inc.
	Slide-A-Lyzer R MINI Dialysis Units 7,000 MWCO	Thermo Scientific
Plates/Petridishes	Petri dishes for bacteriology 92/16 mm	SARSTEDT
	96 well Plate Microfluor	Brand
	96-deep well block	Costar
Eppis	Low Protein Binding Microcentrifuge Tubes (1.5 mL)	Thermo Scientific™
Pipettes	Eppendorf Research R (adjustable) 2.5 ml pipette	Eppendorf
	Eppendorf Multipette R plus	Eppendorf
	Research plus3	Eppendorf
Pipette tips	TipOne RRPT 10 ml (#S1180-3810), 200 ml (#S1180-8810), 1000 ml (#S1182-1830) Pipette-tips 10 ul (#70.1130), 200 ul (70.760.002), 1000 ul (70.762)	STARLAB
Syringes	Hamilton Syringe 1705N 50ml	Hamilton

## 2.1.1.3 CHEMICAL REAGENTS

Table 3 : Overview of Chemicals/Reagents used in this study.

Chemicals/Reagents	Company
2-Mercaptoethanol	Sigma
2-Propanol	AppliChem
4-Benzoyl-L-phenylalanine	Chem-Impex International, Inc.
3-(N-morpholino) propanesulfonic acid (MOPS)	Gerbu
Acetic Acid	Sigma
Acetonitrile	Sigma
Alpha-Factor Mating Pheromone	ZymoResearch
Ampicillin sodium salt pure	AppliChem
Adenosine-5'-triphosphate (ATP)	Sigma-Aldrich, USA
Ammoniumperoxosulphate (APS)	Serva Electrophoresis
dNTP Mix, 10 mM	Thermo Scientific
Boric acid extra pure	Riedel-de Haen
BSA - Albumin bovine serum	Sigma
Bromphenol blue	SERVA
Calcium chloride (CaCl <sub>2</sub> )	Roth
Difco™ Skim Milk	BD
di-Sodium Hydrogen Phosphate 2-Hydrate	Roth
Dithiothreitol	BioChemica, AppliChem
Desthiobiotin	IBA Lifesciences
EDTA	Roth
Ethanol absolute	VWR
GelRed	Biotium
Glycerol bidistilled	VWR
Glutathione (GSH, reduced)	Merck
Glycine	ROTH
Guanidine hydrochloride pure	AppliChem
4-(2-hydroxyethyl)-1-piperazineethanesulfonic acid (HEPES)	SERVA
Hydrochloric acid (HCl)	ITW Reagents
Hydroxyurea	Sigma
Instant Blue	Expedeon
Imidazole	AppliChem
Isopropyl-b-D-thiogalactopyranosid	Roth
Kanamycin sulfate	AppliChem
L-Glutathione reduced	Sigma
Leupeptin	Sigma
Manganese (II) chloride (MnCl <sub>2</sub> )	Sigma
Magnesium chloride (MgCl <sub>2</sub> )	J.T. Baker
Methanol	Merck
Nicotinamide adenine dinucleotide (NAD <sup>+</sup> )	Sigma
Nocodazole	Sigma
O-Phenanthroline	Sigma
Protease Inhibitor Cocktail	Roche
Pefablock™	Sigma
Polyethylene glycol (PEG3350)	Sigma

Ponceau S	Sigma
Pepstatin A	Sigma
peqGOLD Universal Agarose	PEQLAB
Phenol-Chloroform, pH 4.5	Invitrogen™
Phenylmethyl sulfonic acid (PMSF)	Serva Electrophoresis GmbH
PhosSTOP™	Sigma
Phos-tag (TM) Acrylamide AAL-107	FUJIFILM Wako Chemicals
Phenol-Chloroform, pH 4.5	Ambion
Potassium chloride	Applichem
PRO-Q™ Diamond stain	Invitrogen™ Molecular Probes™
Rotiphorese R Gel 30 (37,5:1): 30 % Acrylamide/Bisacrylamide	Roth
Rotiphorese R Gel 40 (29:1): 40 % Acrylamide/Bisacrylamide	Roth
SDS ultrapure	Roth
Sodium butyrate	ACROS Organics
Sodium chloride	AppliChem
Sodium dihydrogen phosphate dihydrate	AppliChem
Spectinomycin dihydrochloride pentahydrate	AppliChem
Streptactin Hicapacity beads	IBA Lifesciences
Sytox Green	Invitrogen
Tetra-methylethylenediamine (TEMED)	ROTH
Trichloroacetic acid	Sigma
Tris-(2-Carboxyethyl)-Phosphine (TCEP)	Sigma
Tris	Roth
Triton X-100	Roth
Tween R 20	Merck
Urea	Merck
Zinc chloride	Sigma
Y-PER™	Thermo Scientific

## 2.1.2 BUFFERS AND SOLUTIONS

### 2.1.2.1 BUFFER RECIPES

**Table 4 : Overview of commonly used buffers and solutions.**

Buffer/Solution	Ingredients
PBS (1x)	137 mM NaCl, 2.7 mM KCl ,10 mM Na <sub>2</sub> HPO <sub>4</sub> , 1.8 mM KH <sub>2</sub> PO <sub>4</sub> pH 7.4
TBS (1x)	50 mM Tris-HCl, pH 7.5 ,150 mM NaCl
TBST (1x)	TBS, 0.05% Tween-20
Single-stranded DNA	10 mg/mL salmon testes DNA (w/v)
Tris-Acetate Running Buffer (20x)	1 M Tricine, 1 M Tris Base, 70 mM SDS
Transfer Buffer for NuPage	25mMBicine, 25mMBis-Tris, 1.05mMEDTA, 1.3 mM Sodium Bisulfite, pH 7.2 (wo adjustments), 10 % (v/v) Methanol
TES buffer	10 mM Tris-Cl, pH 7.5 10 mM EDTA 0.5% SDS

SDS Sample Buffer (1x)	2.5% glycerol ,12.5 mM Tris-HCl, pH 6.8 ,25 mM DTT, 0.5% SDS (w/v) ,0.025% bromophenol blue (w/v)
MOPS Running buffer (1x)	50 mM MOPS,50 mM Tris base ,1 mM EDTA ,0.1% SDS (w/v) pH 7.7
TE Buffer (10x)	100 mM Tris-HCl, pH 8.0, 10 mM EDTA, pH 8.0
PEG Solution (50%)	50% PEG 4000 (w/v)
PIC (1x)	75 µM pefabloc SC,150 nM leupeptin,37.5 µM O-phenanthroline,500 nM pepstatin A, Sterilized using 0.2 µm syringe filter
2x luciferin buffer	40 mM Tricine, 200 µM EDTA, 7.4 mM MgSO <sub>4</sub> , 2 mM NaHCO <sub>3</sub> , 34 mM DTT, 0.5 mM ATP and 0.5 mM luciferin, pH 7.8
pBPA-stock solution	100 mM 4-Benzoyl-L-phenylalanine in 120 mM NaOH, filter sterile; store at -20C
Ni-NTA wash buffer	20 mM HEPES pH 7.5, 200 mM NaCl, 20 mM imidazole, 1 mM DTT
Gel filtration buffer	20 mM HEPES pH 7.5, 100 mM NaCl, 10 mM DTT
Luciferase wash buffer	20 mM Tris/HCl pH 8, 10 mM imidazole, 200 mM NaCl, 10 mM DTT
Luciferase storage buffer	20 mM Tris pH 8, 50 mM NaCl, 10 mM DTT or 1 mM TCEP
Towbin-transfer buffer	25 mM Tris, 192 mM Glycine, 20% methanol, pH 8.3
PonceauS Solution	0.5% PonceauS (w/v), 5% TCA (w/v)
Single-stranded DNA	10 mg/mL salmon testes DNA (w/v)
Lysis Buffer	1x PBS, 2x PIC, 2 mM PMSF
Extraction buffer	7 M Guanidinium-HCl 20 mM Tris-HCl, pH 7.5 ,10 mM DTT
Urea Dialysis Buffer	7 M Urea, 10 mM Tris-HCl, pH 8.0, 1 mM EDTA, pH 8.0, 100 mM NaCl ,5 mM β-ME, 1 mM PMSF
Urea Loading Buffer	7 M Urea, 10 mM Tris-HCl, pH 8.0, 1mM EDTA, pH 8.0, 1x PIC, 1 mM PMSF ,1 mM DTT
Resolving Gel Solution (PhosTag)	30% (w/v) Acrylamide Solution :1.4 mol/L Bis-Tris/HCl Solution, pH 6.8; 5.0 mmol/L Phos-tag™ Solution; 10 mmol/L ZnCl <sub>2</sub> Solution; 10%APS; TEMED
Stacking Gel Solution (PhosTag)	30% (w/v) Acrylamide Solution; 1.4 mol/L Bis-Tris/HCl Solution, pH 6.8; 10%APS; TEMED
Running Buffer (PhosTag)	0.5 mol/L Tris base, 0.5 mol/L MOPS, 10% SDS, 0.5 mol/L Sodium Bisulfite Solution, pH. 7.8
TAF Buffer	20 mM Tris-HCl, pH 7.5, 20 mM NaN <sub>3</sub> , 20 mM NaF
IP buffer (1.2x)	168 mM NaCl,12 mM Tris-HCl, pH 8.0 ,1.2 mM EDTA, pH 8.0, 0.12% SDS (w/v) , 0.12% Na-deoxycholate (w/v) ,1.2% Triton X-100 (w/v)
TFB1 Buffer	100 mM RbCl, 50 mM MnCl <sub>2</sub> , 30 mM KAc, 10 mM CaCl <sub>2</sub> , 15% Glycerol, pH 5
TFB2 Buffer	10 mM MOPS, 10 mM RbCl, 75 mM CaCl <sub>2</sub> , 15% Glycerol, pH 8
Resuspension Buffer	1x TE Buffer, 0.1 M LiOAc

### 2.1.2.2 MEDIA

**Table 5 : Overview of media used in this study.**

Media	Ingredients
LB	5 g/L NaCl, 5 g/L Yeast Extract, 10 g/L Bactotryptone
YPA	20 g/L Bactotryptone, 10 g/L Yeast Extract, 0.04 g/L adenine
SD	1.7 g/L Yeast Nitrogen Base without Amino Acids & Ammonium Sulfate, 5 g/L Ammonium Sulfate, 2 g/L Dropout amino acid mix, 0.8 mL/L 4MNaOH

Carbon sources: (w/v) of either Glucose or Galactose in H<sub>2</sub>O

### 2.1.2.3 ANTIBIOTICS

**Table 6 : Overview of antibiotics used in growth media and agar plates.**

Antibiotic	Work concentration[ $\mu\text{g}/\text{mL}$ ]	Company
Ampicillin (Amp)	100	AppliChem, Darmstadt
Chloramphenicol (Cm)	50	AppliChem, Darmstadt
Kanamycin (Kan)	50	AppliChem, Darmstadt
Spectinomycin (Spec)	50	AppliChem, Darmstadt

### 2.1.2.4 ENZYMES

**Table 7 : Overview of enzymes used.**

Enzyme	Supplier
DNaseI	AppliChem
Trypsin	Sigma
Phusion DNA Polymerase	Thermo Scientific
Expand™ High Fidelity PCR System	Roche
Lysozyme	Boehringer Mannheim
Proteinase K	Thermo Scientific
Shrimp Alkaline Phosphatase (SAP)	Fermentas
Calf Intestine Alkaline Phosphatase (CIAP)	Fermentas
T4 DNA Ligase	Thermo Scientific
Restriction Endonucleases	New England Bio labs
PNK	New England Bio labs
RNase A	Sigma
Sumo Protease	Dortmund Protein Facility (DPF), MPI
Lyticase	Sigma-Aldrich
Zymolase	Zymo Research
Superscript-III reverse transcriptase	Invitrogen

### 2.1.2.5 STANDARD MARKERS

**Table 8 : Overview of standard markers used.**

Markers	Supplier
GeneRuler™ 100bp Plus DNA Ladder	Thermo Scientific
GeneRuler™ 1 kb DNA Ladder	Thermo Scientific
PageRuler™ Prestained Protein Ladder	Thermo Scientific

### 2.1.2.6 ANTIBODIES

Table 9 : Overview of antibodies used.

Company	Target	Host	Dilution
<b>Primary</b>			
Abcam (ab9110)	HA	Rabbit	1:10K in 3% BSA-PBS
Active Motif (39167)	Histone H4 acetyl Lys16	Rabbit	1:2.5K in 3% Milk-TBS
Cell Signaling (9701)	Phospho-Histone H3(Ser10)	Rabbit	1:3K in 3% BSA-TBS
Abcam (ab10158)	Histone H4	Rabbit	1:2.5K in 3% Milk-TBS
Abcam (ab6556)	GFP	Rabbit	1.5K in 5% Milk-TBS
Millipore (05-419)	Myc	Mouse	1.5K in 3% Milk-TBS
Sigma (F7425)	Flag	Rabbit	1:10K in 5% Milk-TBS
<b>Secondary</b>			
Abcam (ab6721)	Rabbit	Goat	1:10K in 3% Milk-TBS
Abcam (ab6789)	Mouse	Goat	1:10K in 3% Milk-TBS

### 2.1.2.7 ANTIBODY CONJUGATED BEADS

Table 10 : Overview of antibody conjugated beads used.

Conjugate	Bead Material	Manufacturer
Anti-HA	Agarose	Sigma
Anti-Flag	Agarose	Sigma
GFP nanobodies	Agarose	This study
Streptactin	Agarose	IBA Lifesciences

### 2.1.3 KITS

Table 11 : Overview of kits used.

Kit	Purpose	Supplier
peqGOLD Plasmid Miniprep Kit I,(#12-6943-02)	Isolation of Plasmid DNA from bacterial cultures	PEQLAB
QIAGEN Plasmid Mini Kit (cat. No 12123)	Isolation of Plasmid DNA from bacterial cultures	Qiagen
QIAquick Gel extraction Kit	Purification of DNA from gels	Qiagen
QIAquick PCR purification Kit	Purification of DNA from PCR	Qiagen

### 2.1.4 PEPTIDES

Table 12 : Overview of peptides used for ITC.

Peptide	Sequence	Source
H4K16Ac	NH <sub>2</sub> -KGGAK <sub>Ac</sub> RHRKIL-COOH	Sascha Gentz, DPF, MPI
H3S10D	NH <sub>2</sub> -ARTKQTARKDGTGGKAPRKQLK(Biotin)-COOH	Sascha Gentz, DPF, MPI

## 2.1.5 SOFTWARES

Table 13 : Overview of softwares used.

Software	Version	Supplier
Illustrator CS6	16.0.0	Adobe
Excel	16.16.21	Microsoft
Word	16.16.20	Microsoft
FlowJo	10	Becton, Dickinson & Company
Chimera	1.9	UCSF
Fiji	1.0	National Institutes of Health
ApE- A Plasmid Editor	2.0.45	M.Wayne Davis
SnapGene Vielr	2.6.2	GSL Biotech LLC
GraphPad Prism	8	Dr. Harvey Motulsky
SciDavis	1.22	Miquel Garriga
ChemDraw	17.1	PerkinElmer
Origin	7.0	MicroCal

## 2.1.6 STRAINS

A complete list of all the strains used in this study is added to the supplementary.

## 2.1.7 PLASMIDS

A complete list of all the plasmids used in this study is added to the supplementary.

## 2.1.8 PRIMERS

A complete list of all the primers used in this study is added to the supplementary.

## 2.2 METHODS

### 2.2.1 DNA METHODS

#### 2.2.1.1 TRANSFORMATION OF *S. CEREVISIAE* WITH DNA

The transformation of *S. cerevisiae* was performed by a standard lithium acetate/heat shock method. Prior to the transformation, a 4 mL overnight culture of the yeast cells (**Table 5**) was prepared from a single colony. The next day, the overnight culture was used to inoculate a 50 mL main culture to a final OD<sub>600</sub> of 0.25. The cells were allowed to grow till OD<sub>600</sub> of 0.5 and then collected by centrifugation at 4800 rpm for 2 min

at RT. Subsequently, the cells were washed with sterile ddH<sub>2</sub>O, the pellet dissolved by shaking and the cells again rinsed in water. The resulting pellet was resuspended in 2 mL of Resuspension Buffer (Table 4). From the cell resuspension, 100  $\mu$ L was mixed with 1  $\mu$ g plasmid DNA(s), 10  $\mu$ g of heat inactivated salmon sperm DNA and 600  $\mu$ L PEG Solution (Table 4) and incubated for 30 min at 30 °C with gentle shaking. The heat shock was then performed at 42 °C for 15 min. Following heat shock, the cells were spun down at 10,000 rpm for 1 min and the supernatant was discarded. The cell pellet was washed with 1 mL dH<sub>2</sub>O and then resuspended in 100  $\mu$ L dH<sub>2</sub>O. Finally, the resuspended cells were plated on selective synthetic complete (SC) agar plates depending on the plasmid's auxotrophic marker (1 sample plate and 1 control plate/strain) and incubated for 2-3 days at 30 °C.

### 2.2.1.2 ISOLATION OF GENOMIC DNA FROM YEAST

Isolation of genomic DNA was performed based on spheroplasting yeast cells (Table 15) followed by precipitation of DNA using ethanol. Briefly, 1 mL of a fresh yeast overnight culture was harvested by centrifugation at 10,000 rpm in a table-top centrifuge for 3 minutes. Cells were resuspended in 250  $\mu$ L buffer P1 substituted with lyticase (final concentration 25 kU/mL). Cells were incubated at 30° C for 10 minutes. Subsequently, 250  $\mu$ L lysis buffer P2 and 50  $\mu$ L of a 3 M sodium acetate solution (pH 5.2) was added. The samples were incubated at 30° C for 10 minutes with gentle shaking. Cells were centrifuged at 14,000 rpm in a pre-chilled table-top centrifuge for 8 minutes at 4° C. The soluble supernatant was transferred to a fresh 2 mL tube and mixed with 1 mL 95 % ethanol by inverting mixing. After incubation at on ice for 10 minutes, the precipitate was collected by centrifugation at 14,000 rpm for 5 minutes at 4° C and the supernatant was discarded. The pellet was washed with 1 mL 70 % ethanol and collected by centrifugation as described above. The supernatant was discarded and the pellet was air dried at RT. Finally, the pellet was resuspended in 250  $\mu$ L water and heated at 50° C with shaking for 10 minutes. The nucleic acid

concentration was determined by UV spectroscopy at 260 nm. The concentration was adjusted to 100 ng/mL (common working concentration) and the DNA was stored at -20°C.

### 2.2.1.3 TRANSFORMATION OF BACTERIA AND PREPARATION OF PLASMID DNA

For preparation of chemically competent *E.coli* cells, an overnight culture of DH10B (Table 14) cells was started at 37°C at 200 rpm, of which 1 mL was inoculated the following day in 100 mL LB medium and grown to an OD<sub>600</sub> upto 0.5. The cells were cooled on ice for 10 min and harvested by centrifugation at 4000 rpm for 5 min. The pellet was suspended in 25 mL TFB1-buffer (Table 4) and incubated on ice for 90 min. The cells were collected as before and suspended in 2 mL TFB2 (Table 4). Cells were aliquoted, flash frozen in liquid nitrogen and stored at -80°C.

Chemically competent *E.coli* DH10B cells prepared as stated above were transformed with plasmids using the heat shock method. A mixture of 50 µL chemical competent cells and 150-500 ng plasmid DNA were incubated on ice for 20 min. After heat shocking for 95 sec at 42 °C, the cells were incubated for further 2 min on ice. For recovery, the cells were resuspended in 1 mL LB medium, followed by incubation for 1 hr at 37 °C and 500 rpm in a Thermoshaker. Transformants were plated on agar media containing the appropriate antibiotics (Table 6) or used for the inoculation of an overnight culture.

Preparation of plasmid DNA from *E.coli* was done using peqGOLD or Qiagen Plasmid Miniprep Kits (Table 11) according to manufacturer's instructions. As stated above after transformation bacterial colonies were incubated in 4 mL LB media containing appropriate antibiotics. Cultures were kept at 37° C in a shaker (approx. 200 rpm) for at least 16 hours. Cells were harvested by centrifugation in a table-top centrifuge at full speed. The cell pellet was subjected to plasmid preparation as described in the

manual based upon the property of DNA. binding to silica gel under high chaotropic salt conditions and subsequent elution under low salt conditions. The DNA was ultimately eluted with 50  $\mu$ L elution buffer and concentration were determined using UV spectroscopy at 260 nm. Plasmids were stored at  $-20^{\circ}$  C or sequenced using Sanger sequencing.

#### **2.2.1.4 PCR BASED STRATEGY FOR QUICKCHANGE MUTAGENESIS**

Quickchange mutagenesis PCR was performed to prepare alanine mutants of Hst2 in pRS plasmid, introduce amber mutants into Hst2 in pCDF plasmids and exchange the His tag of Bmh1 to strep tag in pCDF plasmid. Primers used (Table 18) were designed in an overlapping fashion covering the region of interest: 10 bp upstream and at least 15 bp downstream of the region are complementary to the plasmid template with desired mutation or tag. After PCR amplification, the methylated parent plasmid was digested with 10 U DpnI for at least 1 hour at  $37^{\circ}$  C. The generated plasmid was PCR purified using PCR purification kit (Table 11) and subsequently transformed into chemically competent bacterial cells. The quickchanges were confirmed by sanger sequencing analysis of the plasmids generated.

#### **2.2.1.5 MOLECULAR CLONING FOR YEAST-TWO-HYBRID**

The sequences of Hst2 and putative targets Bmh1/2 were PCR amplified from yeast genomic DNA, PCR product gel extracted, restriction digested and ligated into pGBKT7 bait vector or pGADT7 prey vector (Clontech Laboratories, Inc.). Using the one-step transformation protocol for yeast in stationary phase<sup>175</sup>, the generated vectors containing the putative targets as well as the empty vectors (to test for auto-activation) were transformed into yeast strains AH109 (pGBKT7 bait vectors) or Y187 (pGADT7 prey vector) and transformants were selected on SD plates deficient of tryptophane (SD-Trp) or leucine (SD-Leu), respectively.

### 2.2.1.6 ENDOGENOUS GENE TAGGING IN YEAST

The method relied on PCR based strategy for tagging a protein-coding gene<sup>176</sup>. In general, a PCR product containing desired HA tag and selection marker flanked by homologous regions of the target gene, Bmh1 was generated using pYM24 plasmid. This PCR-product was then transformed into Flag Hst2 BY4741 yeast cells. The success of the homologous recombination was determined by genomically isolating DNA followed by PCR based confirmation, validation by sequencing and visualization of the tag in western blot analysis.

### 2.2.1.7 CREATION OF BY4741 SIZ1,2 KNOCKOUT STRAIN

BY4741 *siz1/siz2*Δ strain was established through genomic integration of the yeast selectable marker *kanMX* gene<sup>177</sup> at the *siz1* locus in BY4741 yeast cells. Standard PCR amplification of the pUG6 plasmid was performed to amplify the *kanMx* region with flanking sequences to the *siz1* ORF. The PCR products were ethanol precipitated and then transformed into wild type BY4741 cells. Genomic integration was selected on YPD plates with G418 (Geneticin) : selection antibiotic and surviving colonies were streaked through another round on G418 YPD plate. Next, *siz2* knockout was created through genomic integration of the *hphnt1* gene at the *siz2* locus in BY4741 *siz1*Δ::KanMX. Standard PCR amplification of the pYM24 plasmid was performed to amplify the *hphnt1* region with flanking sequences to the *siz2* ORF followed by PCR purification, ethanol precipitation, subsequent transformation in BY4741 *siz1*Δ::KanMX followed by final selection on YPD plates with hygromycin selection antibiotic. The initial *siz1*Δ strain and the double knockout *siz1/siz2*Δ were verified by yeast genomic DNA extraction and PCR.

### 2.2.1.8 CRISPR/CAS9 GENOME EDITING IN YEAST

BY4741 Yeast cells containing Flag tagged Hst2 and Gfp tagged Bmh1 were transformed with 2-micron plasmid, pRS425-Cas9-2xSapI and selected on SD leu+ plates, that constitutively expressed the gene encoding the Cas9 endonuclease. In the same plasmid, DNA containing guide RNA sequences were introduced at two SapI sites downstream of the SNR52 promoter. Guide RNAs (gRNAs) targeting the N and C terminus of Hst2 were designed using the online CRISPR design tool (<http://zlab.bio/guide-design-resources>). Phosphorylated and annealed oligos (Table 18) were ligated into SapI digested pRS425 plasmid. To introduce genomic mutations in Hst2 above cells were co-transformed with a 'healing fragment' or homology-directed donor oligos (Table 18). Genomic DNA was isolated from picked single clones and the desired mutations were scored for by Sanger sequencing.

## 2.2.2 PROTEIN METHODS

### 2.2.2.1 SDS POLYACRYLAMIDE ELECTROPHORESIS OF PROTEINS

Sodium dodecyl sulfate polyacrylamide gel electrophoresis (SDS-PAGE) was used to separate a mixture of proteins based on their electrophoretic mobility. This relies on the ability of SDS to denature and surround proteins by a negatively charged detergent micelle which eliminates most of the charge and solubility differences from one protein to another and differentiates them based on the negative charge proportional to their molecular weight. During the course of this study four different types of SDS-PAGE gels were used. First, the common discontinuous SDS-PAGE with a Tris-Glycine buffer system. A discontinuous gel is formed from two acrylamide layers a stacking gel and the resolving gel. Here, three ions are primarily involved: Chloride ( $-$ ), from gel buffer, serves as the leading ion because of highest mobility to the anode in comparison to other ions. Glycine ( $-$ ), the primary anion from the running buffer, serves as the trailing ion, because of more neutral charge and remains behind the more highly

charged chloride ions. Tris base (+), commonly present in the gel and running buffer, maintains a high pH in the resolving region of the gel. The proteins are stacked between the leading chloride and trailing glycine ions. Upon start of electrophoresis, glycine becomes negatively charged in the higher pH resolving gel, which then acts like a sieve separating proteins based on their molecular weight.

Depending on size of target protein, gel types with different acrylamide concentrations were used -10%,15% and 18% (Table 14)

**Table 14 : Composition of Polyacrylamide Gels for SDS-PAGE.**

10% Resolving gel	15 % Resolving gel	18% Resolving gel	4% Stacking gel
375 mM Tris-HCl, pH 8.8	375 mM Tris-HCl, pH 8.8	375 mM Tris-HCl, pH 8.8	125 mM Tris-HCl, pH 6.8
0.1% SDS (w/v)	0.1% SDS (w/v)	0.1% SDS (w/v)	0.1% SDS (w/v)
10% acrylamide	15% acrylamide	18% acrylamide	4% acrylamide
0.2% bisacrylamide	0.4% bisacrylamide	0.6% bisacrylamide	0.11% bisacrylamide
0.1% APS (w/v)	0.1% APS (w/v)	0.1% APS (w/v)	0.05% APS (w/v)
0.04% TEMED (v/v)	0.04% TEMED (v/v)	0.04% TEMED (v/v)	0.1% TEMED (v/v)

The second type of SDS-PAGE was performed with commercially available 3-8% NuPage Tris acetate gels. Here, acetate and tricine ions replace chloride and glycine ions from Tris-glycine system. Moreover, the lower pH result in less gel-induced protein modifications and better separation of higher molecular weight proteins. This system with its own buffers were employed to detect all histone crosslinks.

Third, 4-12% NuPage Bis-Tris gels were used. Here, MOPS: 3-(N-morpholino) propane sulfonic acid replaced the glycine ions. Bis-Tris (+) acts as the common ion with a pH of 6.4 and pH 7.3–7.7 of the system lowers the pH, resulting in better sample integrity and gel stability. MOPS running buffers is mainly used to resolve mid-size proteins and was employed to run enriched histone proteins and their crosslinks.

Fourth, Phos-tag gels were used to specifically separate phosphorylated species of Hst2. 12% Phos-tag SDS-PAGE gels was prepared by adding  $ZnCl_2$  ions and Phos-tag acrylamide in the resolving gel.  $Zn^{2+}$  ions trap phosphorylated proteins and separated species on amount of phosphorylation. In all above cases, samples were loaded after denaturation, boiling in 1x SDS buffer at 95° C for 10 minutes and centrifugation at full speed in a table-top centrifuge for 2 minutes. Electrophoresis was performed at constant voltage of 120V and after electrophoresis, the gel was either stained with a one-step Coomassie-based stain (Instant Blue) or subjected to western blot.

#### **2.2.2.2 TCA PRECIPITATION**

Wildtype and mutant yeast cells were grown to  $OD_{600} = 0.5-1.0$  and harvested equivalent to 12 OD units for each strain at 4000 rpm for 2 minutes. Cells were resuspended in 1 mL ddH<sub>2</sub>O (2 mM PMSF, 1 x PIC) supplemented with 150  $\mu$ L 2 M NaOH and 12  $\mu$ L  $\beta$ -Mercaptoethanol. Samples were incubated at RT for 10 minutes. Lysates were then precipitated by adding 100% TCA to a final concentration of 33% (v/v), centrifuged at 14000 rpm for 5 minutes, and washed twice with 1 mL acetone, further centrifuged as above. Proteins were eluted by boiling in SDS-PAGE loading buffer and run on SDS gels further stained with Coomassie Blue (Instant Blue, Expedeon) or analyzed by western blot.

#### **2.2.2.3 WESTERN BLOT AND DETECTION**

Throughout this study, western blot was a major means to visualize proteins. After SDS-PAGE, proteins were transferred to a methanol activated PVDF (polyvinylidene difluoride) membrane using the wet blot or the semi-dry method. In both cases, the gel was placed on a PVDF membrane and sandwiched between layers of 3 mm Whatman paper on each side. In wet blot transfers, 2-3 sponges were used additionally on each side. Transfer of proteins in wet blot method was either done at constant current of 280mA for 2-3 hours or overnight at 38mA at 4°C. In case of semi-dry method,

electrodes are placed directly in contact with the gel/PVDF membrane sandwich to provide a faster transfer and thus was run for 30 mins. The transfer efficiency was determined by 0.5% PonceauS staining of the membrane. Subsequently, protein expression was verified by protein/tag specific primary antibodies overnight at 4 °C or for 3-4 hours at 37° C. Prior to immunolabelling, the membrane was blocked by incubation with 3% BSA or dried skim milk in PBS or TBS (pH 7.5), respectively, depending on antibodies used to avoid non-specific binding of the antibodies. Primary antibodies were in turn bound by a secondary antibody conjugated to a horseradish peroxidase (HRP) (Table 7). In between binding, membrane was washed with 1x TBS and 0.5% Tween 20 for 10 min, followed by 1x TBS thrice. The detection was done with the Amersham ECL Select or Prime western blotting detection reagent, over a range of exposure times depending on intensity of protein signals.

#### 2.2.2.4 WESTERN BLOT ANALYSIS

For analysis of protein band intensities, the raw tiff images of the western blots were imported into Fiji and inverted. So as to measure each row of protein band across the lanes a single region of interest was defined by selecting the “rectangle” tool and saved as “Selection” from the “File” menu. Protein bands from each lane within this rectangular selection were analyzed by Plot profile method which displayed a “column average plot”, wherein the x-axis represented the horizontal distance through the selection and the y-axis, the vertically averaged pixel intensity or gray value. Next, using “free hand selection” tool, the region consistent to the protein band under the curve from the plot profile was measured, subtracting the background, using “Measure” under “Analyze”. This process was repeated for different protein bands within the rectangular selection and across different lanes. Results were then imported into Excel and the mean intensity of each band was calculated by multiplying the measured area and averaged pixel intensity values. Average mean intensity and standard deviations were further calculated for three biological replicates. The final relative quantification values were the ratio of the mean intensities of different protein bands which were further displayed as a bar or scatter graph to equate them.

#### 2.2.2.5 PROTEIN EXPRESSION AND PURIFICATION

The full-length Hst2 gene from *S. cerevisiae* was cloned into the pCDF expression vector and overexpressed as an N-terminal His<sub>6</sub>-tagged fusion protein (His-yHst2) in *E. coli* BL21 (DE3), initially grown at 37°C in LB containing 50 µg/mL spectinomycin. Next day, the preculture was used 1:50 to inoculate 4 L LB medium and protein expression induced with 0.5 mM IPTG at OD<sub>600</sub> = 0.5, and incubation continued overnight at 15°C. Cells were harvested, suspended in 20 mM HEPES, pH 7.5, 200 mM NaCl, 20mM Imidazole, 3 mM β-mercaptoethanol and 1 mM PMSF supplemented with lysozyme (~0.5 mg/mL), DNase (1 mg), protease inhibitor cocktail (Roche) and disrupted with a pneumatic cell disintegrator. Soluble His-yHst2 was purified by Ni-

NTA affinity chromatography using HisPur™ Ni<sup>2+</sup>-NTA resin, followed by incubation of 1 hr at 4°C and washing with 50 mL Ni-NTA wash buffer (20 mM HEPES pH 7.5, 200 mM NaCl, 20 mM imidazole, 3 mM  $\beta$ -mercaptoethanol) and elution in 5 mL Ni-NTA wash buffer supplemented with 200 mM imidazole. The eluate was concentrated and the buffer exchanged to gel filtration buffer (20 mM HEPES, pH 7.5, 100 mM NaCl, 0.5 mM TCEP) before loading onto a 16/60 Superdex 75 size-exclusion chromatography column (GE healthcare, UK) pre-equilibrated with gel filtration buffer. Absorption at 280 nm was monitored and 2 mL fractions collected. Fractions containing protein were analyzed on a SDS-PAGE, pooled and concentrated in a microfiltrator (Amicon Ultra-15 Centrifugal Unit, 30 kDa, Merck Millipore). The protein was aliquoted (50  $\mu$ L), flash frozen in liquid nitrogen and stored at -80°C.

The full-length Bmh1 gene from *S. cerevisiae* cloned into the pCDF expression vector and overexpressed as an N-terminal Streptavidin-tagged Bmh1 in *E. coli* BL21(DE3). Protein expression conditions are the same as for Hst2. Cells were lysed in 50 mM Tris pH 8, 300 mM NaCl, 3 mM  $\beta$ -mercaptoethanol, 10% glycerol. The supernatant was incubated with Pierce™ High Capacity Streptavidin Agarose, washed with the same buffer and Strep-Bmh1 eluted with additional 10 mM desthiobiotin. Strep-Bmh1 was further purified on a Superdex 200 column (GE Healthcare) in 20 mM Tris pH 8, 100 mM NaCl, 0.5 mM TCEP, 10% glycerol.

Phosphorylated Hst2 S320ph and S324ph were prepared by quickchange mutagenesis-based cloning into pCDF expression vector and overexpressed as an N-terminal His-tagged protein in *E. coli* BL21  $\Delta$ serB (DE3) cells containing pKW2-EF-Sep (a chloramphenicol resistant plasmid containing SepRS2, pSer-tRNAB<sub>4CUA</sub> and EF-Sep)<sup>164</sup> were transformed with pCDF-His-yHst2 S320TAG or S324TAG. Cells were grown at 37°C in LB medium containing 50  $\mu$ g/mL spectinomycin and 34  $\mu$ g/mL chloramphenicol and used next day to inoculate 4 L LB-SC 1:50. Protein expression was induced

at OD<sub>600</sub>=0.5 with 1 mM IPTG, and cells were harvested after 4 h at 37°C. Purification followed the same protocol as for unmodified Hst2. All proteins were stored at -80°C.

For purification of GFP nanobodies and subsequently conjugating them to beads, shuffle express competent *E. coli* cells were transformed with pK63 GFP nanobody plasmid. Overnight cultures of 200mL were started from single colonies at 37°C in LB containing 50 µg/mL kanamycin. Next day, the preculture was used 1:5 to inoculate 4 L LB medium and protein expression induced with 0.5 mM IPTG at OD<sub>600</sub> = 0.5, and incubation continued for 4 hours at 25°C. Cells were harvested, suspended in Ni<sup>2+</sup> wash buffer and 1 mM PMSF supplemented with lysozyme (~0.5 mg/mL), DNase (1 mg), protease inhibitor cocktail (Roche) and disrupted with a pneumatic cell disintegrator. Soluble His-yHst2 was purified by Ni-NTA affinity chromatography using His-Pur™ Ni<sup>2+</sup>-NTA resin, followed by incubation of 1hr at 4°C and washing with 50 mL Ni-NTA wash buffer and elution in 5 mL Ni-NTA wash buffer supplemented with 200 mM imidazole. The eluate was concentrated and dialyzed to 200mM NaHCO<sub>3</sub>, 200mM NaCl pH 8.3 and incubated with 4mL CH-Sepharose 4B beads preswollen in 1mM HCl for 5 hrs at 4 °C. The beads were subsequently washed with NaHCO<sub>3</sub>/NaCl to remove unbound sample blocked with 0.1M Tris pH 8 at RT and stored in 10mL 20% Ethanol solution at 4 °C.

#### **2.2.2.6 IN VITRO KINASE ASSAY**

Recombinant active 1 µg AuroraB delta45/InBox Incenp or Ipl1/Sli15 as well as other human mitotic kinases (Mps1, CDK1/Cyclin8, Haspin, Plk1, Bub1 and Bub1/Bub3) were incubated with 20µg substrate-Hst2 in the absence or presence of 2mM ATP and 1 mM MgCl<sub>2</sub> in a 50 µL total reaction volume. Reactions were incubated at 30°C for 2 hours and terminated by addition of Laemmli SDS sample dilution buffer. Proteins were separated by 10% SDS-PAGE, and phosphorylation was visualized by phospho-specific staining with Invitrogen™ Pro-Q™ Diamond Phosphoprotein Gel Stain.

### 2.2.2.7 ISOTHERMAL CALORIMETRY (ITC)

ITC experiments were performed in 20 mM HEPES pH 8, 100 mM NaCl, 0.5mM TCEP at 30°C using a iTC200 microcalorimeter (MicroCal). 300  $\mu$ M peptide (Table 2.16) were titrated into the cell containing 30 $\mu$ M of Hst2. The reference cell contained water. To obtain the  $K_d$  value, binding isotherms were fitted with the nonlinear least squares method, assuming one set of binding sites, by Origin (Version 7.0, MicroCal).

### 2.2.2.8 CO-PRECIPIATION EXPERIMENTS WITH YEAST LYSATES

BY4741 Yeast cells were transformed with 2-micron pRS-Flag tagged Hst2 plasmid and lysates were prepared by growing these cells in YPD medium to OD<sub>600</sub>=1.7–3.0, resuspended in PBS pH 7.0 supplemented with protease inhibitors (1 mM phenylmethanesulfonylfluoride and each 5  $\mu$ g/mL chymostatin, leupeptin, aprotinin and pepstatin A) as well as with or without Phosphatase inhibitor (PhosSTOP™ Sigma Aldrich). Subsequently, cells were lysed by flash freezing in liquid nitrogen and grinded using RETSCH ZM 200 Ultra Centrifugal Mill, thawed and cleared the supernatant by centrifugation (20000 rpm, 4°C for 15 minutes). The soluble yeast lysate (total protein concentration ~3 mg/ml) was incubated with ANTI-FLAG M2 agarose beads (Table 10) and set on a rotor at 4°C for 1hr. Beads bound protein fractions were further precipitated by centrifugation (1000 rpm at 4°C for 5 minutes), next beads were washed six times with 500  $\mu$ L PBS pH 7.0 with 0.2% Triton® X-100 and ultimately denatured with SDS buffer, analyzed by SDS Page and western blotted with respective antibodies (Table 9) Additionally, similar experiments with untagged Hst2 were performed for negative control.

### 2.2.2.9 *IN VITRO* PULLDOWNS

20  $\mu$ L 50:50 slurry of Pierce. Avidin Agarose Resin were washed three times with PBS (1 min incubation in buffer followed by centrifugation with 1000 rpm at 1 min). 5 mg/mL of individual recombinant proteins Bmh1 and wildtype/phosphoserine containing Hst2 or 1:1 combination of Bmh1 and Hst2 were added and the samples were incubated for 1h at RT while shaking (300 rpm). Unbound fractions were removed by three washing steps. Proteins recovered on the beads were eluted by boiling in SDS-PAGE loading buffer, analyzed by 10% SDS-PAGE and stained with Coomassie Brilliant Blue.

### 2.2.2.10 LUCIFERASE ASSAY

KDAC activity was measured in continuous assay format using Firefly Luciferase (FLuc) K529ac<sup>178</sup>. Reactions contained 200 nM Hst2 (unmodified or phosphorylated), NAD<sup>+</sup> at concentrations from 0 – 4 mM, FLuc K529ac (suitably diluted to match the sensitivity of the luminometer) in 50  $\mu$ l KDAC buffer (25 mM Tris/HCl pH 8.0, 137 mM NaCl, 2.7 mM KCl, 1 mM MgCl<sub>2</sub>, 1 mM GSH). To assay luciferase activity, an equal volume of 40 mM Tricine pH 7.8, 200  $\mu$ M EDTA, 7.4 mM MgSO<sub>4</sub>, 2 mM NaHCO<sub>3</sub>, 34 mM DTT, 0.5 mM ATP and 0.5 mM luciferin was added, and luminescence recorded for 30 min at 30°C in a FluoStar Omega Microplate Reader (BMG Labtech). All experiments were executed in triplicate, averaged and reactions without the enzyme were used for background subtraction. Initial rates were determined from the linear phase of the reactions. The kinetic parameters (apparent  $K_M$  and  $k_{cat}$ ) were obtained by fitting the data to the non-linear regression Michaelis-Menten model in GraphPad Prism 8 software.

## 2.2.3 YEAST METHODS AND CROSSLINKING

### 2.2.3.1 YEAST CULTURING

Wildtype yeast strains (Table 16) were grown and maintained on standard YPD medium. Auxotrophic yeast strains transformed with desired plasmids were cultured in standard SD medium supplemented with the required amino acid(s), allowing propagation and maintenance of plasmid(s) with selectable markers. The carbon source varied due to experimental setup (final concentrations: 2 % (w/v) glucose or galactose. Cells were normally grown at 30 °C with 200 rpm in erlenmayer flasks. For temperature sensitive strains (cdc15-2ts and cdc 28-1/2 ts) altered temperatures were used dependent upon the strain. For yeast growth assays, cells were grown as stated above and OD measured at regular intervals. For plating of yeast cells on nicotinamide plates, serial dilutions of yeast cultures in ddH<sub>2</sub>O were performed and samples were spotted on YPD agar plates supplemented with varied concentrations of nicotinamide with replicator tool.

### 2.2.3.2 YEAST CELL LYSIS

The yeast cell is difficult to lyse because of its rigid cell wall. Therefore, techniques for protein extraction from yeast often involve harsh mechanical treatment while using strong reducing agents, chemicals and pH and temperature extremes. Here, diverse methods were employed for yeast cell lysis. For whole cell lysate, cell pellets of 12 OD units were collected and lysed either following NaOH/TCA protocol or using a commercially available detergent mix called Y-PER. In preparation for immunoprecipitation of histones or colP of Hst2, cell pellets from 1 litre of cell cultures were resuspended in 5 mL lysis buffer (v/v, Table 4) and lysed by flash freezing in liquid nitrogen and disruption by ultra-centrifugal rotor mill (Retsch ZM200). The adherent cell lysate was scraped off the rotor mill and gently transferred into a centrifugation tube and clarified by harvesting with rotor JA-20 at 20.000 rpm for 15 min at 4 °C. Soluble

proteins were subsequently purified from the supernatant and histones extracted from the insoluble cell pellet using high salt and detergents.

### 2.2.3.3 *IN VIVO* CROSSLINKING USING pBPA IN YEAST

Plasmids containing histone amber mutations were cotransformed into BY4741 yeast cells using standard yeast transformation protocol with the plasmid pESC pBPA-RS (LEU). The plasmid pESC pBPA-RS harbors the amber suppressor *E. coli* tyrosyl tRNACUA and the evolved *E. coli* tyrosyl-tRNA synthetase (TyrRS) for the incorporation of pBPA, plated on yeast selection plates and stored at 30°C. After 2-3 days, a single colony of transformed yeast cells was used to inoculate a 4 mL overnight culture. For full-length expression of pBPA mutants, cultures were inoculated at an OD<sub>600</sub> of 0.2-0.3 in fresh SD medium (-Leu, -Ura) supplemented with 1 mM pBPA (4-Benzoyl-L-phenylalanine). Cells were harvested at late exponential phase (approximately 12 units) by centrifugation and resuspended in 200 µL of sterile 1x PBS buffer. Samples were subjected to 365 nm UV irradiation on ice (Vilber Lourmat VL-208.BL, 365nm tubes, 2x8W). The distance from the light source to the samples was approximately 5 cm, typically crosslinking was performed for 7 to 15 min. Samples were either stored at -20°C or processed further for preparation of whole cell lysates.

### 2.2.3.4 IMMUNOPRECIPITATION OF HISTONES AND CROSSLINKS

In order to identify crosslinks of histones<sup>179</sup>, plasmids containing histone amber mutations (URA) were cotransformed into BY4741 yeast cells along with the plasmid pESC pBPA-RS (LEU). Two days before harvest, a single colony of transformed yeast cells was used to inoculate a 20 mL overnight culture (supplemented with 1mM pBPA). The next morning, the entire overnight culture was used to inoculate 4 x 200 mL cultures (each supplemented with 1mM pBPA) and cells were grown over four cell cycles at 30 °C. Then, each 100 mL cell culture were used to inoculate 900 mL main cell culture (+1 mM pBPA), which were grown as 8x1L cultures separately overnight at 30 °C. The

next morning, the main culture were harvested by centrifugation with rotor JA-8.1000 (Beckman Coulter, Krefeld) at 4800 rpm and 4 °C for 15 min, washed with dH<sub>2</sub>O and resuspended in 20 mL PBS media. 4 L of above pelleted yeast cells were irradiated with 365 nm UV-light from a distance of ~5 cm at 4 °C for 15 mins from a UV cross-linking apparatus (Vilber Lourmat lamp, 2x 8 W, 365 nm tubes, 32 W, 230 V #VL-208.BL) and the other 4L were treated as control. Preparation of cell lysis was performed by resuspending the cells in 1:1 v/v lysis buffer (Table 4). The cells were lysed by flash freezing in liquid nitrogen and disruption by ultra-centrifugal rotor mill (Retsch ZM200). The adherent cell lysate was scraped off the rotor mill and gently transferred into a centrifugation tube and then clarified by centrifugation with rotor JA-20 (Beckman Coulter, Krefeld) at 20,000 rpm for 20 min at 4 °C. To extract chromatin associated proteins from the insoluble pellet fraction, 25 mL extraction buffer (Table 4) was added to the sample, followed by vortexing and incubation for 1 h at room temperature on a tumbler. The protein extract was clarified by centrifugation with rotor JA-20 (Beckman Coulter, Krefeld) at 20,000 rpm for 30 min at 4 °C, and the resulting supernatant was collected and filled the supernatant into a dialysis membrane tube (MWCO 6–8 kDa, e.g., Spectra/Por<sup>®</sup>) and dialysed two times against 1 L dialysis buffer at RT. If a precipitate after dialysis was visible, it was spun for 3 mins at 3500 rpm at RT and the supernatant was used for further steps. Isolation of histone proteins from supernatant was performed by affinity chromatography with a 5 mL ion exchange HiTrap SP FF column (GE Healthcare), equilibrated in urea loading buffer (Table 4). Elution of histone proteins was performed by washing the column with 100% urea elution buffer, containing 1 M NaCl. The resulting peak fractions were pooled and concentrated with a 10k MWCO Amicon ultra-centrifugal concentrator (Merck, Darmstadt) to a final concentration of 0.5-1.0 mg/mL. The concentration was determined by standard Bradford test. The concentrated sample was subsequently mixed with a 5-fold excess of 1.2x IP-buffer (Table 4) resulting in a final concentration of 1x IP-buffer in the sample, and incubated with 150 µL slurry of the HA-agarose beads (prewashed once in 1x TBS, once in 1x IP-buffer, followed by centrifugation at 2000 rpm for 1 min) incubated on

a tube roller at 4°C for 3 hrs. Following which the beads were centrifuged at 2000 rpm for 1 min and washed thrice with 1x IP-buffer, 1x TBS (150 mM NaCl +0.05% Tlen 20). Proteins were eluted by resuspending the beads in 50 µL preheated 4x SDS loading buffer at 95 °C, and boiling for 20 min. The prepared sample were then run on 4-12% Bis-Tris NuPage SDS gels in the form of technical triplicates at 120V for 15mins. Gels were stained with Instant Blue to visualize the protein bands.

### 2.2.3.5 IN-GEL TRYPsin DIGESTION OF PROTEINS FOR MS/MS ANALYSIS

For mass spectrometry, samples from the pull-down were digested in gel using proteomics grade trypsin protease (Sigma Aldrich). Before digestion, each gel lane was horizontally cut into small pieces (~1 mm<sup>3</sup> cubes) with a surgeon knife and transferred with a spatula into Protein Low binding Eppendorf tubes (Thermo Scientific Pierce) containing 500 µl of Fixation solution (5:4:1 - H<sub>2</sub>O: EtOH: Acetic acid). The tubes were incubated at 300 rpm in a Thermoshaker overnight at RT, followed by centrifugation at 14000 rpm for 10 secs next day. The supernatant was removed, the gel pieces were resuspended in 200 µl washing solution 1 (3:1 – 25 mM NH<sub>4</sub>HCO<sub>3</sub>: Acetonitrile) and incubated for 30 min at 37°C and 600 rpm. Again, the tubes were centrifuged and the supernatant removed. The gel pieces were washed in 200 µl of washing solution 2 (1:1 – 25 mM NH<sub>4</sub>HCO<sub>3</sub>: Acetonitrile) and incubated for 15 min at 37°C and 600 rpm. Following this the proteins were reduced in 200 µl reducing solution (50 mM DTT in 25 mM NH<sub>4</sub>HCO<sub>3</sub>) for 45 min at 37°C and 600 rpm. The reducing solution was exchanged for alkylating solution (55 mM iodoacetamide in 25 mM NH<sub>4</sub>HCO<sub>3</sub>). The gel pieces were washed subsequently twice with washing solution 2 and once with acetonitrile. The gel pieces were dried in hood for 30 min and resuspended in 75 µl trypsin buffer, followed by an incubation for 15 min at 600 rpm. Following which, the samples were incubated at 30°C overnight at 350 rpm in 75 µl 25 mM NH<sub>4</sub>HCO<sub>3</sub>. Next day, the reactions were stopped by addition of 10 µl 10% Trifluoroacetic acid and

sonicated for 30 min on ice. Gel pieces were dried using 75  $\mu$ L Acetonitrile. Eluted samples were dried using a Speedvac and stored at  $-20^{\circ}\text{C}$  until measurement.

### 2.2.3.6 NANO HPLC-MS/MS

After tryptic digestion and purification, the protein fragments were analyzed by nano-HPLC-MS/MS by using an Ultimate<sup>TM</sup> 3000 RSLC nano-HPLC system, and a Q Exactive<sup>TM</sup> Plus Hybrid Quadrupole-Orbitrap mass spectrometer equipped with a nano-spray source (all from ThermoFisher Scientific). Briefly, the lyophilized tryptic peptides were suspended in 20  $\mu$ L 0.1% TFA, and 3  $\mu$ L of the samples were injected onto and enriched on a C18 PepMap 100 column (5  $\mu$ m, 100  $\text{\AA}$ , 300  $\mu$ m ID \* 5 mm, Dionex, Germany) using 0.1% TFA, at a flow rate of 30  $\mu$ L/min, for 5 min. Subsequently, the peptides were separated on a C18 PepMap 100 column (3  $\mu$ m, 100  $\text{\AA}$ , 75  $\mu$ m ID \* 50 cm) using a linear gradient, starting with 95% solvent A/5% solvent B and increasing to 30.0% solvent B in 90 min, with a flow rate of 300 nL/min (solvent A: water containing 0.1% formic acid; solvent B: acetonitrile containing 0.1% formic acid). The nano-HPLC apparatus was coupled online with the mass spectrometer using a standard coated Pico Tip emitter (ID 20  $\mu$ m, Tip-ID 10  $\mu$ m, New Objective, Woburn, MA, USA). Signals in the mass range of m/z 300 to 1650 were acquired at a resolution of 70,000 for full scan, followed by up to ten high-energy collision-dissociation (HCD) MS/MS scans of the most intense at least doubly charged ions at a resolution of 17,500. Protein interaction partner identification and relative quantification were performed by using MaxQuant<sup>180</sup> v.1.6.1.0, including the Andromeda search algorithm and searching the *Saccharomyces cerevisiae* reference proteome of the UniProt database. Briefly, an MS/MS ion search was performed for enzymatic trypsin cleavage, allowing two missed cleavages. Carbamidomethylation was set as a fixed protein modification, and oxidation of methionine and acetylation of the N-terminus were set as variable modifications. The mass accuracy was set to 20 ppm for the first search, and to 4.5 ppm for the second search. The false discovery rates for peptide and protein

identification were set to 0.01. Only proteins for which at least two peptides were quantified were chosen for further validation. Relative quantification of proteins was performed by using the label-free quantification algorithm implemented in MaxQuant. All experiments were performed in technical duplicates of biological duplicates. Statistical data analysis was performed using Perseus<sup>181</sup> v.1.6.1.1. Label-free quantification (LFQ) intensities were log-transformed (log<sub>2</sub>); samples from pulldown experiments using Flag-HST2 were grouped together and samples from control experiments were also grouped together. Proteins had to be quantified at least three times in at least one of the groups to be retained for further analysis. Missing values were imputed using small normal distributed values (width 0.3, down shift 1.8), and a t-test ( $\alpha = 0.01$ , FDR = 0.05) was performed. Proteins that were statistically significant outliers and enriched in samples from experiments using Flag-HST2 were considered as hits. For the identification of HST2 phosphorylation sites the MaxQuant search was repeated with the same parameters, but phosphorylation of S, T, and Y were included as variable modifications.

### 2.2.3.7 CELL CYCLE SYNCHRONIZATIONS IN YEAST

Cell cycle synchronizations were performed in W303a cells with a temperature-sensitive *cdc15-2* allele containing plasmids encoding H2B or H3 pBPA-mutants. An overnight culture of 4 ml in SC-Ura/Leu minimal medium (supplemented with 1 mM pBPA) was diluted to an OD<sub>600</sub> = 0.2 in 50 ml YPD and incubated with shaking at 25°C until an OD<sub>600</sub> of 0.5 was reached. Cells were then shifted for 2 h to 37°C with shaking to arrest cells in telophase<sup>182</sup>. Following complete arrest (as determined by FACS analysis<sup>183</sup>) cells were released into 50 ml YPD at an OD<sub>600</sub> = 0.5 at 25°C. Samples were taken at indicated time points, crosslinked and processed as described above.

To synchronize cells in G<sub>1</sub>, the mating pheromone alpha-factor (GenScript) was added to log phase cultures grown to OD<sub>600</sub> = 0.4–0.6 (MATa yeast strains BY4741) to a final concentration of 15 µg/mL. Cells were incubated for 1 hr at 30°C at which time an

additional dose of 7.5  $\mu\text{g}/\text{mL}$  of  $\alpha$ -factor was added and cells incubated for one more hour. Cells were monitored periodically by microscopy. Cells were collected by centrifugation at 4000 rpm for 2 mins and processed for further experiments. To synchronize cells in metaphase, one dose of nocodazole (Sigma) to a final concentration of 15  $\mu\text{g}/\text{mL}$  was added to log phase cultures ( $\text{OD}_{600} \approx 0.5$ ) for 2hrs. The cells were monitored by microscopy and collected and precipitated as above. To synchronize cells in S phase, 100mM hydroxyurea (sigma) were added to exponentially growing cells in YPD ( $\text{OD}_{600} \approx 0.3$ ) and incubated culture for two hours at 30°C, after which they were monitored by microscopy and collected and precipitated as above.

### 2.2.3.8 FACS ANALYSIS IN YEAST

For the analysis of the DNA content<sup>183</sup>, yeast cells were grown in (YPD) medium to an  $A_{600}$  of approximately 0.4–0.6.  $1 \times 10^6$  cells were fixed in 70% ethanol overnight at 4°C, harvested, resuspended in 1 mL of 50 mM citrate buffer, pH 7.4 and sonicated for 10 seconds at setting 30% (1 sec on, 1 sec off) to disperse any potential clumps of cells. Cells were harvested, resuspended in 1 mL of 50 mM citrate buffer containing 0.25 mg/mL RNase-A (Sigma) and incubated for 2 hours at 50C. Proteinase-K(Sigma) (1 mg) was added and cells were incubated for additional 2 hours. Cells were harvested and resuspended in 1 mL of 50 mM citrate buffer, pH 7.4, containing 20  $\mu\text{g}/\text{mL}$  Sytox green (Sigma). Cells were incubated for 30 minutes at room temperature (RT), sonicated as above for 5 seconds and analyzed on a FACS BD Accuri™ C6 Plus flow cytometer (BD Biosciences), acquisition of  $1 \times 10^4$  events. The proportion of cells in each cell cycle stage was assessed with Flowjo software (version 9.0.2, Tree Star Inc, San Carlo, CA), Watson pragmatic model which fits the Gaussian DNA distribution curves to the stages of the cell cycle. Cell doublets were removed prior to analysis by plotting the area versus the width of FL-2 channel using the Flowjo software.

### 2.2.3.9 LIVE CELL IMAGING OF YEAST

For observation and confirmation of yeast cell synchronized in different stages of cell cycle based on their morphological feature, 1mL of yeast cells was collected by harvesting at 14000 rpm for 2 mins, followed by suspension of cells in 200  $\mu$ L of TAF buffer (Table 4). 1-5  $\mu$ L of cells were spread onto a microscope slide (Superfrost Microscope Slides from Thermo Scientific). The cover slip was sealed with nail polish and the slides were imaged immediately. Imaging was performed using Zeiss LSM 900 with the Zeiss Objective 63x using immersion oil.

### 2.2.3.10 YEAST-TWO-HYBRID STUDIES

Yeast two-hybrid allows detection of interaction between two proteins based on the reconstitution of a functional transcription factor (TF) which allows the transcription of a reporter gene leading to growth or change of phenotype of yeast cells. Here, HST2 was cloned into GAL4 transcription factor DNA binding domain containing pGBKT7 vector using EcoRI/Sall sites and BMH1/2 genes cloned into GAL4 transcription factor DNA activation domain containing pGADT7 vector using EcoRI/BamHI sites. Using the one-step transformation protocol for yeast in stationary phase,<sup>63</sup> the generated vectors containing the putative targets as well as the empty vectors (to test for auto-activation) were transformed into yeast strains AH109 (pGBKT7 bait vectors) or Y187 (pGADT7 prey vector) and transformants were selected on SD plates deficient of tryptophane (SD-Trp) or leucine (SD-Leu), respectively. Subsequently, all different combinations of the AH109 yeast strain containing the bait vectors and the Y187 yeast strain containing the prey vectors were mated and plated on SD plates deficient of tryptophane and leucine (SD-Trp-Leu) and grown for 3 days at 30 °C. Protein-protein interactions were subsequently screened by resuspending a single colony from the mating plates in 50  $\mu$ l 0.9 % NaCl solution and plating 3  $\mu$ l thereof on SD-Trp-Leu plates containing X- $\alpha$ -Gal with and without histidine and growing the cells for 3–4 days at 30 °C. The strength of interaction was estimated from the comparative growth

of yeast cells on minimal media lacking either adenine or histidine or both. Mating of yeast cells (Y2HGold or AH109 strain) containing either the pGBKT7–53 or pGBKT7-Lam vectors with yeast cells (Y187 strain) containing the pGADT7-T vector (all Clontech Laboratories, Inc.) served as positive and negative controls, respectively.

### 2.2.3.11 RNA ISOLATION FROM YEAST

RNA isolation from yeast is based on extraction using phenol: chloroform method. Addition of this mix causes phase separation of the sample into a lower organic phase mainly constituting proteins and upper aqueous phase containing nucleic acids, because of unique properties of phenol. Moreover, at lower pH of 4-6, DNA remains in the organic phase leaving RNA in the upper aqueous phase. Addition of chloroform removes protein contaminations and improves the efficiency of RNA extraction. Here, 4 mL of overnight wildtype and *siz1,2* knockout strains were harvested by centrifugation at 14000 rpm for 2 minutes at indicated time points before and after galactose induction. From these cell pellets, total RNA was extracted using the hot-acidic phenol method. Briefly, cells were resuspended in 600 µl of freshly prepared TES buffer (10 mM Tris-Cl, pH 7.5 10 mM EDTA 0.5% SDS). 600 µl of acidic-phenol (Ambion) was added and the solution was immediately vortexed vigorously for 30 seconds. Samples were incubated at 65°C for 90 min under rotation at 300 rpm. The solution was kept on ice for 10 minutes and spinned down at 14000 rpm for 10 minutes at 4°C. The aqueous top layer was transferred to a new tube and 600 µl of chlorophorm was added and immediately vortexed. Cells were centrifuged as above after which the aqueous layer was transferred to a new pre-chilled eppendorf tube. RNA was precipitated overnight at –20°C with 2.5 volumes of 100% ethanol and 10% (v/v) sodium acetate, pH 5.4 and washed with 75% ethanol. After drying on ice, RNA was eluted with RNase free water and stored at –80°C. The quality of RNA was checked by running on 12 % denaturing RNA Urea-PAGE gels. cDNA was generated using the superscript-III reverse transcriptase (Invitrogen) according to the manufacturer's

protocol. Briefly, 1-2 µg of total RNA was used in a 20 µl reaction mixture using random primer mix or oligodT-20 (Invitrogen). Relative amounts of cDNAs of GAL1 genes were measured by real time quantitative PCR (RT-qPCR). Expression of GAL1 gene was normalized to expression of  $\beta$ -Actin (ACT1) from the same RNA preparation. Oligo sequences used are mentioned in Table 18.

#### 2.2.3.12 RT-PCR ANALYSIS

GAL1 and ACT1 gene expression levels samples were quantified by quantitative real-time PCR on a CFX96 Touch Real-Time PCR Detection System. In contrast to a conventional PCR, where the amplified product is detected by an end-point analysis, in real-time PCR the amplified product is detected and measured as the reaction progresses. This is done by including a fluorescent molecule such as SYBR Green I which binds to double stranded DNA as it accumulates. Increase in fluorescent signal is proportional to quantitatively increase in amount of DNA. Enrichment of GAL1 gene levels in relative quantification to housekeeping gene such as actin was calculated using the  $\Delta C_t$  method as follows:  $1/(2^{[C_t - C_{t_{control}}]})$ .

## 3 RESULTS

### 3.1 IDENTIFICATION OF CHROMATIN INTERACTION TOPOLOGY WITH GENETICALLY ENCODED UV-CROSSLINKER

So as to profile interactions encompassing core histones in their innate setting, a chemical proteomics approach was employed (Figure 10). This strategy which was pioneered by Chin and Schultz, entails the addition of photo-activatable crosslinker amino acid in histones in retort to amber (UAG) stop codons<sup>150,184</sup>. This is followed by photo crosslinking with long-wavelength ultraviolet light (365 nm) that consequences in the creation of binary covalent adducts between *p*-benzoyl-L-phenylalanine (pBPA) and aliphatic side chains of other amino acids by radical mechanism. These are then purified from whole cell lysates by acid extraction or enrichment and purification of histones under high salt denaturing conditions, as explained here, which are ultimately quantitated by western blot or analyzed by Mass spectrometry.

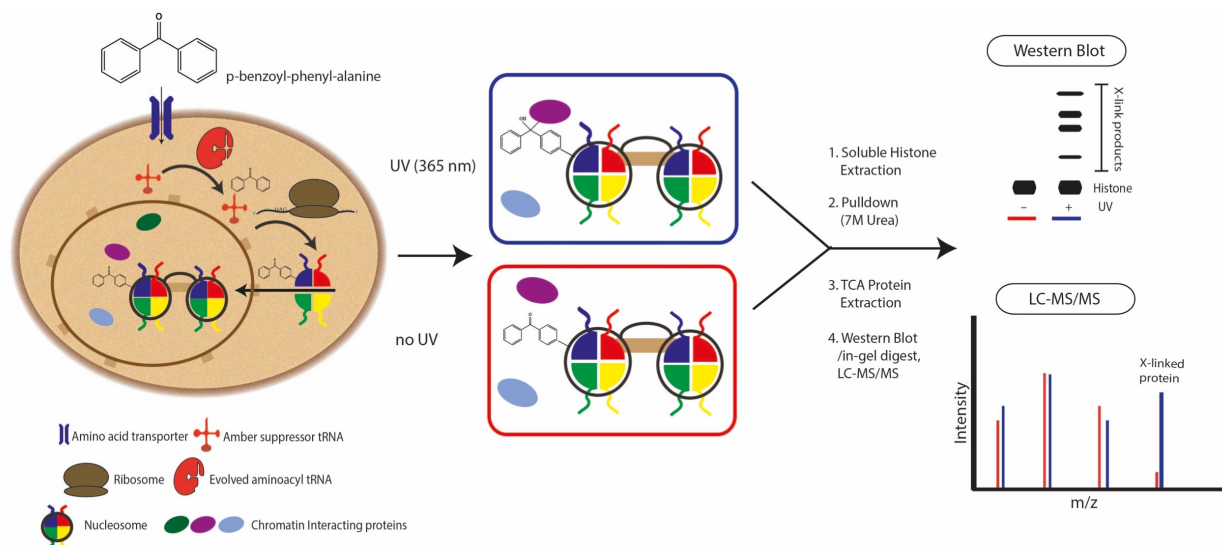


**Figure 10 : Chromatin Crosslinking pipeline with encoded UV-Crosslinker, pBPA**

So as to identify site-specific protein interactors of histones, a pipeline was established which allowed purification and enrichment of histones containing BPA under denaturing conditions, refolding of histones and identification of crosslinked interacting proteins to those sites by western blotting merged with quantitative Mass spectrometry.

The chief rewards of pBPA mediated photo crosslinking is that it permits identification of exceedingly transient interactors in their native setting which are often neglected by routine immunoprecipitation methods and it accelerates investigation of the interaction topology of proteins at single amino acid resolution. In a pursuit to exploit these potentials, the interactome of the nucleosome in living yeast was mapped by a comprehensive crosslink screening of a library of HA-epitope-tagged histone pBPA mutants. Using the structure of nucleosome, hundred discrete sites across its surface were selected to be modified to amber codon (pdb: 1ID3). BY4741 yeast cells were then co transformed with pESC BPARS plasmid expressing evolved orthogonal tRNA and tRNA synthetase for the incorporation of pBPA in retort to the amber codon as well as pRS plasmid which contained individual histone amber mutants.

Since I was probing the native system to my advantage, one of the scenarios that could not be excluded was the magnitude of toxicity produced by the amber suppressor system to the cells. To test this when I compared the growth rates of cells expressing some of the pBPA-containing histones, or only the HA-tagged histones to wildtype cells, I detected a decrease in growth rate (Figure 11A) and a rise in doubling time (upto ~3 hours) in the former cases (Figure 11B). This signified that manufacture of fragment by termination or mutation of histones did stress the cells to some extent. May be the alteration in carbon source affected the growth rate as the mutants were grown in minimal medium as opposed to wildtype cells grown in complete medium. Nevertheless, the biological inferences made must still be constant with the native setting because the mutant histones were manufactured as extra copy and simply represented a minute fraction of the whole histone amounts.

Furthermore, addition of the non-toxic crosslinker pBPA and exposure to non-damaging UV light ensured that the experiments preserved biological interactions. Samples after UV radiation and without UV as negative controls were isolated from whole

cell lysates following NaOH/TCA extraction protocol, the crosslinks were then run on 3-8% SDS-PAGE gels and HA-tagged-histones investigated by western blots using anti-HA antibody. The mapping of interaction interface by inspection of a large set of histone amber mutants ensued in a crosslink pattern exclusive for each individual histone site (Figure 12, Figure 13).

The screening was accomplished across representative positions encompassing the histone surfaces from the N-terminal domain through the central globular domain to the C-terminal domain. Across all sites, the quantities of full-length HA-epitope-tagged histones were akin in amounts (H3-HA: 17 kDa, H2B-HA: 16 kDa, H2A-HA: 15 kDa and H4-HA: 12 kDa). The crosslinks to histones were UV dependent and migrated slower on SDS gels due to higher molecular weights. They were highly diverse in addition to being exclusive simultaneously. This reproducible pattern could be characterized by molecular weight and individual densities. Crosslink band at ~30 kDa roughly indicated inter histone interactions. Moreover, proximal sites often showed similar pattern indicating an overlap of interaction topology.

Certain sites such as H2A: S17, H113, Q114, N115; H2B: K46, T51, H112, S115, K123; H3: A29, R53, K56, R69, E73, E76 and H4: R23, A56, Q27, A56, R67 displayed highly dense crosslink pattern signifying conceivable 'hot-spots' of associations and post translational modifications, while others just a modest number of crosslinks. In general, crosslink patterns were richer at N terminal tails which also harbor several acetylated and methylated amino-acid residues and assist as recognition sites for numerous proteins with reader domains such as Bromo, Chromo, PHD, Tudor, MBT<sup>185</sup>.

Although isolation of whole cell lysate and analysis by western blots helped us visualize chromatin interactors at spatio-temporal resolution, it did not help in identification of the trapped interaction partners. In subsequent section I combined *in vivo*

crosslinking with immunoprecipitation and a quantitative mass spectrometry-based approach for establishing identities of those interactors.

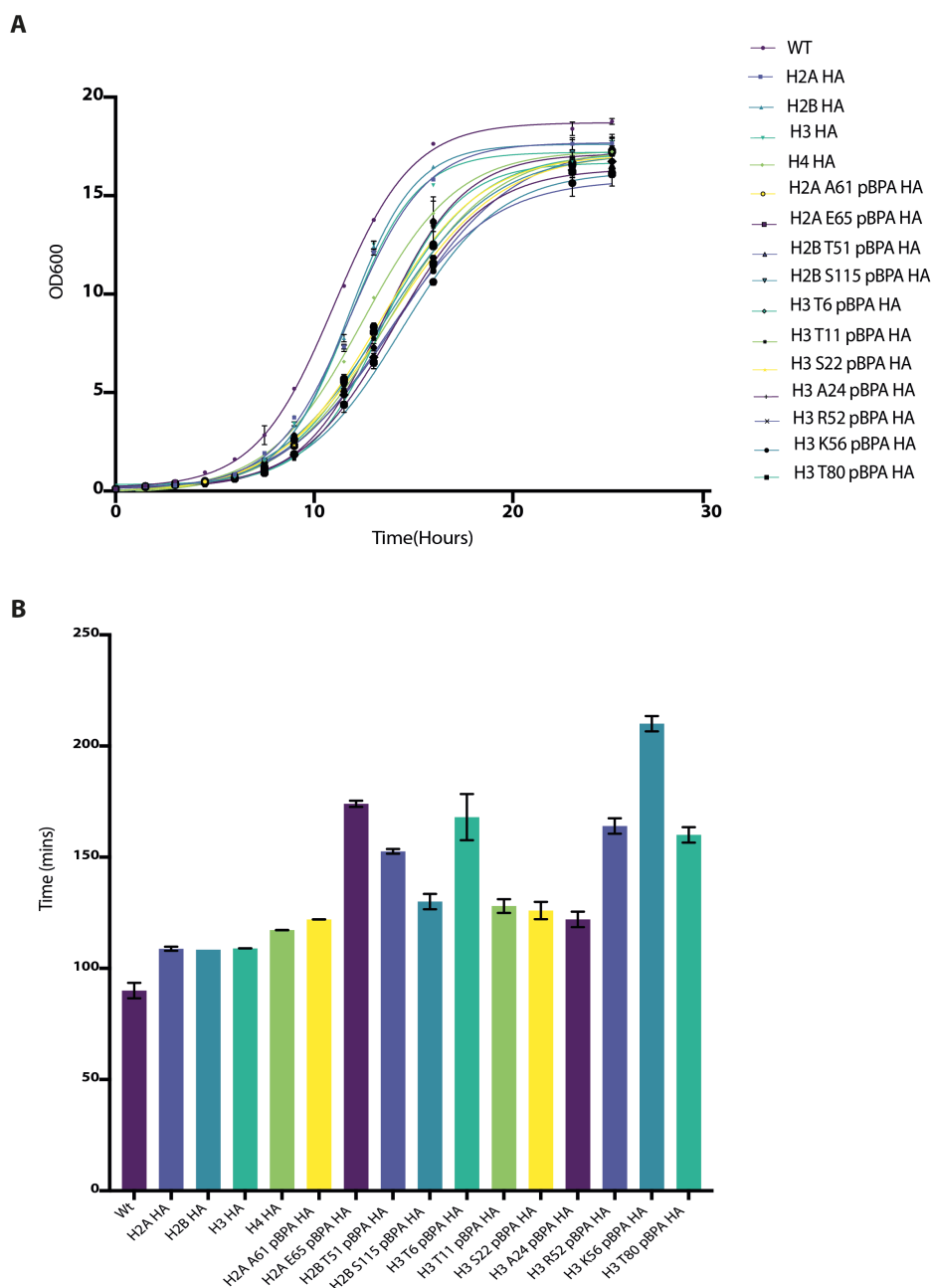


**Figure 11 : Comparative growth of Wildtype and Histone mutants.**

(A) BY4741 Wildtype yeast cells were grown in YPD medium and histone mutants expressing HA - tagged pBPA histone and aaRS/tRNA pair were grown in minimal medium (SD -Leu,-Ura). Overnight cultures were diluted to  $OD_{600} = 0.1$  and growth was examined at specified time points for biological triplicates of all samples. Growth curves were plotted using Boltzmann sigmoidal curve fitting option in Graphpad Prism 8 Software. Data are represented as mean  $\pm$  SD.

(B) Doubling time of Wildtype and Histone mutants was estimated using growth curve in (A). Data are represented as mean  $\pm$  SD.

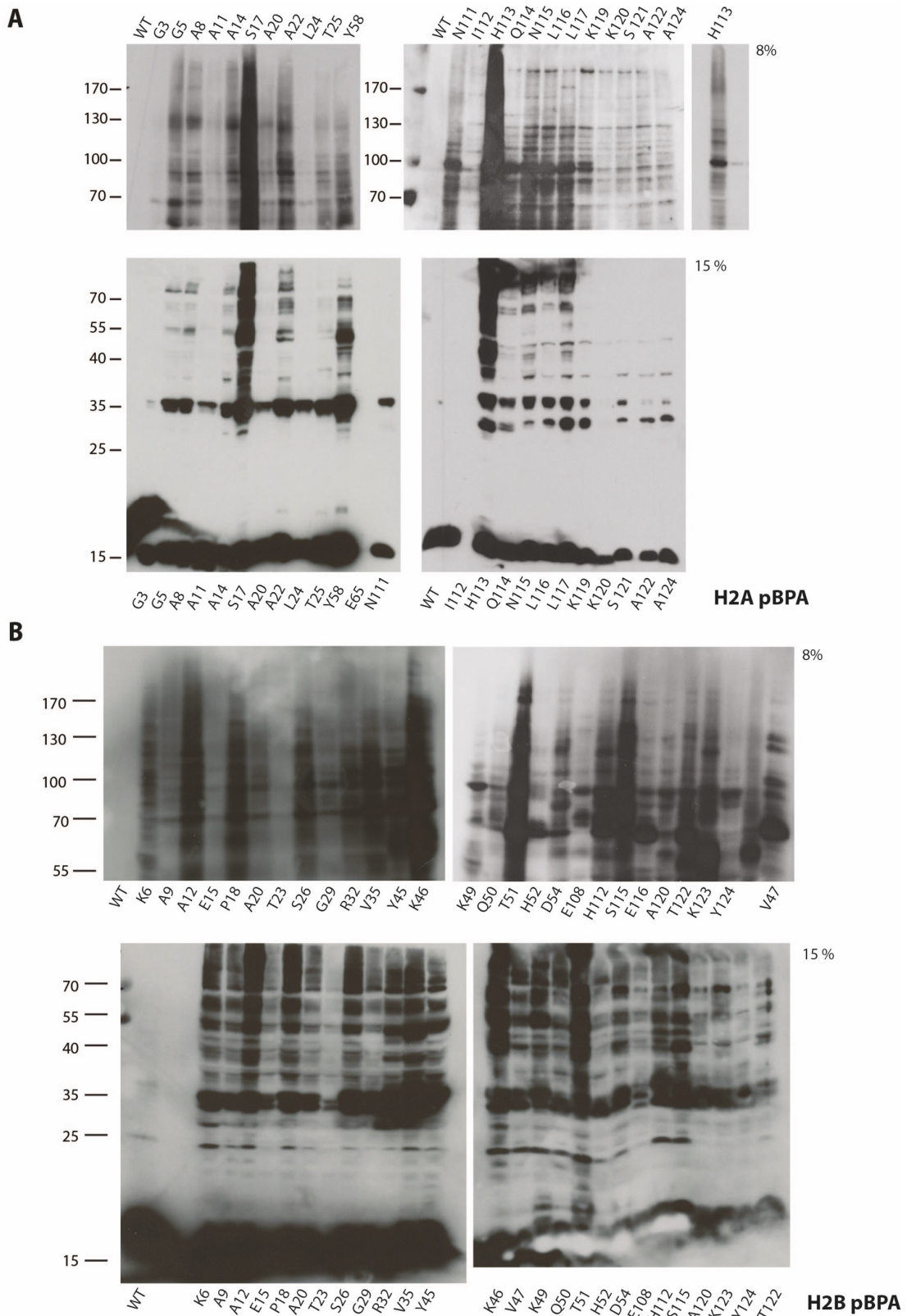


**Figure 12 : *in vivo* crosslink pattern throughout Histone H2A and H2B.**

Western Blot evaluation of histone (A) H2A- and (B) H2B-pBPA crosslink products. Yeast cells containing the specified pBPA-expressing histone were UV-irradiated and whole cell lysates examined by SDS-PAGE and Western Blot by means of anti-HA antibodies. (Data from Bryan J. Wilkins).

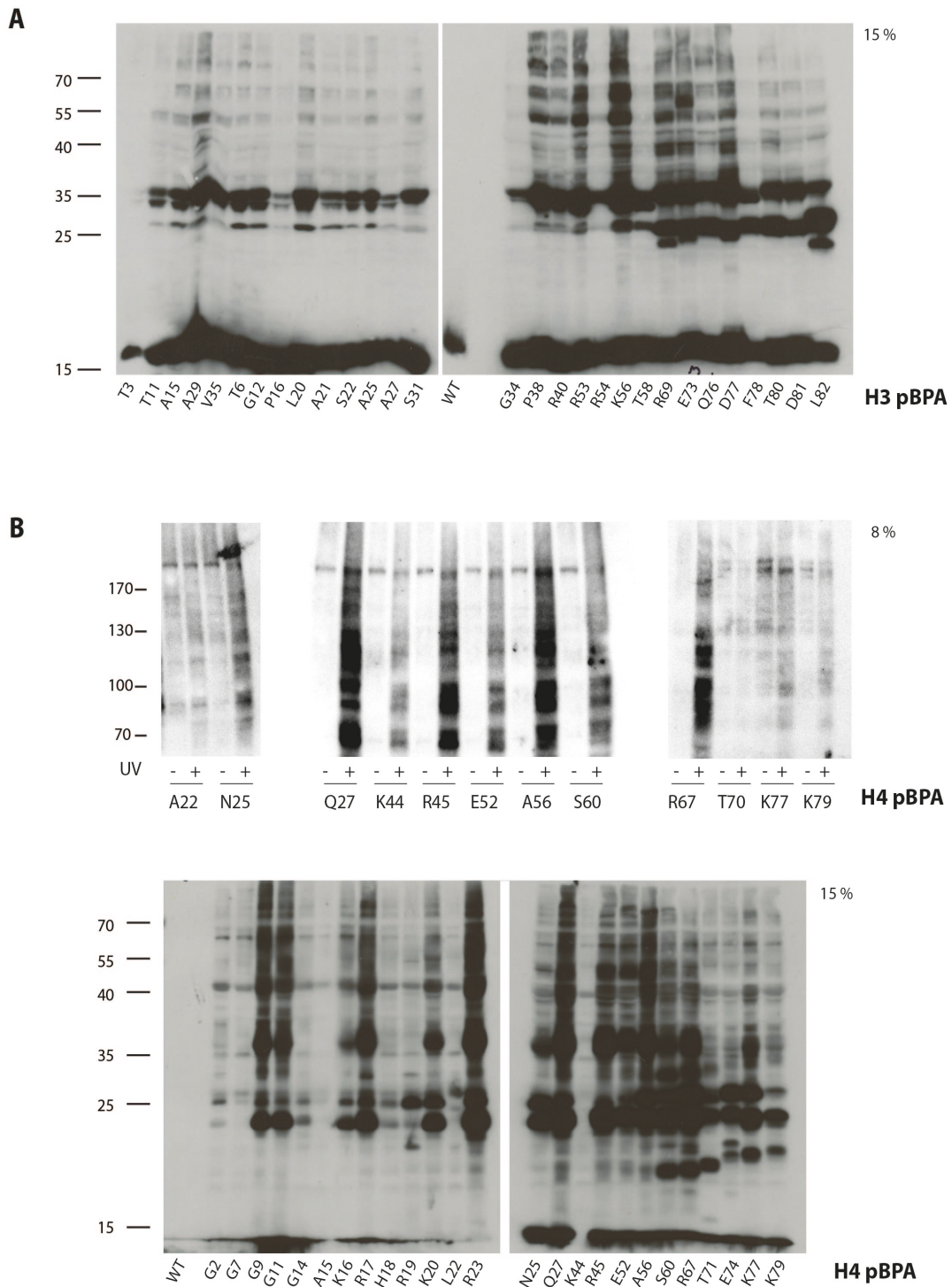


**Figure 13 : *in vivo* crosslink pattern throughout Histone H3 and H4.**

Western Blot analyses of histone (A) H3- and (B) H4-pBPA crosslink products. Yeast cells containing the specified pBPA-expressing histone were UV-irradiated and whole cell lysates examined by SDS-PAGE and Western Blot using anti-HA antibodies. (Data from Bryan J. Wilkins).

## 3.2 INVESTIGATION OF PROTEINS ASSOCIATING WITH HISTONES AT SINGLE AMINO ACID RESOLUTION

Identification of interaction partners of a protein of interest at its diverse domains not only yields a vast amount of structural information details but also provides insights into its functions. Nevertheless, identification of site-specific components of chromatin can be arduous due to the fact that chromatin attracts many cytosolic proteins that non-specifically bind to DNA by ionic interactions once cells are lysed. By *in vivo* photo crosslinking this problem can be overcome by freezing and detecting covalent interactions with intact chromatin. All experiments were performed in asynchronous BY4741 cells expressing the pESC BPARS plasmid for the incorporation of pBPA in response to the amber suppression codon as well as distinct histone amber mutants. Non-UV treated samples served as control. As described in 2.2.3.4 Immunoprecipitation of Histones and Crosslinks, this multistep purification approach led to an increase in the amount and purity of protein of interest, i.e. histones, and also allowed investigation of exclusive binders across its different interfaces.

### 3.2.1 ANALYSIS OF HISTONE H2B T51 pBPA AND CROSSLINK PRODUCTS

I chose a set of amino acid positions across histones which showed enriched crosslinking efficiency from the crosslinking survey (Figure 12 and Figure 13) for identification and characterization of their individual crosslink proteins. For example, to identify interactors that rely upon the sequence surrounding position T51 for interaction with histone H2B, yeast cells harboring histone H2B T51pBPA mutant (Figure 14A) were grown and UV-treated or non-UV-treated. The IP procedure included mechanical cell disruption, protein extraction with chaotropic agents, affinity purification and antibody-mediated protein isolation. After enrichment there was an obvious formation of UV-dependent crosslinking as seen by additional bands of crosslink products exclusively present in all replicates with UV light (Figure 14B). After in-gel digestion, proteins were identified by mass spectrometry and analyzed directly using MaxQuant

search. While simple MS/MS analysis of crosslinked, immunopurified samples can sometimes deliver a suitable candidate list, more sensitive detection of crosslinked species can be obtained by comparing crosslinked and non-crosslinked samples. The comparison can be performed computationally, using normalized spectral index quantification to compare MS/MS data obtained from crosslinked or non-crosslinked samples. This entire analysis was repeated for three biological replicates which were further compared to determine the potential hits present exclusively with UV crosslinked sample as visualised by a Venn Diagram (Figure 15A). 31 proteins (10% of all potential hits) were consistently and significantly enriched potential hits common to all UV dependent samples in three independent experiments and absent in non-UV treated samples.

To obtain biological information about these potential hits, a Gene Ontology analysis was carried out using the online tool '<http://geneontology.org/>'<sup>186,187</sup>. Results are presented as a bar chart ranked by fold enrichment of genes in UV crosslinked samples (Figure 15B). I used asynchronous cell populations and identified number of direct binders of H2B T51 amino acid position. Gene ontology (GO term) analysis revealed a strong overrepresentation of proteins from chromatin remodeling families, DNA helicases or ATP dependent chromatin interactors which dictate chromatin dynamics by their action on DNA or histones. With few exceptions of heat shock proteins and chaperons the top hits represent general histone binding proteins which are involved in regulatory processes such as chromatin remodeling and transcription: mainly RSC (Rsc2, Sth1, Sfh1), ISW1 (Ioc2, Ioc3) and CHD1. Intriguingly, RSC and ISW1 have recently been reported to be antagonistic in their mechanism of actions<sup>188,189</sup>.

Many of the proteins identified overlap in their domain organization or functions. For example, both Sth1 and Rsc2 house 1 and 2 bromodomains each. Many proteins also showed acetyl transferase activities. The repeated detection of the majority of these proteins indicates that they represent an inherent part of the sample. Although this

also holds true for non-specific binding proteins, the validation of STH1 as an interaction partner of H2B at position T51 (Figure 23, Figure 25) proves that interactions captured and identified by the described procedure here can be further validated for direct binding confirmations.

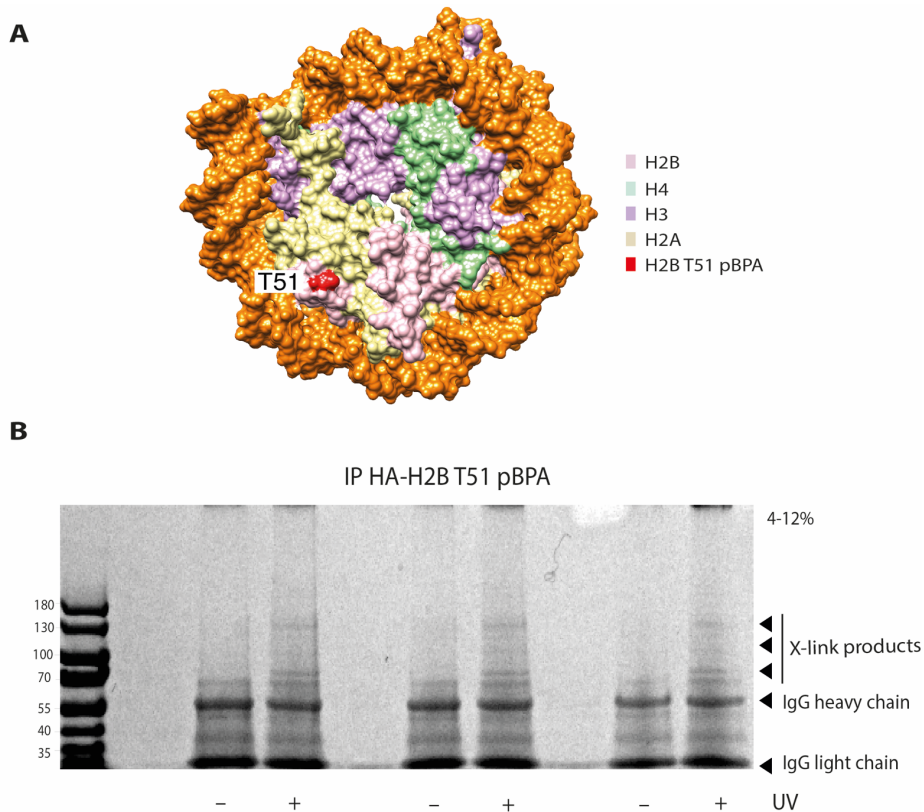


**Figure 14 : Immunoprecipitation of H2B T51pBPA crosslink products for MS analysis.**

(A) Schematic illustration showing H2B T51 pBPA site highlighted in red (pdb 11D3)

(B) Yeasts producing H2B-HA T51pBPA were irradiated with UV or left untreated. Crosslink products were precipitated under denaturing conditions with anti-HA beads and detected by colloidal Coomassie staining. Peptides were extracted from six consecutive slices from both samples (+/- UV) and analysed by MS.

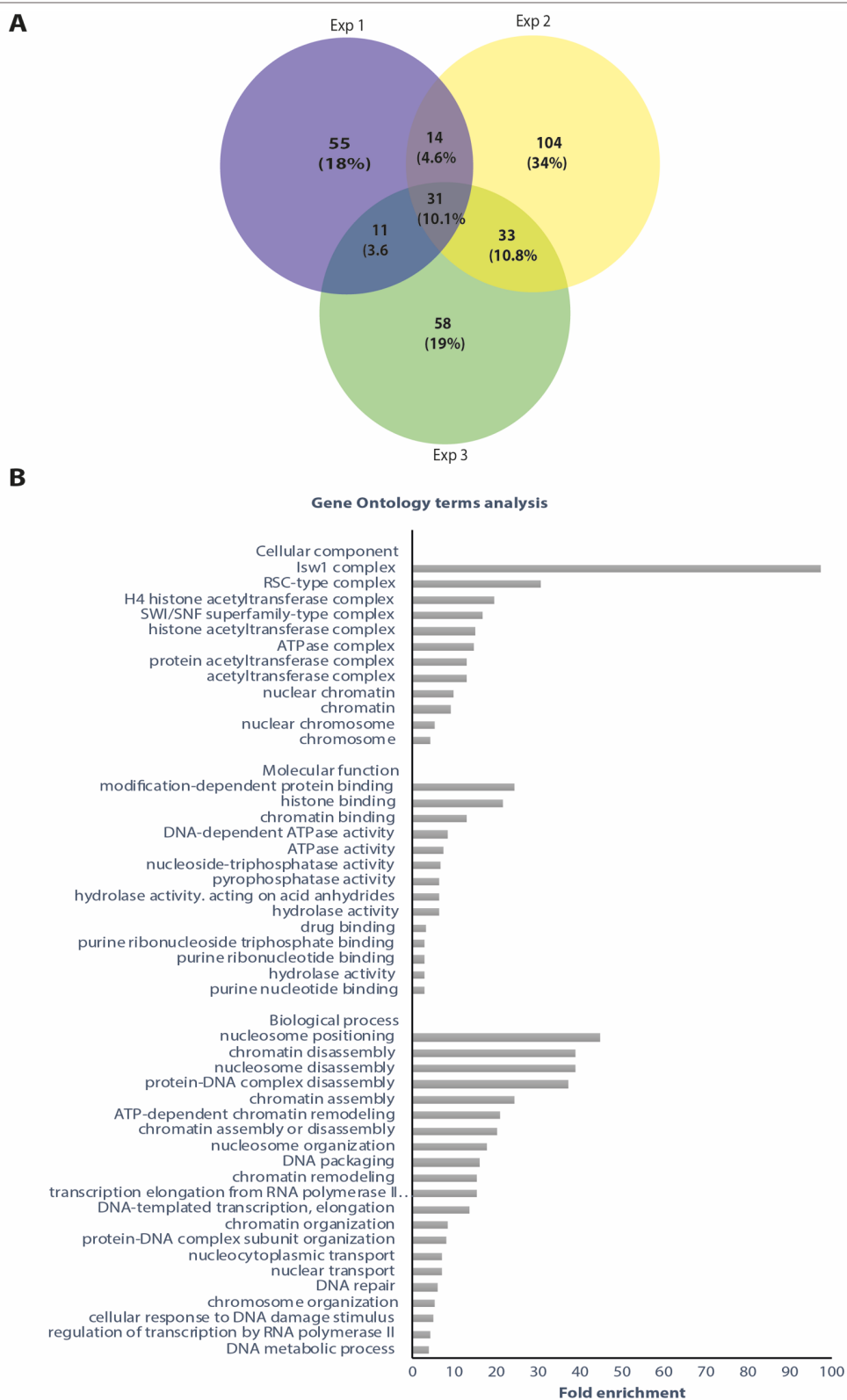
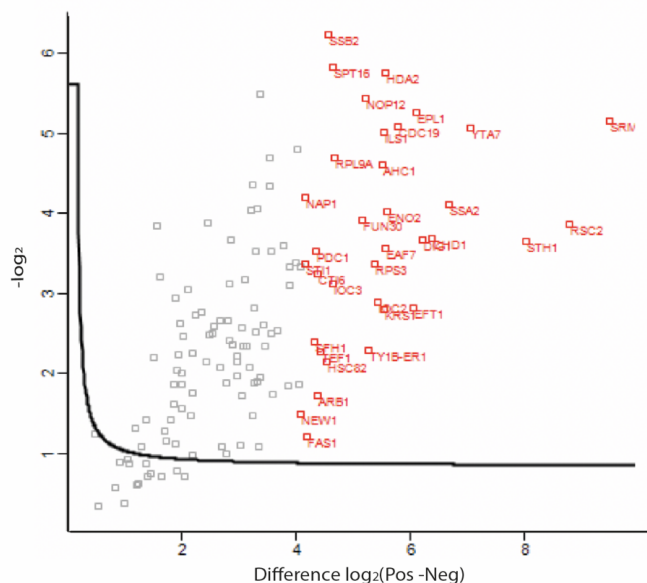


**Figure 15 : MS analysis of H2B T51pBPA crosslink products.**

(A)Venn diagram showing number of proteins exclusively crosslinking to H2B T51 pBPA site *in vivo* in three biological replicates. (B) Gene ontology analysis of exclusive binders identified in A. Analysis was performed using the online tool “The Gene Ontology Resource”.

**A**



**B**

S.No	Gene names	Protein names	Difference $\log_2(\text{pos-neg})$	$-\log_2P$
1	SRM1	Guanine nucleotide exchange factor SRM1	9.5	5.1
2	RSC2	Chromatin structure-remodeling complex subunit RSC2	8.8	3.9
3	STH1	Nuclear protein STH1/NPS1	8.0	3.7
4	YTA7	Tata-binding homolog 7	7.1	5.1
5	SSA2	Heat shock protein SSA2	6.7	4.1
6	CHD1	Chromo domain-containing protein 1	6.4	3.7
7	DIG1	Down-regulator of invasive growth 1	6.2	3.7
8	EPL1	Enhancer of polycomb-like protein 1	6.1	5.2
9	EFT1	Elongation factor 2	6.1	2.8
10	CDC19	Pyruvate kinase 1	5.8	5.1
11	ENO2	Enolase 2	5.6	4.0
12	EAF7	Chromatin modification-related protein EAF7	5.6	3.6
13	HDA2	HDA1 complex subunit 2	5.6	5.8
14	KRS1	Lysine--tRNA ligase. cytoplasmic	5.5	2.8
15	ILS1	Isoleucine--tRNA ligase. cytoplasmic	5.5	5.0
16	AHC1	Protein AHC1	5.5	4.6
17	IOC2	ISWI one complex protein 2	5.4	2.9
18	RPS3	40S ribosomal protein S3	5.4	3.4
19	TY1B	Transposon Ty1-ER1 Gag-Pol polyprotein	5.3	2.3
20	NOP12	Nucleolar protein 12	5.2	5.4
21	FUN30	ATP-dependent helicase FUN30	5.2	3.9
22	RPL9A	60S ribosomal protein L9-A	4.7	4.7
23	SPT16	FACT complex subunit SPT16	4.7	5.8
24	IOC3	ISWI one complex protein 3	4.6	3.1
25	SSB2;SSB1	Heat shock protein SSB2;Heat shock protein SSB1	4.6	6.2
26	HSC82	ATP-dependent molecular chaperone HSC82	4.6	2.1
27	TEF1	Elongation factor 1-alpha	4.4	2.3
28	ARB1	ABC transporter ATP-binding protein ARB1	4.4	1.7
29	CTI6	Histone deacetylase complex subunit CTI6	4.4	3.2
30	PDC1	Pyruvate decarboxylase isozyme 1	4.4	3.5
31	SFH1	Chromatin structure-remodeling complex subunit SFH1	4.3	2.4

**Figure 16 : MS analysis of H2B T51pBPA crosslink products.**

(A) Volcano plot highlighting statistically enriched exclusive H2B T51pBpa binders in red.

(B) Table showing list of proteins enriched at H2B T51 site upon UV irradiation from one of the biological replicate experiments.

### 3.2.2 ANALYSIS OF HISTONE H3 T80 pBPA AND CROSSLINK PRODUCTS

Akin to H2B T51, I investigated H3 T80 amino acid residue for its interactors. Unlike H2B T51 residue which resides near SHL +6 position, H3 T80 is near the SHL +2 location from the nucleosome structure (Figure 17A)<sup>5</sup>. Since these residues are quite apart and essentially at different interfaces of the nucleosome they provide a sound experimental basis for comparison and differentiation of interface specific chromatin binders to the nucleosome.

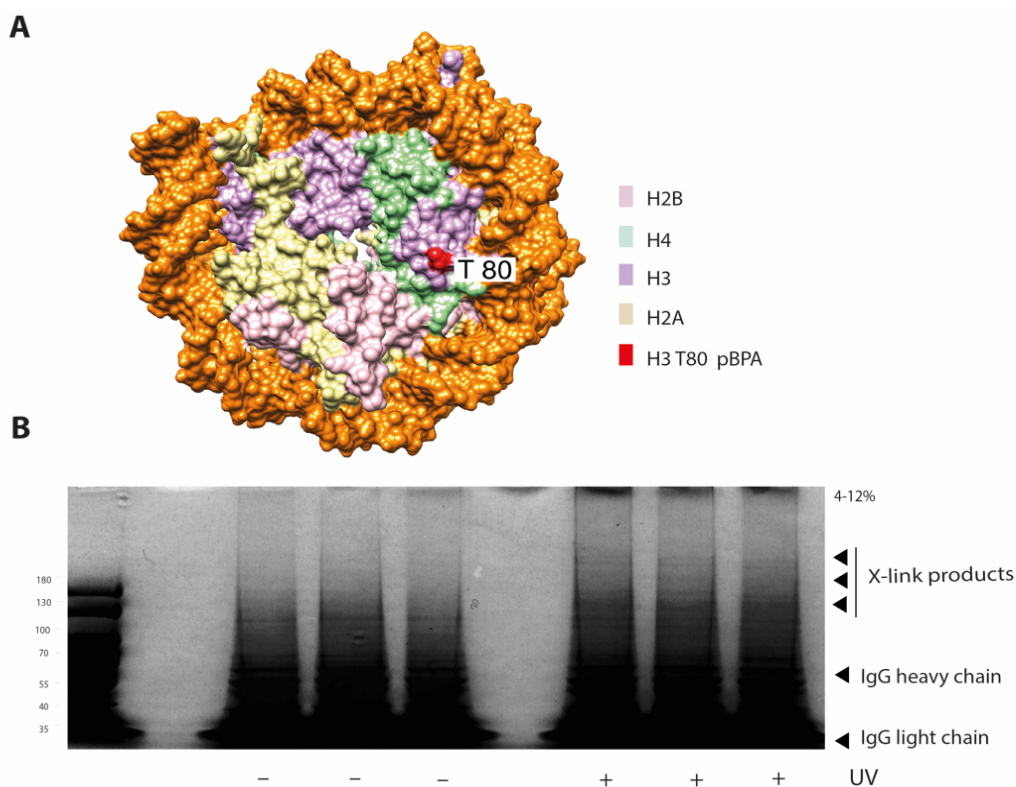


**Figure 17 : Immunoprecipitation of H3 T80 pBPA crosslink products for MS analysis.**

(A) Schematic illustration showing H3 T80 pBPA site highlighted in red (pdb 1ID3)

(B) Yeasts producing H3-HA T80pBPA were irradiated with UV or left untreated. Crosslink products were precipitated under denaturing conditions with anti-HA beads and detected by colloidal Coomassie staining. Peptides were extracted from six consecutive slices from both samples (+/- UV) and analysed by MS.

Following crosslinking, immunoprecipitation yielded in crosslinked proteins exclusively to T51 position (Figure 17B). This was followed by gel extraction of proteins and MS analysis as described before. This entire analysis was repeated for two biological replicates which were further compared to determine the potential hits present exclusively with UV crosslinked sample as visualised by a Venn Diagram (Figure 18A). 34 proteins (10% of all potential hits) were consistently and significantly enriched potential hits common to all UV dependent samples in two independent experiments and absent in non-UV treated samples. Gene ontology analysis was performed as described before using the online tool (Figure 18B). Upon comparison of results from both histone site analysis, only 5 proteins including Sth1, Nop12, Swc3, Top2 and Yta7 were commonly crosslinked to both sites. Rest of the proteins were distinguishable site-specific binders. For H3 T80 site, the top crosslink hits were majorly involved in processes concerning RNA, be it metabolism, modification or processing. Naturally, there were also chromatin binders including STH1 which was later validated by epitope tagging and gel shift assays in *in vivo* crosslinking experiments (Figure 24, Figure 25) as a direct binder of H3 T80 site.

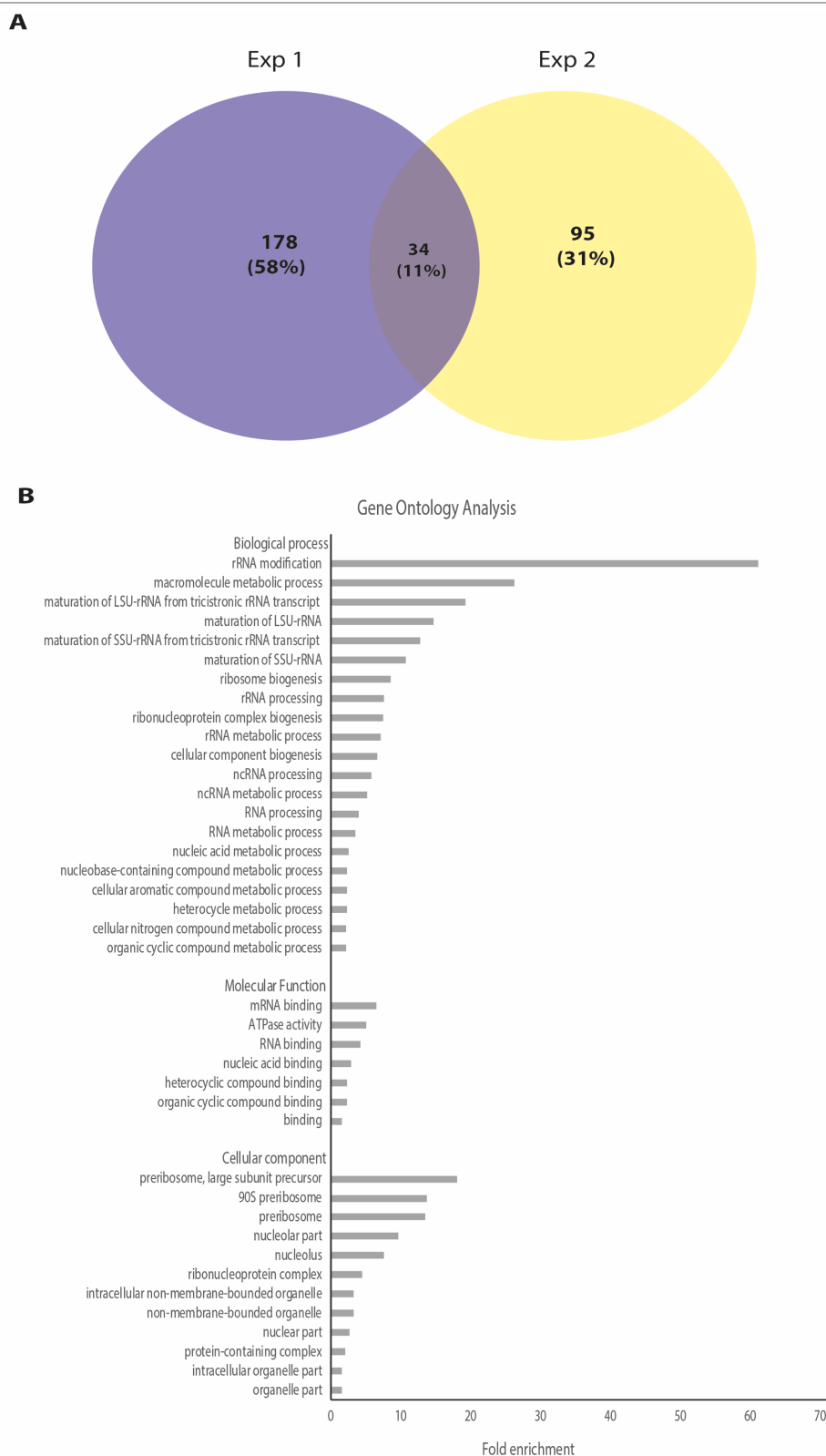


**Figure 18 : MS analysis of H2B T80pBPA crosslink products.**

(A)Venn diagram showing number of proteins exclusively crosslinking to H3 T80 pBPA site *in vivo* in three biological replicates. (B) Gene ontology analysis of exclusive binders identified in A. Analysis was performed using the online tool "The Gene Ontology Resource".

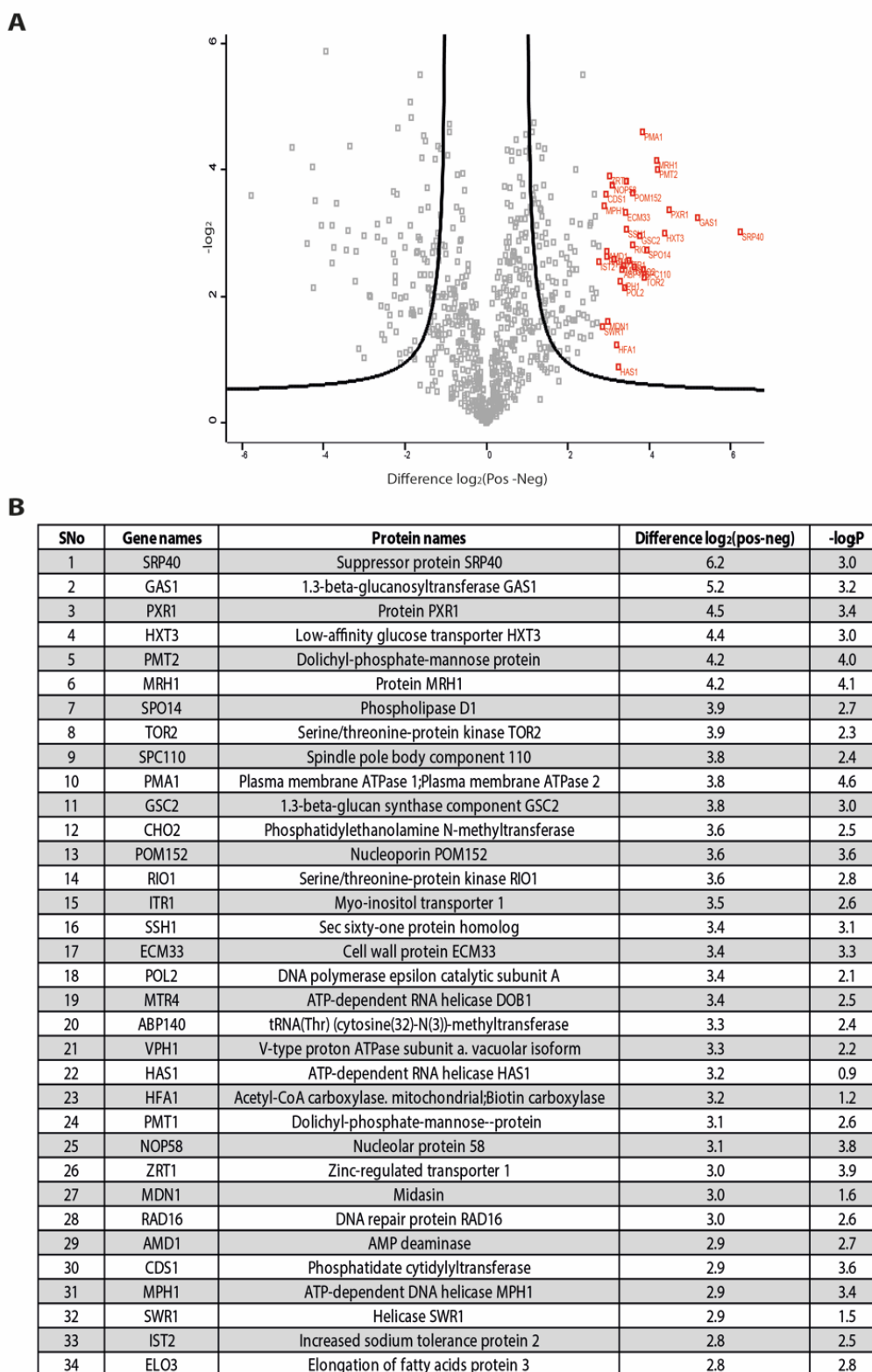


**Figure 19 : MS analysis of H2B T80pBPA crosslink products.**

(A) Volcano plot highlighting statistically enriched exclusive H3 T80 pBpa binders in red.

(B) Table showing list of proteins enriched at H3 T80 site upon UV irradiation from one of the biological replicate experiments.

### 3.2.3 IMMUNOPRECIPITATION OF HISTONES AND CROSSLINKS AT DIVERSE SITES

Next endeavors to identify crosslink products at various histone sites suffered from a number of problems. For most of these sites isolation and immunoprecipitation (IP) of histones worked appropriately. In the process of establishing and optimizing the immunoprecipitation protocol, a multitude of parameters were tested for beneficial effects on quality and quantity of isolated crosslink products. However, some histone amber mutant sites such as H3 S22, showed no obvious enrichment of crosslink products (Figure 20).

For rest of histones amber sites such as H3 T6 and H3 K56, even though there was an obvious UV dependent crosslink enrichment (Figure 20) major obstacle in these cases was a heavy contamination of samples with polyethylene glycol (PEG) which disabled detection of crosslinking peptides in MS analysis. Later using glasswares devoid of detergents helped reduce PEG contaminations in subsequent analysis.

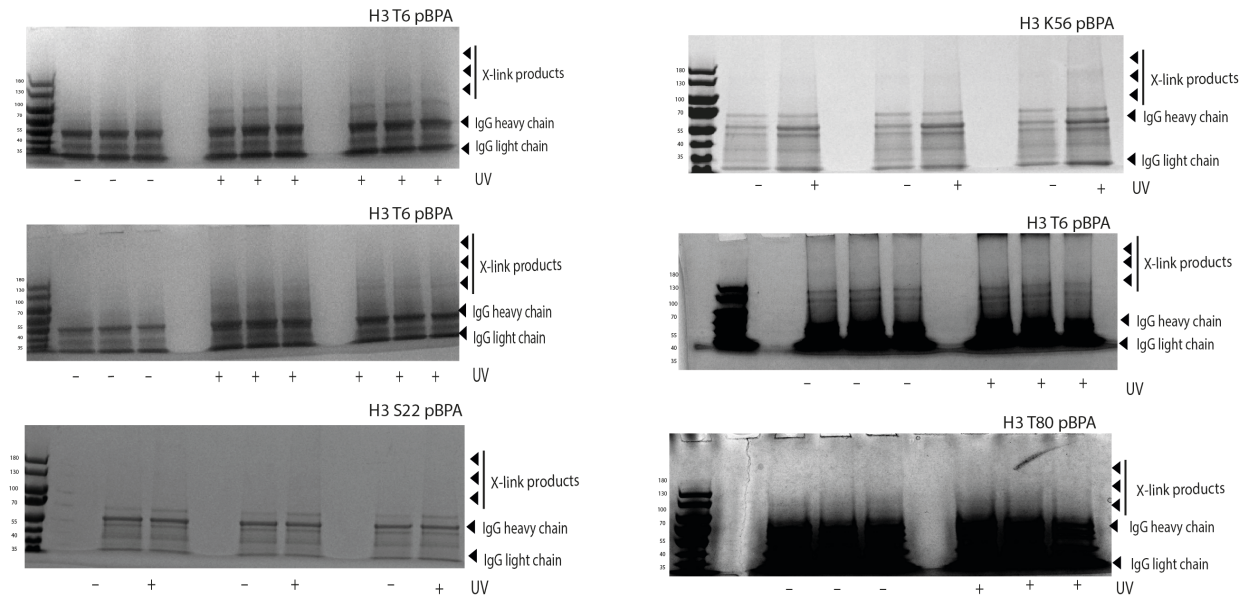


**Figure 20 : Immunoprecipitation of diverse histones and crosslink products for MS analysis.**

Yeasts producing diverse H3-HA pBPA mutants were irradiated with UV or left untreated. Crosslink products were precipitated under denaturing conditions with anti-HA beads and ran on 4-12 % tris acetate gels and detected by colloidal Coomassie staining.

### 3.3 INVESTIGATION OF RSC-NUCLEOSOME INTERACTION *IN VIVO* USING GCE

Until now large-scale crosslinking studies enabled the identification of interactors of chromatin. So as to characterize these discrete chromatin interactors, explicitly nucleosome bound chromatin remodeling complexes, a comprehensive mapping study of particular chromatin remodeling complex subunit, Sth1, the ATPase core subunit of the RSC complex in yeast was performed<sup>52</sup>. This was done by means of the molecular weight shift method (Figure 21) which entails comparison of crosslink pattern between two independent yeast strains. Strain II contains a genomically tagged variant of the candidate protein to be investigated, Sth1 in this case. Addition of a tag results in a shift in the crosslink band in this strain corresponding to the weight of the tag and thus enables identification of a map of crosslink sites of the candidate protein.

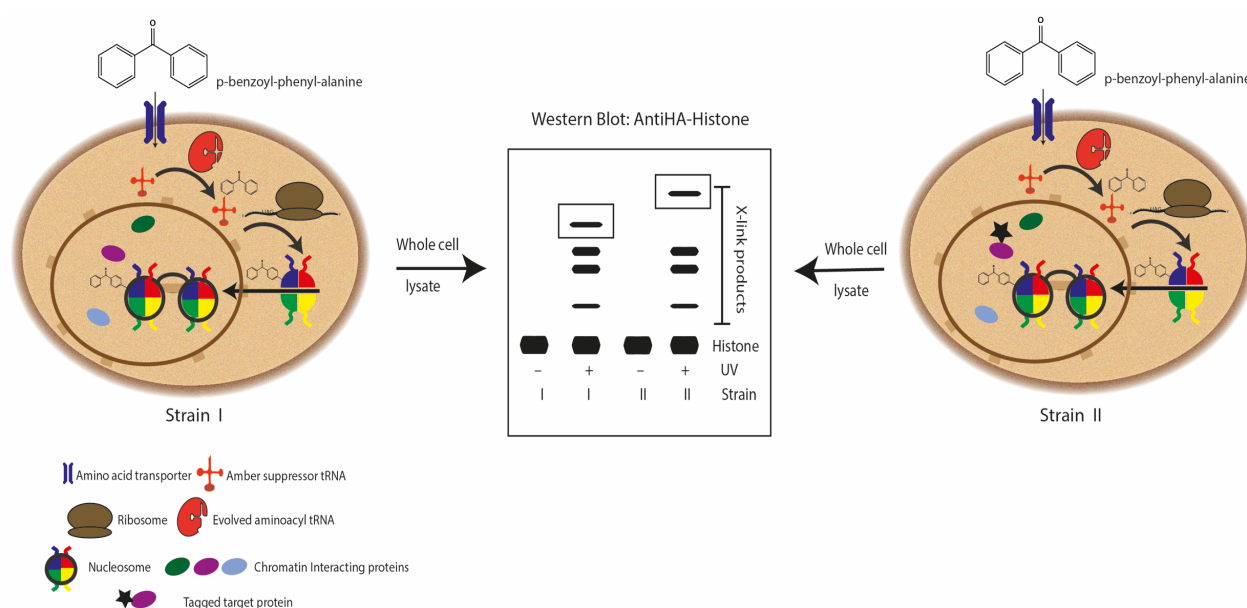


**Figure 21: Molecular weight shift method.**

The molecular weight shift method is implemented by two discrete crosslink experiments in distinctive yeast strains. Strain II comprises a genomically tagged variant of the candidate crosslink partner which would outcome in an additional molecular weight shift in a crosslink experiment employing this strain.



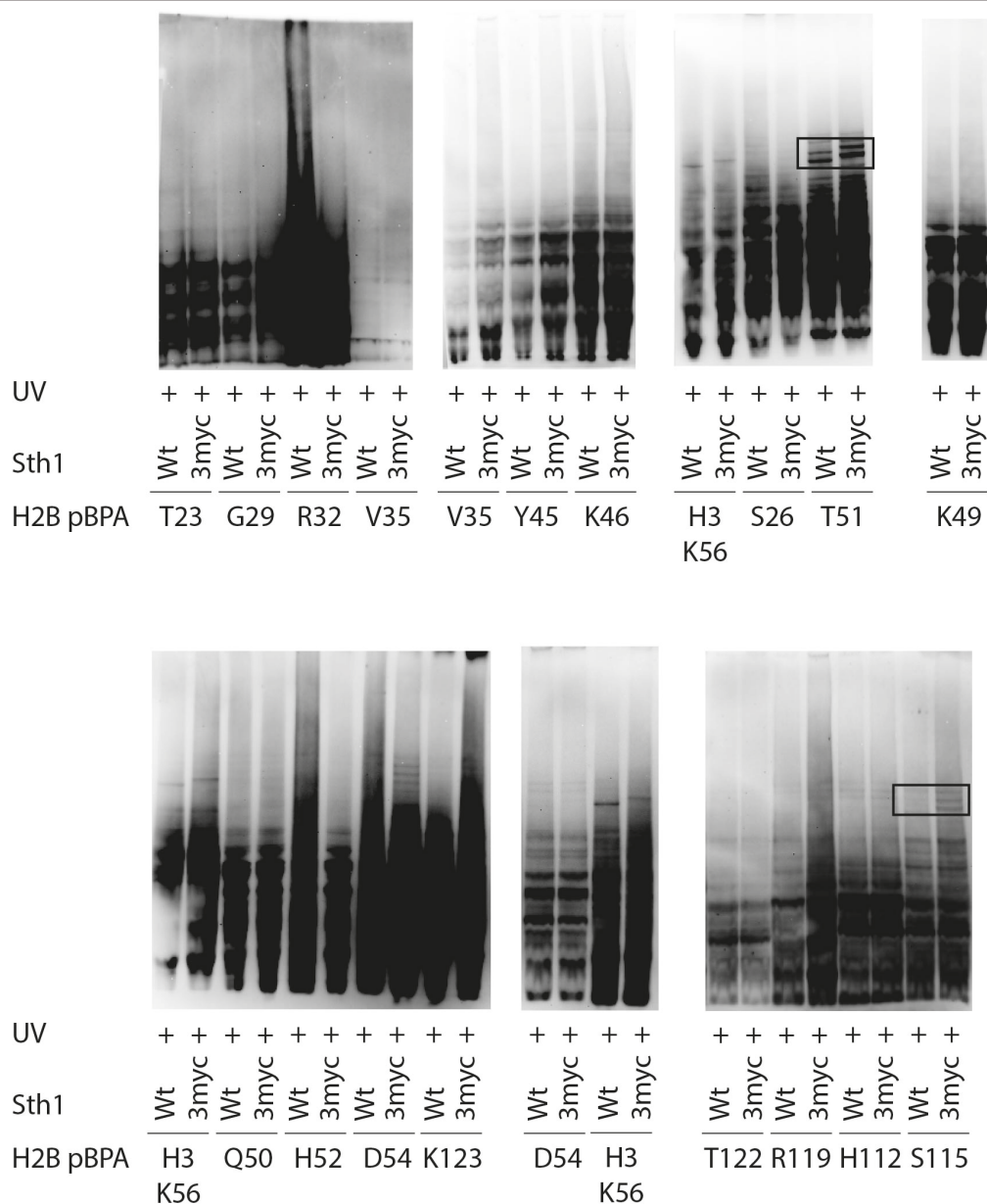


**Figure 23 : Identification of Sth1-histone H2B crosslink products.**

Yeast cells (wild-type or Sth1-3myc) containing the designated pBPA-containing histone were UV-irradiated and whole cell lysates examined by SDS-PAGE and Western Blot using anti-HA antibodies. Boxed areas indicate bands corresponding to Sth1-tagging (Data from Bryan J. Wilkins).

As a result of this comparative crosslinking analysis, nine positions on the nucleosome were identified to be crosslinking sites (Figure 25A). I mapped these sites onto the structure of the nucleosome core particle to envisage the footprint of Sth1 (Figure 25B).

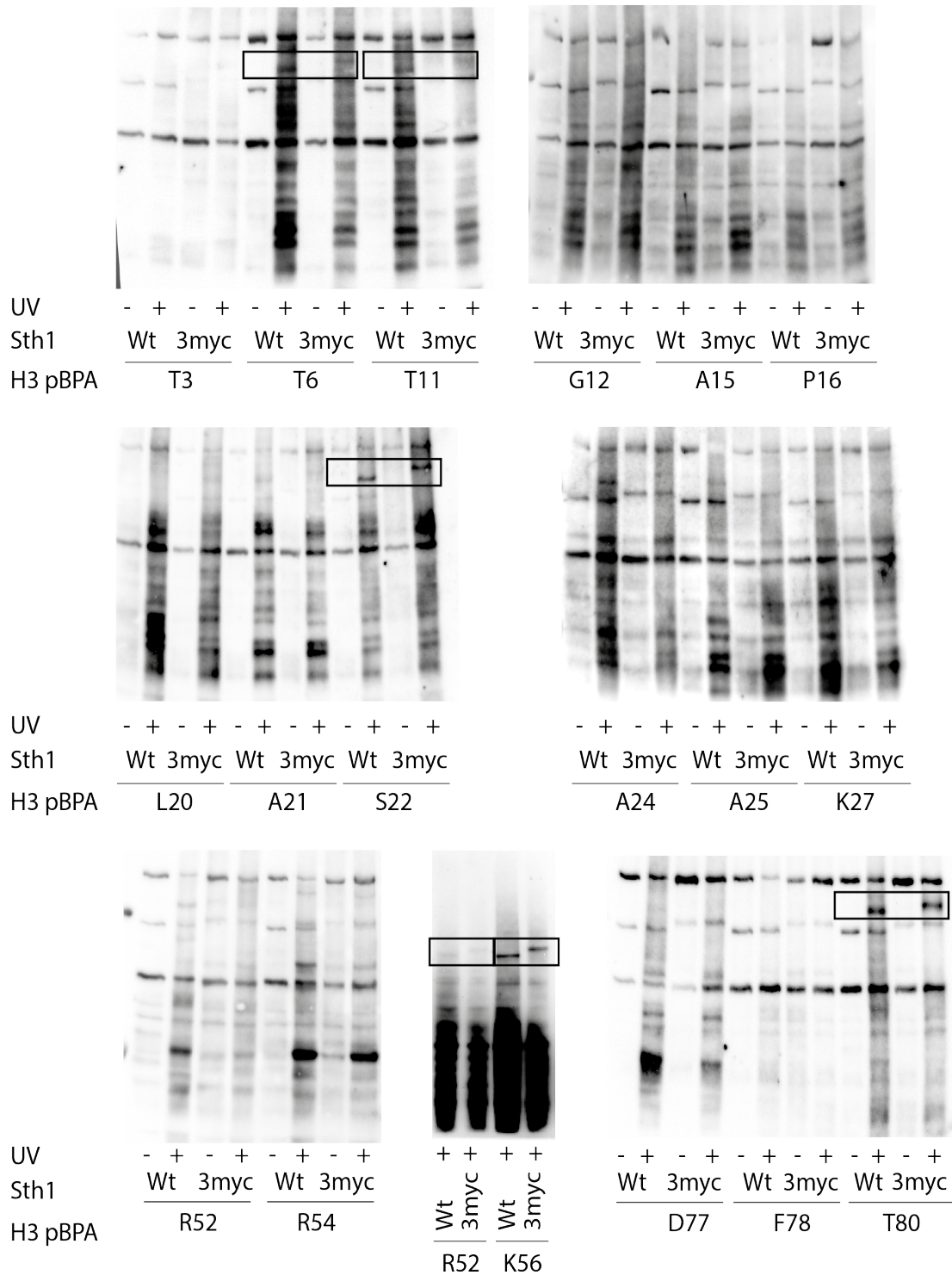


**Figure 24 : Identification of Sth1-histone H3 crosslink products.**

Yeast cells (wild-type or Sth1-3myc) expressing the indicated pBPA-containing histone were UV-irradiated and whole cell lysates examined by SDS-PAGE and western blot using anti-HA antibodies.

Boxed areas show bands sensitive to Sth1-tagging (Data from Bryan J. Wilkins)

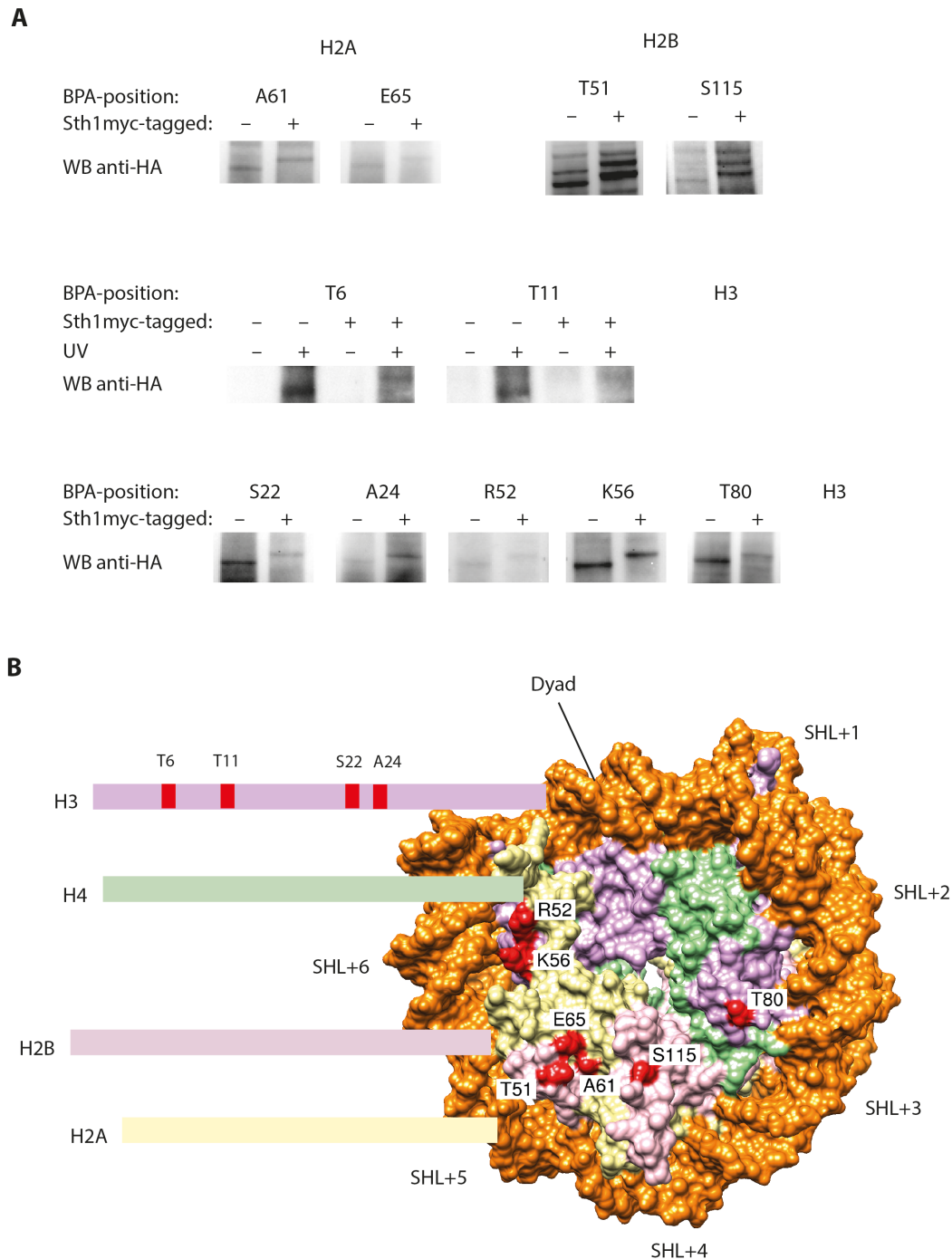


**Figure 25 : Mapping the interaction surface of Sth1 on the nucleosome *in vivo*.**

(A) Yeast cells (wild-type or Sth1-3myc) expressing histones with pBPA at the indicated position were UV irradiated and crosslink products analysed by SDS-PAGE and western blot employing anti-HA antibodies identifying the pBPA-containing histone. The change in mobility ensuing from the myc-tag recognizes a crosslink product with Sth1. H2B-Sth1 crosslinks emerge as a double band due to H2B SUMOylation. (B) Graphical representation of the sites identified in A and B on the structure of the nucleosome. (Figure was prepared using pdb-file 1ID3 and Chimera).

### 3.3.2 STH1 RELIES ON H3 K14 ACETYLATION MARK FOR INTERACTION WITH HISTONE H3

Dispersed over five subunits, the RSC complex hosts eight of the 15 bromodomains annotated in the budding yeast genome<sup>190</sup>. In spite of possessing the highest number of acetyl binding reader domains, functions of only few of them have been reckoned so far. Example, lysine acetylation sites recognized by the RSC complex are H3 K14ac and Rsc4 K25ac via the double bromodomain of the Rsc4 subunit<sup>191</sup>. Structurally, Sth1 is composed of five major domains: the N-terminal domain (NTD), the domain preceding the HSA helix (preHSA), HSA, motor, and the C-terminal extension and BD<sup>67</sup>. H3 K14 is crucial for the interaction of Sth1 with the N-terminal H3 tail<sup>192</sup>. Additionally, H3 K14 acetylation is described to serve as a recognition site to maintain RSC on nucleosomes<sup>193</sup>, hence H3 K14 was mutated to alanine on the equivalent H3 copy having amber mutation. This experiment conferred that K14 is needed for interaction of Sth1 with the tip of the H3 tail, because amber mutation only affected crosslinking of H3 T6pBPA and T11pBPA to Sth1 (Figure 26A). Akin to the H3 K14A mutation, deletion of Gcn5 gene led to the same effect that is obliteration of crosslinking between H3 tail and Sth1 (Figure 26B)<sup>194,195,196</sup>

Could *in vivo* crosslinking with pBPA help? Investigations were carried out from H2A A61pBPA–nucleosomes with or without a genomic H3 K14 mutation to alanine (Figure 26C, left panel)<sup>197</sup>. The crosslinking of Sth1 was only somewhat abridged by this mutation. Thus, H3 K14 does not seem necessary for RSC recruitment as known previously.<sup>198</sup> Nevertheless, the nucleosomes that interact with RSC may be regulated by RSC itself. In this situation, mutation of H3 K14 in nucleosomes deprived of the crosslinker must move RSC binding to crosslinker-bearing nucleosomes which still retain H3 K14ac mark. Consequently, crosslinking experiments from H3 S22 in the backdrop of a strain bearing the H3K14ac mutation in the genomic copy of H3 (Figure 26C, middle panel) were performed.

Crosslinking from H3 S22pBPA was not disturbed by genomic H3 K14A mutation . Whether the Sth1 bromodomain singularly associates with H3 tails that are segment of the nucleosome bound by RSC or whether H3 tails from adjacent nucleosomes are likewise its substrates remain unknown. Therefore, crosslinking experiments from H3 tip which is H3 T6pBPA in the genetic background of H3 K14A cells were performed (Figure 26C, right panel). Say the bromodomain of Sth1 only networks with H3 tails that share the identical nucleosome that the complex is bound to, the mutation of the native H3 must not perturb the crosslinking efficiency. Conversely, if Sth1 networks with H3 tails of adjacent nucleosomes, the mutation would nullify the competition with their histone tails and hence lead to a surge in crosslinking. Indeed, the K14A mutation of the native H3 allele augmented crosslinking between Sth1 and H3 T6pBPA fifteen times (Figure 26D), representing that the bromodomain of Sth1 is capable of interacting with acetylated H3 tails of adjacent nucleosomes.

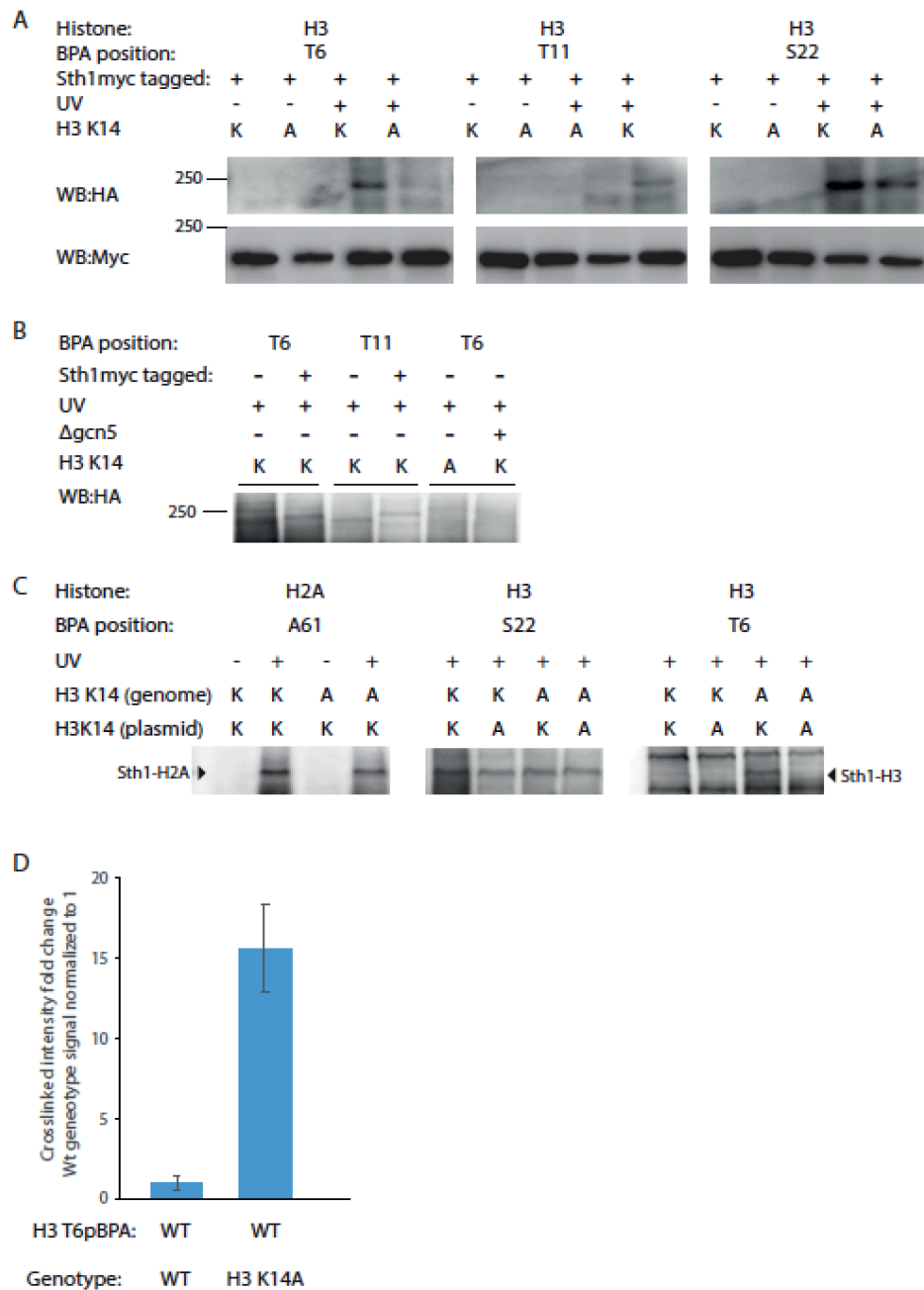


**Figure 26 : H3K14 acetylation moderates interaction of Sth1 with nucleosomes**

(A) Crosslinking from sites in the H3 tail in Sth1-3myc cells. Anti-myc immunoprecipitates were analysed by western blot with anti-HA antibodies. (B) Deletion of *gcn5* meddles with H3 T6pBPA crosslinking to Sth1. WCEs of crosslinked samples were irradiated with UV-light and whole cell extracts analysed by western blot with anti-HA antibodies. (C) Result of mutating endogenous H3 K14 to alanine on crosslinking to Sth1. Yeast cells (wild-type or H3 K14A) expressing H3 T6pBPA, H3 S22pBPA or H2A A61pBPA with or without K14A mutation were analyzed as in B. D) Quantitative comparison of crosslinking efficiencies from H3 T6pBPA in wild-type and H3 K14A yeasts. Error bars are standard deviations of five independent experiments.(Experiments performed in the lab of Bryan J.Wilkins)

### 3.2.3 RSC FAVOURABLY INTERACTS WITH SUMOYLATED H2B *IN VIVO*

Having a closer look at the crosslinking pattern, it was almost immediate to recognize that there was a unique crosslinking pattern of Sth1 only for histone H2B- as opposed to other histones. At position T51 and S115 of H2B-Sth1 crosslinks, there was a double band as opposed to a single band for crosslinks at other sites. Moreover, the second crosslink band was shifted by ~10kDa in both strains with or without Myc tag on Sth1 (Figure 25). Candidates of histone post translational modifications which can account for such mass shifts of ~10kDa include ubiquitination (1 ubiquitin protein has size of 8.6 kDa) and SUMOylation (1 SUMO protein has size of 12kDa). Therefore, initially I hypothesized that the mass shift might be a result of H2B K123 ubiquitination, most prominent site of H2B ubiquitination in *S. cerevisiae*<sup>199</sup>. However, the crosslinking pattern of ubiquitination-deficient mutant H2B T51pBPA K123R was not any different from that of H2B T51pBPA wildtype (Figure 27A). Next upon testing additional sites of H2B ubiquitination - K46, K49 and K111<sup>200</sup> mutants to arginine, I observed no change in crosslinking pattern too (Figure 27A). So, ubiquitination did not seem to be the additional factor on H2B required for interaction with Sth1 from our *in vivo* crosslinking studies. Therefore, I then mutated combinations of lysine residues- K6, K7, K16 and K17 on H2B known to be SUMOylated in *S.cerevisiae* to arginine<sup>25</sup>. Here, I observed that mutating these residues led to loss of the upper band of H2B-Sth1 crosslink. Intriguingly, mutating either pair of lysine residues in the H2B N-terminus (K6/7 or K16/17) was adequate to eliminate the slower migrating band. Fittingly, mutations of the same sites have formerly been shown to eradicate H2B SUMOylation. Finally, when I examined a strain deficient in E3 SUMO ligases Siz1 and Siz2 in *S.cerevisiae* requisite for H2B SUMOylation<sup>201</sup>, similar to mutating lysine residues crucial for SUMOylation, the ligases deficient strain should an abolishment of the upper crosslinking band (Figure 27C), clearly authenticating it to be the SUMOylated form of H2B. Densitometric quantification of both bands suggesting that 20-30% of H2B that crosslinked with Sth1 was SUMOylated (Figure 27D).

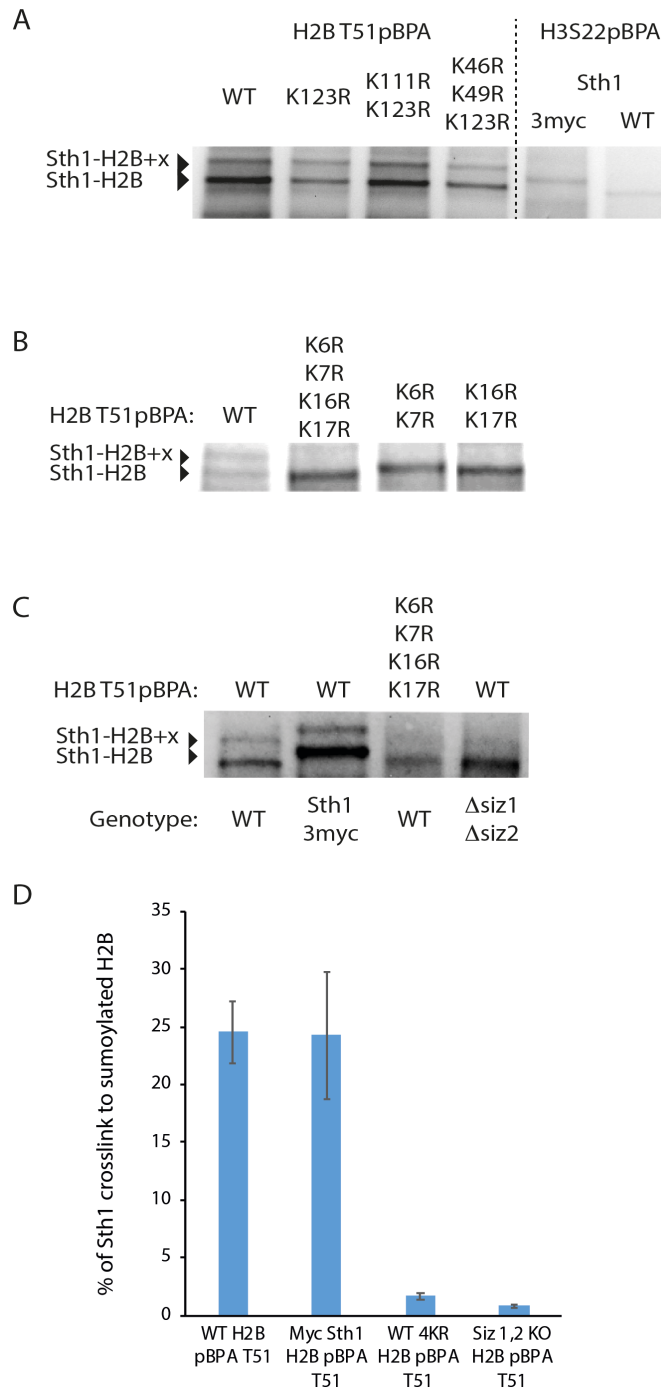


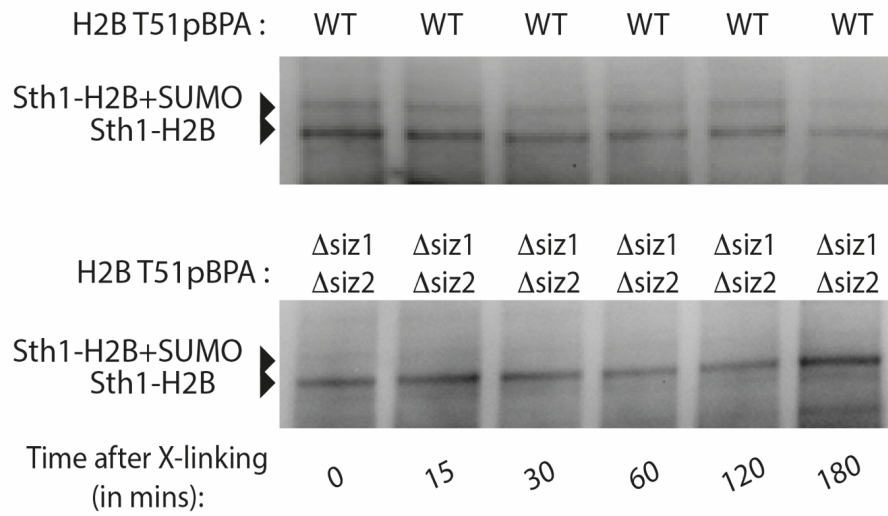
**Figure 27 : RSC specially interacts with SUMOylated H2B *in vivo*.**

(A) Crosslink pattern of H2B T51pBPA is not disturbed by mutation in lysine residues stated to be subject to ubiquitinylation. Crosslinks to H3 S22pBPA are used as indication to identify Sth1-H2B crosslink. B) Effect of mutating H2B SUMOylation positions on H2B T51pBPA crosslink pattern. (C) Consequence of deletion of siz1 and siz2 on H2B T51pBPA crosslink pattern. (D) Intensities of upper and lower crosslink bands were quantified by densitometry. Error bars are standard deviations of five independent experiments. In all panels, yeasts expressing H2B T51pBPA with the designated mutations were UV-irradiated and whole cell lysates analysed by SDS-PAGE and western Blot by means of anti-HA antibodies.

### 3.2.4 RSC RECOGNIZES PREVIOUSLY SUMOYLATED NUCLEOSOMES *IN VIVO*

Next, I asked if I could further dissect the relationship between RSC and SUMOylated nucleosomes. In other words, I decided to use our *in vivo* crosslinking setup to answer if RSC crosslinks to already SUMOylated nucleosomes or acts as a part of a complex machinery which probably recruits SUMO modification to specific nucleosomes. To carry out this experiment I co transformed both wildtype and Siz1,2 knockout yeast cells with amber suppression machinery plasmid as well as HA-tagged histone H2B T51 pBPA amber mutant as used in section 3.2.3 Immunoprecipitation of Histones and crosslinks at diverse sites and crosslinked cells for 10 minutes. Whole cell lysates collected at this timepoint were labelled as 0 minute and the rest of the crosslinked sample was permitted to regrow in YPD medium. Samples were subsequently gathered at indicated time points to temporally monitor the crosslinking pattern. From HA blots I observed a double band crosslink pattern, *i.e.* the crosslink of Sth1 to both wildtype and SUMOylated H2B histones to remain consistent across time points from the time of crosslinking in wildtype cells and expectedly only lower band in Siz1,2 knockout strain. This proves that RSC distinguishes previously SUMOylated nucleosomes and once crosslinked it persists covalently bound to them (Figure 28A). Densitometric quantification of both bands suggested nearly 20% of H2B that interacts with Sth1 is SUMOylated (Figure 28B). If RSC would have mediated SUMOylation on H2B histone, I would have expected a single lower band in wildtype cells depicting crosslink of Sth1 only to wildtype H2B initially and a gradual appearance of upper second band indicative of deposition of SUMO protein on histone H2B by RSC.

**A**



**B**

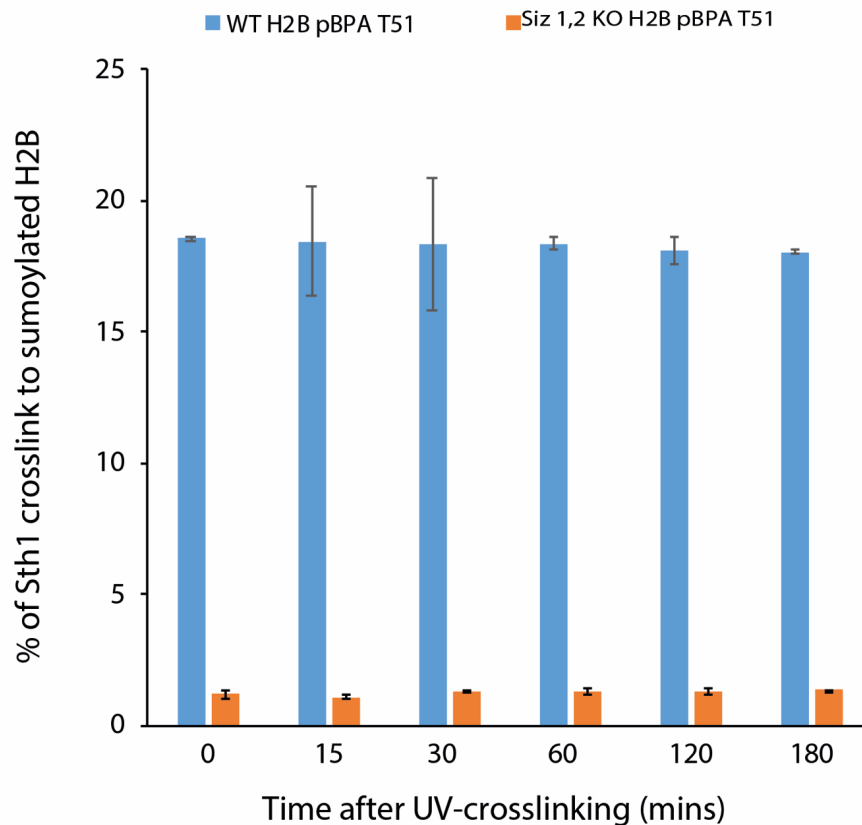


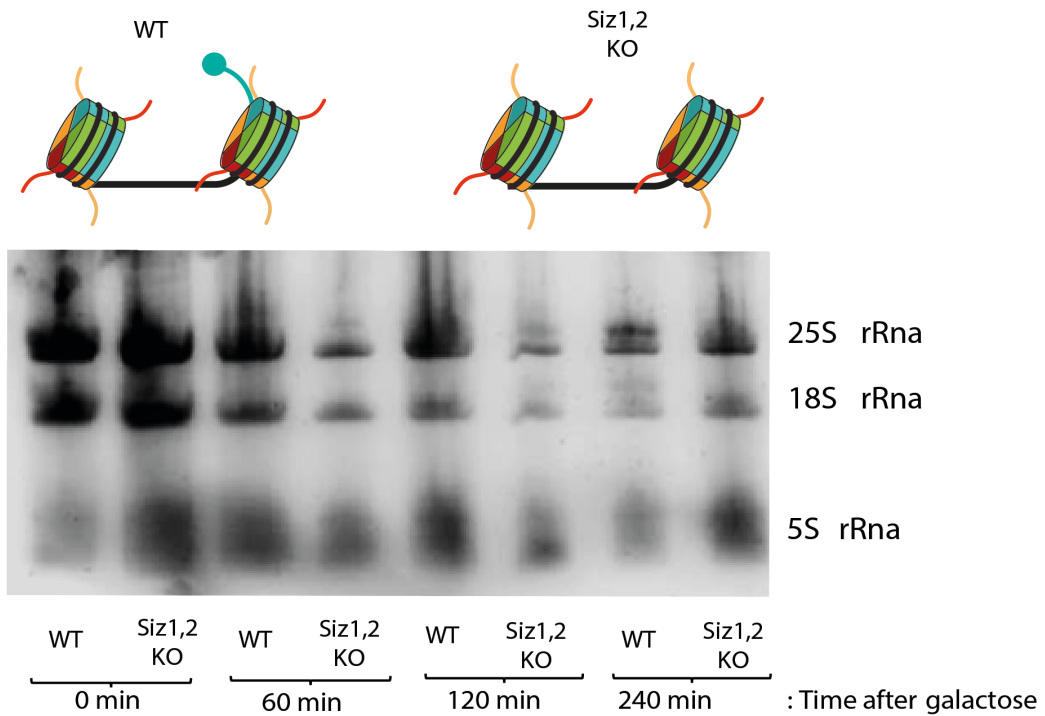
**Figure 28 : RSC recognizes previously SUMOylated nucleosomes.**

(A) Crosslink pattern of H2B T51pBPA through distinctive samples gathered at specified time points after UV crosslinking at 0 minute. In wildtype and *siz1,2* knockout cells. In all panels, yeasts with H2B T51pBPA and the indicated mutations were UV-irradiated and whole cell lysates analyzed by SDS-PAGE and western blot using anti-HA antibodies. (B) Intensities of upper and lower crosslink bands were quantified by densitometry. Error bars are standard deviations of two separate experiments.

### 3.2.5 INDUCTION OF GAL1 GENE AS A READOUT OF RSC INTERACTION WITH SUMOYLATED NUCLEOSOMES

Nucleosomes act as encroachers of promoters and thereby suppressors of basal transcription levels. RSC complex destabilizes or disposes nucleosomes off DNA to free up space for binding of factors such as activator protein Gal4 which in turn regulate induction of GAL genes under special conditions<sup>56</sup>. On one hand, upon RSC depletion, GAL1 gene levels have been shown to be reduced. This is because in absence of RSC, Gal4 must compete with broadly bound nucleosomes for binding to the (Upstream activating sequence) UASg, whereas in its presence the UASg is held readily accessible to Gal4. On the other hand, previous works have demonstrated that a fusion of SUMO to H2B also reduces GAL1 transcription levels<sup>201</sup>. Is it possible that the presence of modifications such as SUMOylation on nucleosomes dictates the fate of such promoter occupying nucleosomes by regulating action of RSC complex? To test this hypothesis, I decided to monitor the level of GAL1 gene induction in Wildtype and Siz1,2 knockout strains. I grew cells in presence of glucose (not raffinose) and shifted them to galactose to trigger GAL1 induction. This is because RSC showed effect only in former case<sup>56</sup>. I isolated RNA at indicated time points pre and post induction with galactose. Following RNA isolation (Figure 29A), I prepared cDNA and then measured the levels of Gal gene using real time qPCR. I observed no significant difference in GAL1 induction levels in Siz1,2 knockout strain as compared to wildtype strain, consistent with previous findings that SUMOylation generally represses GAL1 transcription<sup>201</sup>(Figure 29B). However, these results fail to reveal a direct contribution of RSC in this scenario. To obtain such insights RSC will have to be probed, ideally with temporary depletion strategies such as AID tagging of its nonessential subunits and combined with excess, nominal presence or absence of SUMOylation on histone H2B.

A



B

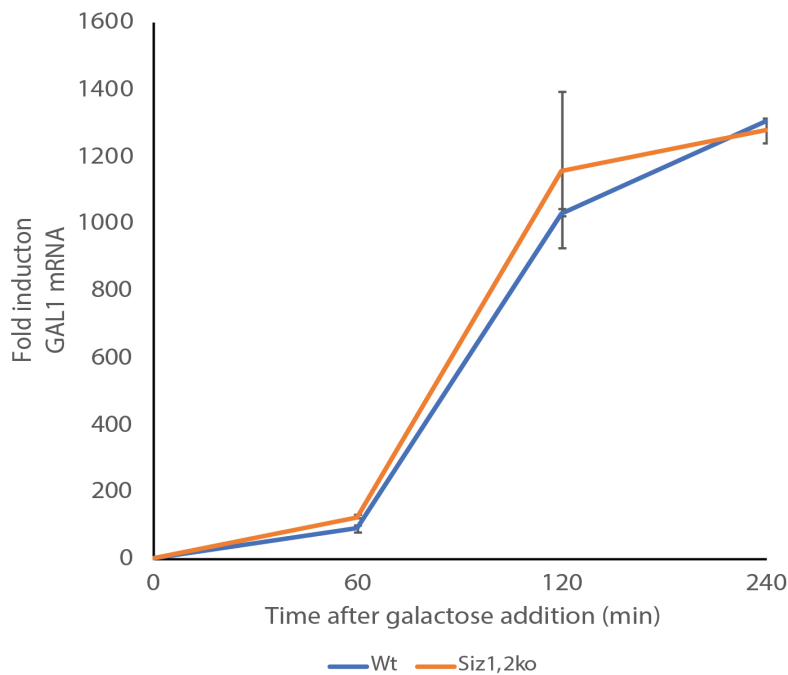


**Figure 29 : Effect of SUMOylation on GAL1 mRNA levels.**

(A) WT and Siz1,2 knockout cells were grown in YPD media containing glucose until reached  $OD_{600}=0.5$  and then shifted to media lacking glucose but containing galactose. Samples were collected at indicated timepoints and RNA isolated using hot acid phenol protocol. Quality of extracted RNA was checked by running on 12% denaturing Urea-PAGE RNA gels. (B) cDNA were prepared from RNA isolated in A. (B) GAL1 mRNA levels were measured by real time qPCR and normalizations done on ACT1 levels. Error bars are standard deviations of the means of two independent experiments.

### 3.2.6 VARIATION OF STH1-NUCLEOSOME INTERACTIONS THROUGH THE CELL CYCLE

Chromatin structure alters with the passage of cell cycle. During interphase it is generally more open and accessible whereas it is maximally compacted in mitosis. At this time the tight packaging of DNA renders it inaccessible to regulatory factors and enzymes such as transcription factors, RNA polymerases and ATP dependent chromatin remodelers<sup>202</sup>. To investigate whether RSC binding to chromatin is modulated by changes in chromatin structure, I examined the crosslinking efficiency of histones to Sth1 during the cell cycle. To this end, I utilized a temperature-sensitive strain of yeast *cdc15-2* such that mutation in this essential kinase leads to synchronisation of yeasts in mitosis when cells are grown at non-permissive temperature and then regrowth upon shifting cells to permissive temperature. Thus, following this temperature shift protocol, cells were collected at different time points upon synchronisation, photo crosslinked and subsequently analysed the crosslink products by SDS-PAGE and western blot (Figure 30A). Synchronisation of cells in different cell-cycle stages were confirmed by FACS analysis of the samples (Figure 30C). Out of the four positions studied, two (H3 S22 and K56) exhibited no change in crosslinking efficiency between mitosis and interphase, denoting that the during the cell cycle, RSC remodelling complex is retained on the nucleosomes . Conversely, for rest of the two positions (H3 T80 and H2B T51), I noticed a reciprocal alteration in intensity between mitosis and interphase, signifying that changes in chromatin structure lead to minute dynamic effects on RSC binding to the nucleosomes (Figure 30B).

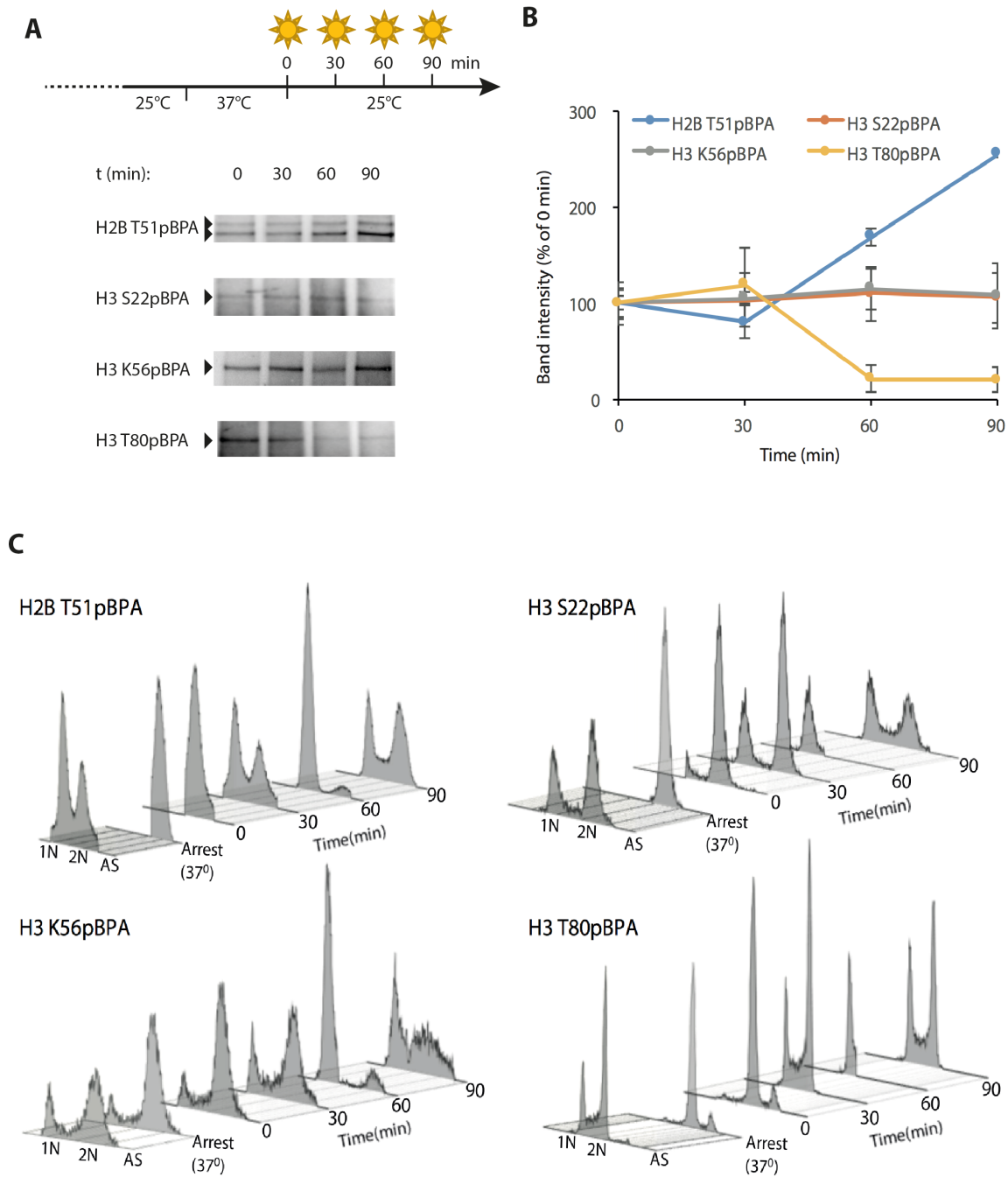


**Figure 30 : Outcome of the cell cycle stage on Histone-Sth1 crosslink efficiency.**

(A) Yeast cells (*cdc15-2*) expressing the specified pBPA-containing histones were synchronized using the elucidated temperature-shift protocol. Samples were irradiated and whole cell lysates analyzed by SDS-PAGE and western blot using anti-HA antibodies. (B) Band intensities of 3-4 separate replicates of the experiment shown in A were quantified by densitometry using Fuji software. Error bars are standard errors of the mean. (C) FACS analysis of synchronized yeast populations analyzed in A and B.

### 3.3 INVESTIGATION OF H3S10 PHOSPHORYLATION MEDIATED RECRUITMENT OF DEACETYLASE HST2

This part of my thesis was dedicated in deciphering the mechanism by which one of the erasers of lysine acetylation, Sirtuin Hst2 is recruited to H3 S10 phosphorylation to mediate chromosome condensation, which is prerequisite for regulating essential genome functions such as DNA segregation during cell division.

#### 3.3.1 RECRUITMENT OF DEACETYLASE HST2 TO H3S10PH IN MITOSIS

During mitosis, proper compaction of chromatin into rod shaped chromosomes is decisive for the faithful segregation of genetic information to recipient daughter cells. This process is of considerable risk, as a letdown in any of its steps can lead to stark pathological conditions such as aneuploidy and cancers. One of the key hallmarks of eukaryotic mitosis is phosphorylation at S10 on histone. H3 S10 phosphorylation was originally identified as a major site of mitotic phosphorylation on condensed chromosomes<sup>203,204</sup>.

However, the meticulous mechanism by which this phosphorylation drives mitotic chromosome condensation is not lucidly understood. Using Genetic Code Expansion in *S.cerevisiae* our lab had previously described a condensin-independent driving force of mitotic chromosome condensation where phosphorylation at H3 S10 recruits Hst2 to deacetylate H4 K16, triggering condensation<sup>117</sup>.

Preceding pull-down experiments with synthetic H3 peptides phosphorylated at Ser10 have shown to competently recover Hst2 from whole-cell extracts, relative to a non-phosphorylated control, demonstrating the significance of phosphorylation at H3 S10 in recruiting Hst2, directly or indirectly, to condensing chromatin<sup>117</sup>. In contrast, recombinantly expressed Hst2 in *E. coli* did not show interaction with H3S10D peptide whereas it was able to interact with its known substrate, H4K16ac peptide with an

affinity of  $\sim 730$  nM as measured by ITC, denoting that additional factors or PTMs on Hst2 are required (Figure 31A,B).

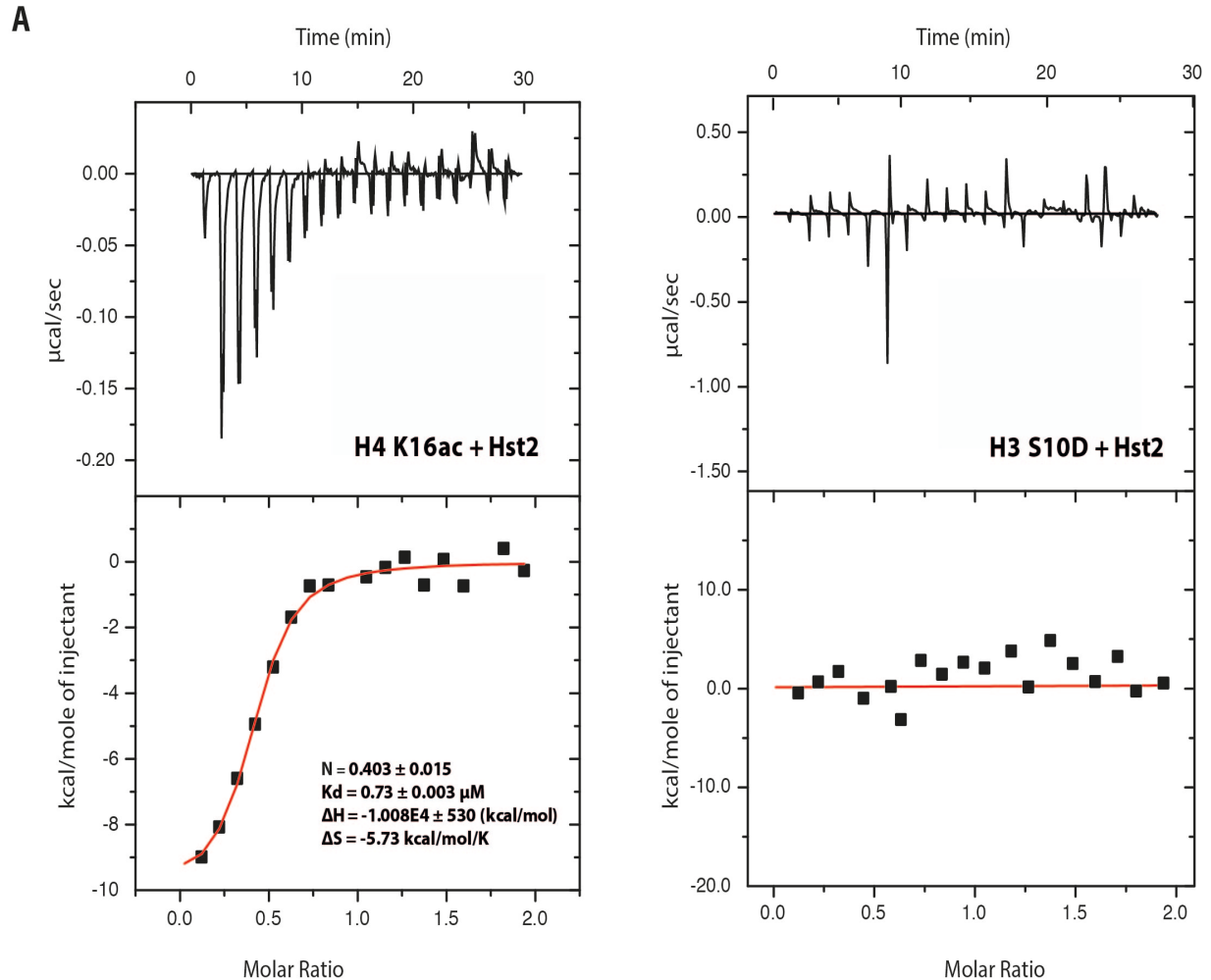


Figure 31 : Hst2 shows no interaction with H3S10D peptide *in vitro*.

(A) Thermogram and binding isotherm of peptide (300  $\mu$ M, injected) binding to Hst2 (30  $\mu$ M in reservoir) (fit  $\pm$  error of the fit). (B) Derived thermodynamic parameters.

### 3.3.2 CHARACTERIZATION OF HST2 INTERACTION PARTNERS AND PTMS USING PROTEOMICS

So as to recognize the mechanism by which Hst2 is recruited to the Histone H3 tail, factors were screened that might function as mediators between the H3 tail and Hst2. Epitope-tagged Hst2 was purified from yeast extracts using anti-FLAG antibodies (Figure 32A) and the co-purifying proteins were analyzed by mass spectrometry. Cells expressing untagged Hst2 served as control. Interestingly, MS analysis revealed several novel interactors of Hst2 with high fold difference as compared to the negative control. Gene ontology revealed a strong overrepresentation of proteins involved in key chromatin related processes, such as replication: Mcm4, Mcm6 and Mcm2 (Figure 32B). I confirmed the interaction of Hst2 with Mcm2, a component of the MCM helicase, and cyclin dependent kinase Cdc28 by co precipitations (Figure 33A,B). While no direct genetic or physical interaction between Hst2 with MCM helicase is previously reported, Hst2 knockout was identified in a chemical-genetic screen as one of the mutants that specifically failed to grow in the presence of low doses of 1-NM-PP1 which is a highly specific inhibitor of the *cdc28-as1* allele<sup>205</sup>. As a follow up experiment, here I used increasing concentrations of nicotinamide (0 to 20 mM) to inhibit yeast sirtuins and examined their growth in combination with temperature sensitive mutations in Cdc28. As compared to wildtype strains, *cdc28-1/2* ts cells showed loss of viability at 37 degrees, however grew normally at permissive temperatures, irrespective of nicotinamide and by extension Hst2 inhibition (Figure 33C).

In the same experiment I also analyzed enriched Hst2 for the presence of PTMs. Previously reported structure of Hst2 shows the N and C terminus of the protein with a conserved catalytic core similar to other sirtuins<sup>206</sup>. However, regions of the C-terminus remain unstructured possibly due to high flexibility. Due to the occurrence of several serine residues in the same region I looked for phosphorylations by MS/MS. This analysis identified the 1 residue formerly defined as being altered, S340<sup>207</sup>, but also

numerous novel phosphorylations which had not been reported before, involving 5 serine and 2 threonine phosphorylation sites. Importantly, some of these phosphorylations were found on adjacent serine residues in the unstructured C terminus of the protein and one at the unstructured N terminus with both elevated intensities and probabilities (Figure 32C). Three serine phosphorylation sites (S316, S320 and S324) cluster downstream of the nuclear export sequence (NES) in the C-terminus (Figure 32D) and may consequently contribute to nuclear export <sup>208</sup>.

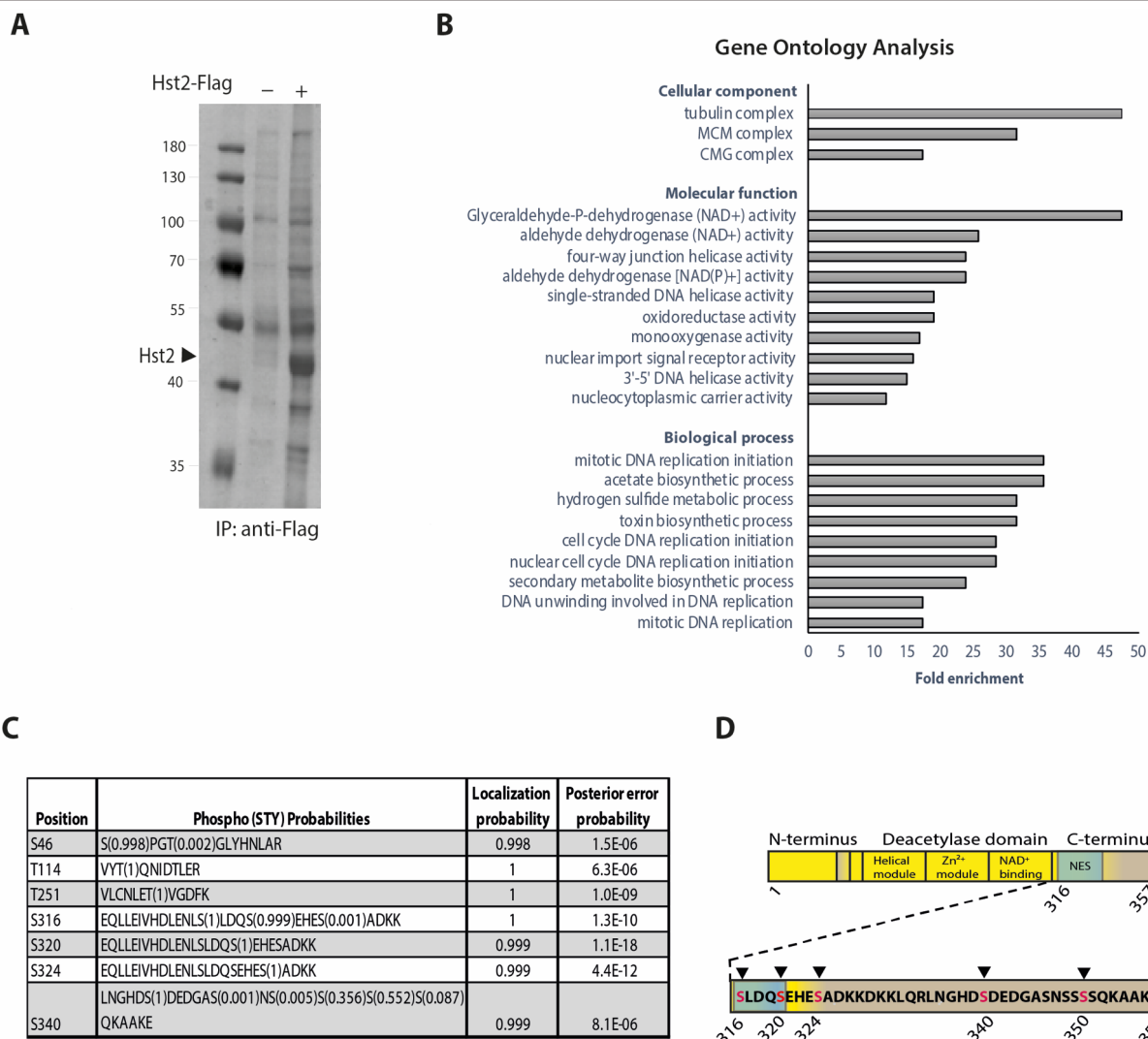


**Figure 32 : Identification of Hst2 interaction partners and PTMs by MS analysis.**

(A) Immunoprecipitation of Flag-tagged Hst2. Yeast cells expressing Flag-Hst2 were isolated with ANTI-FLAG® M2 beads, analyzed by 10% SDS-PAGE and stained with Instant Blue. Cells expressing untagged Hst2 acted as control.

(B) Gene ontology analysis of differentially linked proteins recognized in A. Analysis was implemented using the online tool “The Gene Ontology Resource”.

(C) Phosphorylation sites recognized on Hst2 by MS/MS analysis.

(D) Schematic representation of Hst2 C-terminal phosphorylation sites. NES: Nuclear Export Sequence (amino acids 306-317).

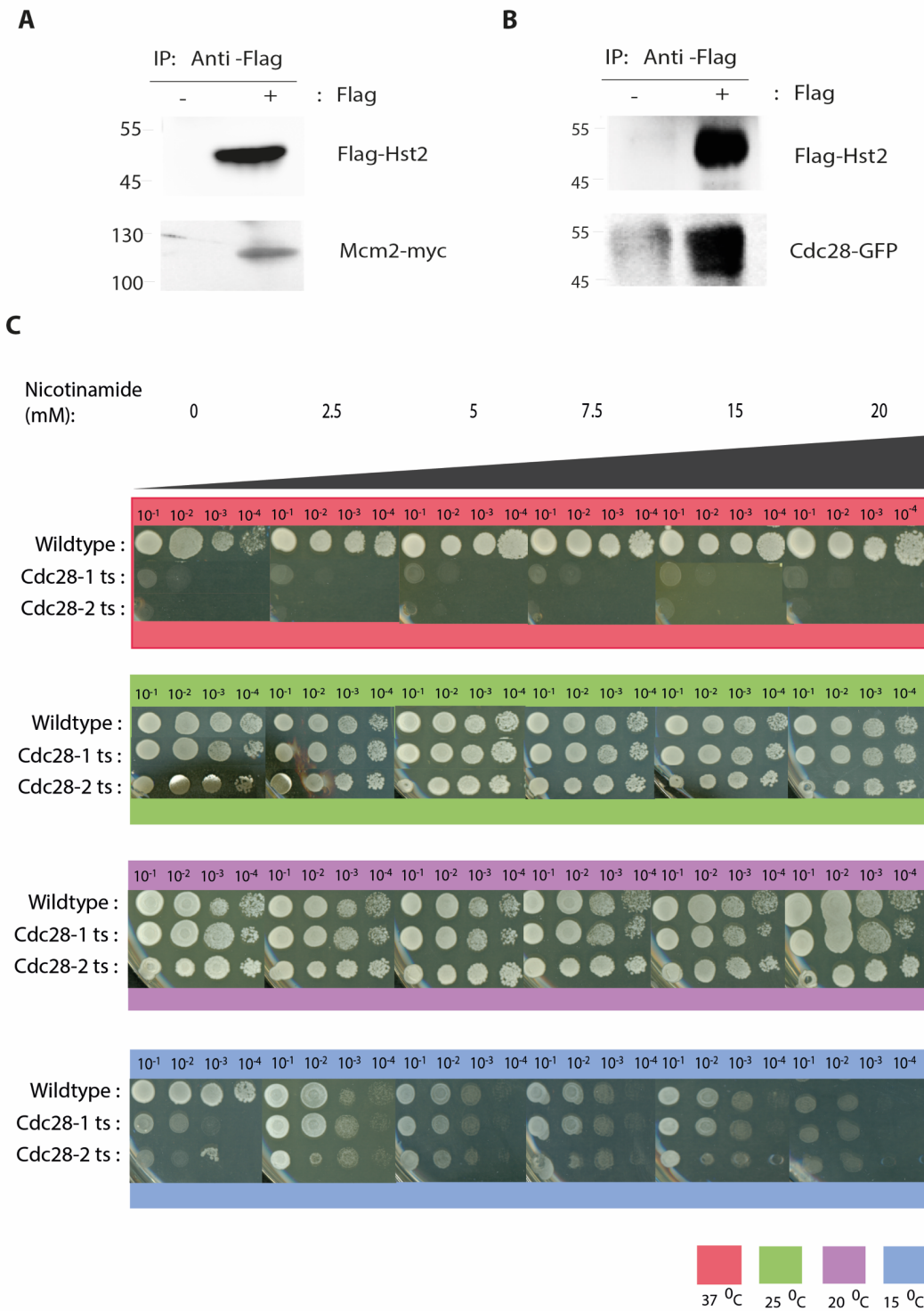


**Figure 33 : Interaction of Hst2 with Mcm2 and Cdc28.**

Flag-IPs from lysates of yeast cells overexpressing Hst2 with or without N-terminal Flag-tag and carrying either a 9xmyc-tag on Mcm2 (A) or GFP-tag on Cdc28 (B) were analyzed by SDS-PAGE and western blot using the indicated antibodies. (C) Serial dilutions (fourfold) of the indicated strains were spotted on YPD media with or without nicotinamide. Plates were grown at indicated temperatures for 48 hours.

### 3.3.3 CANDIDATE PROTEINS AS MISSING LINK IN CHROMOSOME CONDENSATION CASCADE

I postulated that phosphorylation of Hst2 is essential for its recruitment to H3 S10ph. Representative candidate moderators of interactions between two phosphorylated proteins are 14-3-3 proteins<sup>209-211</sup> (Figure 34A). They are ubiquitously expressed in eukaryotes and have been shown to be involved in myriad of key cellular procedures for example cell division, transcription, ion channels trafficking, proteasome functioning, in addition to in the development of diseases involving neurodegenerative disorders and cancer<sup>212,213,214,215</sup>. Nevertheless, their function in the conservation of chromatin architecture remains obscure. The interaction of 14-3-3 proteins with H3 S10ph is well well-known throughout diverse organisms<sup>216-218</sup>. Conversely, numerous KDACs are known to network with 14-3-3 proteins in a phosphorylation-dependent manner<sup>219</sup>. As, SirT2 interacts with 14-3-3  $\beta/\gamma$  in humans<sup>220</sup> and the homologous Sir2.1 and PAR-5/FTT-2 interact in nematodes<sup>221,222</sup>. In budding yeast 14-3-3 proteins are characterized by Bmh1 and Bmh2 and known to have high affinity to H3S10ph in addition to H3S10phK14ac peptides<sup>217</sup> (Figure 34B). Hence, I hypothesized that these proteins might operate as molecular bridge between H3 S10ph and phosphorylations on Hst2 that I discovered above.

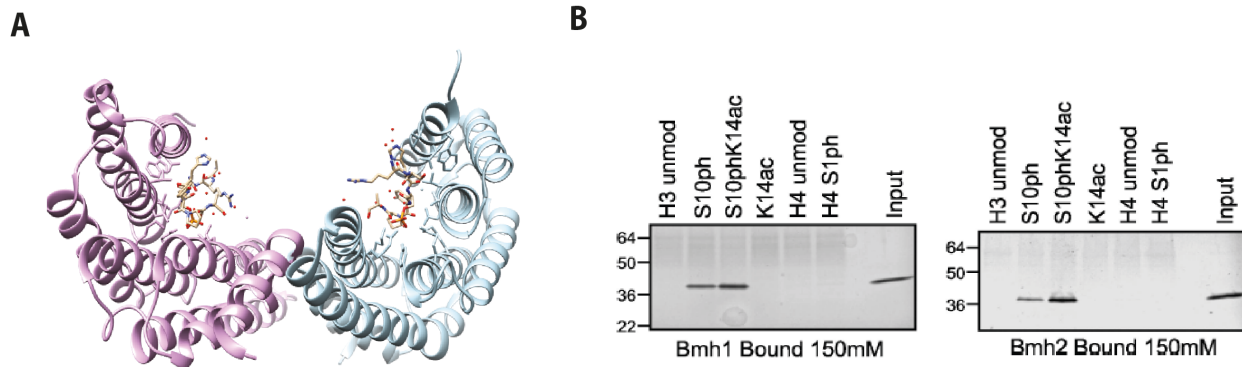


**Figure 34 : 14-3-3 proteins as candidates for recruiting Hst2 to H3S10ph.**

(A) Crystal structure of 14-3-3 bound to the phosphoserine peptide RLYHpSLP ( Figure prepared using pdb 1QJA<sup>223</sup>). (B) Recombinant Bmh1 and Bmh2 directly bind to H3S10 phK14ac peptides and also bind to H3S10ph peptides at lower ionic strength<sup>217</sup>. (Figure taken from Walter *et.al.*, 2008 <sup>217</sup>)

### 3.3.4 EFFECT OF BMH1/2 KNOCKOUTS ON H4K16AC LEVELS

Consequently, I tested whether depletion of the budding yeast 14-3-3 proteins, Bmh1 and Bmh2, impedes with deacetylation of H4 K16 by Hst2 in mitosis, an recognized hallmark of short-range chromatin compaction<sup>117</sup>. I examined the influence of individual depletion of Bmh1 and Bmh2 protein on H4 K16ac levels. Upon synchronization of cells with nocodazole and arrest in G2/M stage of mitosis as seen by elevated levels of H3 S10Ph the level of H4 K16ac sturdily reduced in wild type strain. As the role of Hst2 in mitosis as H4K16 deacetylase is well-known, strain depleted of HST2 were incapable of deacetylating H4K16 (Figure 35A). Startlingly, strain depleted of BMH1 exhibited comparable outcome as HST2 knockout that is persistence of H4K16ac levels specially, in cells synchronized with nocodazole. This was nonetheless not observed with full effect for strain deleted with BMH2. With these results I hypothesized that Bmh1 and Hst2 are in the identical pathway for H4K16ac and this interaction must be quite exclusive in mitosis.

Intriguingly, strain having a C-terminus deletion of Hst2 labelled as Hst2 aa1-295 showed the similar effect on H4K16ac levels as a complete Hst2 knockout, denoting that the C- terminus of the protein is vital for its full catalytic activity and consequence

on H4 K16ac levels *in vivo*. I established cell cycle synchronizations by gathering fractions of cells after arrest and measuring the DNA content by FACS analysis (Figure 35B). Additionally, when I observed the different cell types under microscope they all looked normal in shape, showing no obvious phenotypic defects of individual protein knockouts and successful synchronization specific morphologies: dumbbell shaped in G2/M phase for nocodazole synchronized cells (Figure 35C).

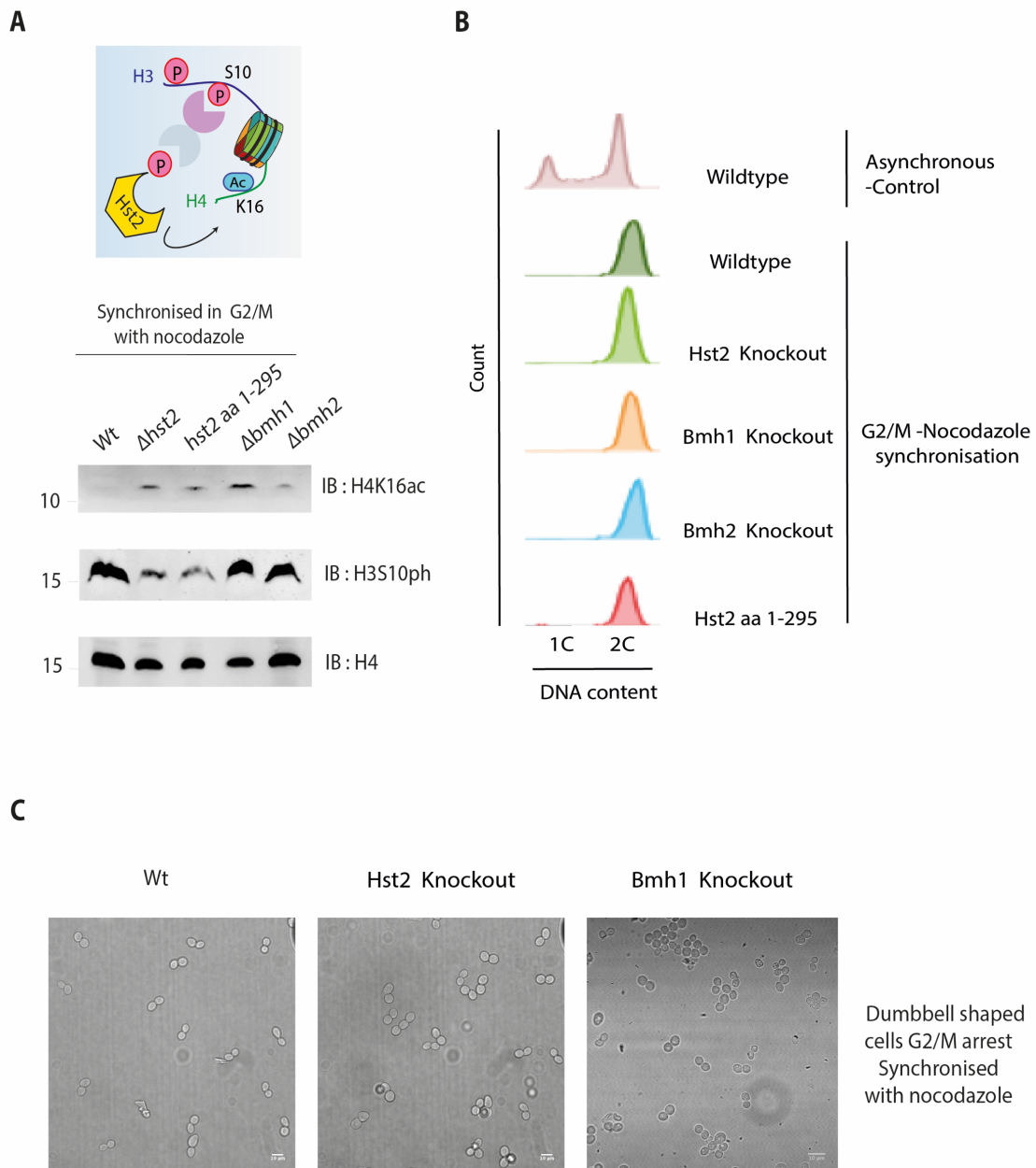


**Figure 35 : Hst2 and Bmh1 knockout have same effect on H4K16ac.**

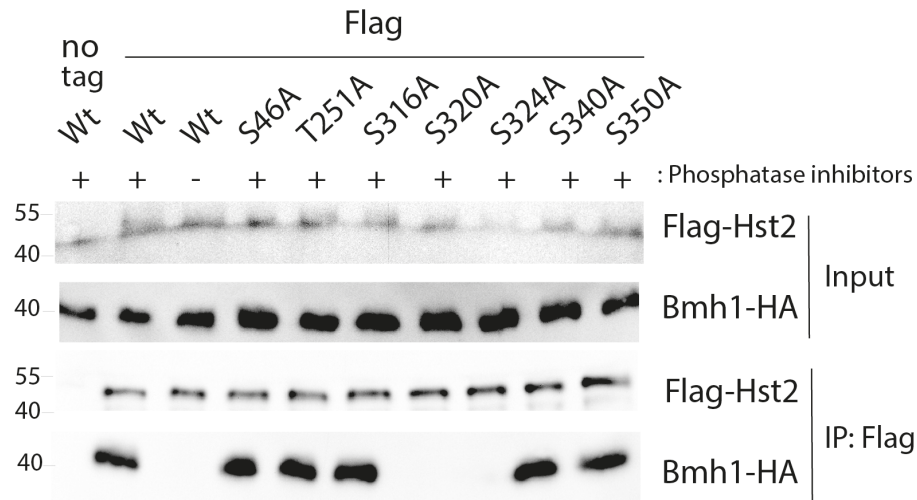
(A) Illustration depicting the hypothesis that 14-3-3 dimer (shown in purple) act as a scaffold between phosphorylation on H3 S10 and Hst2 and therefore might have a similar effect on H4K16ac. Wild type and mutant yeast cells were arrested with nocodazole or alpha factor; acid extracts of whole cell lysates were eluted by boiling in SDS-PAGE loading buffer, run on 18 % SDS gels and analyzed by Western blot with the indicated antibodies: anti H4K16ac (Active Motif (39167)), anti H3S10ph (Cell Signalling), anti H4 (Abcam). Representative blots from triplicate biological experiments. (B) Flow Cytometry analysis of DNA content of samples in A. (C) Morphological features of samples synchronised with nocodazole. Images were taken at 63x magnification using Zeiss LSM 800 Microscope. Scale bar represents 10  $\mu$ m.

### 3.3.5 CHARACTERIZATION OF INTERACTION BETWEEN HST2 AND BMH1 *IN VIVO*

Next, I tested whether Bmh1 and Hst2 interact physically, I isolated overexpressed Flag tagged Hst2 using anti-flag beads from yeast cells endogenously labelled with HA tag on Bmh1. I coprecipitated Bmh1 only with full length Flag tagged Hst2 as compared to untagged control. Moreover, this interaction appeared to be dependent on phosphorylation because it was abolished in the absence of phosphatase inhibitors (Figure 36A). Taking cue from this I decided to examine the interaction with the alanine mutants of Hst2 specially at the N- and C- terminus phosphosites that I identified using MS/MS earlier (Figure 36A). From the pulldown assays I concluded that the C terminus phosphorylations on residues S320 of Hst2 were essential for interaction with Bmh1 as alanine mutants for these positions abolished the binding which was not the case for alanine mutant at the N-terminus, S46A (Figure 3.28A). Thus, Hst2 and Bmh1 interaction is mediated by phosphorylations on the C-terminus of Hst2. Interestingly, mutation of Ser-320 to alanine alone was sufficient to completely abolish Bmh1 binding. Because optimal sequence motifs for 14-3-3 proteins are RX<sub>2</sub>-3-(pS/pT)-X-P<sup>224</sup>, I consider it unlikely that Bmh1 requires the presence of both phosphorylations for binding. It seems more likely that the two phosphorylation sites interact functionally, such that phosphorylation of one site relies on the presence of a serine residue at the other site.

Since, overexpression of Hst2 might have artificially induced the interaction with Bmh1, I repeated the pulldown experiments at endogenous protein levels. Therefore, I precipitated Bmh1-GFP from yeast lysates with genomically FLAG-tagged Hst2 (Figure 36B). Hst2-FLAG specifically co-eluted with Bmh1 depending on the GFP-tag on the latter, confirming that the Hst2-Bmh1 interaction also occurs at endogenous protein concentrations.

**A**



**B**

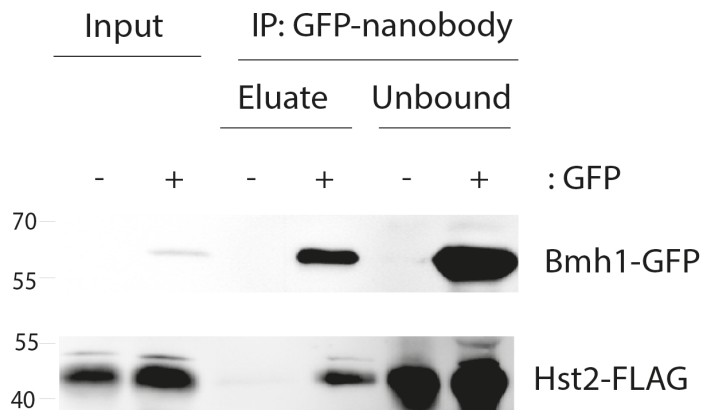


**Figure 36 : Hst2 and Bmh1 interact *in vivo*.**

(A) Interaction of Bmh1 with Hst2 *in vivo* depends on phosphorylation of Hst2 S320 or S324. Flag-Hst2 proteins were immuno-purified from overexpressing yeast cells and proteins analyzed by western blot with the indicated antibodies. (B) Bmh1 interacts with Hst2 *in vivo* at endogenous levels. Bmh1-GFP was isolated from yeast cells with or without genomically Flag-tagged Hst2 using GFP-nanobody beads. Bound proteins were eluted with SUMO protease (releasing the nanobody) and analyzed by western blot.

Next, I asked whether the Hst2-Bmh1 interaction is influenced by the cell cycle stage. Therefore, I repeated the pulldown experiments at endogenous protein levels with cell cycle synchronized yeast cultures (Figure 37A). Pulldown experiments with lysates from yeasts blocked in G1-phase with alpha-factor or S-phase with hydroxyurea should

very little interaction of Hst2 with Bmh1. In contrast, I observed efficient interaction of Hst2 with Bmh1 when cells were blocked in metaphase with nocodazole (Figure 37B,C). This result agrees with our model that Bmh1 recruits Hst2 to chromatin in mitosis when it is needed for short-range chromosome compaction.

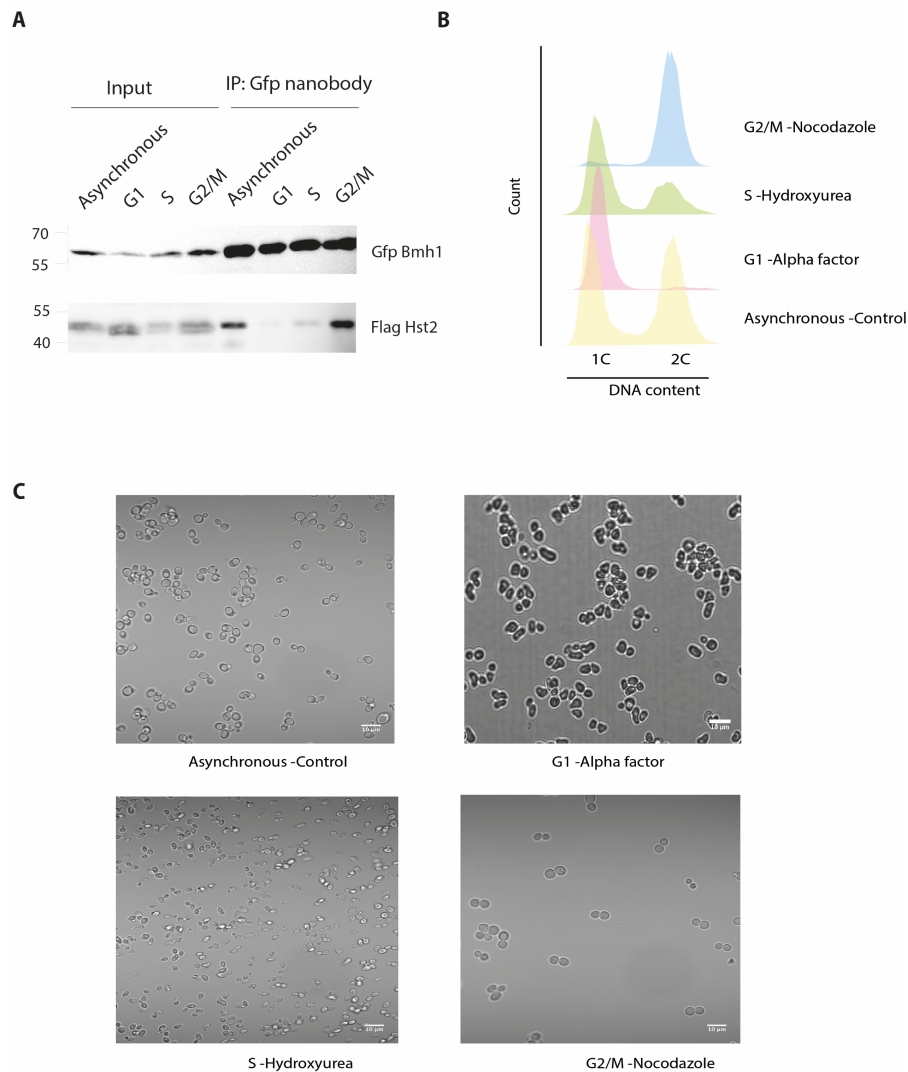


**Figure 37 : Bmh1 interacts with Hst2 in vivo at endogenous levels only in G2/M.**

(A) Yeast cells with genomically Flag-tagged Hst2 and GFP-tagged Bmh1 either asynchronous or arrested with  $\alpha$ -factor (G1), Hydroxyurea (S phase) or nocodazole (G2/M), respectively, were lysed and Bmh1-GFP isolated and bound protein analyzed as in Fig 3.28. (B) Flow Cytometry analysis of DNA content of samples in A. (C) Morphological features of samples synchronised with nocodazole. Images were taken at 63x magnification using Zeiss LSM 800 Microscope. Scale bar represents 10  $\mu$ m.

### 3.3.6 INTERACTION BETWEEN WILDTYPE HST2 AND BMH1

I also made use of yeast two-hybrid (Y2H) to evaluate the interaction between Hst2 and 14-3-3 proteins in yeast. The Y2H results are shown in A. As expected diploid yeast cells indicated as positive control showed interaction between Gal4 DNA-BD fused with murine p53 and Gal4 AD fused with SV40 large T-antigen to activate all reporters and show a white phenotype (SD/-Leu, SD/-Trp; SD/-Leu/-Trp/-His; SD/-Leu/-Trp/-Ade; SD/-Leu/-Trp/-His) or blue phenotype (SD/-Leu/-Trp/-His/-Ade/ X- $\alpha$ -gal), whereas diploid negative labelled yeast cells with Gal4 BD fused with lamin only showed no growth on any of the plates. Hst2 alone should show no signs of autoactivation. However, the screen failed to show any direct interactions between Hst2 and Bmh1 /Bmh2 (Figure 38A). This could be due to a number of reasons such as improper folding or prevention of posttranslational modification of the tagged proteins.

Moreover, in line with our previous results showing the necessity of phosphorylation for interaction of Hst2 and Bmh1, I performed a binding experiment with 20  $\mu$ M each of His-Tag Hst2 and Strep tag Bmh1. SEC elution profile and SDS-PAGE analysis showed an initial void peak of aggregated proteins (large blue and small grey peaks), followed by a dimeric peak of Bmh1 (orange colored) a possible oligomeric (tri/dimeric) peaks of wildtype Hst2 and ultimately monomeric Hst2 (grey peak). From the coelution profile and SDS gel it was evident that there is no interaction between wildtype Hst2 and dimeric Bmh1 proteins (Figure 38B).

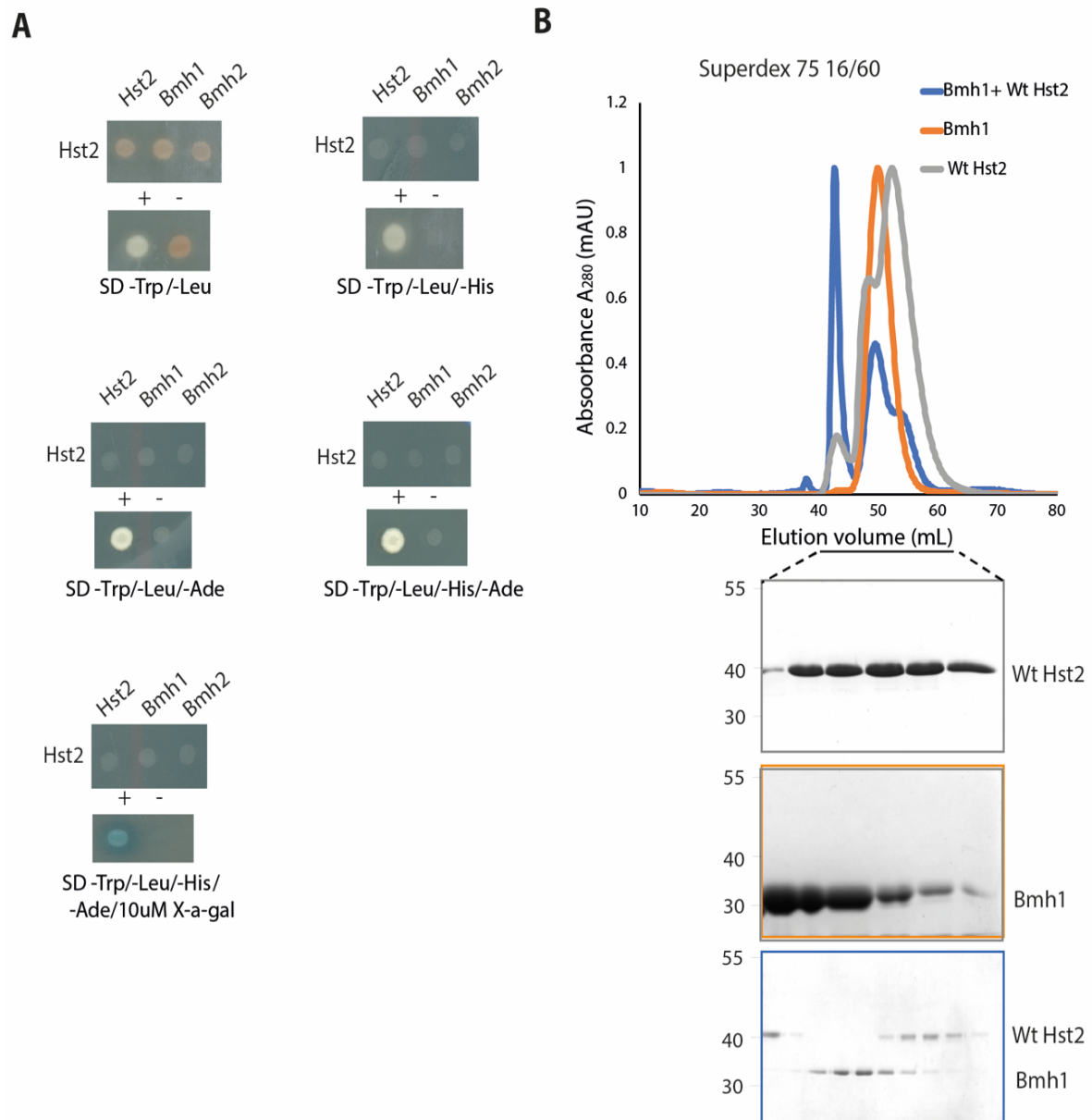


**Figure 38 : Wildtype Hst2 shows no interaction with Bmh1/2.**

(A) Yeast two-hybrid analysis of Hst2 and Bmh1,2 grown on synthetic dextrose (SD) media selection plates with different combinations of amino acids as depicted. " + " represents the positive control of the yeast two-hybrid, the combination of pGADT7 and pGBKT7-53. " - " shows the negative control of yeast two-hybrid, the pGADT7-T co-transformed with pGBKT7-lam. (B) SEC elution profiles and SDS-PAGE analysis of binding experiments with 20  $\mu$ M each of His-Tag Hst2 and Strep tag Bmh1.

### 3.3.7 PURIFICATION OF GENETICALLY ENCODED PHOSPHORYLATED HST2

So far I knew that phosphorylations are essential for interaction between Hst2 and Bmh1 therefore I prepared singly phosphorylated Hst2 proteins in *E. coli* for all further experiments using genetic code expansion<sup>164</sup>. Thereby, phosphoserine is encoded in response to amber (UAG) stop codons by an archaeal phosphoseryl-tRNA synthetase/tRNA<sub>CUA</sub> pair presented in an *E. coli* strain lacking phosphoserine phosphatase SerB. Suppression of amber codons substituting the codon for phosphorylated serine residues in Hst2 outcomes in the creation of site-specifically phosphorylated protein. I expressed pKW SepRS/tRNA<sub>CUA</sub> and pCDF-His- Hst2 plasmid comprising amber codons at serine residues S320 and S324 in DH10B  $\Delta$ serB cells and were able to purify phosphoserine containing Hst2 by Ni-NTA IMAC and Gel filtration chromatography (Figure 39A). SEC elution profiles showed an initial void peak of aggregates followed by elution of phosphoserine containing Hst2. Phosphorylations on Hst2 were confirmed by shift in mass from ESI measurements (Figure 39B) as well as by depletion of phosphorylated Hst2 species upon treatment with phosphatases which initially got separated on a 12% phostag gel (Figure 39C).

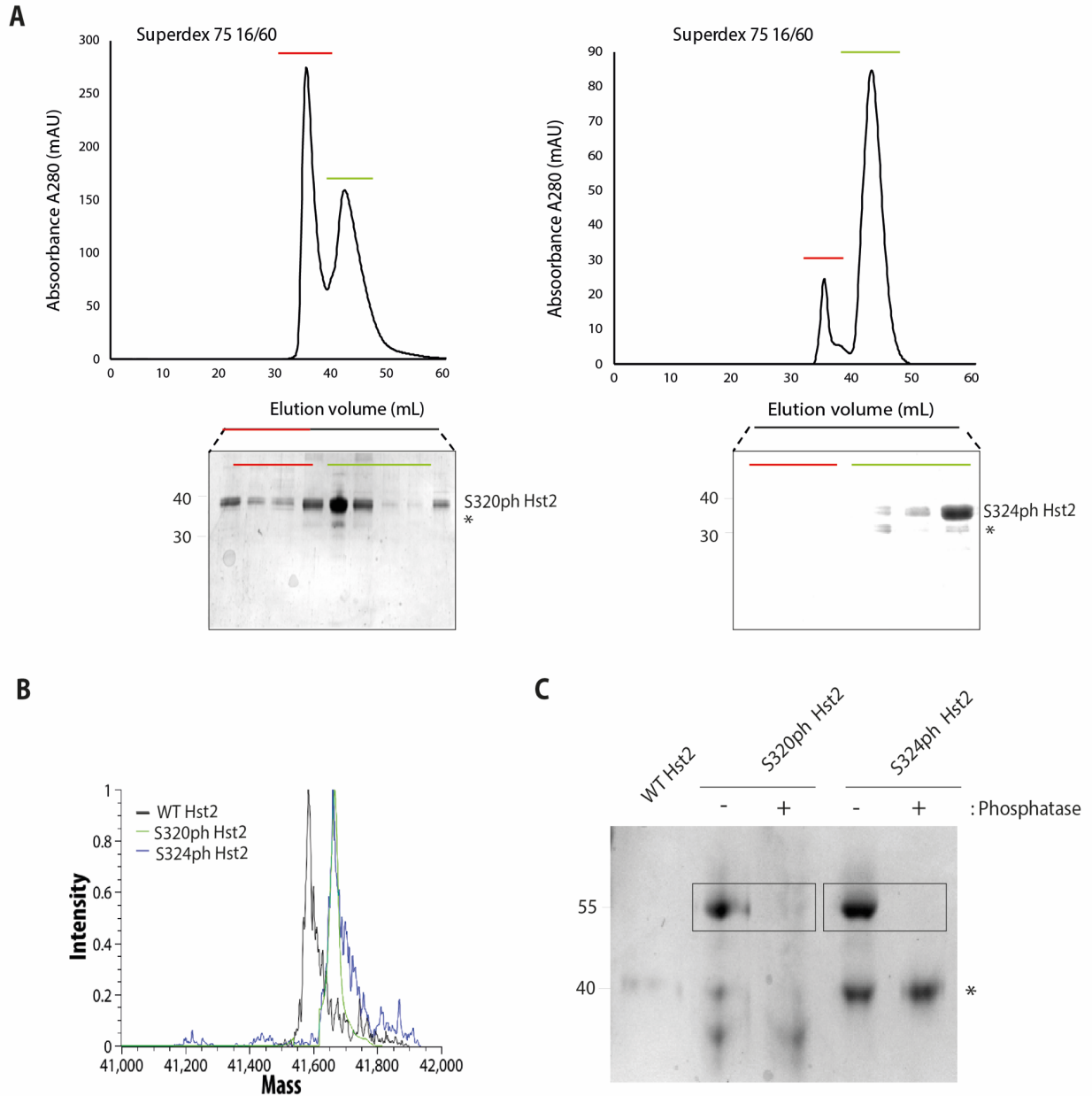


**Figure 39 : Purification of singly phosphorylated Hst2 by GCE.**

(A) SEC elution profiles and SDS-PAGE analysis of His-Tag Wt Hst2, Strep tag Bmh1, His tag PS 320 and PS 324 Hst2. \* symbol denotes truncation products from incomplete phosphoserine Incorporation. (B) Graphical representation of mass shift corresponding to phosphorylated Hst2: S320ph or S324ph (41,660 kDa) as compared to wildtype Hst2 (41,580 kDa) as measured by ESI-MS. (C) Recombinantly purified Phosphoserine Hst2 were phosphorylated. 10% phostag gel Coomassie stained showing recombinant wildtype Hst2 (41,580 kDa) and Phosphoserine 320 or 324 Hst2 with higher migrating bands representing phosphorylated species which further depleted upon treatment with calf intestinal phosphatase.

### 3.3.8 CHARACTERIZATION OF INTERACTION BETWEEN PHOSPHORYLATED HST2 AND BMH1 *IN VITRO*

Next, I used the above produced Hst2 S320ph and Hst2 S324ph and compared their ability to bind to Strep-tagged Bmh1 with unphosphorylated Hst2 (Figure 40A). Only S320ph Hst2 was efficiently recovered in these pulldown experiments, while unmodified Hst2 did not associate with Bmh1. Hence, this serine residue is individually sufficient to mediate the interaction *in vitro*. The phosphorylation of Hst2 may have further functions in the regulation of Hst2 activity. For example, phosphorylation of S316 could govern nuclear export of Hst2 because this residue is part of the NES. Furthermore, the C-terminal  $\alpha$ -helix of Hst2 has been shown to interfere with NAD<sup>+</sup>-binding<sup>206</sup>. Therefore, I measured the activity of recombinant Hst2 with or without phosphorylation of S320 or S324 in dependence of NAD<sup>+</sup>-concentration using acetylated Firefly luciferase as substrate<sup>178</sup> (Figure 40B). The phosphorylated forms of Hst2 both showed a threefold increase in  $V_{max}$  and a threefold decrease in  $K_M$  for NAD<sup>+</sup>, resulting in an nearly tenfold greater catalytic efficiency. The augmented catalytic efficiency was relapsed by preincubation of the phosphorylated proteins with calf intestine phosphatase (CIP), corroborating that the occurrence of the phosphorylation is crucial for the effect (Figure 40 B,C).

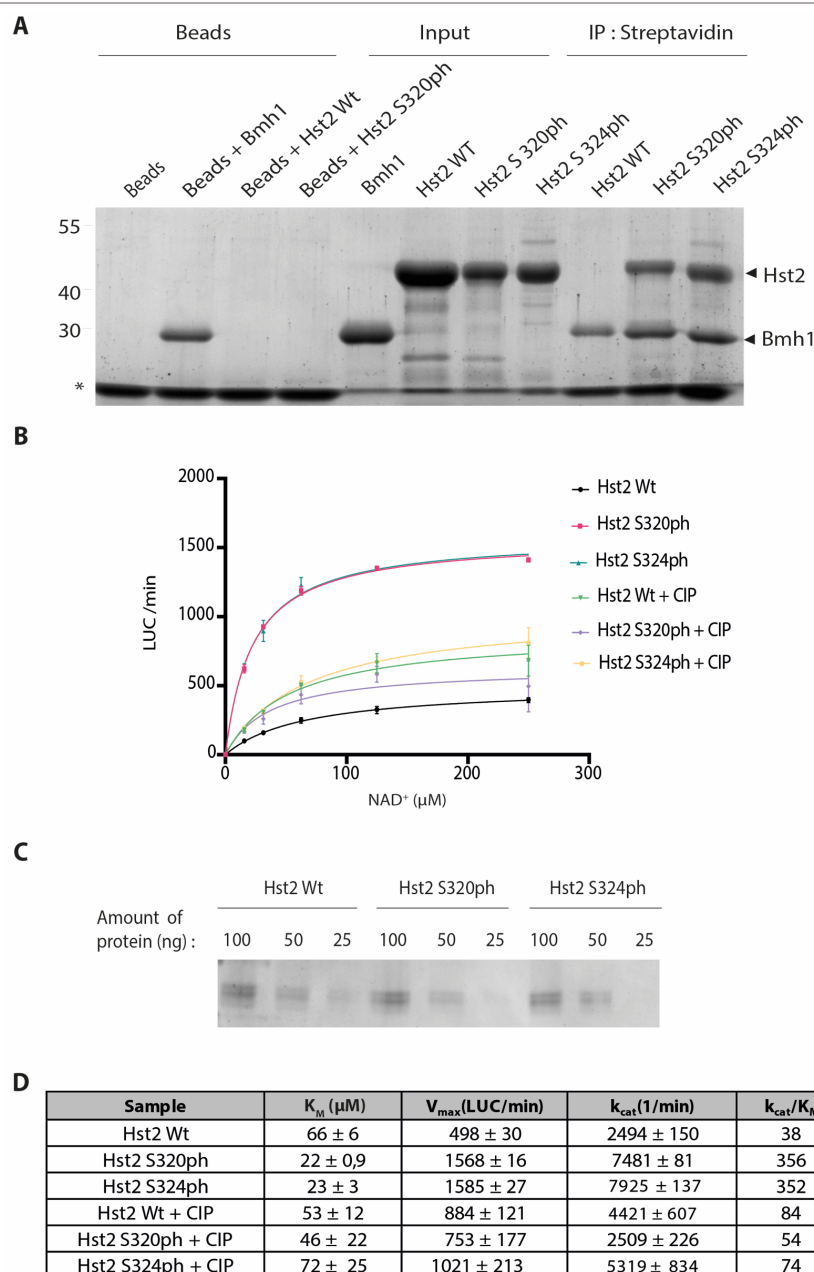


**Figure 40 : Phosphorylation of Hst2 enhances catalytic activity and mediates interaction with Bmh1 *in vitro*.**

(A) Bmh1 binds to singly phosphorylated Hst2 *in vitro*. Phospho-forms of Hst2 produced in *E. coli* were incubated with Strep-tagged Bmh1 on streptavidin beads. Bound proteins were eluted with SDS sample buffer, analyzed by 10% SDS-PAGE and stained with Instant Blue. \* denotes streptavidin bead specific band. (B) Kinetic analysis of Hst2 and the phospho-forms S320ph and S324ph. Deacetylation of FLuc K529ac by Hst2 isoforms was measured in continuous assay format. CIP was used to eradicate phosphorylation of Hst2. (C) Equal amounts of Hst2 proteins analyzed by 10% SDS-PAGE as loading control for B. (D) Kinetic factors of Hst2 and phospho-Hst2. Error values are estimated using a root mean least squares approach from a double-reciprocal plot.

### 3.3.9 EFFECT OF INDIVIDUAL PHOSPHOSITE MUTANTS ON H4K16AC LEVELS USING CRISPR/CAS9 GENOME EDITING

Finally, I tested the requirement of individual phospho-sites in Hst2 for H4 K16 deacetylation in mitosis. Therefore, I set out to create point mutants of Hst2 in which S316, S320 or S324 is replaced with alanine using CRISPR/Cas9. The major advantage of this technique is that it is a scarless method of genome editing and allows the facile construction of endogenous, homozygotic loss of phosphorylation alleles. As described in section 2.2.1.8 CRISPR/Cas9 Genome editing in Yeast, Hst2 C-terminus target gRNA was successfully cloned into pRS425-Cas9-2xSapI, that constitutively expressed the gene encoding the Cas9 endonuclease. Following this the cells were co-transformed with the above plasmid and the homology directed repair oligos for the three serine sites (S316, S320 and S324) respectively and plated on SD +Leu plates. Post transformation there were no clones on the control plate *i.e.*, without repair oligos and few clones on experimental plates. From these 4 clones per plate were picked for sequencing. As evident from the sanger sequencing electropherogram (Figure 41), there appeared to be an overlap of peaks and presence of artifacts beneath the peak suggesting a mix up of clones. Therefore, I decided not to pursue with these strains for further experiments.

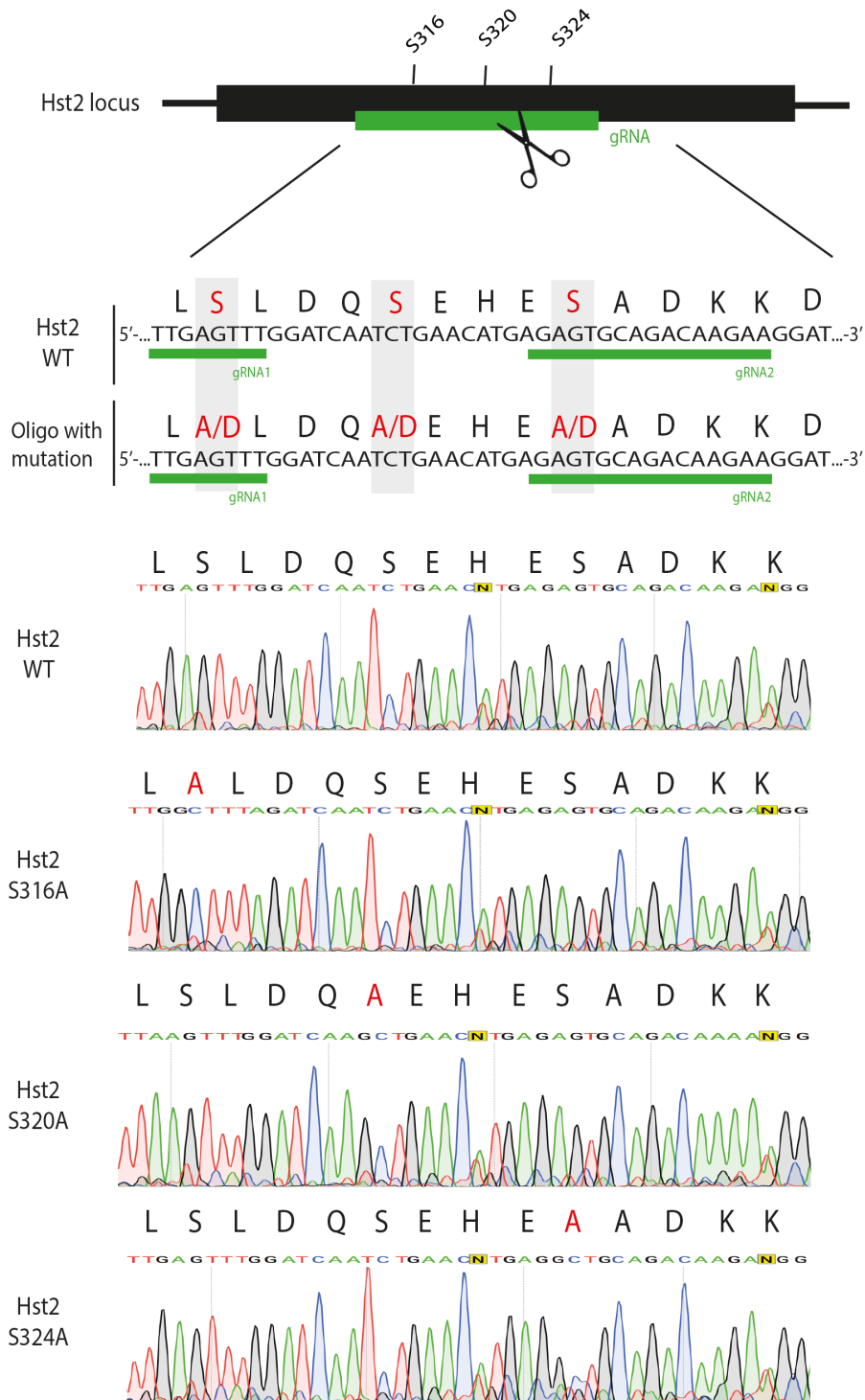
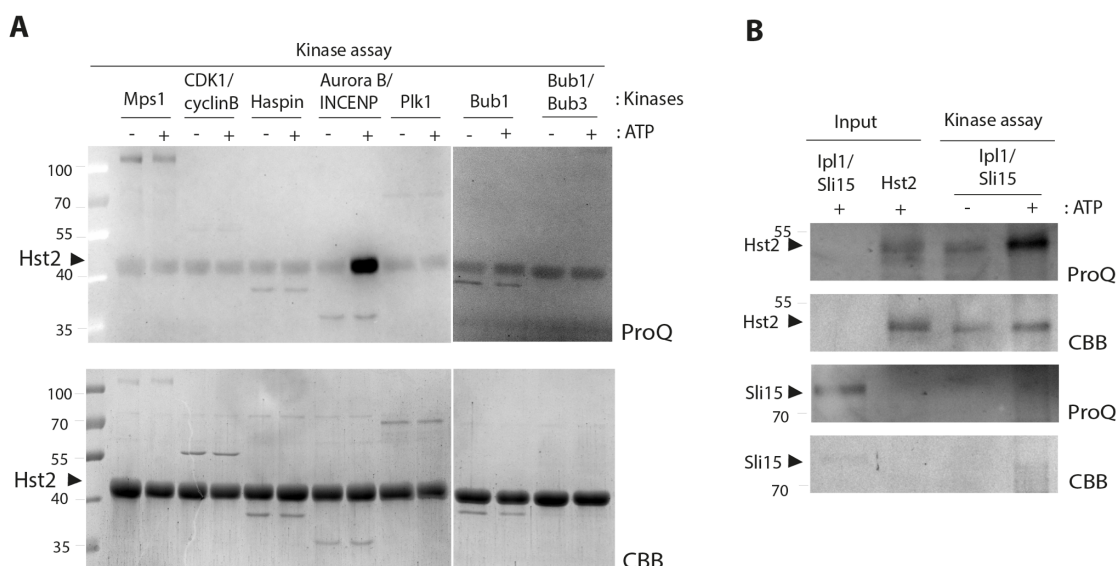


**Figure 41 : Genome Editing of Hst2.**

CRISPR/Cas9 genome-editing technology used to make the individual phosphosite mutations in HST2 in yeast cells. The guide RNA (gRNA) was designed to target Cas9 to cut in the C- terminus of HST2 gene and the mutations were introduced through homology-directed repair using a donor-oligos that carried the mutation. Chromatograms of the Sanger sequencing of cells with HST2 wild type and Hst2 S316A, S320A, S324A are shown.

### 3.3.10 INVESTIGATING POTENTIAL KINASES OF HST2

An open question that remains is the identity of the kinase which phosphorylates Hst2 in mitosis at the C-terminal region. I incubated numerous mitotic specific kinases with Hst2 in the absence or presence of ATP and intriguingly only found Aurora B/INBOX-INCENP phosphorylating Hst2 *in vitro* (Figure 42A) as well as yeast Aurora B homolog: Ipl1-1/Sli15 complex doing the same (Figure 42B). Upon MS analysis of the phosphorylated Hst2 I found several serine residues on Hst2 to be phosphorylated by human Aurora B/ INBOX-INCENP. However, none (S320 or S324) that are relevant for interaction between Hst2 and Bmh1. AuroraB /Ipl1 kinases play a major role in mitosis by regulating diverse substrates<sup>225</sup>. The fact that it is the kinase which regulates phosphorylation of H3 S10 prompted us to believe that it could be the kinase which also phosphorylates Hst2 for Bmh1 mediated interaction with H3 S10 phosphorylation in mitosis. Unfortunately, our current results do not support this hypothesis. Further investigations such as MS measurement of phosphorylations on Hst2 by Ipl1 *in vitro* and *in vivo* in yeast strains carrying deletions, temperature sensitive or analog sensitive alleles of mitotic kinase Ipl1 would assist in drawing conclusions. Moreover, most of the phosphosites identified here do not match the reported consensus sequence of phosphorylation by Aurora B kinase<sup>226</sup>.



Position	Phospho (STY) Probabilities	Localization probability	Intensity
S2	MS(0.971)VS(0.028)T(0.001)ASTEMSVRK	0.970831	3.05E+06
S38	VIFMVGAGIS(0.006)T(0.185)S(0.809)CGIPDFRSPGTGLYHNLAR	0.809347	7.10E+07
S46	VIFMVGAGISTS(0.001)CGIPDFRS(0.851)PGT(0.149)GLYHNLAR	0.850601	2.04E+07
T49	S(0.003)PGT(0.997)GLYHNLAR	0.99689	5.62E+07
S94	ELYPGNFRPS(1)K	1	7.73E+08
T114	RVYT(1)QNIDTLER	0.999999	7.17E+07
T208	IT(0.333)T(0.333)S(0.333)GKHPQQPLVIVVGTSLAVYPFASLPPEIIPRK	0.333333	
T209	IT(0.333)T(0.333)S(0.333)GKHPQQPLVIVVGTSLAVYPFASLPPEIIPRK	0.333333	
S210	IT(0.333)T(0.333)S(0.333)GKHPQQPLVIVVGTSLAVYPFASLPPEIIPRK	0.333333	
S225	HPQQPLVIVVGT(0.453)S(0.477)LAVY(0.252)PFAS(0.819)LPPEIIPR		
S233	HPQQPLVIVVGT(0.453)S(0.477)LAVY(0.252)PFAS(0.819)LPPEIIPR		
T251	RVLCNLET(1)VGDFK	1	2.2E+07
T262	RPT(1)DLIVHQYSDEFAEQLVEELGWQEDFEK	1	7.0E+09
S270	RPTDLIVHQYS(1)DEFAEQLVEELGWQEDFEK	0.999999	5.7E+07
S301	ILTAQGGMGDNS(1)K	0.999961	5.5E+06
S316	EQLLEIVHDLENLS(0.998)LDQS(0.002)EHESADKK	0.998318	2.4E+08

**Figure 42 : AuroraB delta45/InBox Incenp and Ipl-1/Sli15 phosphorylate Hst2 *in vitro*.**

(A) Human AuroraB delta45/InBox Incenp phosphorylates Hst2 *in vitro*. 10% SDS gels stained with phosphospecific ProQ stain (upper panel) and Coomassie (lower panel) showing phosphorylation of recombinant wildtype Hst2 by Aurora B kinase in the presence of ATP.

(B) Yeast Aurora Ipl-1/Sli15 phosphorylates Hst2 *in vitro*. 10 % 10% SDS gels stained with phosphospecific ProQ stain (upper panel) and Coomassie (lower panel) showing phosphorylation of recombinant wildtype Hst2 by Aurora B kinase in presence of ATP.

(C) MS/MS analysis of recombinant Hst2 by Aurora kinase from Fig5A showing several phospho residues with high intensities and probabilities.

## DISCUSSION

During the course of this study I explored multiple questions relevant in the context of chromatin biology. First part of my thesis focused on site-specifically incorporating genetically encoded crosslinker *p*-benzoyl-L-phenylalanine (pBPA) in living yeast, this helped in visualization of interaction landscape of chromatin. This was followed by an enrichment protocol for histones combined with a mass spectrometry-based pipeline for the identification of crosslink partners. Though it was possible to obtain biological information of interactors of few histone sites, the procedure needs to be repeated for diverse histone sites. Next, GCE enabled mapping of interaction topology of Sth1 protein onto histones *in vivo*. Novel roles of H3K14 acetylation and SUMOylation in modulation of RSC complex were identified. Lastly, a previously unknown role of 14-3-3 protein, Bmh1 in chromatin compaction by recruiting phosphorylated Hst2 to H3 tail was unraveled.

### 4.1 *IN VIVO* CROSSLINKING OF HISTONES IN *S. CEREVISIAE*

Building on established *in vivo* crosslinking strategies in my lab<sup>117,158</sup>, a complete library of amber site mutants across the histone surfaces for their suitability of pBPA incorporation and crosslinking pattern in asynchronous yeast cells (Figure 12, Figure 13). This disclosed that each histone protein has a distinctive interaction topology which is in turn context specific. The information acquired here can be used as a template for future investigations by uniting biochemical and proteomics-based characterization of individual crosslink proteins in different mutant strain backgrounds and at different stages of the cell cycle.

Unbiased proteomics helped in identification of new factors that encompass the local chromatin composition. The chief advantages were crosslinking efficiency of pBPA, its reversibility upon unuse and low cost for large scale experiments. The entire procedure had numerous benefits over conventional pulldown protocols as well as ChIP-

based methods. Though recent methods have extended biotin-based proximity labeling techniques such as BioID and APEX<sup>227</sup> for interactome mapping they nevertheless face issues for example effects on substrate bioavailability or surge in cellular oxidative stress. ChIP based methods require ChIP-grade antibodies which can be quite difficult to produce as well as expensive in nature. The site-specific incorporation of the crosslinker amino acids offered details on how proteins interact and probed only direct interactions as compared to typically employed formaldehyde crosslinking in ChIP<sup>228</sup>, which crosslinks proteins via lysine side chains and may produce large aggregates. The usage of non-damaging UV light offered temporal control over crosslinking reactions. Furthermore, this mode which is chiefly based on protein-protein interactions and could be accompanied with ChIP based on protein-DNA interactions, similar to ChIP-SICAP (chromatin immunoprecipitation merged with selective isolation of chromatin-associated proteins).

Genetically encoded pBPA has demonstrated to be a feasible and competent tool for capturing moderate affinity and transient protein-protein interactions *in vivo* on several occurrences. For instance, group of Anna K. Mapp had identified the recruitment mechanism of Swi/Snf remodeling complex to gene promoters to be dependent on transcriptional activators VP16 and Gal4 via direct interactions with its ATPase subunit Snf2<sup>229</sup>. Similar to the approach I utilized here of pBPA mediated crosslinking coupled with MS/MS based identification of dynamic histone interactome, they used the benzophenone diradical crosslinking along with shotgun proteomics for the identification of new interaction networks of the transcriptional activator, Gal4 in the cellular setting of budding yeast. They revealed that Gal4 makes contacts with two subunits within the Snf1/AMPK complex: Snf1 and Gal83 and provided insights into mechanism of cooperativity displayed by the activator in ultimately delivering a rapid transcriptional response to external stimulus<sup>230</sup>. In another study by the group of Tarun Kapoor, they used this approach combined with SILAC to identify post-translational modification (PTM) mediated interactions. Their investigation led to identification of MORC3 as a

binder of trimethylated lysine-4 at the histone H3 N-terminus (H3K4Me3)<sup>231</sup>. These above examples illustrate that pBPA mediated UV crosslinking merged with advanced proteomics techniques can help ensnare critical protein-protein interactions in their native context.

Here, the approach was successfully applied and assisted recognizing direct covalent binders at two distinct histone sites i.e., H2B T51 and H3 T80. Most of these interaction specificities are not fully characterized previously, hence provide new insights into chromatin networks. For H2B T51 site, exclusive UV crosslinked interactors are mostly nuclear proteins and participants of larger complexes involved in key processes such as chromatin remodeling, chromatin assembly and other key regulatory processes such as Spt16 which was also identified to crosslink to genomically-tagged H2B:3myc strains at position Y972 in an independent screen from my lab<sup>158</sup>. The observed interactions also agree with available structural information. For example, Srm1 is the yeast homolog of the RanGEF Rcc1, which has been shown to interact with this region of the nucleosome<sup>232</sup>. Few cytosolic proteins such as heatshock proteins, elongation factors, chaperons and cytoplasmic ligases were also identified. In routine proteomics analysis, these proteins are discarded as contaminants because of their higher abundance in cell<sup>233</sup>. Here detection of cytosolic proteins was not unexpected as histones are synthesized in the cytoplasm, and here I irradiated asynchronous yeast populations. In the process of assembly of histones, chaperons or ribosomal proteins could very well crosslink to some amber histone sites. Example, one mitochondrial protein Hsc82 was identified which could assist as a chaperone in communication with others. It was also previously reported to interact with Nap1 protein<sup>234</sup> which is a very well-known histone chaperone. Otherwise, these proteins could serve as mediator of cytosol-to-nucleus communication. For H3 T80 site, major interactors were involved in RNA metabolism and only few in chromatin related processes. For both sites I identified several differential binders except for five proteins such as Sth1, Nop12, Swc3, Top2 and Yta7. Out of which I was able to validate direct interaction between Sth1

and histones H2B T51 and H3 T80 by western blot shift assays (Figure 25). Similarly, validation experiments can be performed for other proteins recognized here to further explore their roles in site specific interaction.

While the crosslinking approach applied here was successful in acquiring some biological information for the abovementioned histone sites, it suffered from several caveats for further analysis of other histone sites (Figure 20), such as the following: it was limited by the very low amount of material obtained after growing several liters of yeast cultures, bringing into question the feasibility of further experiments. Quantitative mass spectrometry-based quantification requires relatively high amount of crosslink peptides to be detected. The current method was founded on large number of different crosslink products formed from the same position on histone proteins, such that the amount of material of each individual crosslink product was very low which would eventually restrict quantitative measurements by mass spectrometry. To improve this, labelling proteins with heavy isotopes in culture (SILAC) or by chemical labelling with isobaric tags (iTRAQ) may be used. These would also require amendments made in the MS/MS analysis setup, which is presently partial towards peptides of high abundance and exceedingly sensitive to contaminant proteins such as keratins or detergents such as PEG, which was a major hindrance here. Enhanced peptide detection specially for low abundant peptides, higher signal -to noise -ratios and better ion statistics quantification could improve results manifold to greatly escalate the inventory of chromatin interactors.

In terms of choice of crosslinker, even though pBPA has its own advantages, the low molar absorptivity and quantum yield of the crosslinker could constrain crosslinking yields. Mechanism wise pBPA experiences an  $n$  to  $\pi^*$  transition to form a diradical species, and the triplet state then reacts with protein functional groups via a sequential abstraction–recombination mechanism. Over the years numerous labs have created variants of pBPA with additional moieties such as lipid tools and linkers to

heighten its crosslinking efficiency<sup>235</sup>. In a topical study halogenated pBPAs were designed, with the intention that addition of these electron withdrawing groups onto the benzophenone framework would lead to reduction of the excitation energy gap for the  $n$  to  $\pi^*$  transition of the carbonyl oxygen's electrons, and surge the reactivity of the benzophenone core to ultimately raise the crosslinking yield of the molecule<sup>236</sup>. The use of bromine and chlorine isotopes in turn could conceivably be preferred in proteomics over approaches like SILAC to improve identification of crosslinks.

While *in vivo* crosslinking is a powerful approach to map protein interaction networks it can be experimentally very arduous particularly in terms of reproducibility and still subject to various corrections as suggested above. Because of these reasons, mapping at numerous other histone sites were withdrawn during the course of this thesis. With improvements in experimental designs and advancements in proteomics, information obtained in future with this method will be eventually helpful for the development of therapeutically useful small molecule modulators of protein-protein interactions. In terms of structural biology studies this approach will be beneficial for mapping multisubunit complexes which presently persist as an immense challenge. Information acquired by *in vivo* crosslinking could be predominantly useful to construct models of the nucleosome-bound state of the recognized proteins. These models would be valued because it is very difficult to procure such information by other methods. Only few nucleosome complexes have been crystallized to this point and nucleosome occupancy of several and stability of chromatin complexes is regularly low in Cryo-EM structures<sup>237</sup>.

## 4.2 INSIGHTS INTO RSC COMPLEX INTERACTION WITH NUCLEOSOME *IN VIVO*

While RSC has been extensively studied and its recent high-resolution maps have provided unprecedented structural insights into its functions<sup>69,67,68</sup>, there are pertinent questions that still remain unanswered, most of them involving its interaction with its substrate in the native context. To overcome this limitation, here I leveraged photo

crosslinking with large scale mapping studies in living yeast. I used electrophoretic mobility shift assays to disclose the footprint of Sth1, the catalytic subunit of RSC onto the nucleosome *in vivo*. Out of the 12 identified sites of crosslinking *in vivo*, the most profuse crosslinks of Sth1 resided in histone H3 comparable to the chromatin remodeler INO80<sup>238,239</sup>, specially at the N-terminal tail. Drawing on structural information of the nucleosome-bound RSC complex, crosslink reactions from the H3  $\alpha$  N-helix (R52, K56) almost certainly target the motor domain of Sth1, constant with the observation that mutations in this helix have a robust consequence on RSC remodeling activity<sup>240</sup>. Intriguingly, no crosslinks of Sth1 with histone H4 while its N-terminal tail has been revealed to bind at the interface of the SnAC and ATPase motor of Sth1 in the CryoEM structure were found here<sup>69</sup>.

Additional noteworthy crosslinking interactions of Sth1 were with parts of the histones H2A and H2B that constitute an acidic patch on the octamer surface<sup>241</sup>. RSC has been disclosed to sandwich histone octamer from both sides of acidic patch concurrently, on one side with Sth1 SnAC and other with Sfh1<sup>69</sup>. Crosslinking interactions of SnAC domain of Sth1 almost certainly ensue with H2A A61, E65; H2B T51, S115; H3 T80 while positions in the H3-tail possibly target its bromodomain in agreement with latest structural studies<sup>242</sup>.

Our observations additionally demonstrate that Sth1 relies on H3 K14 acetylation modification. Though, opposing prevalent belief, our results suggest that this modification is dispensable for its recruitment as removal of H3 K14ac had slight effect on binding of the RSC complex to the nucleosome. Recruitment of the complex must consequently be controlled by surplus mechanisms, for example through the zinc finger clusters of Rsc3 and Rsc30 (part of DNA interacting motif)<sup>69</sup> which identify a CGCG DNA element positioned upstream of the transcription start site<sup>243</sup> or universal regulatory factors of transcription and DNA sequence motifs like poly(dA)/(dT) elements<sup>244, 245</sup>. Our data propose that the bromodomain of Sth1 binds the K14ac mark of H3 tails

of adjacent nucleosomes. This property would be well-suited with the concept that RSC provides to the creation of a nucleosome depleted areas at yeast promoters<sup>63, 244</sup>.

Our results unraveled a novel pronounced preference of RSC for binding SUMOylated H2B *in vivo*. Protein SUMOylation outcomes in a myriad of effects, including changes in cellular localization or stability, modulation of protein–protein or protein–DNA interactions, or antagonizing other lysine modifications such as Ubiquitylation<sup>246,247</sup>. SUMOylation is chiefly involved in transcription regulation and contains components that modify chromatin structure<sup>248,249</sup>. All four core histones are known to be SUMOylated<sup>201</sup> with likely other unknown sites. However, their exact roles in cellular context remains elusive. Molecular evidence for regulation of chromatin remodeling by histone SUMOylation is still unexplored. Here, the crosslinking reactions of RSC from H2B positions formed a double band with the greater band being about 20-30% of the lower band intensity. Conversely, SUMOylation affects only about 5% of H2B molecules<sup>201</sup>, denoting that RSC has a convincing thermodynamic inclination for these nucleosomes. Using an online SUMO interacting prediction tool it appears that several subunits of the complex (specially Arp9, Rsc58, Rsc4, Rsc3, Sth1) have a high SUMO interacting prediction score<sup>250</sup>. Taking this as a starting point, these subunits can be depleted or inactivated *in vivo* (taking in consideration their effect on complex stability) to display the crosslinking outline. Next I asked, whether H2B SUMOylation modulates RSC activity *in vivo* or whether H2B SUMOylation depends on RSC activity. Though, RSC subunits have been formerly recognised in Siz1 pulldown<sup>251</sup> and could also be involved in course of deposition of this modifications onto nucleosomes, upon following the crosslinking reaction and supervising the double band pattern over a time course I propose that H2B SUMOylation ensures preferred interaction of RSC to nucleosomes *in vivo*. H2B SUMOylation has a repressive effect whereas Siz1,2 knock-out strain seems to show no significant effect on GAL1 transcription levels<sup>201</sup>. To evaluate whether RSC has a direct role in it, auxin (indole-3-acetic acid [IAA])-inducible degradation system that allows for rapid and reversible degradation of proteins could

be used. In short AID tagging of nonessential subunits of RSC such as used previously<sup>252</sup> could be combined with conditions having no SUMOylated nucleosomes as well as fused constitutive SUMOylation. Readout of GAL1 induction levels might be able to shed light on the involvement of RSC in transcriptional regulation and its dependence on SUMOylation. How would the interaction affinities of RSC complex with H2B-SUMOylated nucleosomes vary *in vitro*? Using ATPase or remodeling assays we detected only a marginally increased affinity RSC to SUMOylated substrate. Collectively, these data indicate that *in vivo* the state is severely complex, RSC recruitment encompasses a crosstalk amongst various histone modifications and engagement with additional elements such as histone variants and transcription factors<sup>253</sup>.

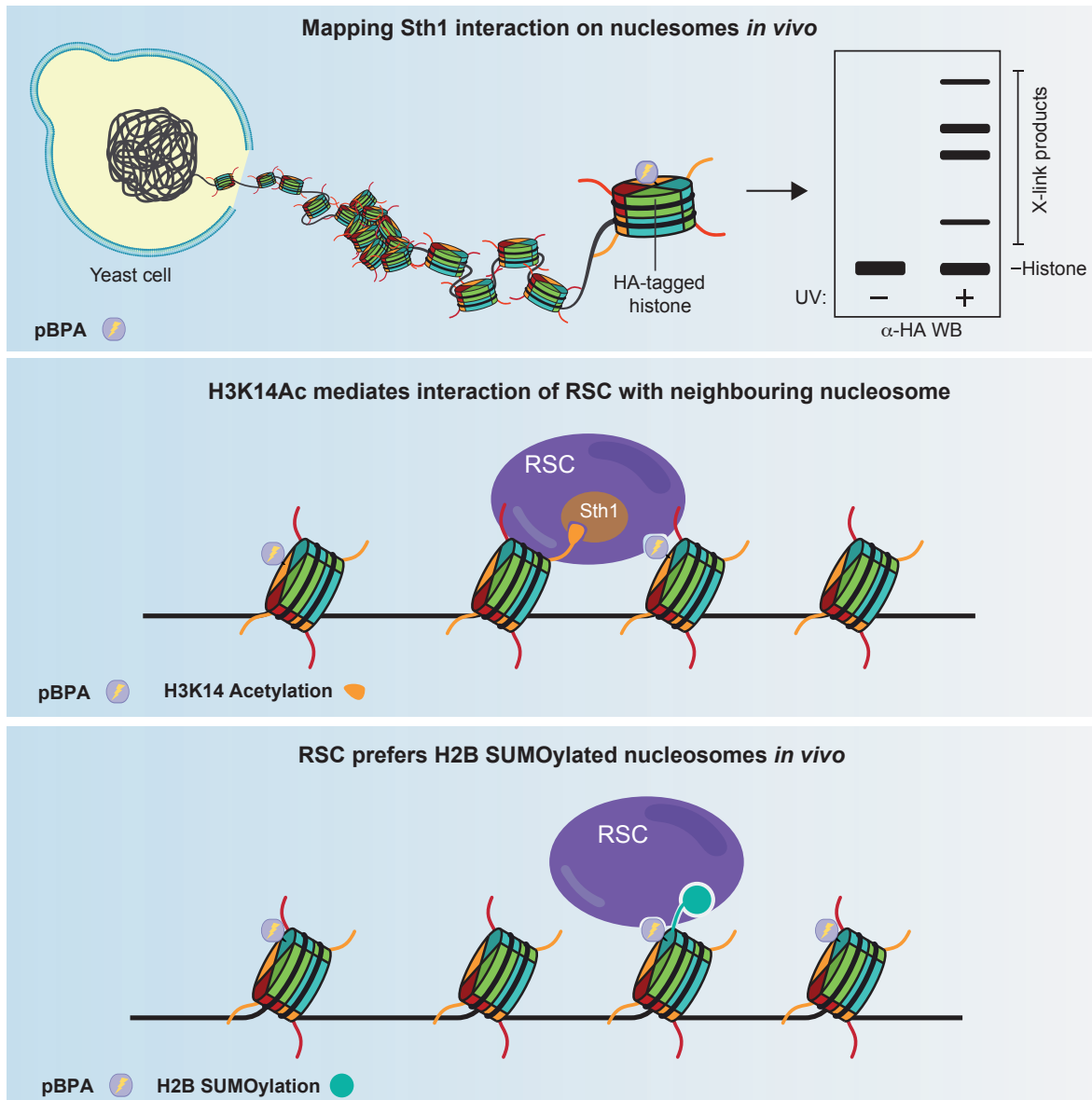


**Figure 43 : Modulation of RSC complex by histones and their PTMs.**

(Figure from Jain *et.al.*, 2020<sup>253</sup>)

Lastly, I examined the dynamics of RSC-nucleosome interactions with alterations in cell cycle stages and found that the crosslinking efficiencies from two sites (H3 S22 and K56) exhibited hardly any changes at distinctive cell cycle stages signifying that RSC contacts to nucleosomes are not lost rather upheld throughout the duration of the cell cycle. This implies that its activity is not regulated by ejection from chromatin by condensation in mitosis, as has been previously perceived for the homologous human chromatin remodeler BRG-1<sup>63</sup>. Additional positions such as H3 T80 and H2B T51 displayed mutual changes in crosslinking intensities in mitosis and interphase.

Intriguingly, position H3 T80 is only obscured in the structure of SNF2 bound at SHL+2, while H2B T51 is only concealed in the alternative configuration of SNF2 bound at SHL+6<sup>254</sup>. Otherwise, the variations in crosslinking efficiencies alongside the cell cycle stages could be the outcome of cell cycle deviations in histone PTMs. For example, H3 K56ac exhibits prominent cell cycle variation<sup>255</sup>. Whereas H3 K56ac does not disturb RSC interaction and remodelling, it could affect RSC interaction at the  $\alpha$ N-helix of H3<sup>169</sup>.

Our method could be valuable to examine the inclination of protein complexes for individual histone variants. As it has been revealed that RSC favourably remodels H2A.Z-containing nucleosomes at promoters<sup>15</sup>, by associating crosslinking efficiencies from corresponding positions amid two histone variants, it must be feasible to detect such inclinations. Precisely, crosslinking from sites adjacent to the acidic patch of recognised H2A and H2A.Z might be used to assess whether RSC specially inhabits on nucleosomes with the uncanonical version. Nevertheless, so as to permit such assessments, expression levels of both isoforms must be prudently equalised.

Whereas this strategy delivered us insights explicitly into Sth1 interaction, the potential of this method can be stretched to mapping other subunits of the complex, mapping interaction systems of proteins or resolving structural conformations for example as has been stated beforehand<sup>257</sup>. Addition of pBPA in distinctive sites of histone deacetylase 8 (HDAC8), aided in identification of HDAC8 definite substrates with larger catalytic efficiency following covalent capture, co-immunoprecipitation, and mass spectrometric analysis<sup>257</sup>. For ISWI complex, UV crosslinking was used to investigate its solution structure. Sites within its ATPase domain were discretely substituted with pBPA and subsequent crosslinks were mapped onto previously published crystal structures of ISWI-related ATPases. This facilitated examining structures and conformations of the protein which were not amenable to conventional structural techniques

<sup>256</sup>.

Furthermore, vital queries such as in what way mutations in distinctive domains of Sth1 would disturb or help its binding to the nucleosome could be answered by employing the same set of experiments that I used above. Global proteomic analysis have disclosed PTMs on RSC residues, these could be additionally mutated to explore the impact of these modifications which continue to be largely unknown.

### 4.3 IDENTIFICATION OF 14-3-3 PROTEIN Bmh1 IN TRIGGERING SHORT RANGE CHROMOSOME CONDENSATION

In *S. cerevisiae*, condensation process is previously known to begin at the centromeres in mitosis<sup>116</sup>. Here, Aurora Kinase B phosphorylates H3 S10 which ultimately leads to unmasking of H4 K16ac by Sirtuin, Hst2<sup>117,120</sup>. Another pathway encompasses the phosphorylation and activation of Shugoshin downstream of Aurora B. Here, I reveal that binding of Hst2 to H3S10 phosphorylation mark in mitosis is facilitated by Bmh1 which concurrently binds the phosphorylated H3 tail and C-terminally phosphorylated Hst2. Furthermore, phosphorylation of Hst2 at its C-terminus residue S320 is important for its interaction with Bmh1. *In vitro* it was sufficient to induce an interaction with Hst2. *In vivo*, mutation of this residue to alanine abrogated Bmh1 binding and to ability to stimulate the downstream deacetylation of H4 K16ac.

Thus, I dissected another important regulatory pathway that is mediated by 14-3-3 proteins *in vivo* which was formerly unreported. Until today, the mechanistic, structural and temporal insights into responses facilitated by 14-3-3 proteins are generally absent. This is aggravated by the shortage of co-crystal structures of 14-3-3 proteins with their bound partners either due their temporary phospho-mediated interaction which are arduous to reconstitute *in vitro* or occurrence of flexible or intrinsically disordered regions in partner proteins. Structural studies of 14-3-3 dimer proteins have

recognized conserved amphiphatic grooves in their alpha helical subunits which expedite accommodation of phosphomotifs of binding partner which then is believed to require electrostatic interactions adjoining the phosphosites with their amphiphatic residues. Fitting to the molecular anvil hypothesis consecutive binding of phosphomotifs at the amphiphatic groove mediates a conformational change in binding partner regulating their functions. Because optimal sequence motifs for 14-3-3 proteins are R-X<sub>2-3</sub>-(pS/pT)-X-P<sup>224,260</sup>, Our results uncover that Bmh1 mostly aids in recruitment of Hst2, which is chiefly cytoplasmic, to H3 tails to enable chromatin compaction in mitosis (Figure 44). Furthermore, at C-terminus of Bmh1 and Bmh2 reside poly-glutamine stretches which might mediate their interaction with nucleic acids and ultimately contribute to phase separation along with their interaction with Hst2<sup>261,262</sup>.

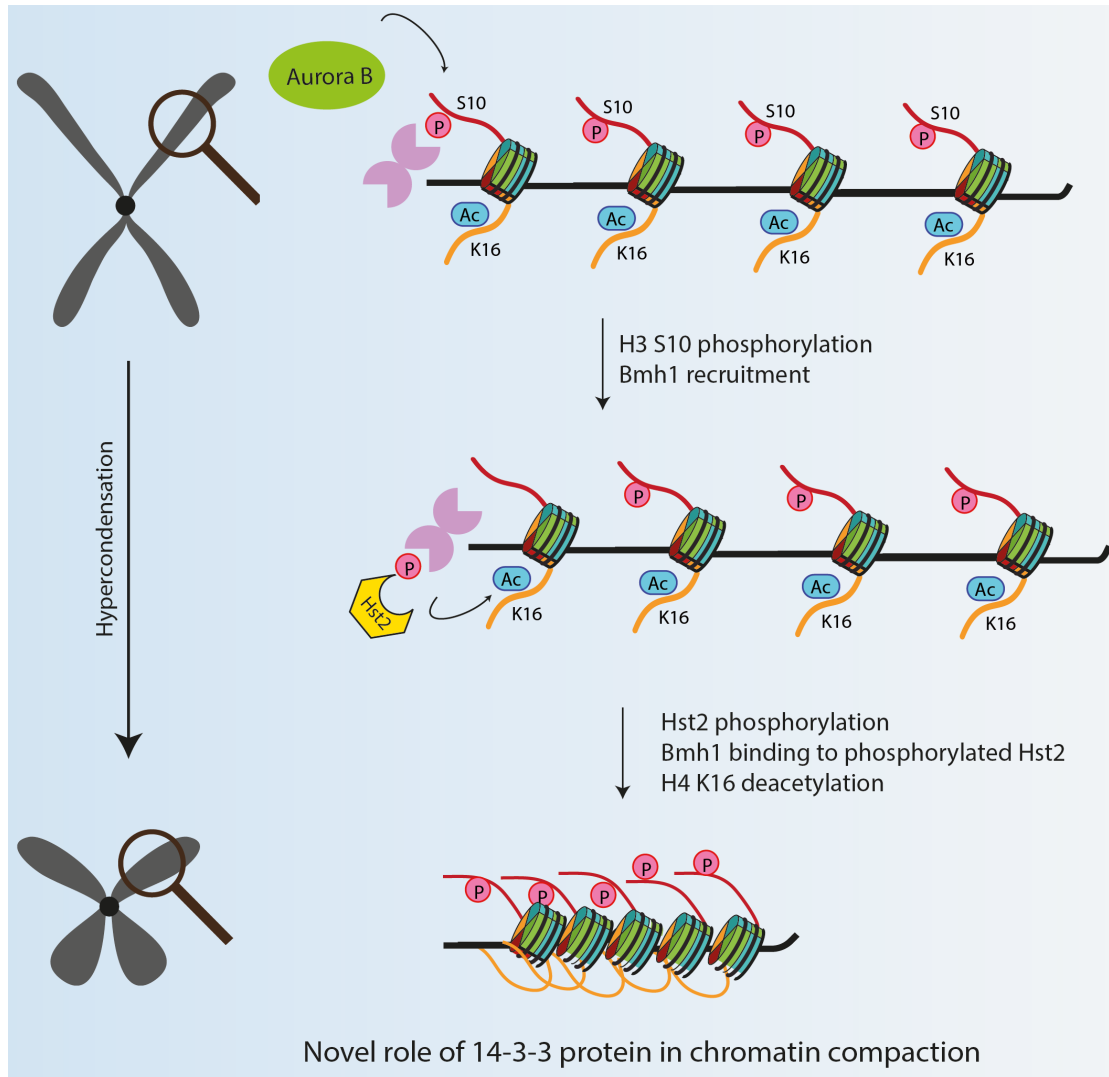


**Figure 44 : Model for histone tails mediated chromatin compaction.**

(Figure adapted from *Jain et.al., 2020*<sup>263</sup>)

Here I revealed the influence of deleting 14-3-3 proteins on H4 K16 acetylation levels. Bmh1 deletion had a marked effect on H4K16ac as compared to Bmh2, this could simply be due to much higher levels of Bmh1 in cells as compared to Bmh2<sup>264</sup>. Both these proteins have a high (~93%) amino acid identity and are described to display a good level of redundancy for most cellular functions. For example, Bmh2 overexpression had revealed to rescue the Bmh1 deletion mutant to lead to reduced Fin1 kinetochore localization and prolongation of the spindle assembly checkpoint (SAC)<sup>265</sup>. Despite their overlapping functions, both these proteins play unique roles as well, example Bmh1 was revealed to be needed for the efficient forward transport of Pmp2 and

not Bmh2<sup>266</sup>. These two yeast 14-3-3 proteins have been described to have different subcellular localization patterns<sup>267</sup> alongwith regulation of distinctive subset of genes<sup>268</sup>. For example, Bmh2 and not Bmh1 primarily regulates genes involved in ribosome biogenesis and nitrogen catabolite repression<sup>268</sup>. While single deletion mutants do not show noticeable growth-defects compared to wild type, the Bmh1 Bmh2 double mutant is described to be lethal in most yeast strains<sup>269,270</sup>. Hence, was not tested for its effect on H4K16ac here. But bearing in mind their similarity in amino acid composition and individual effect on H4K16ac, they are most likely redundant in recruiting Hst2 to H3 10ph in cells. Further experiments in this direction, say by over-expressing Bmh2 in Bmh1 deletion mutant and also examining for its direct physical interaction with Hst2 will help shed light on the role of Bmh2 in this process.

I could apprehend the functional consequence of phosphorylation on deacetylase activity of Hst2 using genetically encoded form of this modification. This aspect has been formerly studied for other Sirtuins such as phosphorylation of mammalian Sirtuin1 has shown to increase its activity<sup>271,272,273</sup>. Here, I saw an approximately 10-fold increase in catalytic efficiency of Hst2 upon phosphorylation which was appreciably reduced upon treatment with phosphatase. The X-ray crystal structure of the full-length Hst2 has been revealed to include a central catalytic core domain that is feature of other Sirtuin homologs, and C- and N-terminal domains that cooperate with the NAD<sup>+</sup> and acetyl-lysine substrate-binding sites, respectively. The C- terminal  $\alpha$ 13 helix is known to act as an autoinhibitor by moderately blocking the cofactor NAD<sup>+</sup>-binding<sup>206</sup>. Results from the kinetic analysis of effect of phosphorylation of Hst2 here appear to release this autoinhibition. Alternatively, unphosphorylated Hst2 C-terminus acts alike a mixed noncompetitive inhibitor which is concealed by phosphorylation. Binding of the C-terminus to the catalytic domain decreases the affinity for NAD<sup>+</sup> (increasing  $K_M$ ) and additionally slackens catalysis (decreasing  $V_{max}$ ). Moreover, Hst2 homologue in humans, SirT2 seems to be catalytically regulated by phosphorylation of at its C terminal

as well , suggesting a conserved mechanism by which phosphorylation serves to regulate these enzymes <sup>274,275</sup>.

It will be noteworthy to test how the mechanisms of chromatin compaction laid out here function in eukaryotes with much more convoluted chromosome structure, such as humans. A good commencing point for such investigations would be to check the recruitment mechanism of 14-3-3 proteins in Hst2 homologues in such cells. A critical question arising from our results was the distinctiveness of the kinase that phosphorylates the serine rich motif of Hst2. Using an *in vitro* kinase assay I speculate Ipl1, yeast Aurora kinase phosphorylates Hst2. However, further studies would be needed to potentiate these results.

Finally, our results can be recapitulated *in vitro* with phosphorylated Hst2 and Bmh1 being recruited to H3 S10ph peptides or reconstituted designer chromatin arrays which harbor FRET sensors. This will give us deeper understanding into the effect of the chromatin environment on Hst2 recruitment and will ultimately allow us to study the cascade of modification events leading to the condensation of the array. This will permit understandings of the kinetic properties of the condensation process and assist in experiments addressing a potential spreading of the cascade from kinetochore proximal to distal regions of the chromosome arm.

Regarding structural biology, the eventual aim comprises of a full three-dimensional model of the Hst2 interaction with H3 tail in its holo-form or bound to a nucleosome mediated by Bmh1 complex by means of structure determination techniques for example X-ray crystallography or Cryo-electron microscopy and Tomography. Former structural studies of nucleosomes and histone tails have not been obvious because of their reported flexible, unstructured nature. Addition of 14-3-3 protein

Bmh1 could impart rigidity to a segment of the phosphorylated H3 tail and provide understandings into its mechanism of bridging interactions with the deacetylase Hst2.

## SUPPLEMENTARY INFORMATION

### SUPPLEMENTARY TABLES

**Table 15 : Overview of *E.coli* strains used during this study.**

Strain	Genotype	Reference
<i>E.coli</i>	DH10B: F mcrA D(mrr-hsdRMS-mcrBC) F80dlacZDM15 DlacX74 endA1 recA1 D(ara,leu)7697 araD139 galU galK nupG rpsL	Invitrogen
<i>E.coli</i> BL21 (DE3)	F- ompT hsdSB(rB- mB-) gal dcm I (DE3)	Millipore
<i>E.coli</i> BL21 (DE3) <i>serB</i>	fhuA2 [lon] ompT gal ( $\lambda$ DE3) [dcm] $\Delta$ hsdS $\Delta$ serB  [ $\lambda$ DE3 = $\lambda$ sBamHlo $\Delta$ EcoRI-B int:::(lacI::PlacUV5::T7 gene1) i21 $\Delta$ nin5]	Addgene
<i>E.coli</i> SHuffle® Express Competent	fhuA2 [lon] ompT ahpC gal $\lambda$ att::pNEB3-r1-cDsbC (SpecR, lacIq) $\Delta$ trxB sulA11 R(mcr-73::miniTn10--TetS)2 [dcm] R(zgb-210::Tn10 --TetS) endA1 $\Delta$ gor $\Delta$ (mcrC-mrr)114::IS10	New England BioLabs
<i>E.coli</i> Rosetta 2	F- <i>ompT hsdS<sub>B</sub>(r<sub>B</sub>- m<sub>B</sub>-) gal dcm</i> pRARE2 (Cam <sup>R</sup> )	Novagen

**Table 16 : Overview of yeast strains used during this study.**

Strain	Genotype	Reference
BY4741	Mat a his3 $\Delta$ 1 leu2 $\Delta$ 0 met15 $\Delta$ 0 ura3 $\Delta$ 0 a his3 $\Delta$ 1 leu2 $\Delta$ 0 met15 $\Delta$ 0 ura3 $\Delta$ 0	AG Neumann
BY4741Bmh1-GFP/Hst2-Flag	[BY4741] pFA6a-GFP(S65T)-His3M Hst2-Flag:KanMX	AG Neumann
BY4741 Hst2-Flag	[BY4741] Hst2-Flag:HIS	AG Neumann
BY4741Bmh1-HA	[BY4741] Bmh1-3HA:hphNt1	This study
BY4741 $\Delta$ hst2	[BY4741] Hst2::KanMX	Yeast ko Collection (GE DHARMACON)
BY4741 $\Delta$ bmh1	[BY4741] Bmh1::KanMX	Yeast ko Collection (GE DHARMACON)
BY4741 $\Delta$ bmh2	[BY4741] Bmh2::KanMX	Yeast ko Collection (GE DHARMACON)
BY4741 Hst2 1-294	[BY4741] HST2::pRS303-Hst2_1-294	AG Neumann
BY4741Mcm2-9Myc	[BY4741] Trp::KanMX Mcm2-9Myc::KITrp1	AG Neumann
BY4741 Cdc28-Gfp	[BY4741] Cdc28-Gfp:His	AG Neumann
BY4741 Sth1-3myc	[BY4741] Sth1-3Myc::HIS3MX6	AG Neumann
BY4741 $\Delta$ gcn5	[BY4741] gcn5::HIS3	AG Neumann
BY4741 $\Delta$ siz2	[BY4741] siz1::kanMX siz2::hphNT1	This study
BJ3505 Rsc2-TAP	MATa pep4::HIS3 prb1- $\Delta$ 1.6R lys2-208 trp1- $\Delta$ 101 ura3-52 gal2 can1 rsc2- TAP::KITRP leu2 $\Delta$ ::KAN	AG Neumann
W303a cdc15-2	MATa leu2-3,112 trp1-1 can1-100 ura3-1 ade2-1 his3-11,15 phi+ cdc15-2	<sup>276</sup>

S288C H3	MATa his3Δ200 leu2Δ0 lys2Δ0 trp1Δ63 ura3Δ0 met15Δ0 can1::MFA1pr-HIS3 hht1-hhf1::NatMX4 hht2-hhf2::[HHTS-HHFS]*-URA3	197
S288C H3 K14A	MATa his3Δ200 leu2Δ0 lys2Δ0 trp1Δ63 ura3Δ0 met15Δ0 can1::MFA1pr-HIS3 hht1-hhf1::NatMX4 hht2-hhf2::[HHTS K14A-HHFS]*-URA3	197
AH109	MATa, trp1-901, leu2-3, 112, ura3-52, his3-200, gal4Δ, gal80Δ, LYS2 : : GAL1UAS-GAL1TATA-HIS3, GAL2UAS-GAL2TATA-ADE2, URA3 : : MEL1UAS-MEL1TATA-lacZ	Clontech's Matchmaker
Y187	MATa, ura3-52, his3-200, ade2-101, trp1-901, leu2-3, 112, gal4Δ, met-, gal80Δ, URA3 : : GAL1UAS-GAL1TATA-lacZ	Clontech's Matchmaker
BY4741Bmh1GFP/Hst2S316A-Flag	[BY4741]pFA6a-GFP(S65T)-His3M Hst2 S316A-Flag:KanMX	This study
BY4741 Bmh1-GFP/Hst2S320A-Flag	[BY4741]pFA6a-GFP(S65T)-His3M Hst2 S320A-Flag:KanMX	This study
BY4741 Bmh1-GFP/Hst2S324A-Flag	[BY4741]pFA6a-GFP(S65T)-His3M Hst2 S324A-Flag:KanMX	This study
Cdc 28-1 ts	[BY4741] Cdc 28-1 ts:: KanMX	AG Neumann
Cdc 28-2 ts	[BY4741] Cdc 28-2 ts:: KanMX	AG Neumann

Table 17 : Overview of plasmids used in this study.

Vector	Insert	Auxotrophic marker/Antibiotic resistance	Source
pESC	BPARS-tRNACUA	Leu/Amp	AG Neumann
pRS426	H2A-HA-L66TAG	Ura/Amp	AG Neumann
pRS426	H2A-HA-WT	Ura/Amp	AG Neumann
pRS426	H2A-HA-E57TAG	Ura/Amp	AG Neumann
pRS426	H2A-HA-Y58TAG	Ura/Amp	AG Neumann
pRS426	H2A-HA-L59TAG	Ura/Amp	AG Neumann
pRS426	H2A-HA-A60TAG	Ura/Amp	AG Neumann
pRS426	H2A-HA-A61TAG	Ura/Amp	AG Neumann
pRS426	H2A-HA-E62TAG	Ura/Amp	AG Neumann
pRS426	H2A-HA-I63TAG	Ura/Amp	AG Neumann
pRS426	H2A-HA-L64TAG	Ura/Amp	AG Neumann
pRS426	H2A-HA-E65TAG	Ura/Amp	AG Neumann
pRS426	H2A-HA-L66TAG	Ura/Amp	AG Neumann
pRS426	H2A-HA-A67AG	Ura/Amp	AG Neumann
pRS426	H2A-HA-D90TAG	Ura/Amp	AG Neumann
pRS426	H2A-HA-D91TAG	Ura/Amp	AG Neumann
pRS426	H2B-HA-WT	Ura/Amp	AG Neumann
pRS426	H2B-HA-A12-T6AG	Ura/Amp	AG Neumann

pRS426	H2B-HA-R32-TAG	Ura/Amp	AG Neumann
pRS426	H2B-HA-T51-TAG	Ura/Amp	AG Neumann
pRS426	H2B-HA-S115-TAG	Ura/Amp	AG Neumann
pRS426	H2B-HA-T122-TAG	Ura/Amp	AG Neumann
pRS426	<b>H2B-HA-K123-TAG</b>	Ura/Amp	AG Neumann
pRS426	H3-HA-WT	Ura/Amp	AG Neumann
pRS426	H3-HA-T6TAG	Ura/Amp	AG Neumann
pRS426	H3-HA-A15TAG	Ura/Amp	AG Neumann
pRS426	H3-HA-A21TAG	Ura/Amp	AG Neumann
pRS426	H3-HA-A29TAG	Ura/Amp	AG Neumann
pRS426	H3-HA-P38TAG	Ura/Amp	AG Neumann
pRS426	H3-HA-R52TAG	Ura/Amp	AG Neumann
pRS426	H3-HA-K56TAG	Ura/Amp	AG Neumann
pRS426	H3-HA-R69TAG	Ura/Amp	AG Neumann
pRS426	H3-HA-E73TAG	Ura/Amp	AG Neumann
pRS426	H3-HA-Q76TAG	Ura/Amp	AG Neumann
pRS426	H3-HA-T80TAG	Ura/Amp	AG Neumann
pRS426	H3-HA-L82TAG	Ura/Amp	AG Neumann
pRS426	H4-HA-WT	Ura/Amp	AG Neumann
pRS426	H4-HA-G9TAG	Ura/Amp	AG Neumann
pRS426	H4-HA-R17TAG	Ura/Amp	AG Neumann
pRS426	H4-HA-R19AG	Ura/Amp	AG Neumann
pRS426	H4-HA-K20TAG	Ura/Amp	AG Neumann
pRS426	H4-HA-R23TAG	Ura/Amp	AG Neumann
pRS426	H4-HA-Q27TAG	Ura/Amp	AG Neumann
pRS426	H4-HA-R45TAG	Ura/Amp	AG Neumann
pRS426	H4-HA-A56TAG	Ura/Amp	AG Neumann
pRS426	H4-HA-A56TAG	Ura/Amp	AG Neumann
pRS426	H4-HA-A56TAG	Ura/Amp	AG Neumann
pRS426	H4-HA-S60TAG	Ura/Amp	AG Neumann
pRS426	H4-HA-R67TAG	Ura/Amp	AG Neumann
pRS426	H4-HA-E74TAG	Ura/Amp	AG Neumann
pRS426	H4-HA-K77TAG	Ura/Amp	AG Neumann
pRS423	Hst2 +/- 500bp (Sc)	His/Amp	AG Neumann
pRS423	Hst2 n Flag +/- 500bp (Sc)	His/Amp	This study
pRS423	Hst2 S46A n Flag +/- 500bp (Sc)	His/Amp	This study
pRS423	Hst2 T251A n Flag +/- 500bp (Sc)	His/Amp	This study
pRS423	Hst2 S316A n Flag +/- 500bp (Sc)	His/Amp	This study
pRS423	Hst2 S320 n Flag +/- 500bp (Sc)	His/Amp	This study
pRS423	Hst2 S324A n Flag +/- 500bp (Sc)	His/Amp	This study
pRS423	Hst2 S340A n Flag +/- 500bp (Sc)	His/Amp	This study
pRS423	Hst2 S350A n Flag +/- 500bp (Sc)	His/Amp	This study
pGBKT7	Myc-Hst2	Trp/Kan	This study
pAGDT7	HA-Bmh1/Bmh2	Leu/Amp	This study
pRS425	pRS425-CRISPR/Cas9-2xSap1	Leu/Amp	Bruce Flutcher
pRS425	pRS425-CRISPR/Cas9-2xSap1- Hst2_S316_gRNA	Leu/Amp	This study
pRS425	pRS425-CRISPR/Cas9-2xSap2- Hst2_S324_gRNA	Leu/Amp	This study
pCDF-Duet	Hst2 - His	Spec	AG Neumann

pCDF	Bmh1- His	Spec	AG Neumann
pCDF	Bmh1- Strep	Spec	This study
pGBKT7	Myc-Hst2	Trp/Kan	This study
pAGDT7	HA-Bmh1	Leu/Amp	This study
pAGDT7	HA-Bmh2	Leu/Amp	This study
pUG6	loxP-KanMX-loxP	Amp	Euroscarf vector
pYM24	3X HA (hphNT1)	Amp	AG Neumann
pKW2-EF-Sep	SepRS2, pSer-tRNAB4CUA and EF-Sep	Cmp	<sup>164</sup>
pK63 gfp-nanobody	His14-tag-2xProtA SUMO GFPNanobody myc	Kan	AG Neumann

**Table 18 : Overview of primers used in this study.**

Oligo name	Sequence(5'-3')
CR_O_S46A_Stu1	GGATATCCACTTCTTGTGGGATACCAGACTTCCGAGCTCCCG-GAACAGGCCTGTACCATAACTTGGCCAGGTTGAAGTTGCCGTACC
CR_O_S46D_Stu1	GGATATCCACTTCTTGTGGGATACCAGACTTCCGAGATCCCG-GAACAGGCCTGTACCATAACTTGGCCAGGTTGAAGTTGCCGTACC
CR_O_S316A_BspH1	GGATAACTCTAAAGAGCAATTACTTGAAATTGTTTCATGATTTAGA-GAATTTGGCTTTAGATCAATCTGAACATGAGAGTGCAGACAAGAA
CR_O_S316D_BspH1	GGATAACTCTAAAGAGCAATTACTTGAAATTGTTTCATGATTTAGA-GAATTTGGATTTAGATCAATCTGAACATGAGAGTGCAGACAAGAA
CR_O_S320A_Mse1	AATTGTACATGATTTAGAGAATTTAAGTTTGGATCAA-GCTGAACATGAGAGTGCAGA-CAAAAAGGATAAGAAGCTACAGCGTCTCAATGG
CR_O_S320D_Mse1	AATTGTACATGATTTAGAGAATTTAAGTTTGGATCAA-GATGAACATGAGAGTGCAGA-CAAAAAGGATAAGAAGCTACAGCGTCTCAATGG
CR_O_S324A_Mse1	GAAATTGTACATGATTTAGAGAATTTAAGTTT-GGATCAATCTGAACATGAGGCTGCAGA-CAAAAAGGATAAGAAGCTACAGCGTCTCAAT
CR_O_S324D_Mse1	GAAATTGTACATGATTTAGAGAATTTAAGTTT-GGATCAATCTGAACATGAGGATGCAGA-CAAAAAGGATAAGAAGCTACAGCGTCTCAAT
CR_O_S316,20,24A_BspH1	AAGAGCAATTACTTGAAATTGTTTCATGATTTAGAGAATTTGGCTTTA-GATCAAGCTGAACATGAGGCTGCAGACAAGAAGGATAAGAAGC
CR_O_S316,20,24D_BspH1	AAGAGCAATTACTTGAAATTGTTTCATGATTTAGAGAATTTGGATTTA-GATCAAGATGAACATGAGGATGCAGACAAGAAGGATAAGAAGC
CR_gRNA_S46_fp	ATCGATACCAGACTTCCGATCTC
CR_gRNA_S46_Rp	AACGAGATCGGAAGTCTGGTATC
CR_gRNA_S316_Fp	ATCTGATTTAGAGAATTTGAGTT
CR_gRNA_S316_Rp	AACAACCTCAAATTCTCTAAATCA
CR_gRNA_S324_Fp	ATCACATGAGAGTGCAGACAAGA
CR_gRNA_S324_Rp	AACTCTTGCTGCACTCTCATGT
CR_s46_pcr_fp	ATGTCGCTATCTGTGCC
CR_s46_pcr_rp	TACTCTCTCAAACG
CR_S316_pcr_Fp	GCACCTCACTAGCCGTTT
CR_S316_pcr_Rp	CTTTAGCGGCTTTTTGTG

CR_O_S46A_Stu1	GGATATCCACTTCTTGTGGGATACCAGACTTCCGAGCTCCCG- GAACAGGCCTGTACCATAACTTGGCCAGGTTGAAGTTGCCGTACC
CR_O_S46D_Stu1	GGATATCCACTTCTTGTGGGATACCAGACTTCCGAGATCCCG- GAACAGGCCTGTACCATAACTTGGCCAGGTTGAAGTTGCCGTACC
CR_O_S316A_BspH1	GGATAACTCTAAAGAGCAATTACTTGAAATTGTTCATGATTTAGA- GAATTTGGCTTTAGATCAATCTGAACATGAGAGTGCAGACAAGAA
CR_O_S316D_BspH1	GGATAACTCTAAAGAGCAATTACTTGAAATTGTTCATGATTTAGA- GAATTTGGATTTAGATCAATCTGAACATGAGAGTGCAGACAAGAA
CR_O_S320A_Mse1	AATTGTACATGATTTAGAGAATTTAAGTTTGGATCAA- GCTGAACATGAGAGTGCAGA- CAAAAAGGATAAGAAGCTACAGCGTCTCAATGG
CR_O_S320D_Mse1	AATTGTACATGATTTAGAGAATTTAAGTTTGGATCAA- GATGAACATGAGAGTGCAGA- CAAAAAGGATAAGAAGCTACAGCGTCTCAATGG
CR_O_S324A_Mse1	GAAATTGTACATGATTTAGAGAATTTAAGTTT- GGATCAATCTGAACATGAGGCTGCAGA- CAAAAAGGATAAGAAGCTACAGCGTCTCAAT
Hst2_Phosphoser- ine_S316amber_FP	GAGAATTTGTAGTTGGATCAATCTGAACATGAGAGTGC
Hst2_Phosphoser- ine_S316amber_RP	CAGATTGATCCAACACTACAAATTCTCTAAATCATGTACAATTC
Hst2_Phosphoser- ine_S320amber_FP	TTGGATCAATAGGAACATGAGAGTGCAGACAAG
Hst2_Phosphoser- ine_S320amber_RP	CTCATGTTCTTATTGATCCAAACTCAAATTCTC
Hst2_QCS316,20,24A_Fp	GAGAATTTGGCTTTGGATCAAGCTGAACATGAGGCTGCAGACAA- GAAGGATAAGAAGC
Hst2_QCS316,20,24A_Rp	CTTGTCTGCAGCCTCATGTTTCAGCTTGATCCAAA- GCCAAATTCTCTAAATCATGTAC
Hst2_QCS316,20,24D_Fp	AGAGAATTTGGATTTGGATCAAGATGAACATGAGGATGCAGACAA- GAAGGATAAGAAGC
Hst2_QCS316,20,24D_Rp	CTTGTCTGCATCCTCATGTTTCATCTT- GATCCAAATCCAAATTCTCTAAATCATGTAC
Hst2_Phosphoser- ine_S46amber_FP	CTTCCGATAGCCGGGAACTGGCCTGTACCATAAC
Hst2_Phosphoser- ine_S46amber_RP	CAGTTCCCGGCTATCGGAAGTCTGGTATCCCACAAG
Hst2_QCS46A_Fp	CTTCCGAGCTCCGGGAACTGGCCTGTAC
Hst2_QCS46A_Rp	GTTCCCGGAGCTCGGAAGTCTGGTATCCCAC
Hst2_QCS46D_Fp	CTTCCGAGATCCGGGAACTGGCCTGTAC
Hst2_QCS46D_Rp	GTTCCCGGATCTCGGAAGTCTGGTATCCCAC
Hst2_QC_S320A_Fp	TGGATCAAGCTGAACATGAGAGTGCAGAC
Hst2_QC_S320A_Rp	TCATGTTTCAGCTTGATCCAAACTCAAATTC
Hst2_QC_S320D_Fp	TGGATCAAGATGAACATGAGAGTGCAGAC
Hst2_QC_S320D_Rp	TCATGTTTCATCTTGATCCAAACTCAAATTC
Hst2_QC_S324A_Fp	AACATGAGGCTGCAGACAAGAAGGATAAGAAGC
Hst2_QC_S324A_Rp	TTGTCTGCAGCCTCATGTTTCAGATTGATCCAAACT
Hst2_QC_S324A_Fp	AACATGAGGATGCAGACAAGAAGGATAAGAAGC
Hst2_QC_S324A_Rp	TTGTCTGCATCCTCATGTTTCAGATTGATCCAAACT
H2B_amber51T_Fp	TGAAGCAAACCTCACCTGACACTGGTATTTC

H2B_amber51T_Rp	TCAGGGTGAGTTTGCTTCAAACCTTG
GAL1_ORF_840bp_Fp	TGCTCGATCCTTCTTTTCCA
GAL1_ORF_840bp_Rp	TTGCGAACACCCTTGTTGTA
GAL1_ORF_330_Fp	AAGTTTCGATTTGCCGTTGGAC
BMH1_CTAG_FP	CATCAGCAACAGCAGCCACCTGCTGCCGCCGAAGGTGAAGCAC- CAAAGCGTACGCTGCAGGTCGAC
BMH1_CTAG_RP	GTTCTTTTTTTTTCTTTTTTTAGTAATTTCTCTTTAGATTTATCAGAA- TACTTAATCGATGAATTCGAGCTCG
BMH1 CTAG PYM F	ACAGCAGCCACCTGCTGCCGCCGAAGGTGAAGCACCAAAGCG- TACGCTGCAGGTCGAC
BMH1 CTAG PYM R	TTTTTTTAGTAATTTCTCTTTAGATTTATCAGAA- TACTTAATCGATGAATTCGAGCTCG
BMH1 CTAG CHK F	TTGGCTGAATTTCTAGTGG
BMH1_CTAG_FP	CATCAGCAACAGCAGCCACCTGCTGCCGCCGAAGGTGAAGCAC- CAAAGCGTACGCTGCAGGTCGAC
BMH1_CTAG_RP	GTTCTTTTTTTTTCTTTTTTTAGTAATTTCTCTTTAGATTTATCAGAA- TACTTAATCGATGAATTCGAGCTCG
BMH1_HISTOSTREP_FP	ATGGGCAGCAGCTGGAGCCACCCGCAGTTCGAAAA- GAGCCAAGGATCCGAAAACC
BMH1_HISTOSTREP_RP	GGATCCTT- GGCTCTTTTCGAACTGCGGGTGGCTCCAGCTGCTGCCCATGG- TATATC

SUPPLEMENTARY FIGURES

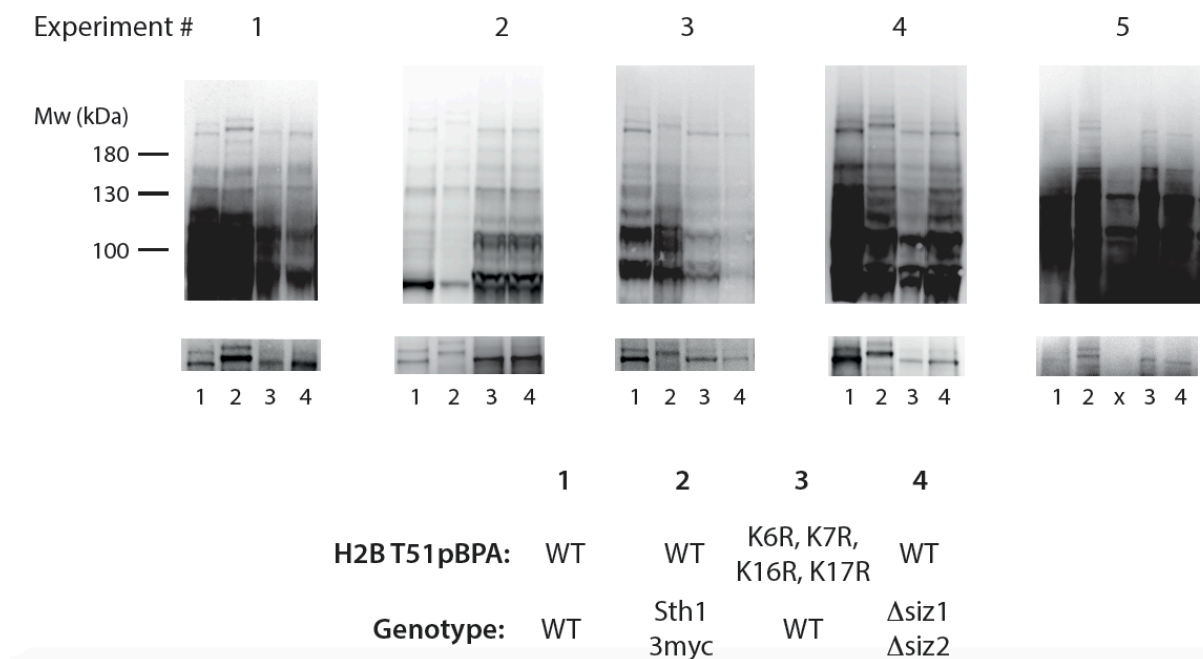


**Figure S 1: Sth1 prefers interaction with SUMOylated H2B.**

Full sized blots for Figure 27. Five independent Biological replicates. In all panels, yeasts expressing H2B T51pBPA with the indicated mutations were UV-irradiated and whole cell lysates analysed by SDS-PAGE and Western Blot using anti-HA antibodies.

Experiment #:

1

2

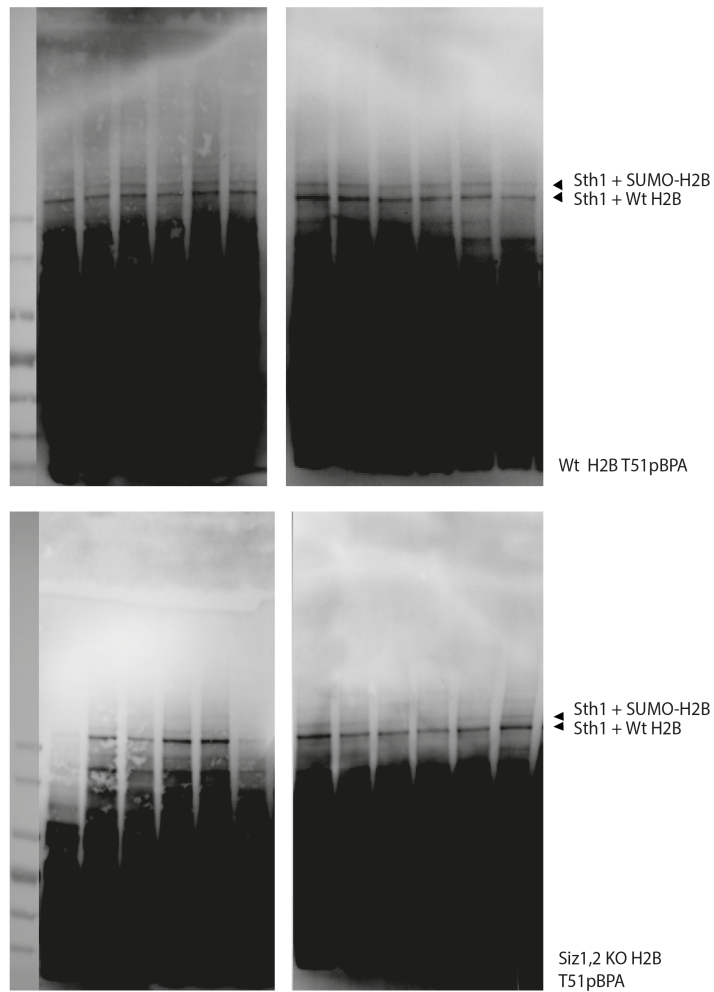


**Figure S 2 : Sth1 recognizes previously SUMOylated nucleosomes.**

Full sized blots for Figure 28. Two independent Biological replicates. In all panels, yeasts expressing H2B T51pBPA with the indicated mutations were UV-irradiated and whole cell lysates analysed by SDS-PAGE and Western Blot using anti-HA antibodies

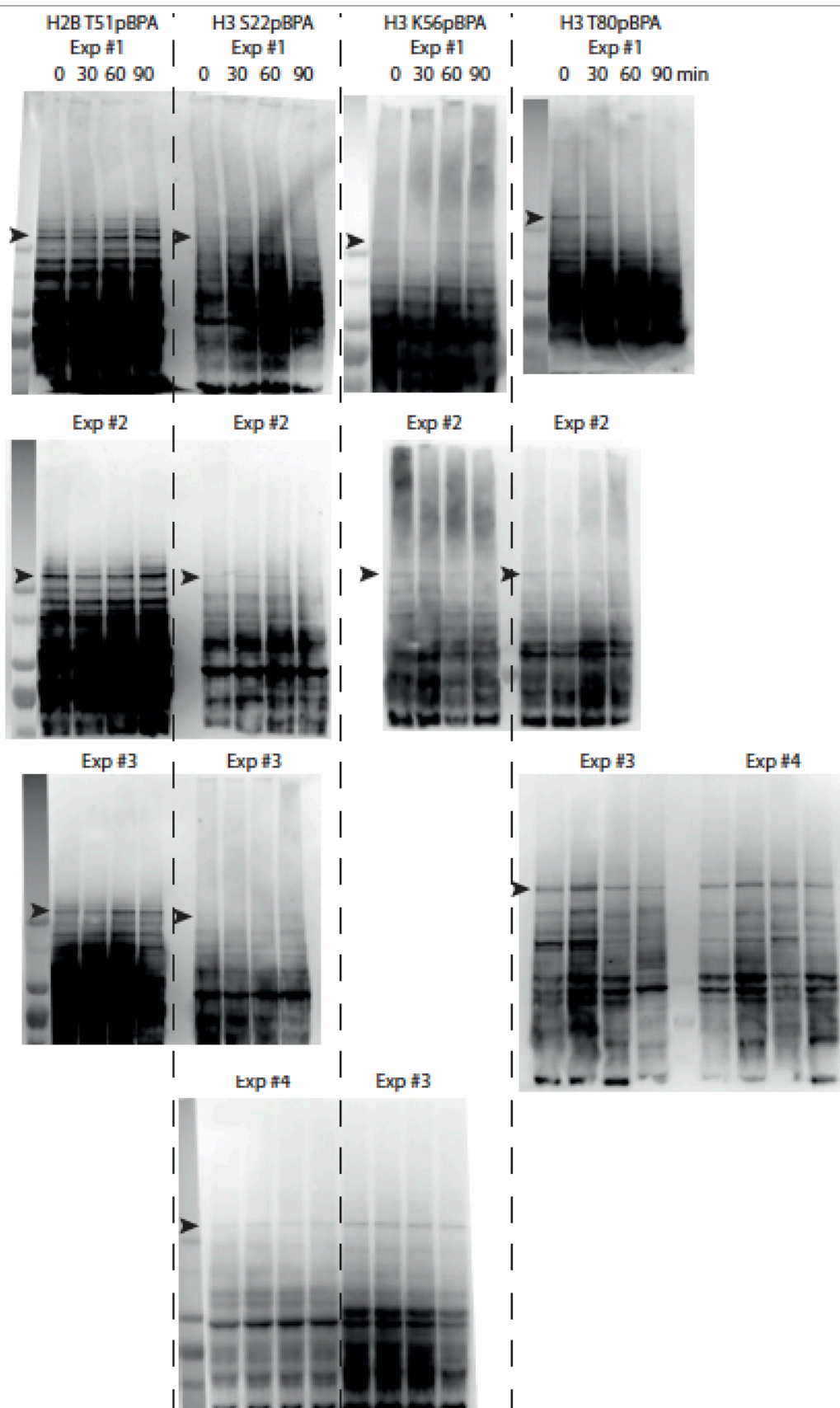
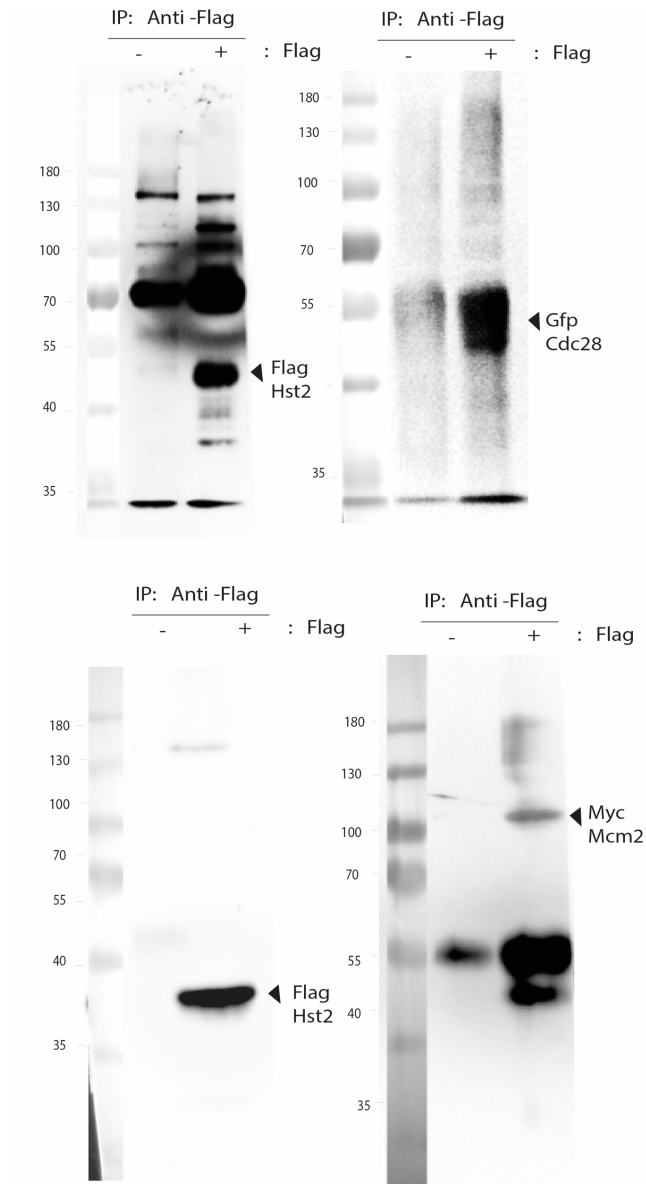


Figure S 3 : Cell cycle dependence of Sth1-histone crosslinks.

Full sized bots used for Figure 30 and for quantification of densitometric analysis.



**Figure S 4 : Novel Interaction partners of Hst2.**

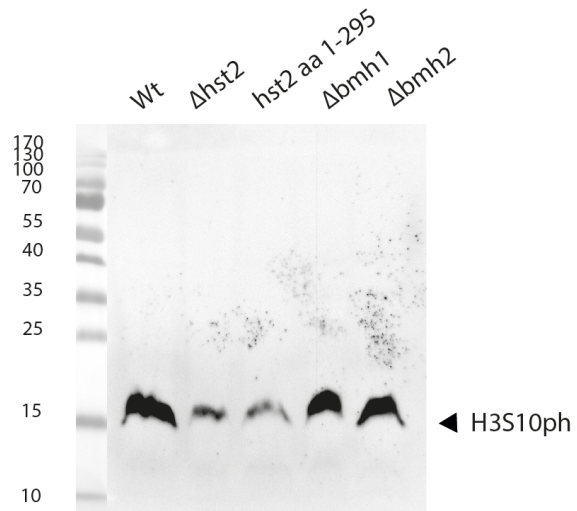
Full sized blots of co-IPs of Hst2 with Cdc28 and Mcm2 as shown in Figure 33.



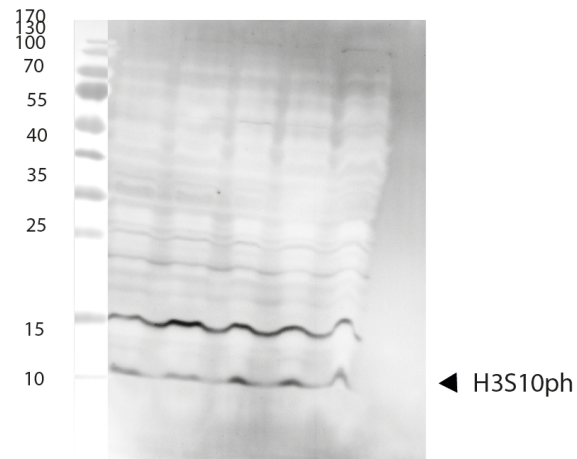
Experiment #:

Synchronised  
with nocodazole

1



2



3

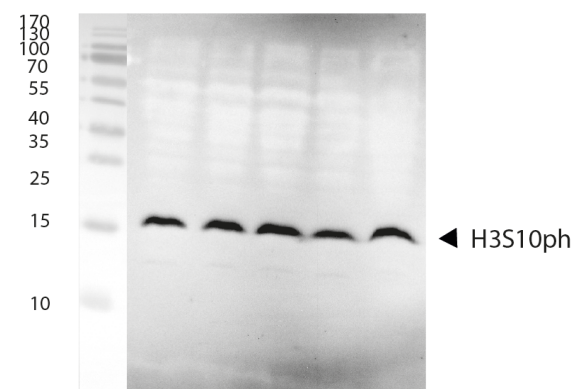


Figure S 6 : Hst2 and Bmh1 knockout have the same effect on H4K16ac levels.

Full sized blots of images used in Figure 35.

Experiment #:

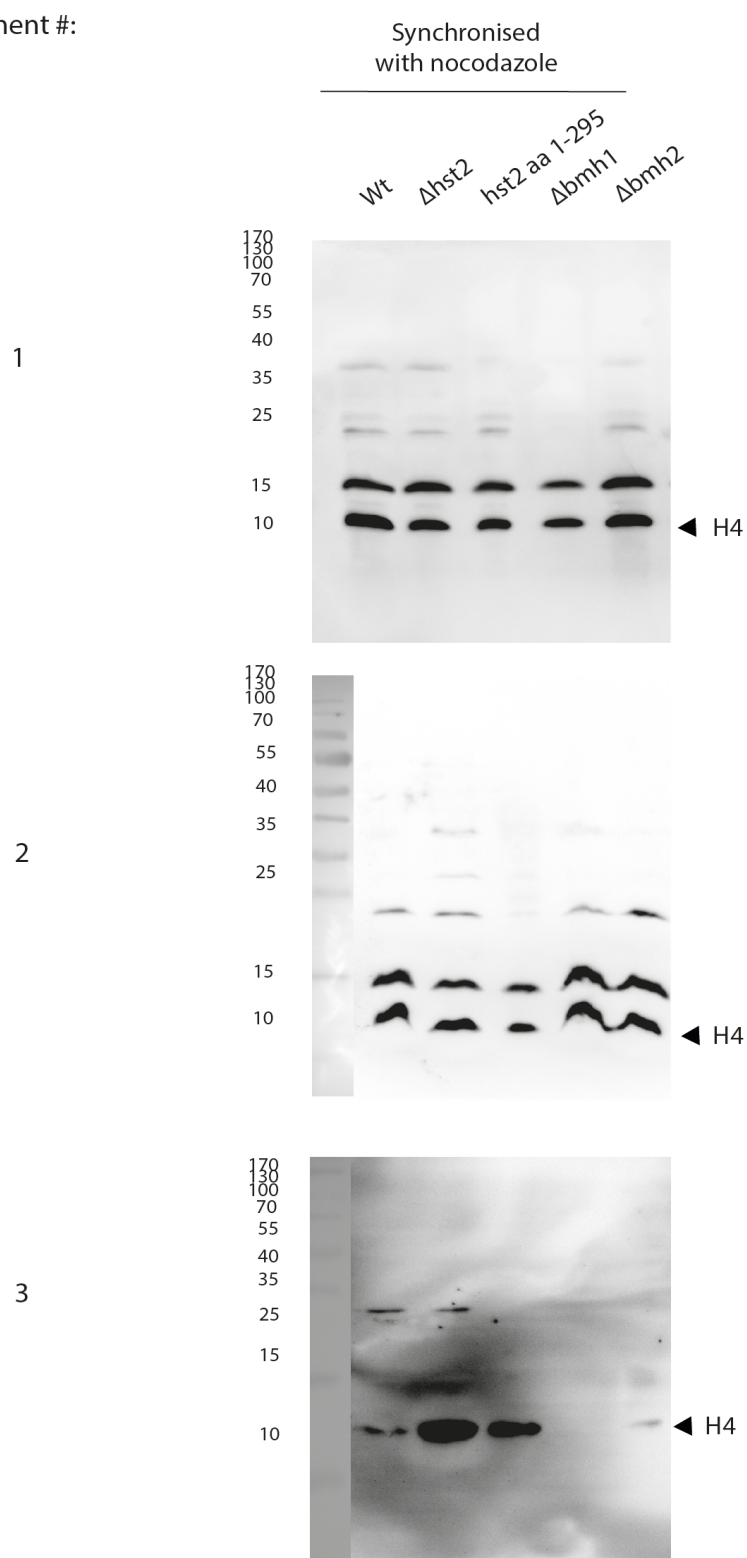
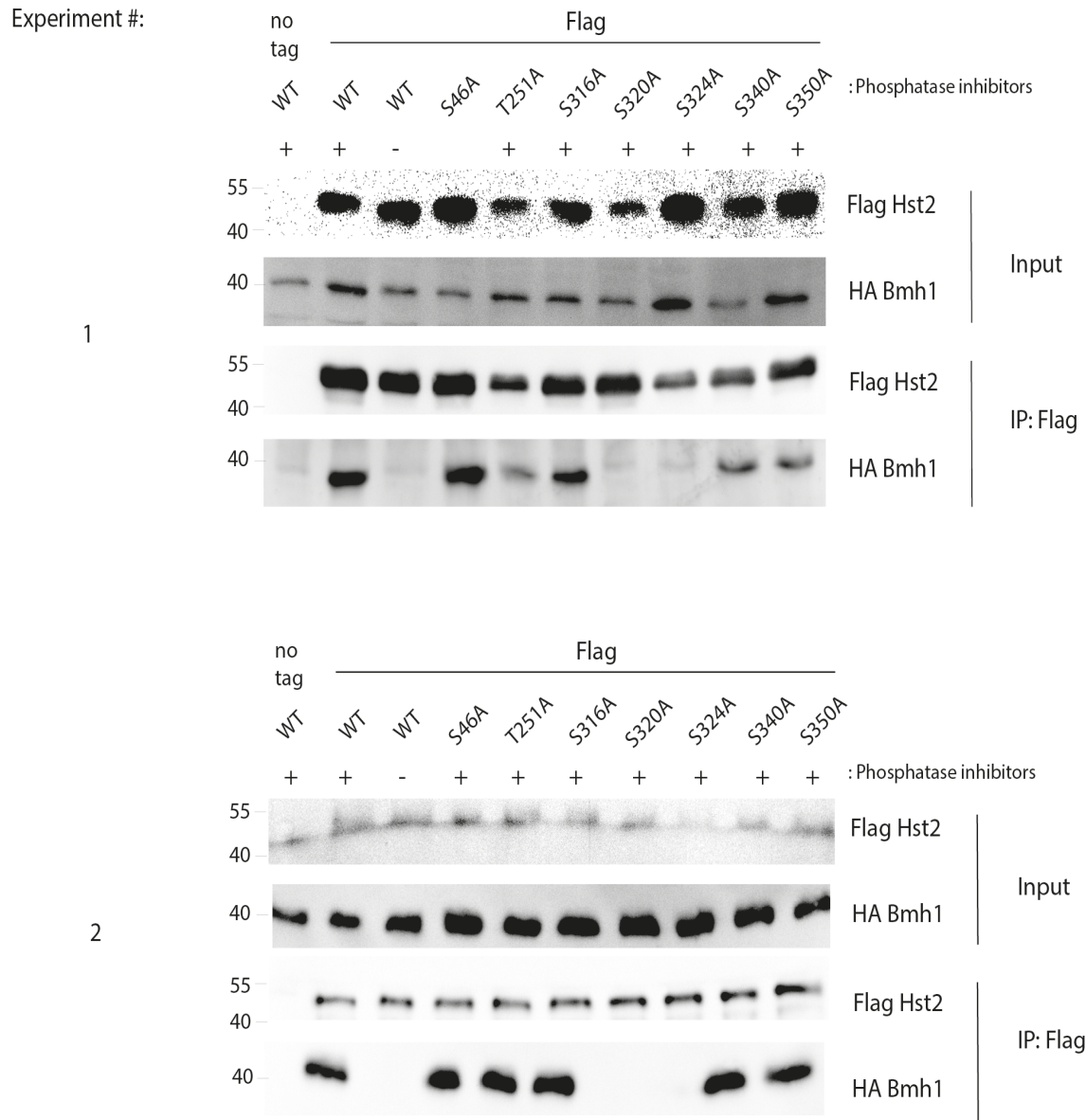


Figure S 7 : Hst2 and Bmh1 knockout have the same effect on H4K16ac levels.

Full sized blots of images used in Figure 35.



**Figure S 8 : Interaction of Hst2 and Bmh1 upon overexpression.**

Biological Duplicate experiments of Blots used for images in Figure 36.

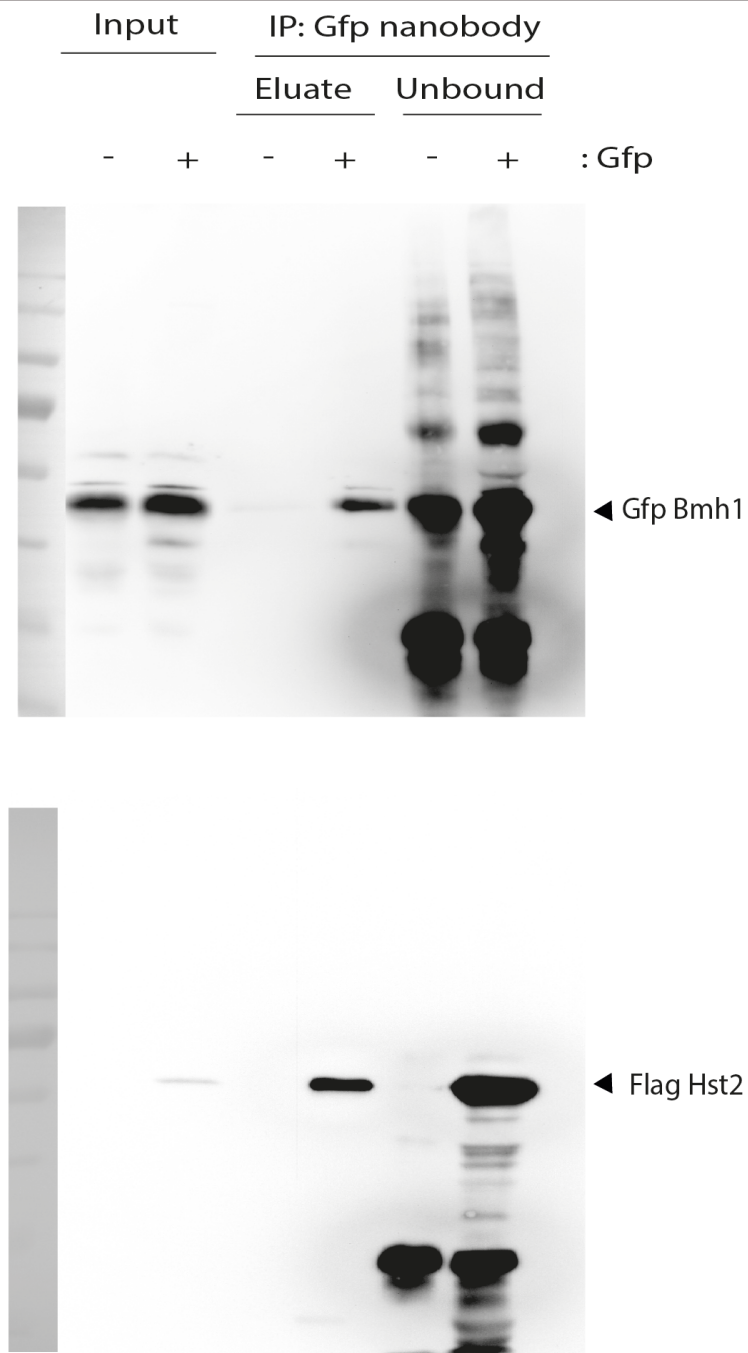


**Figure S 9 : Interaction of Hst2 and Bmh1 at endogenous levels.**

Full sized blots used for images in Figure 36.

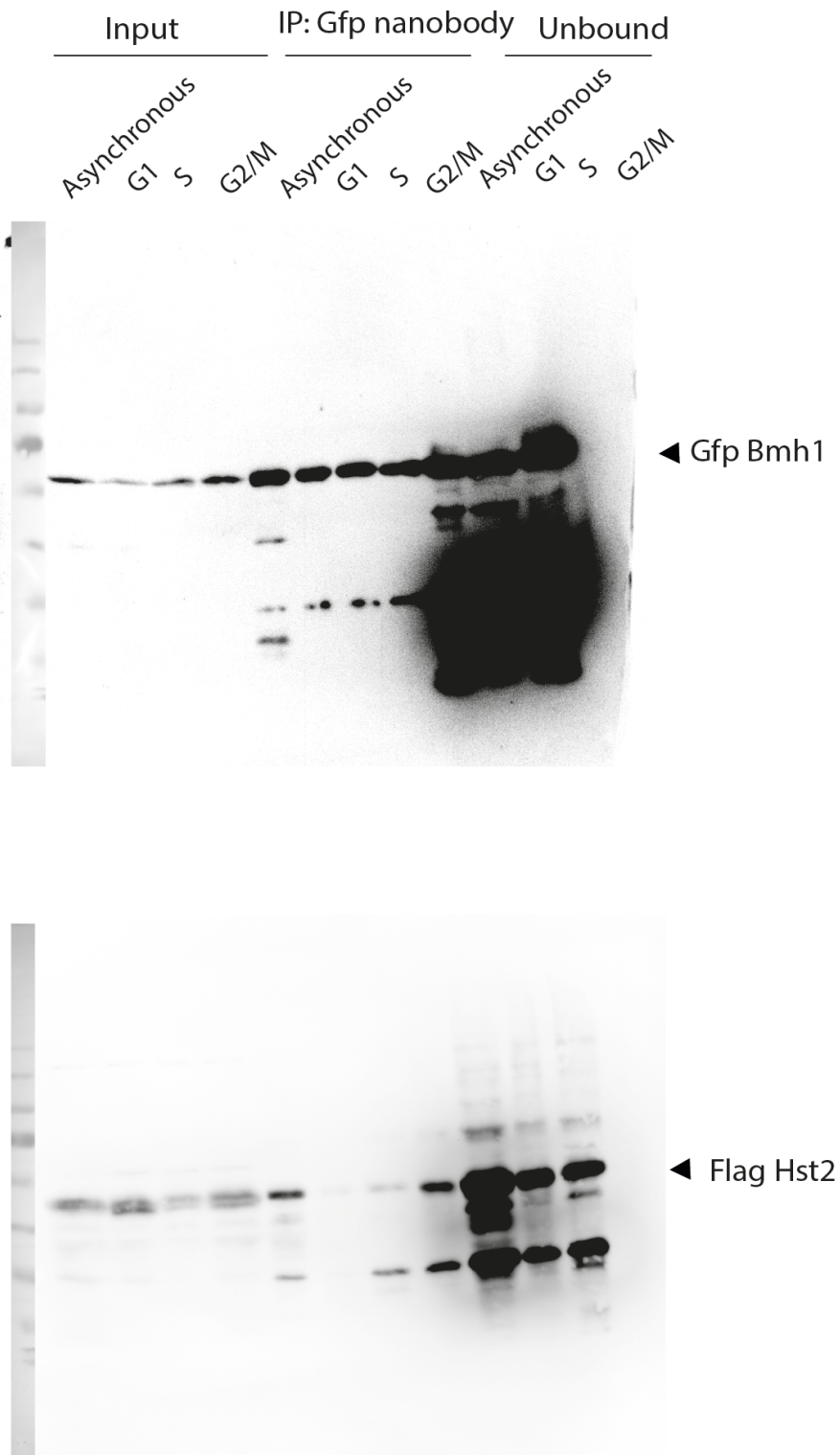


Figure S 10 : Interaction of Hst2 and Bmh1 in terms of cell cycle at endogenous levels.

Full sized blots used for images in Figure 37.

## REFERENCES

1. Dahm, R. Discovering DNA: Friedrich Miescher and the early years of nucleic acid research. *Human Genetics* **122**, 565–581 (2008).
2. Avery, O. T., Macleod, C. M. & McCarty, M. STUDIES ON THE CHEMICAL NATURE OF THE SUBSTANCE INDUCING TRANSFORMATION OF PNEUMOCOCCAL TYPES: INDUCTION OF TRANSFORMATION BY A DESOXYRIBONUCLEIC ACID FRACTION ISOLATED FROM PNEUMOCOCCUS TYPE III. *J Exp Med* **79**, 137–158 (1944).
3. WATSON, J. D. & CRICK, F. H. Molecular structure of nucleic acids; a structure for deoxyribose nucleic acid. *Nature* **171**, 737–738 (1953).
4. Horn, P. J. & Peterson, C. L. Chromatin Higher Order Folding--Wrapping up Transcription. *Science* **297**, 1824 (2002).
5. Luger, K., Mäder, A. W., Richmond, R. K., Sargent, D. F. & Richmond, T. J. Crystal structure of the nucleosome core particle at 2.8 Å resolution. *Nature* **389**, 251–260 (1997).
6. Kornberg, R. D. Structure of Chromatin. *Annu. Rev. Biochem.* **46**, 931–954 (1977).
7. Hansen, J. C. Conformational Dynamics of the Chromatin Fiber in Solution: Determinants, Mechanisms, and Functions. *Annu. Rev. Biophys. Biomol. Struct.* **31**, 361–392 (2002).
8. Arents, G., Burlingame, R. W., Wang, B. C., Love, W. E. & Moudrianakis, E. N. The nucleosomal core histone octamer at 3.1 Å resolution: a tripartite protein assembly and a left-handed superhelix. *Proc Natl Acad Sci USA* **88**, 10148 (1991).
9. Luger, K., Mäder, A. W., Richmond, R. K., Sargent, D. F. & Richmond, T. J. Crystal structure of the nucleosome core particle at 2.8 Å resolution. *Nature* **389**, 251–260 (1997).
10. Weintraub, H. & Van Lente, F. Dissection of chromosome structure with trypsin and nucleases. *Proc Natl Acad Sci U S A* **71**, 4249–4253 (1974).
11. Osley, M. A. THE REGULATION OF HISTONE SYNTHESIS IN THE CELL CYCLE. *Annu. Rev. Biochem.* **60**, 827–861 (1991).
12. Smith, M. M. & Stirling, V. B. Histone H3 and H4 gene deletions in *Saccharomyces cerevisiae*. *Journal of Cell Biology* **106**, 557–566 (1988).
13. Lucchini, R. & Sogo, J. M. Replication of transcriptionally active chromatin. *Nature* **374**, 276–280 (1995).
14. Goldman, J. A., Garlick, J. D. & Kingston, R. E. Chromatin remodeling by imitation switch (ISWI) class ATP-dependent remodelers is stimulated by histone variant H2A.Z. *J Biol Chem* **285**, 4645–4651 (2010).
15. Cakiroglu, A. et al. Genome-wide reconstitution of chromatin transactions reveals that RSC preferentially disrupts H2AZ-containing nucleosomes. *Genome Res* **29**, 988–998 (2019).

16. Kraus, A. J. *et al.* Distinct roles for H4 and H2A.Z acetylation in RNA transcription in African trypanosomes. *Nature Communications* **11**, 1498 (2020).
17. Kharerin, H., Bhat, P. J. & Padinhateeri, R. Role of nucleosome positioning in 3D chromatin organization and loop formation. *Journal of Biosciences* **45**, 14 (2020).
18. Arimura, Y. *et al.* Cancer-associated mutations of histones H2B, H3.1 and H2A.Z.1 affect the structure and stability of the nucleosome. *Nucleic Acids Res* **46**, 10007–10018 (2018).
19. Nacev, B. A. *et al.* The expanding landscape of ‘oncohistone’ mutations in human cancers. *Nature* **567**, 473–478 (2019).
20. Bannister, A. J. & Kouzarides, T. Regulation of chromatin by histone modifications. *Cell Res* **21**, 381–395 (2011).
21. Mersfelder, E. L. & Parthun, M. R. The tale beyond the tail: histone core domain modifications and the regulation of chromatin structure. *Nucleic Acids Res* **34**, 2653–2662 (2006).
22. Fenley, A. T., Anandkrishnan, R., Kidane, Y. H. & Onufriev, A. V. Modulation of nucleosomal DNA accessibility via charge-altering post-translational modifications in histone core. *Epigenetics & Chromatin* **11**, 11 (2018).
23. Tessarz, P. & Kouzarides, T. Histone core modifications regulating nucleosome structure and dynamics. *Nat Rev Mol Cell Biol* **15**, 703–708 (2014).
24. Soufi, Y. & Soufi, B. Mass Spectrometry-Based Bacterial Proteomics: Focus on Dermatologic Microbial Pathogens. *Front Microbiol* **7**, 181–181 (2016).
25. Su, X., Ren, C. & Freitas, M. A. Mass spectrometry-based strategies for characterization of histones and their post-translational modifications. *Expert review of proteomics* **4**, 211–225 (2007).
26. Chen, Y. *et al.* Lysine Propionylation and Butyrylation Are Novel Post-translational Modifications in Histones. *Mol Cell Proteomics* **6**, 812 (2007).
27. Tan, M. *et al.* Identification of 67 histone marks and histone lysine crotonylation as a new type of histone modification. *Cell* **146**, 1016–1028 (2011).
28. Zhang, Z. *et al.* Identification of lysine succinylation as a new post-translational modification. *Nat Chem Biol* **7**, 58–63 (2011).
29. Xie, Z. *et al.* Lysine succinylation and lysine malonylation in histones. *Mol Cell Proteomics* **11**, 100–107 (2012).
30. Dai, L. *et al.* Lysine 2-hydroxyisobutyrylation is a widely distributed active histone mark. *Nat Chem Biol* **10**, 365–370 (2014).
31. Tan, M. *et al.* Lysine glutarylation is a protein posttranslational modification regulated by SIRT5. *Cell Metab* **19**, 605–617 (2014).
32. Yun, M., Wu, J., Workman, J. L. & Li, B. Readers of histone modifications. *Cell Research* **21**, 564–578 (2011).
33. Dhalluin, C. *et al.* Structure and ligand of a histone acetyltransferase bromo-domain. *Nature* **399**, 491–496 (1999).
34. Yap, K. L. & Zhou, M.-M. Structure and mechanisms of lysine methylation recognition by the chromodomain in gene transcription. *Biochemistry* **50**, 1966–1980 (2011).

35. Hershko, A. & Ciechanover, A. THE UBIQUITIN SYSTEM. *Annu. Rev. Biochem.* **67**, 425–479 (1998).
36. Musselman, C. A., Lalonde, M.-E., Côté, J. & Kutateladze, T. G. Perceiving the epigenetic landscape through histone readers. *Nat Struct Mol Biol* **19**, 1218–1227 (2012).
37. Delcuve, G. P., Khan, D. H. & Davie, J. R. Roles of histone deacetylases in epigenetic regulation: emerging paradigms from studies with inhibitors. *Clinical Epigenetics* **4**, 5 (2012).
38. Nakagawa, T. & Guarente, L. Sirtuins at a glance. *J. Cell Sci.* **124**, 833 (2011).
39. Roh, T.-Y., Cuddapah, S. & Zhao, K. Active chromatin domains are defined by acetylation islands revealed by genome-wide mapping. *Genes Dev* **19**, 542–552 (2005).
40. Kim, J. & Kim, H. Recruitment and biological consequences of histone modification of H3K27me3 and H3K9me3. *ILAR J* **53**, 232–239 (2012).
41. Suganuma, T. & Workman, J. L. Crosstalk among Histone Modifications. *Cell* **135**, 604–607 (2008).
42. Zee, B. M., Levin, R. S., DiMaggio, P. A. & Garcia, B. A. Global turnover of histone post-translational modifications and variants in human cells. *Epigenetics Chromatin* **3**, 22–22 (2010).
43. Doerr, A. In pursuit of PTMs. *Nature Methods* **12**, 20–20 (2015).
44. Jenuwein, T. & Allis, C. D. Translating the Histone Code. *Science* **293**, 1074 (2001).
45. Lawrence, M., Daujat, S. & Schneider, R. Lateral Thinking: How Histone Modifications Regulate Gene Expression. *Trends Genet* **32**, 42–56 (2016).
46. Audia, J. E. & Campbell, R. M. Histone Modifications and Cancer. *Cold Spring Harb Perspect Biol* **8**, a019521 (2016).
47. Rando, O. J. & Winston, F. Chromatin and transcription in yeast. *Genetics* **190**, 351–387 (2012).
48. Takada, S., Brandani, G. B. & Tan, C. Nucleosomes as allosteric scaffolds for genetic regulation. *Current Opinion in Structural Biology* **62**, 93–101 (2020).
49. Narlikar, G. J., Sundaramoorthy, R. & Owen-Hughes, T. Mechanisms and functions of ATP-dependent chromatin-remodeling enzymes. *Cell* **154**, 490–503 (2013).
50. Clapier, C. R., Iwasa, J., Cairns, B. R. & Peterson, C. L. Mechanisms of action and regulation of ATP-dependent chromatin-remodelling complexes. *Nat. Rev. Mol. Cell Biol.* **18**, 407–422 (2017).
51. Yan, L., Wu, H., Li, X., Gao, N. & Chen, Z. Structures of the ISWI–nucleosome complex reveal a conserved mechanism of chromatin remodeling. *Nature Structural & Molecular Biology* **26**, 258–266 (2019).
52. Cairns, B. R. et al. RSC, an essential, abundant chromatin-remodeling complex. *Cell* **87**, 1249–1260 (1996).
53. Cairns, B. R. et al. Two Functionally Distinct Forms of the RSC Nucleosome-Remodeling Complex, Containing Essential AT Hook, BAH, and Bromodomains. *Molecular Cell* **4**, 715–723 (1999).

54. Jiang, C. & Pugh, B. F. A compiled and systematic reference map of nucleosome positions across the *Saccharomyces cerevisiae* genome. *Genome Biol* **10**, R109 (2009).
55. Rhee, H. S. & Pugh, B. F. Genome-wide structure and organization of eukaryotic pre-initiation complexes. *Nature* **483**, 295–301 (2012).
56. Floer, M. et al. A RSC/Nucleosome Complex Determines Chromatin Architecture and Facilitates Activator Binding. *Cell* **141**, 407–418 (2010).
57. Parnell, T. J., Huff, J. T. & Cairns, B. R. RSC regulates nucleosome positioning at Pol II genes and density at Pol III genes. *EMBO J* **27**, 100–110 (2008).
58. Spain, M. M. et al. The RSC complex localizes to coding sequences to regulate Pol II and histone occupancy. *Mol Cell* **56**, 653–666 (2014).
59. Brahma, S. & Henikoff, S. RSC-Associated Subnucleosomes Define MNase-Sensitive Promoters in Yeast. *Mol Cell* **73**, 238-249.e3 (2019).
60. Kubik, S. et al. Sequence-Directed Action of RSC Remodeler and General Regulatory Factors Modulates +1 Nucleosome Position to Facilitate Transcription. *Mol Cell* **71**, 89-102.e5 (2018).
61. Musladin, S., Krietenstein, N., Korber, P. & Barbaric, S. The RSC chromatin remodeling complex has a crucial role in the complete remodeler set for yeast PHO5 promoter opening. *Nucleic Acids Res* **42**, 4270–4282 (2014).
62. Muñoz, S., Minamino, M., Casas-Delucchi, C. S., Patel, H. & Uhlmann, F. A Role for Chromatin Remodeling in Cohesin Loading onto Chromosomes. *Mol Cell* **74**, 664-673.e5 (2019).
63. Wippo, C. J. et al. The RSC chromatin remodelling enzyme has a unique role in directing the accurate positioning of nucleosomes. *The EMBO Journal* **30**, 1277–1288 (2011).
64. Chai, B., Huang, J., Cairns, B. R. & Laurent, B. C. Distinct roles for the RSC and Swi/Snf ATP-dependent chromatin remodelers in DNA double-strand break repair. *Genes Dev* **19**, 1656–1661 (2005).
65. Hsu, J.-M., Huang, J., Meluh, P. B. & Laurent, B. C. The yeast RSC chromatin-remodeling complex is required for kinetochore function in chromosome segregation. *Mol Cell Biol* **23**, 3202–3215 (2003).
66. Sing, T. L. et al. The budding yeast RSC complex maintains ploidy by promoting spindle pole body insertion. *J Cell Biol* **217**, 2445–2462 (2018).
67. Ye, Y. et al. Structure of the RSC complex bound to the nucleosome. *Science* **366**, 838 (2019).
68. Patel, A. B. et al. Architecture of the chromatin remodeler RSC and insights into its nucleosome engagement. *eLife* **8**, e54449 (2019).
69. Wagner, F. R. et al. Structure of SWI/SNF chromatin remodeller RSC bound to a nucleosome. *Nature* **579**, 448–451 (2020).
70. Kubik, S. et al. Nucleosome Stability Distinguishes Two Different Promoter Types at All Protein-Coding Genes in Yeast. *Mol Cell* **60**, 422–434 (2015).

71. Saha, A., Wittmeyer, J. & Cairns, B. R. Chromatin remodeling through directional DNA translocation from an internal nucleosomal site. *Nat Struct Mol Biol* **12**, 747–755 (2005).
72. Zhang, Y. et al. DNA translocation and loop formation mechanism of chromatin remodeling by SWI/SNF and RSC. *Mol Cell* **24**, 559–568 (2006).
73. Harada, B. T. et al. Stepwise nucleosome translocation by RSC remodeling complexes. *eLife* **5**, e10051 (2016).
74. Materne, P. et al. Histone H2B ubiquitylation represses gametogenesis by opposing RSC-dependent chromatin remodeling at the *ste11* master regulator locus. *eLife* **5**, e13500 (2016).
75. Clapier, C. R. et al. Regulation of DNA Translocation Efficiency within the Chromatin Remodeler RSC/Sth1 Potentiates Nucleosome Sliding and Ejection. *Molecular Cell* **62**, 453–461 (2016).
76. Kadoch, C. & Crabtree, G. R. Mammalian SWI/SNF chromatin remodeling complexes and cancer: Mechanistic insights gained from human genomics. *Sci Adv* **1**, e1500447 (2015).
77. Kadoch, C. et al. Proteomic and bioinformatic analysis of mammalian SWI/SNF complexes identifies extensive roles in human malignancy. *Nat Genet* **45**, 592–601 (2013).
78. Masliah-Planchon, J., Bièche, I., Guinebretière, J.-M., Bourdeaut, F. & Delattre, O. SWI/SNF chromatin remodeling and human malignancies. *Annu Rev Pathol* **10**, 145–171 (2015).
79. He, S. et al. Structure of nucleosome-bound human BAF complex. *Science* eaaz9761 (2020) doi:10.1126/science.aaz9761.
80. Rowley, M. J. & Corces, V. G. Organizational principles of 3D genome architecture. *Nature Reviews Genetics* **19**, 789–800 (2018).
81. Bouwman, B. A. & de Laat, W. Getting the genome in shape: the formation of loops, domains and compartments. *Genome Biology* **16**, 154 (2015).
82. Bonev, B. & Cavalli, G. Organization and function of the 3D genome. *Nature Reviews Genetics* **17**, 661–678 (2016).
83. Naumova, N. et al. Organization of the Mitotic Chromosome. *Science* **342**, 948 (2013).
84. Kinoshita, K. & Hirano, T. Dynamic organization of mitotic chromosomes. *Curr Opin Cell Biol* **46**, 46–53 (2017).
85. Earnshaw, W. C., Halligan, B., Cooke, C. A., Heck, M. M. & Liu, L. F. Topoisomerase II is a structural component of mitotic chromosome scaffolds. *J Cell Biol* **100**, 1706–1715 (1985).
86. Gasser, S. M., Laroche, T., Falquet, J., Boy de la Tour, E. & Laemmli, U. K. Metaphase chromosome structure. Involvement of topoisomerase II. *J Mol Biol* **188**, 613–629 (1986).
87. Saitoh, N., Goldberg, I. G., Wood, E. R. & Earnshaw, W. C. ScII: an abundant chromosome scaffold protein is a member of a family of putative ATPases with an unusual predicted tertiary structure. *J Cell Biol* **127**, 303–318 (1994).

88. Strunnikov, A. V., Hogan, E. & Koshland, D. SMC2, a *Saccharomyces cerevisiae* gene essential for chromosome segregation and condensation, defines a subgroup within the SMC family. *Genes Dev* **9**, 587–599 (1995).
89. Hirano, T. & Mitchison, T. J. A heterodimeric coiled-coil protein required for mitotic chromosome condensation in vitro. *Cell* **79**, 449–458 (1994).
90. Kschonsak, M. et al. Structural Basis for a Safety-Belt Mechanism That Anchors Condensin to Chromosomes. *Cell* **171**, 588–600.e24 (2017).
91. Terakawa, T. et al. The condensin complex is a mechanochemical motor that translocates along DNA. *Science* **358**, 672–676 (2017).
92. Hassler, M. et al. Structural Basis of an Asymmetric Condensin ATPase Cycle. *Molecular Cell* **74**, 1175–1188.e9 (2019).
93. Elbatsh, A. M. O. et al. Distinct Roles for Condensin's Two ATPase Sites in Chromosome Condensation. *Molecular Cell* **76**, 724–737.e5 (2019).
94. Ganji, M. et al. Real-time imaging of DNA loop extrusion by condensin. *Science* **360**, 102 (2018).
95. Kong, M. et al. Human condensin I and II drive extensive ATP-dependent compaction of nucleosome-bound DNA. *bioRxiv* 683540 (2019) doi:10.1101/683540.
96. Kim, E., Kerssemakers, J., Shaltiel, I. A., Haering, C. H. & Dekker, C. DNA-loop extruding condensin complexes can traverse one another. *Nature* **579**, 438–442 (2020).
97. Golfier, S., Quail, T., Kimura, H. & Brugués, J. Cohesin and condensin extrude DNA loops in a cell-cycle dependent manner. *eLife* **9**, e53885 (2020).
98. Lavoie, B. D., Hogan, E. & Koshland, D. In vivo dissection of the chromosome condensation machinery: reversibility of condensation distinguishes contributions of condensin and cohesin. *Journal of Cell Biology* **156**, 805–815 (2002).
99. Vas, A. C. J., Andrews, C. A., Kirkland Matesky, K. & Clarke, D. J. In vivo analysis of chromosome condensation in *Saccharomyces cerevisiae*. *Molecular biology of the cell* **18**, 557–568 (2007).
100. Gibcus, J. H. et al. A pathway for mitotic chromosome formation. *Science* **359**, eaao6135 (2018).
101. Samejima, K. et al. Mitotic chromosomes are compacted laterally by KIF4 and condensin and axially by topoisomerase II $\alpha$ . *J Cell Biol* **199**, 755–770 (2012).
102. Perišić, O., Portillo-Ledesma, S. & Schlick, T. Sensitive effect of linker histone binding mode and subtype on chromatin condensation. *Nucleic Acids Research* **47**, 4948–4957 (2019).
103. Billett, M. A. & Barry, J. M. Role of histones in chromatin condensation. *Eur J Biochem* **49**, 477–484 (1974).
104. Larson, A. G. et al. Liquid droplet formation by HP1 $\alpha$  suggests a role for phase separation in heterochromatin. *Nature* **547**, 236–240 (2017).
105. Tatavosian, R. et al. Nuclear condensates of the Polycomb protein chromobox 2 (CBX2) assemble through phase separation. *J Biol Chem* **294**, 1451–1463 (2019).

106. Garcia-Ramirez, M., Rocchini, C. & Ausio, J. Modulation of chromatin folding by histone acetylation. *J Biol Chem* **270**, 17923–17928 (1995).
107. Shogren-Knaak, M. et al. Histone H4-K16 acetylation controls chromatin structure and protein interactions. *Science* **311**, 844–847 (2006).
108. Dorigo, B. et al. Nucleosome arrays reveal the two-start organization of the chromatin fiber. *Science* **306**, 1571–1573 (2004).
109. Görisch, S. M., Wachsmuth, M., Tóth, K. F., Lichter, P. & Rippe, K. Histone acetylation increases chromatin accessibility. *J Cell Sci* **118**, 5825–5834 (2005).
110. Risca, V. I., Denny, S. K., Straight, A. F. & Greenleaf, W. J. Variable chromatin structure revealed by in situ spatially correlated DNA cleavage mapping. *Nature* **541**, 237–241 (2017).
111. Zane, L., Chapus, F., Pegoraro, G. & Misteli, T. HiHiMap: single-cell quantitation of histones and histone posttranslational modifications across the cell cycle by high-throughput imaging. *MBoC* **28**, 2290–2302 (2017).
112. Xu, D., Bai, J., Duan, Q., Costa, M. & Dai, W. Covalent modifications of histones during mitosis and meiosis. *Cell Cycle* **8**, 3688–3694 (2009).
113. Dai, J. & Higgins, J. M. G. Haspin: a mitotic histone kinase required for metaphase chromosome alignment. *Cell Cycle* **4**, 665–668 (2005).
114. Hsu, J. Y. et al. Mitotic phosphorylation of histone H3 is governed by Ipl1/aurora kinase and Glc7/PP1 phosphatase in budding yeast and nematodes. *Cell* **102**, 279–291 (2000).
115. Funabiki, H. & Wynne, D. J. Making an effective switch at the kinetochore by phosphorylation and dephosphorylation. *Chromosoma* **122**, 135–158 (2013).
116. Kruitwagen, T., Chymkowitch, P., Denoth-Lippuner, A., Enserink, J. & Barral, Y. Centromeres License the Mitotic Condensation of Yeast Chromosome Arms. *Cell* **175**, 780-795.e15 (2018).
117. Wilkins, B. J. et al. A Cascade of Histone Modifications Induces Chromatin Condensation in Mitosis. *Science* **343**, 77–80 (2014).
118. Peplowska, K., Wallek, A. U. & Storchova, Z. Sgo1 regulates both condensin and Ipl1/Aurora B to promote chromosome biorientation. *PLoS Genet* **10**, e1004411 (2014).
119. Metwaly, G. Y. et al. Phospho-regulation of the Shugoshin - Condensin interaction at the centromere in budding yeast. *bioRxiv* 2019.12.16.877894 (2019) doi:10.1101/2019.12.16.877894.
120. Kruitwagen, T., Denoth-Lippuner, A., Wilkins, B. J., Neumann, H. & Barral, Y. Axial contraction and short-range compaction of chromatin synergistically promote mitotic chromosome condensation. *eLife* **4**, e10396 (2015).
121. Antonin, W. & Neumann, H. Chromosome condensation and decondensation during mitosis. *Current Opinion in Cell Biology* **40**, 15–22 (2016).
122. Booth, D. G. et al. Ki-67 is a PP1-interacting protein that organises the mitotic chromosome periphery. *eLife* **3**, e01641 (2014).
123. Cuylen, S. et al. Ki-67 acts as a biological surfactant to disperse mitotic chromosomes. *Nature* **535**, 308–312 (2016).

124. Ohta, S. *et al.* The protein composition of mitotic chromosomes determined using multiclassifier combinatorial proteomics. *Cell* **142**, 810–821 (2010).
125. Petrova, B. *et al.* Quantitative analysis of chromosome condensation in fission yeast. *Mol Cell Biol* **33**, 984–998 (2013).
126. Neumann, H. Rewiring translation - Genetic code expansion and its applications. *FEBS Lett* **586**, 2057–2064 (2012).
127. Neumann, H., Neumann-Staubitz, P., Witte, A. & Summerer, D. Epigenetic chromatin modification by amber suppression technology. *Curr Opin Chem Biol* **45**, 1–9 (2018).
128. Ambrogelly, A., Palioura, S. & Söll, D. Natural expansion of the genetic code. *Nat Chem Biol* **3**, 29–35 (2007).
129. Xie, J. & Schultz, P. G. Adding amino acids to the genetic repertoire. *Curr Opin Chem Biol* **9**, 548–554 (2005).
130. Nakamura, Y., Gojobori, T. & Ikemura, T. Codon usage tabulated from international DNA sequence databases: status for the year 2000. *Nucleic Acids Res* **28**, 292 (2000).
131. Wang, L., Brock, A., Herberich, B. & Schultz, P. G. Expanding the genetic code of *Escherichia coli*. *Science* **292**, 498–500 (2001).
132. Chin, J. W. Expanding and reprogramming the genetic code of cells and animals. *Annu Rev Biochem* **83**, 379–408 (2014).
133. Liu, C. C. & Schultz, P. G. Adding new chemistries to the genetic code. *Annu Rev Biochem* **79**, 413–444 (2010).
134. Mukai, T. *et al.* Codon reassignment in the *Escherichia coli* genetic code. *Nucleic Acids Res* **38**, 8188–8195 (2010).
135. Johnson, D. B. F. *et al.* RF1 knockout allows ribosomal incorporation of unnatural amino acids at multiple sites. *Nat Chem Biol* **7**, 779–786 (2011).
136. Schmied, W. H., Elsässer, S. J., Uttamapinant, C. & Chin, J. W. Efficient multisite unnatural amino acid incorporation in mammalian cells via optimized pyrrolysyl tRNA synthetase/tRNA expression and engineered eRF1. *J Am Chem Soc* **136**, 15577–15583 (2014).
137. Neumann, H., Wang, K., Davis, L., Garcia-Alai, M. & Chin, J. W. Encoding multiple unnatural amino acids via evolution of a quadruplet-decoding ribosome. *Nature* **464**, 441–444 (2010).
138. Wang, K., Neumann, H., Peak-Chew, S. Y. & Chin, J. W. Evolved orthogonal ribosomes enhance the efficiency of synthetic genetic code expansion. *Nature Biotechnology* **25**, 770–777 (2007).
139. Park, H.-S. *et al.* Expanding the Genetic Code of *Escherichia coli* with Phosphoserine. *Science* **333**, 1151 (2011).
140. Fan, C., Ip, K. & Söll, D. Expanding the genetic code of *Escherichia coli* with phosphotyrosine. *FEBS Lett* **590**, 3040–3047 (2016).
141. Dorman, G. & Prestwich, G. D. Benzophenone Photophores in Biochemistry. *Biochemistry* **33**, 5661–5673 (1994).

142. Preston, G. W. & Wilson, A. J. Photo-induced covalent cross-linking for the analysis of biomolecular interactions. *Chem Soc Rev* **42**, 3289–3301 (2013).
143. Staros, J. V., Bayley, H., Standing, D. N. & Knowles, J. R. Reduction of aryl azides by thiols: Implications for the use of photoaffinity reagents. *Biochemical and Biophysical Research Communications* **80**, 568–572 (1978).
144. Wittelsberger, A., Thomas, B. E., Mierke, D. F. & Rosenblatt, M. Methionine acts as a “magnet” in photoaffinity crosslinking experiments. *FEBS Letters* **580**, 1872–1876 (2006).
145. Weber, P. J. & Beck-Sickinger, A. G. Comparison of the photochemical behavior of four different photoactivatable probes. *J Pept Res* **49**, 375–383 (1997).
146. Chin, J. W., Martin, A. B., King, D. S., Wang, L. & Schultz, P. G. Addition of a photocrosslinking amino acid to the genetic code of *Escherichiacoli*. *Proc Natl Acad Sci U S A* **99**, 11020–11024 (2002).
147. Mori, H. & Ito, K. Different modes of SecY–SecA interactions revealed by site-directed *in vivo* photo-cross-linking. *Proc Natl Acad Sci USA* **103**, 16159 (2006).
148. Das, S. & Oliver, D. B. Mapping of the SecA·SecY and SecA·SecG interfaces by site-directed *in vivo* photocross-linking. *J Biol Chem* **286**, 12371–12380 (2011).
149. Schlieker, C. *et al.* Substrate recognition by the AAA+ chaperone ClpB. *Nature Structural & Molecular Biology* **11**, 607–615 (2004).
150. Chin, J. W. *et al.* An expanded eukaryotic genetic code. *Science* **301**, 964–967 (2003).
151. Mehnert, M., Sommer, T. & Jarosch, E. Der1 promotes movement of misfolded proteins through the endoplasmic reticulum membrane. *Nature Cell Biology* **16**, 77–86 (2014).
152. Carvalho, P., Stanley, A. M. & Rapoport, T. A. Retrotranslocation of a misfolded luminal ER protein by the ubiquitin-ligase Hrd1p. *Cell* **143**, 579–591 (2010).
153. Stanley, A. M., Carvalho, P. & Rapoport, T. Recognition of an ERAD-L substrate analyzed by site-specific *in vivo* photocrosslinking. *FEBS Lett* **585**, 1281–1286 (2011).
154. Schulz, C. *et al.* Tim50’s presequence receptor domain is essential for signal driven transport across the TIM23 complex. *J Cell Biol* **195**, 643–656 (2011).
155. Shiota, T. *et al.* Molecular architecture of the active mitochondrial protein gate. *Science* **349**, 1544 (2015).
156. Mohibullah, N. & Hahn, S. Site-specific cross-linking of TBP *in vivo* and *in vitro* reveals a direct functional interaction with the SAGA subunit Spt3. *Genes Dev* **22**, 2994–3006 (2008).
157. Neumann, H., Neumann-Staubitz, P., Witte, A. & Summerer, D. Epigenetic chromatin modification by amber suppression technology. *Current Opinion in Chemical Biology* **45**, 1–9 (2018).
158. Hoffmann, C. & Neumann, H. *In Vivo* Mapping of FACT–Histone Interactions Identifies a Role of Pob3 C-terminus in H2A–H2B Binding. *ACS Chem. Biol.* **10**, 2753–2763 (2015).

159. Hiragami-Hamada, K. et al. Dynamic and flexible H3K9me3 bridging via HP1 $\beta$  dimerization establishes a plastic state of condensed chromatin. *Nature Communications* **7**, 11310 (2016).
160. Van Oss, S. B. et al. The Histone Modification Domain of Paf1 Complex Subunit Rtf1 Directly Stimulates H2B Ubiquitylation through an Interaction with Rad6. *Mol Cell* **64**, 815–825 (2016).
161. Hino, N. et al. Protein photo-cross-linking in mammalian cells by site-specific incorporation of a photoreactive amino acid. *Nat Methods* **2**, 201–206 (2005).
162. Daggett, K. A. & Sakmar, T. P. Site-specific in vitro and in vivo incorporation of molecular probes to study G-protein-coupled receptors. *Current Opinion in Chemical Biology* **15**, 392–398 (2011).
163. Lee, S. et al. A Facile Strategy for Selective Incorporation of Phosphoserine into Histones. *Angewandte Chemie International Edition* **52**, 5771–5775 (2013).
164. Rogerson, D. T. et al. Efficient genetic encoding of phosphoserine and its non-hydrolyzable analog. *Nat Chem Biol* **11**, 496–503 (2015).
165. Huguenin-Dezot, N. et al. Synthesis of Isomeric Phosphoubiquitin Chains Reveals that Phosphorylation Controls Deubiquitinase Activity and Specificity. *Cell Reports* **16**, 1180–1193 (2016).
166. Beránek, V. et al. Genetically Encoded Protein Phosphorylation in Mammalian Cells. *Cell Chemical Biology* **25**, 1067-1074.e5 (2018).
167. Zhang, M. S. et al. Biosynthesis and genetic encoding of phosphothreonine through parallel selection and deep sequencing. *Nature Methods* **14**, 729–736 (2017).
168. Luo, X. et al. Genetically encoding phosphotyrosine and its nonhydrolyzable analog in bacteria. *Nature Chemical Biology* **13**, 845–849 (2017).
169. Neumann, H. et al. A Method for Genetically Installing Site-Specific Acetylation in Recombinant Histones Defines the Effects of H3 K56 Acetylation. *Molecular Cell* **36**, 153–163 (2009).
170. Rodriguez, Y., Hinz, J. M., Laughery, M. F., Wyrick, J. J. & Smerdon, M. J. Site-specific Acetylation of Histone H3 Decreases Polymerase  $\beta$  Activity on Nucleosome Core Particles in Vitro. *J Biol Chem* **291**, 11434–11445 (2016).
171. Mo, F. et al. Acetylation of Aurora B by TIP60 ensures accurate chromosomal segregation. *Nature Chemical Biology* **12**, 226–232 (2016).
172. Xuan, W., Yao, A. & Schultz, P. G. Genetically Encoded Fluorescent Probe for Detecting Sirtuins in Living Cells. *J. Am. Chem. Soc.* **139**, 12350–12353 (2017).
173. Gattner, M. J., Vrabel, M. & Carell, T. Synthesis of  $\epsilon$ -N-propionyl-,  $\epsilon$ -N-butyryl-, and  $\epsilon$ -N-crotonyl-lysine containing histone H3 using the pyrrolysine system. *Chem Commun (Camb)* **49**, 379–381 (2013).
174. Kim, C. H., Kang, M., Kim, H. J., Chatterjee, A. & Schultz, P. G. Site-Specific Incorporation of  $\epsilon$ -N-Crotonyllysine into Histones. *Angewandte Chemie International Edition* **51**, 7246–7249 (2012).
175. Chen, D. C., Yang, B. C. & Kuo, T. T. One-step transformation of yeast in stationary phase. *Curr Genet* **21**, 83–84 (1992).

176. Knop, M. *et al.* Epitope tagging of yeast genes using a PCR-based strategy: more tags and improved practical routines. *Yeast* **15**, 963–972 (1999).
177. Wach, A., Brachat, A., Pöhlmann, R. & Philippsen, P. New heterologous modules for classical or PCR-based gene disruptions in *Saccharomyces cerevisiae*. *Yeast* **10**, 1793–1808 (1994).
178. Spinck, M., Ecke, M., Sievers, S. & Neumann, H. Highly Sensitive Lysine Deacetylase Assay Based on Acetylated Firefly Luciferase. *Biochemistry* **57**, 3552–3555 (2018).
179. Hoffmann, C., Neumann, H. & Neumann-Staubitz, P. Trapping Chromatin Interacting Proteins with Genetically Encoded, UV-Activatable Crosslinkers In Vivo. in *Noncanonical Amino Acids: Methods and Protocols* (ed. Lemke, E. A.) 247–262 (Springer New York, 2018). doi:10.1007/978-1-4939-7574-7\_16.
180. Cox, J. & Mann, M. MaxQuant enables high peptide identification rates, individualized p.p.b.-range mass accuracies and proteome-wide protein quantification. *Nature Biotechnology* **26**, 1367–1372 (2008).
181. Tyanova, S. *et al.* The Perseus computational platform for comprehensive analysis of (prote)omics data. *Nature Methods* **13**, 731–740 (2016).
182. Surana, U. *et al.* Destruction of the CDC28/CLB mitotic kinase is not required for the metaphase to anaphase transition in budding yeast. *The EMBO Journal* **12**, 1969–1978 (1993).
183. Haase, S. B. Cell Cycle Analysis of Budding Yeast Using SYTOX Green. *Current Protocols in Cytometry* **26**, 7.23.1-7.23.4 (2004).
184. Chin, J. W. & Schultz, P. G. In vivo photocrosslinking with unnatural amino Acid mutagenesis. *Chembiochem* **3**, 1135–1137 (2002).
185. Zhang, T., Cooper, S. & Brockdorff, N. The interplay of histone modifications – writers that read. *EMBO reports* **16**, 1467–1481 (2015).
186. Ashburner, M. *et al.* Gene ontology: tool for the unification of biology. The Gene Ontology Consortium. *Nat Genet* **25**, 25–29 (2000).
187. The Gene Ontology Resource: 20 years and still GOing strong. *Nucleic Acids Res* **47**, D330–D338 (2019).
188. Parnell, T. J., Schlichter, A., Wilson, B. G. & Cairns, B. R. The chromatin remodelers RSC and ISW1 display functional and chromatin-based promoter antagonism. *eLife* **4**, e06073 (2015).
189. Kubik, S. *et al.* Opposing chromatin remodelers control transcription initiation frequency and start site selection. *Nature Structural & Molecular Biology* **26**, 744–754 (2019).
190. Kasten, M. *et al.* Tandem bromodomains in the chromatin remodeler RSC recognize acetylated histone H3 Lys14. *The EMBO Journal* **23**, 1348–1359 (2004).
191. VanDemark, A. P. *et al.* Autoregulation of the rsc4 tandem bromodomain by gcn5 acetylation. *Mol Cell* **27**, 817–828 (2007).
192. Chen, G., Li, W., Yan, F., Wang, D. & Chen, Y. The Structural Basis for Specific Recognition of H3K14 Acetylation by Sth1 in the RSC Chromatin Remodeling Complex. *Structure* **28**, 111-118.e3 (2020).

193. Duan, M.-R. & Smerdon, M. J. Histone H3 lysine 14 (H3K14) acetylation facilitates DNA repair in a positioned nucleosome by stabilizing the binding of the chromatin Remodeler RSC (Remodels Structure of Chromatin). *J Biol Chem* **289**, 8353–8363 (2014).
194. Muchardt, C., Reyes, J. C., Bourachot, B., Leguoy, E. & Yaniv, M. The hbrm and BRG-1 proteins, components of the human SNF/SWI complex, are phosphorylated and excluded from the condensed chromosomes during mitosis. *EMBO J* **15**, 3394–3402 (1996).
195. Zhang, W., Bone, J. R., Edmondson, D. G., Turner, B. M. & Roth, S. Y. Essential and redundant functions of histone acetylation revealed by mutation of target lysines and loss of the Gcn5p acetyltransferase. *EMBO J* **17**, 3155–3167 (1998).
196. Kuo, M. H. *et al.* Transcription-linked acetylation by Gcn5p of histones H3 and H4 at specific lysines. *Nature* **383**, 269–272 (1996).
197. Dai, J. *et al.* Probing nucleosome function: a highly versatile library of synthetic histone H3 and H4 mutants. *Cell* **134**, 1066–1078 (2008).
198. Lorch, Y., Cairns, B. R., Zhang, M. & Kornberg, R. D. Activated RSC-nucleosome complex and persistently altered form of the nucleosome. *Cell* **94**, 29–34 (1998).
199. Robzyk, K., Recht, J. & Osley, M. A. Rad6-Dependent Ubiquitination of Histone H2B in Yeast. *Science* **287**, 501 (2000).
200. Swaney, D. L. *et al.* Global analysis of phosphorylation and ubiquitylation cross-talk in protein degradation. *Nat Methods* **10**, 676–682 (2013).
201. Nathan, D. *et al.* Histone sumoylation is a negative regulator in *Saccharomyces cerevisiae* and shows dynamic interplay with positive-acting histone modifications. *Genes Dev* **20**, 966–976 (2006).
202. Yokoyama, H. & Gruss, O. J. New mitotic regulators released from chromatin. *Front Oncol* **3**, 308 (2013).
203. Gurley, L. R., D’Anna, J. A., Barham, S. S., Deaven, L. L. & Tobey, R. A. Histone phosphorylation and chromatin structure during mitosis in Chinese hamster cells. *Eur J Biochem* **84**, 1–15 (1978).
204. Hendzel, M. J. *et al.* Mitosis-specific phosphorylation of histone H3 initiates primarily within pericentromeric heterochromatin during G2 and spreads in an ordered fashion coincident with mitotic chromosome condensation. *Chromosoma* **106**, 348–360 (1997).
205. Chymkowitz, P. *et al.* Cdc28 kinase activity regulates the basal transcription machinery at a subset of genes. *Proceedings of the National Academy of Sciences of the United States of America* **109**, 10450–10455 (2012).
206. Zhao, K., Chai, X., Clements, A. & Marmorstein, R. Structure and autoregulation of the yeast Hst2 homolog of Sir2. *Nature Structural Biology* **10**, 864 (2003).
207. Albuquerque, C. P. *et al.* A multidimensional chromatography technology for in-depth phosphoproteome analysis. *Molecular & cellular proteomics: MCP* **7**, 1389–1396 (2008).
208. Wilson, J. M., Le, V. Q., Zimmerman, C., Marmorstein, R. & Pillus, L. Nuclear export modulates the cytoplasmic Sir2 homologue Hst2. *EMBO Rep* **7**, 1247 (2006).

209. Braselmann, S. & McCormick, F. Bcr and Raf form a complex in vivo via 14-3-3 proteins. *EMBO J* **14**, 4839–4848 (1995).
210. Vincenz, C. & Dixit, V. M. 14-3-3 proteins associate with A20 in an isoform-specific manner and function both as chaperone and adapter molecules. *J Biol Chem* **271**, 20029–20034 (1996).
211. Obsil, T., Ghirlando, R., Klein, D. C., Ganguly, S. & Dyda, F. Crystal structure of the 14-3-3zeta:serotonin N-acetyltransferase complex. a role for scaffolding in enzyme regulation. *Cell* **105**, 257–267 (2001).
212. Tzivion, G., Dobson, M. & Ramakrishnan, G. FoxO transcription factors; Regulation by AKT and 14-3-3 proteins. *Biochim Biophys Acta* **1813**, 1938–1945 (2011).
213. Gardino, A. K. & Yaffe, M. B. 14-3-3 proteins as signaling integration points for cell cycle control and apoptosis. *Semin Cell Dev Biol* **22**, 688–695 (2011).
214. Fan, X. et al. 14-3-3 Proteins Are on the Crossroads of Cancer, Aging, and Age-Related Neurodegenerative Disease. *Int J Mol Sci* **20**, (2019).
215. Freeman, A. K. & Morrison, D. K. 14-3-3 Proteins: diverse functions in cell proliferation and cancer progression. *Seminars in cell & developmental biology* **22**, 681–687 (2011).
216. Macdonald, N. et al. Molecular basis for the recognition of phosphorylated and phosphoacetylated histone h3 by 14-3-3. *Mol Cell* **20**, 199–211 (2005).
217. Walter, W. et al. 14-3-3 Interaction with Histone H3 Involves a Dual Modification Pattern of Phosphoacetylation. *Mol. Cell. Biol.* **28**, 2840 (2008).
218. Winter, S. et al. 14-3-3 proteins recognize a histone code at histone H3 and are required for transcriptional activation. *EMBO J* **27**, 88–99 (2008).
219. Healy, S., Khan, D. H. & Davie, J. R. Gene expression regulation through 14-3-3 interactions with histones and HDACs. *Discov Med* **11**, 349–358 (2011).
220. Jin, Y.-H. et al. Sirt2 interacts with 14-3-3 beta/gamma and down-regulates the activity of p53. *Biochem Biophys Res Commun* **368**, 690–695 (2008).
221. Berdichevsky, A., Viswanathan, M., Horvitz, H. R. & Guarente, L. C. elegans SIR-2.1 interacts with 14-3-3 proteins to activate DAF-16 and extend life span. *Cell* **125**, 1165–1177 (2006).
222. Wang, Y. et al. C. elegans 14-3-3 proteins regulate life span and interact with SIR-2.1 and. *Mech Ageing Dev* **127**, 741–747 (2006).
223. Rittinger, K. et al. Structural analysis of 14-3-3 phosphopeptide complexes identifies a dual role for the nuclear export signal of 14-3-3 in ligand binding. *Mol Cell* **4**, 153–166 (1999).
224. Kakiuchi, K. et al. Proteomic analysis of in vivo 14-3-3 interactions in the yeast *Saccharomyces cerevisiae*. *Biochemistry* **46**, 7781–7792 (2007).
225. KE, Y. W., DOU, Z., ZHANG, J. & YAO, X. B. Function and regulation of Aurora/Ipl1p kinase family in cell division. *Cell Research* **13**, 69–81 (2003).
226. Deretic, J., Kerr, A. & welburn, J. P. I. A rapid computational approach identifies SPICE1 as an Aurora kinase substrate. *MBoC* **30**, 312–323 (2018).
227. Trinkle-Mulcahy, L. Recent advances in proximity-based labeling methods for interactome mapping. *F1000Res* **8**, F1000 Faculty Rev-135 (2019).

228. Fullwood, M. J. & Ruan, Y. CHIP-based methods for the identification of long-range chromatin interactions. *J Cell Biochem* **107**, 30–39 (2009).
229. Krishnamurthy, M. *et al.* Caught in the act: covalent cross-linking captures activator-coactivator interactions in vivo. *ACS Chem Biol* **6**, 1321–1326 (2011).
230. Dugan, A. *et al.* Discovery of Enzymatic Targets of Transcriptional Activators via in Vivo Covalent Chemical Capture. *J. Am. Chem. Soc.* **138**, 12629–12635 (2016).
231. Li, X. *et al.* Quantitative chemical proteomics approach to identify post-translational modification-mediated protein-protein interactions. *J Am Chem Soc* **134**, 1982–1985 (2012).
232. Makde, R. D., England, J. R., Yennawar, H. P. & Tan, S. Structure of RCC1 chromatin factor bound to the nucleosome core particle. *Nature* **467**, 562–566 (2010).
233. Gavin, A.-C. *et al.* Functional organization of the yeast proteome by systematic analysis of protein complexes. *Nature* **415**, 141–147 (2002).
234. Calvert, M. E. K. *et al.* Phosphorylation by casein kinase 2 regulates Nap1 localization and function. *Mol Cell Biol* **28**, 1313–1325 (2008).
235. Murale, D. P., Hong, S. C., Haque, Md. M. & Lee, J.-S. Photo-affinity labeling (PAL) in chemical proteomics: a handy tool to investigate protein-protein interactions (PPIs). *Proteome Science* **15**, 14 (2017).
236. Joiner, C. M., Breen, M. E. & Mapp, A. K. Electron-deficient p-benzoyl-l-phenylalanine derivatives increase covalent chemical capture yields for protein-protein interactions. *Protein Sci* **28**, 1163–1170 (2019).
237. Wilson, M. D. & Costa, A. Cryo-electron microscopy of chromatin biology. *Acta Crystallogr D Struct Biol* **73**, 541–548 (2017).
238. Ayala, R. *et al.* Structure and regulation of the human INO80–nucleosome complex. *Nature* **556**, 391–395 (2018).
239. Eustermann, S. *et al.* Structural basis for ATP-dependent chromatin remodelling by the INO80 complex. *Nature* **556**, 386–390 (2018).
240. Somers, J. & Owen-Hughes, T. Mutations to the histone H3 alpha N region selectively alter the outcome of. *Nucleic Acids Res* **37**, 2504–2513 (2009).
241. Zhou, K., Gaullier, G. & Luger, K. Nucleosome structure and dynamics are coming of age. *Nature Structural & Molecular Biology* **26**, 3–13 (2019).
242. Chen, G., Li, W., Yan, F., Wang, D. & Chen, Y. The Structural Basis for Specific Recognition of H3K14 Acetylation by Sth1 in the RSC Chromatin Remodeling Complex. *Structure* **28**, 111-118.e3 (2020).
243. Badis, G. *et al.* A library of yeast transcription factor motifs reveals a widespread function for Rsc3 in targeting nucleosome exclusion at promoters. *Mol Cell* **32**, 878–887 (2008).
244. Krietenstein, N. *et al.* Genomic Nucleosome Organization Reconstituted with Pure Proteins. *Cell* **167**, 709-721.e12 (2016).
245. Lorch, Y., Maier-Davis, B. & Kornberg, R. D. Role of DNA sequence in chromatin remodeling and the formation of nucleosome-free regions. *Genes Dev* **28**, 2492–2497 (2014).

246. Verger, A., Perdomo, J. & Crossley, M. Modification with SUMO. A role in transcriptional regulation. *EMBO Rep* **4**, 137–142 (2003).
247. Johnson, E. S. Protein modification by SUMO. *Annu Rev Biochem* **73**, 355–382 (2004).
248. Wohlschlegel, J. A., Johnson, E. S., Reed, S. I. & Yates, J. R. 3rd. Global analysis of protein sumoylation in *Saccharomyces cerevisiae*. *J Biol Chem* **279**, 45662–45668 (2004).
249. Zhou, W., Ryan, J. J. & Zhou, H. Global analyses of sumoylated proteins in *Saccharomyces cerevisiae*. Induction of protein sumoylation by cellular stresses. *J Biol Chem* **279**, 32262–32268 (2004).
250. Zhao, Q. *et al.* GPS-SUMO: a tool for the prediction of sumoylation sites and SUMO-interaction motifs. *Nucleic Acids Research* **42**, W325–W330 (2014).
251. Srikumar, T., Lewicki, M. C. & Raught, B. A global *S. cerevisiae* small ubiquitin-related modifier (SUMO) system interactome. *Mol Syst Biol* **9**, (2013).
252. Klein-Brill, A., Joseph-Strauss, D., Appleboim, A. & Friedman, N. Dynamics of Chromatin and Transcription during Transient Depletion of the RSC Chromatin Remodeling Complex. *Cell Reports* **26**, 279-292.e5 (2019).
253. Jain, N. *et al.* Interaction of RSC chromatin remodelling complex with nucleosomes is modulated by H3 K14 acetylation and H2B SUMOylation in vivo. *iScience* 101292 (2020) doi:10.1016/j.isci.2020.101292.
254. Liu, X., Li, M., Xia, X., Li, X. & Chen, Z. Mechanism of chromatin remodelling revealed by the Snf2-nucleosome structure. *Nature* **544**, 440 (2017).
255. Ozdemir, A., Masumoto, H., Fitzjohn, P., Verreault, A. & Logie, C. Histone H3 lysine 56 acetylation: a new twist in the chromosome cycle. *Cell Cycle* **5**, 2602–2608 (2006).
256. Forné, I., Ludwigsen, J., Imhof, A., Becker, P. B. & Mueller-Planitz, F. Probing the conformation of the ISWI ATPase domain with genetically encoded photoreactive crosslinkers and mass spectrometry. *Mol Cell Proteomics* **11**, M111.012088 (2012).
257. Lopez, J. E., Haynes, S. E., Majmudar, J. D., Martin, B. R. & Fierke, C. A. HDAC8 Substrates Identified by Genetically Encoded Active Site Photocrosslinking. *J Am Chem Soc* **139**, 16222–16227 (2017).
258. Soulard, A. *et al.* The rapamycin-sensitive phosphoproteome reveals that TOR controls protein kinase A toward some but not all substrates. *Mol Biol Cell* **21**, 3475–3486 (2010).
259. Holt, L. J. *et al.* Global analysis of Cdk1 substrate phosphorylation sites provides insights into evolution. *Science* **325**, 1682–1686 (2009).
260. Liu, D. *et al.* Crystal structure of the zeta isoform of the 14-3-3 protein. *Nature* **376**, 191–194 (1995).
261. Yaffe, M. B. *et al.* The structural basis for 14-3-3:phosphopeptide binding specificity. *Cell* **91**, 961–971 (1997).
262. Langdon, E. M. *et al.* mRNA structure determines specificity of a polyQ-driven phase separation. *Science* **360**, 922 (2018).

263. Jain, N., Janning, P. & Neumann, H. 14-3-3 protein Bmh1 triggers short-range compaction of mitotic chromosomes by recruiting sirtuin deacetylase Hst2. *bioRxiv* 2020.06.09.142752 (2020) doi:10.1101/2020.06.09.142752.
264. Ghaemmaghami, S. et al. Global analysis of protein expression in yeast. *Nature* **425**, 737–741 (2003).
265. Jones, N. Bmh1/Bmh2 Redundancy in the Control of the Spindle Assembly Checkpoint in Yeast Cells. in (2018).
266. Michelsen, K. et al. A multimeric membrane protein reveals 14-3-3 isoform specificity in forward transport in yeast. *Traffic* **7**, 903–916 (2006).
267. Huh, W.-K. et al. Global analysis of protein localization in budding yeast. *Nature* **425**, 686–691 (2003).
268. Trembley, M. A., Berrus, H. L., Whicher, J. R. & Humphrey-Dixon, E. L. The yeast 14-3-3 proteins BMH1 and BMH2 differentially regulate rapamycin-mediated transcription. *Biosci Rep* **34**, e00099 (2014).
269. van Heusden, G. P. et al. The 14-3-3 proteins encoded by the BMH1 and BMH2 genes are essential in the yeast *Saccharomyces cerevisiae* and can be replaced by a plant homologue. *Eur J Biochem* **229**, 45–53 (1995).
270. Roberts, R. L., Mösch, H. U. & Fink, G. R. 14-3-3 proteins are essential for RAS/MAPK cascade signaling during pseudohyphal development in *S. cerevisiae*. *Cell* **89**, 1055–1065 (1997).
271. Sasaki, T. et al. Phosphorylation regulates SIRT1 function. *PLoS One* **3**, e4020–e4020 (2008).
272. Kang, H., Jung, J.-W., Kim, M. K. & Chung, J. H. CK2 is the regulator of SIRT1 substrate-binding affinity, deacetylase activity and cellular response to DNA-damage. *PLoS One* **4**, e6611 (2009).
273. Guo, X. et al. The NAD<sup>+</sup>-dependent protein deacetylase activity of SIRT1 is regulated by its oligomeric status. *Scientific Reports* **2**, 640 (2012).
274. Movahedi Naini, S., Sheridan, A. M., Force, T., Shah, J. V. & Bonventre, J. V. Group IVA Cytosolic Phospholipase A<sub>2</sub> Regulates the G<sub>2</sub>-to-M Transition by Modulating the Activity of Tumor Suppressor SIRT2. *Mol. Cell. Biol.* **35**, 3768 (2015).
275. Pandithage, R. et al. The regulation of SIRT2 function by cyclin-dependent kinases affects cell motility. *The Journal of cell biology* **180**, 915–929 (2008).
276. Spellman, P. T. et al. Comprehensive identification of cell cycle-regulated genes of the yeast *Saccharomyces cerevisiae* by microarray hybridization. *Mol Biol Cell* **9**, 3273–3297 (1998).

## ACKNOWLEDGEMENTS

I am deeply indebted to my supervisor, Prof. Dr. Heinz Neuman, for providing me a platform to learn and grow in science. I present my heartiest gratitude for all these years of advice and constant support. I am grateful for his continuous trust and patience, being an inspiring teacher.

I want to thank Prof. Dr. Andrea Musacchio and Dr. Gerben Vader, for their advice and feedback as members of my thesis committee. The fruitful discussions contributed considerably to my thesis. Furthermore, I want to thank Prof. Dr. Stefan Raunser for inspiring me with his great scientific vision in our department. I would like to acknowledge all the present and past members of Department III, for I have learned a lot from them. They were always willing to discuss the results in all progress report sessions and I highly appreciated their suggestions. I thank everyone for sharing reagents, ideas, creating a great working atmosphere and helping me getting familiar with german culture.

I would like to acknowledge all my lab mates for the wonderful time both in and out of the lab. Special thanks to Dr. Petra Neumann Staubitz for being a constant source of encouragement, for creating a refreshing working environment and her patience. I express my deepest gratefulness to Martin Spinck for being my go-to person and a constant help as a critical thinker. I thank Petra Geue for her technical support, preparing all reagents and SDS-PAGE gels. I am deeply indebted to Davide Tamborrini for inspiring me to work harder, for his ideas and contribution to our paper. This work would not have been possible without the help of our past lab member, Dr. Bryan Wilkins and his crosslinking experiments. Thanks are due to Simon Herring, Maria Ecke, Damian Schiller and Simon Kotnig for being part of this journey and always

helping with all the german translations. Special thanks go to Diana Ludwig, Sheila Mainye, Angela Hagemeyer and Anson Shek for standing through thick and thin.

I specially thank Dr. Petra Janning and the HRMS facility at MPI Dortmund for performing and evaluating Mass Spectrometry results. I highly appreciated Petra for her time and scientific suggestions. I am grateful to members specially of Department I for their support with reagents and advice. In particular to Dr. Richard Cardoso da Silva for numerous hours of discussion and constant encouragement if things were not working out. I am grateful to have received enormous scientific inputs from everyone at MPI, Dortmund. The possibility to work in a well-functioning surrounding is a great pleasure. I am happy to have made friends and beautiful memories that I will always cherish in my heart. My profound thanks go to Christa Hornemann and Lucia Sironi for all administrative help, time support and advice. I want to thank the International Max Planck Research School (IMPRS) for financial support.

Last but not the least, I would like to express my immense gratitude to my family and friends, who believed in me and supported me at each and every step. I draw enormous strength from my mother who fought cancer like a hero. I am eternally indebted to my grandparents for making me what I am today. I would like to express my sincerest thanks to my father for supporting my endeavors and dreams. A heartfelt thanks to my sister and brother for their unconditional love, encouragement and confidence in me. I would not have been able to come so far without each and every one of them.